

**ČESKÁ ZEMĚDĚLSKÁ UNIVERZITA V PRAZE**



**FAKULTA AGROBIOLOGIE, POTRAVINOVÝCH A PŘÍRODNÍCH ZDROJŮ  
KATEDRA PEDOLOGIE A OCHRANY PŮD**

**Mapování redistribuce organického uhlíku v erozně  
ovlivněných půdách metodami dálkového průzkumu  
Země a digitálního mapování půd**

.....  
doktorská disertační práce

Autor: **Mgr. Daniel Žížala**

Školitel: **Prof. Dr. Ing. Luboš Borůvka**

Konzultant: **Ing. Vladimír Papaj, Ph.D., VÚMOP, v.v.i.**

**Praha 2018**

## **Prohlášení**

Prohlašuji, že jsem disertační práci na téma „Mapování redistribuce organického uhlíku v erozně ovlivněných půdách metodami dálkového průzkumu Země a digitálního mapování půd“ vypracoval samostatně s použitím uvedené literatury a na základě konzultací a doporučení školitele. Souhlasím se zveřejněním disertační práce dle zákona č. 111/1998 Sb. o vysokých školách v platném znění, a to bez ohledu na výsledek její obhajoby.

V Praze dne 28. 8. 2018

.....

Podpis autora

## **Poděkování**

Na tomto místě bych rád poděkoval mému školiteli prof. Dr. Ing. Luboši Borůvkovi a konzultantu Ing. Vladimíru Papajovi, Ph.D., za jejich pomoc, cenné rady a připomínky, které mi poskytli při zpracování této práce. Rovněž děkuji všem spoluautorům předložených publikací a všem spolupracovníkům z České zemědělské univerzity a Výzkumného ústavu meliorací a ochrany půdy, v.v.i., kteří mi pomohli při mém výzkumu. Dále děkuji celé své rodině za jejich podporu v celé době studia a v celém životě, za trpělivost během zpracovávání mé práce a v neposlední řadě děkuji všem svým přátelům za příjemnění doby, v níž práce vznikala.

Za finanční podporu, která podpořila můj výzkum, bych chtěl poděkovat Národní agentuře pro zemědělský výzkum v rámci projektů QJ1330118 „Monitoring erozního poškození půd a projevů eroze pomocí metod DPZ“, QJ1520028 „Kvantifikace a modelování posunu půdních částic zpracováním půdy a výmolnou erozí v rámci hodnocení celkové ztráty půdy na zemědělsky intenzivně využívaných pozemcích“ a QJ1520028 „Vytvoření podrobných aktuálních map půdních vlastností ČR na základě využití dat Komplexního průzkumu půd a metod digitálního mapování půd“ a Grantové agentuře České republiky v rámci projektu GP13-07516P „Vývoj metod pro mapování koluvizemí na základě půdně-terénního modelování.

## Obsah

1	Úvod.....	1
2	Literární přehled .....	3
2.1	Organický uhlík v půdě a jeho zásoby .....	3
2.2	Dynamika a redistribuce organického uhlíku v půdě.....	5
2.3	Redistribuce půdního organického uhlíku vlivem erozně-akumulačních procesů 8	
2.3.1	Vodní eroze.....	10
2.3.1.1	Erozní části svahu.....	11
2.3.1.2	Transportní části svahu.....	12
2.3.1.3	Akumulační části svahu.....	12
2.3.2	Eroze zpracováním půdy .....	14
2.3.3	Větrná eroze.....	15
2.4	Metody kvantifikace SOC a jeho redistribuce .....	16
2.4.1	Klasické metody .....	16
2.4.2	Pedometrické metody .....	17
2.4.3	Simulační modely .....	20
2.4.4	Spektroskopie.....	22
2.4.4.1	Bodová spektroskopie .....	26
2.4.4.2	Obrazová spektroskopie .....	28
3	Vědecká hypotéza .....	32
4	Cíle práce .....	32
5	Publikované práce.....	33
5.1	Assessment of Soil Degradation by Erosion Based on Analysis of Soil Properties Using Aerial Hyperspectral Images and Ancillary Data, Czech Republic.....	33

5.2	Soil organic carbon and texture retrieving and mapping using proximal, airborne and Sentinel-2 spectral imaging.....	58
5.3	Mapping Soil Degradation using Remote Sensing Data and Ancillary Data - South-East Moravia, Czech Republic.....	97
5.4	Colluvial soils as a soil organic carbon pool in different soil regions .....	113
5.5	Relating extent of colluvial soils to topographic derivatives and soil variables in a Luvisol sub-catchment, Central Bohemia, Czech Republic .....	127
5.6	Influence of former lynchets on soil cover structure and soil organic carbon storage in agricultural land, Central Czechia.....	139
6	Sumární diskuze.....	152
7	Závěr .....	162
8	Seznam použité literatury .....	165
	Příloha.....	200

# 1 Úvod

---

Pokles organického uhlíku v půdě (SOC – *soil organic carbon*), respektive organické hmoty (SOM – *soil organic matter*), kde uhlík je nejzastoupenějším prvkem, je obecně chápán jako hlavní ohrožení pro trvalou udržitelnost obdělávání půdy. Jeho role je klíčová v mnoha produkčních i mimoprodukčních funkcích půdy. Půdní systém je v přírodních stabilních podmínkách považován za dlouhodobě udržitelný. Úbytek určitých půdních komponent je dynamicky nahrazován. V případě přirozené půdní eroze půdy je například odnos půdy přibližně bilančně nahrazován tvorbou půdy zvětráváním a dalšími procesy. Tato rovnováha je však v důsledku vnějších, zejména antropogenních, zásahů ohrožována a dochází k rozvoji řady degradačních procesů. Těmi může být ohrožena i zásoba půdního uhlíku v půdě. Půda představuje značnou zásobárnu uhlíku, po oceánech druhou největší, a je tak důležitým komponentem celého uhlíkového cyklu na Zemi, obzvláště v kontextu očekávaných změn klimatu a využití území. Proto je výzkumu půdního organického uhlíku věnovaná v poslední době značná pozornost.

Tak tomu je i v případě redistribuce organického uhlíku laterálními pohyby vlivem eroze půdy. V tomto ohledu přetrvává v poznání zatím mnoho nejasností a mezi vědeckou komunitou panují rozpory v popisu dynamiky uhlíku v různých fázích erozně-akumulačního procesu. Někteří autoři zmiňují, že nedostatečné poznatky o dynamice uhlíku v půdě a procesech spojených s erozí půdy představují nejslabší článek v obecném poznání celého uhlíkového cyklu. Vědeckými kruhy je tak kladen zvýšený důraz na další výzkum v této oblasti a mimo jiné i na vývoj efektivních metod mapování variability koncentrace a zásob organického uhlíku v půdách. K poznání těchto nedostatků v dosavadních vědomostech a posunu poznání přispívají i nové technologie a postupy. Ty ovšem s sebou přinášejí nové specifické okruhy problémů. Mezi hojně rozšířené způsoby výzkumu půdního organického uhlíku patří například laboratorní metody spektrální analýzy. Tyto metody však pracují v prostorové doméně pouze zprostředkovaně přes vyhodnocení výsledků v rámci vzorkovací sítě. Variabilita obsahu organického uhlíku, obzvláště v komplexním reliéfu, může být značná, a to i na malé vzdálenosti. Na lokální úrovni (jednotlivého pozemku) může variabilita vlivem laterálních pohybů půdy dosahovat míry variability na úrovni krajiny či regionu. V tomto kontextu je zapotřebí

etablovat metody, které umožní prostorové mapování organického uhlíku v dostatečném rozlišení. To mohou umožnit metody obrazové spektroskopie spadající do oboru dálkového průzkumu Země v kombinaci s metodami digitálního mapování půd. Z dosavadních výzkumů vyplývá, že využití těchto technologií, obzvláště v rámci studia silně heterogenního půdního prostředí, má svá specifika. Postupy zpracování a vyhodnocení pomocí těchto metod nejsou v současnosti ještě plně vyvinuty, ověřeny a etablovány a existuje řada problémů, které nebyly dosud plně vyřešeny. Záměrem této disertační práce je tedy zodpovězení otázky, jak je možné a s jakou přesností využít tyto metody pro účely mapování redistribuce organického uhlíku v erozně ovlivněných půdách v podmínkách České republiky a obecně v podmínkách zemědělské krajiny mírného klimatu

## 2 Literární přehled

### 2.1 Organický uhlík v půdě a jeho zásoby

---

Půdní organická hmota je zastoupena ve většině půd pouze v malém množství, v porovnání s minerální složkou půdy (od minimálního zastoupení až do cca 30 %). Její přítomnost je však velice důležitá pro fyzikálně-chemické vlastnosti půd a zásadní pro udržení půdní produktivity a dalších funkcí půdy. Je obecně známo, že obsah organického uhlíku v půdě (tvoří cca 58 % půdní organické hmoty; Dlugoš, 2011) má vliv na formování a stabilitu půdních agregátů a tedy i půdní strukturu jako takovou, pórovitost, vodní režim půd, kationtovou výměnnou kapacitu, pufrální schopnost půd, aktivitu půdních organismů apod. (Banwart et al., 2015; Milne et al., 2015); ve výsledku má tedy i zásadní vliv na úrodnost půdy. Snižování obsahu půdního organického uhlíku vede k degradaci půdy, zhoršení jejích funkcí a zvýšení emisí CO<sub>2</sub> do atmosféry. Obnova, navýšení a ochrana půdního organického uhlíku se tak z tohoto hlediska stává globální prioritou (Banwart et al., 2015; Milne et al., 2015). Na lokální úrovni se obsah a kvalita půdní organické hmoty stává vážným problémem současného stavu půd a celkových podmínek pro zemědělství a kvalitu životního prostředí, zejména vzhledem k negativní bilanci vstupů a výstupů organických látek v půdě (Bielek a Jurčová, 2010).

V současné době je půdní organický uhlík studován hlavně v souvislosti s rolí, kterou může hrát při snižování efektu klimatické změny v souvislosti se zvýšenou hladinou CO<sub>2</sub> v atmosféře. S výjimkou karbonátových hornin a fosilních zdrojů představuje půda největší pozemní zásobárnu uhlíku – uvádí se množství přibližně 2200 Pg C ve svrchním metru půdního pokryvu, z čehož přibližně 1500 Pg připadá na organický C, což je zhruba dvojnásobné množství, než je alokováno v atmosféře a trojnásobné než ve vegetaci (Batjes, 1995; Houghton, 1995; Batjes, 1996; Smith et al., 2015). Odhady celkových zásob organického uhlíku jsou nicméně nejisté (Minasny et al., 2013; Bayer et al., 2015). Todd-Brown et al. (2013) například ukazují rozpětí v zásobách organického půdního uhlíku mezi 510 – 2040 Pg C v závislosti na použití typu modelu systému Země (*Earth system model*). Stejně tak Hiederer a Köchy (2011) uvádějí rozpětí odhadů zásob SOC ve



svrchním metru půdy mezi 991 – 2469 Pg C (504 – 967 Pg C ve svrchní vrstvě půdy a 487 – 1502 Pg C v podorničí). Půda tedy může představovat značný potenciál pro dlouhodobé uložení uhlíku (tzv. sekvestraci uhlíku), nicméně také pro uvolňování uhlíku do atmosféry v závislosti na způsobu využití půdy a způsobu hospodaření (Jastrow et al., 2007; Powlson et al., 2011; Kadlec et al., 2012; Doetterl et al., 2015a). Vlivem různých procesů v půdě dochází ke ztrátám organického uhlíku. Půdy jsou obecně k těmto ztrátám náchylné vlivem degradačních procesů či ekosystémových disturbancí (Frank et al., 2015).

Houghton (2012) uvádí, že mezi roky 1850 – 2005 došlo vlivem kultivace půd k 25-30% úbytku půdního organického uhlíku. Smith et al. (2005a) v jejich výhledu změny zásob SOC v evropských půdách uvádějí, že mezi roky 1990 – 2080 může vlivem klimatické změny sice dojít k zvýšení zásob SOC o 1-7 t.ha<sup>-1</sup>, nicméně v případě započítání změn využití půdy spíše k celkovému úbytku. V těchto modelových odhadech jsou však značné nejistoty (Todd-Brown et al., 2013), zejména vlivem nejasností týkajících se osudu redistribuovaného organického uhlíku a nedostatečného poznání některých biochemických procesů v rámci rozkladu a stabilizace organické hmoty v různých podmínkách (sekvestrace v anoxických podmínkách, akumulace ve vodních ekosystémech, nahrazení na erodovaných plochách, apod.) či vlivu zemědělských činností na stabilizaci organické hmoty. Vliv klimatické změny je také zatím zatížen velkou nejistotou (Schils et al., 2008; Eglin et al., 2010; Falloon et al., 2011; Doetterl et al., 2015b; Smith et al., 2015) – zvýšení CO<sub>2</sub> může vést k většímu růstu biomasy a tedy nahrazení organického uhlíku, ale zvýšená teplota může naopak zvýšit rozklad a oxidaci, zejména v podmínkách dnešního permafrostu (Victoria et al., 2012). Dle Goidts et al. (2009) je stejně tak samotné hodnocení zásob SOC spojeno s velkými nejistotami, které mohou ovlivnit detekci časových změn v zásobě SOC, stejně tak identifikaci hlavních řídicích sil, které je ovlivňují. Jedním zdrojem těchto nejistot mohou být i rozdíly v použitých analytických metodách stanovení koncentrace SOC, využívání pedotransferových funkcí k odvození objemové hmotnosti či nejistoty spojené s použitím geostatistických modelů (Goidts et al., 2009).

Dle Milne et al. (2015) je odhadováno, že v posledních 25 letech čtvrtina půdy na světě trpí degradací v souvislosti se ztrátou organického uhlíku. Přestože mezi globálně nejvýznamnějšími ekosystémy, které nejvíce trpí ztrátou organického uhlíku, jsou řazeny

rašeliníště, aridní a semi-aridní oblasti a tropické lesy (Joosten, 2015), případně oblast permafrostu (Victoria et al., 2012), úbytky SOC v zemědělských půdách jsou značným problémem i v mírném pásmu, byť zde spíše ve vztahu k půdní úrodnosti a mimoprodukčním funkcím zemědělství než ve vztahu k příspěvku ke globální změně klimatu.

Jak uvádějí např. Victoria et al. (2012), Eglin et al. (2010) či Feller a Bernoux (2008), současné vědecké poznání o tom, jak lokální půdní vlastnosti a klimatické podmínky ovlivňují změny v obsahu organického uhlíku a jak fungují všechny toky uhlíku v půdě a mezi vnějším prostředím, jsou zatím nedostatečné a často se rozcházejí.

## **2.2 Dynamika a redistribuce organického uhlíku v půdě**

---

Distribuce SOC je obecně ovlivňována variabilitou klimatu (distribuce srážek, teplota) (Conant et al., 2011), variabilitou půdních vlastností (mateční substrát, textura, obsah a typ jílových minerálů, vlhkost, teplota) (Doetterl et al., 2015b), topografickou polohou, typem vegetace a využití půdy (management obhospodařování) (Joosten, 2015; Stevens et al., 2015). Zásoby SOC jsou také, zejména v současné době, ovlivňovány lidskou aktivitou – změny v krajinném pokryvu a využití půdy (např. odlesnění), odvodnění, orba, management rostlinných zbytků, zhutnění půdy, zvýšené využívání hnojiv, pesticidů a dalších chemikálií apod. (Banwart et al., 2015; Joosten, 2015).

Dynamika organického uhlíku v půdě je obecně ovlivňována dvěma protichůdnými pochody: vytvářením organického uhlíku zejména prostřednictvím vstupů rostlinných zbytků a odumřelých kořenů (nadzemní a podzemní biomasou) a rozkladem organické hmoty mikrobiální biomasou vrcholící mineralizací organického uhlíku (heterotrofní půdní respirací) (Lal, 2010; Dlugoš, 2011; Doetterl et al., 2012). Tyto procesy jsou ve stabilním prostředí vyrovnané. Vlivem působení přírodních a zejména antropogenních faktorů však dochází ke změně rovnováhy, k zvýšené mineralizaci organické hmoty, či k redistribuci organického uhlíku laterálním transportem (Dlugoš, 2011). Přirozená vertikální dynamika organického uhlíku je spojena zejména s distribucí půdní biomasy, pohybem rozpuštěné organické hmoty zejména podél preferenčních cest a bioturbací (VandenBygaart et al., 2015). Dynamika půdního organického uhlíku je nicméně značně komplexní záležitostí i v závislosti na různých vlastnostech organické hmoty a půdy, které ovlivňují míru a podobu procesů mineralizace a chemicko-fyzikální ochrany

organické hmoty v půdě. Organický uhlík se v půdě nachází v různých formách stabilizace – ve volné labilní formě v rámci nevázané relativně nerozložené organické hmoty, ve vázané formě v rámci půdních agregátů a v komplexní formě, kdy je chráněn silnými vazbami na minerální částice. Předmětem redistribuce a mineralizace je pak hlavně labilní forma, nicméně vlivem erozních a sedimentačních procesů může docházet k přechodu mezi jednotlivými formami (rozrušováním agregátů či pohřbením a fyzikální stabilizací) (Kirkels et al., 2014).

Zásoby SOC jsou labilní a zranitelné zejména tím, že se nacházejí v blízkosti povrchu a jsou tak předmětem transportu a transformace na rozdíl od fyzicky vázaných zásob uhlíku v oceánech a horninách. Půdní organická hmota je lehká a má nízkou objemovou hmotnost, takže je jednoduše transportovatelná a díky svému chemickému složení (organické sloučeniny) je za přítomnosti kyslíku předmětem oxidace (Lal, 2003). Vzhledem k těmto vlastnostem dochází k degradaci SOC zejména působením eroze půdy, chemické degradace vlivem oxidace a mineralizace spojené například s orbou či odvodněním a fyzikální degradací spojenou s degradací organických půd (Joosten, 2015). Obsah půdního uhlíku má vysokou prostorovou variabilitu (Minasny et al., 2013). Dle Goidts et al. (2009) variabilita koncentrací SOC na malém území (v řádu několik stovek metrů) může obecně dosahovat stejného rozpětí jako variabilita v regionálním měřítku a to i v případě orné půdy s relativně homogenním půdním pokryvem. Dle rešerše McBratney a Pringle (1999) se prostorová závislost půdního uhlíku v rámci pozemku vyskytuje v rozsahu 20 – 300 m. Variabilita na krátkou vzdálenost je výsledkem komplexního působení řady procesů. Stevens et al. (2015) tyto procesy rozdělují na ty, které působí téměř spojitě v prostoru a ovlivňující rovnováhu SOC v závislosti na topografických vlastnostech (vodní eroze a eroze zpracováním půdy, rozdíly v teplotě a vlhkosti), a procesy, které působí na bázi jednotlivých půdních bloků (způsob obdělávání, aplikace organických a dalších hnojiv, osevní postup, management posklizňových zbytků, změna využití půdy apod.). Stevens et al. (2015) také zdůrazňují nedostatek výzkumů prostorově určených a systematických rozdílů obsahu SOC mezi jednotlivými půdními bloky. Zatímco některé studie jsou zaměřeny na konkrétní půdní bloky, výzkumy na úrovni krajiny nejsou dostatečně přesné pro hodnocení variability mezi jednotlivými bloky a jsou často spojeny s využitím statistických metod s různou mírou nejistoty (Goidts et al., 2009).

K redistribuci půdního materiálu svázané s redistribucí organického uhlíku dochází především vlivem svahových pohybů, vodní a větrnou erozí a erozí zpracováním půdy (Van Oost et al., 2003; Kuhn a Armstrong, 2012). Vzhledem k tomu, že tyto procesy jsou vázány na topografické vlastnosti reliéfu, jejich rozložení a intenzita jsou závislé na pozici v prostoru (Zádorová, 2009; Schwanghart a Jarmer, 2011; Zádorová et al., 2015), což samozřejmě ovlivňuje i prostorovou variabilitu obsahu organické hmoty. Pozice na svahu ovlivňuje však také další faktory, které mají na variabilitu organického uhlíku vliv. Jedná se např. o vlhkost či teplotu půdy. Pozice také ovlivňuje množství biomasy vlivem variability radiačních podmínek důležitých pro její rozvoj (Hancock et al., 2010).

Na úrovni krajiny mají největší dopad na dynamiku SOC změny využití půdy a obdělávání půdy spojené se změnami vstupů organické hmoty, s ovlivněním procesu mineralizace a s laterálními pohyby půdy (Lal, 2004; Van Oost et al., 2007). V rámci hospodaření na zemědělské půdě jsou obvykle sníženy vstupy organické hmoty do půdy oproti přirozenému prostředí vlivem sklizně plodin a odvozu posklizňových zbytků, které často nejsou nahrazovány jinými vstupy. Vlivem odstranění přirozeného půdního krytu je také v některých fázích roku půda vystavena působení vodní a větrné eroze. Vlivem zemědělské činnosti dochází k ovlivnění půdních podmínek (teplota, vlhkost) například orbou či odvodněním a jsou tak ovlivňovány podmínky mineralizace organické hmoty. Konvenční způsoby orby zapracovávají rostlinné zbytky do půdy, zvyšují kontakt s minerální složkou, což vede k rychlejší mineralizaci organické hmoty oxidací (Campbell et al., 1996). Konvenční orba a časté přejezdy po pozemcích kvůli přípravě pro setí vedou k narušení půdních agregátů a vystavení chráněného organického uhlíku mikrobiální činnosti, přičemž narušují i půdní biotu a tak ovlivňují míru mineralizace uhlíku. Orba také ovlivňuje teplotní režim, čímž může být zvýšena náchylnost k fyzikálnímu rozpadu agregátů (Lee et al., 2009). Vlivem orby také dochází k redistribuci organického uhlíku v rámci půdního profilu, například míšením svrchních půdních horizontů s priorávaným podorničím. Pozitivní vliv minimalizačních technologií na zásoby SOC, ve smyslu jejich ochrany, nikoli zvýšení, byl prokázán řadou studií (např. VandenBygaart et al., 2003; Lee et al., 2009; Awale et al., 2013). Dále byl pozorován i pozitivní vliv bezorebných technologií na snížení emisí CO<sub>2</sub> při erozních událostech (Chaplot et al., 2012). Nicméně jak uvádějí Kirkels et al. (2014), existuje stále dost nejasností a další výzkum laterálních a vertikálních toků SOC v rámci orebních technologií je zapotřebí. Využití průmyslových hnojiv může mít pozitivní efekt na zásoby

SOC v půdě vlivem zvýšení primární produkce biomasy (Kirkels et al., 2014), nicméně jen v případě, pokud jsou zbytky plodin vráceny zpět do půdy (Alvarez, 2005).

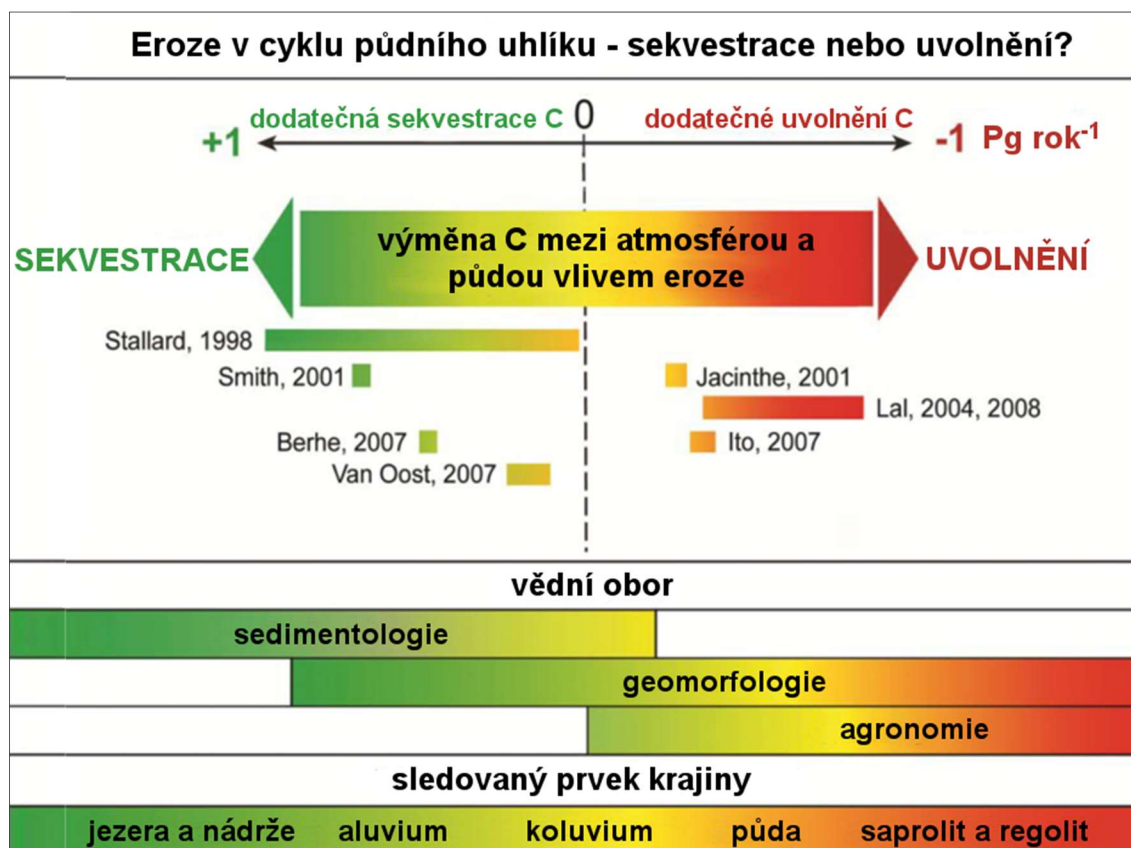
### **2.3 Redistribuce půdního organického uhlíku vlivem erozně-akumulačních procesů**

---

Půdní eroze jakožto nejčastěji zmiňovaný faktor redistribuce SOC je intenzivně studována již zhruba od poloviny 20. století a z geomorfologického pohledu je dobře popsána. Pohyb SOC zemědělskou krajinou prostřednictvím eroze, jeho ovlivnění v různých fázích erozního procesu a sedimentace a zejména jeho osud nejsou však v současnosti plně prozkoumány (Kuhn et al., 2012; Kirkels et al., 2014; Doetterl et al., 2015a). V posledních letech je obsahu SOC a jeho dynamice věnována značná pozornost vzhledem k faktu, že nedostatečné vědomosti o transferu uhlíku mezi půdou a atmosférou představují v současnosti největší nedostatek v poznání celého globálního cyklu uhlíku (Lal, 2003; Sanderman a Chappell, 2013; Kirkels et al., 2014). Jak uvádějí Polyakov a Lal (2008) či Kirkels et al. (2014), koncepční vztahy popisující dynamiku SOC jsou dnes relativně dobře popsány a chápány a mezi odborníky panuje shoda v názoru na dopad eroze na obsah SOC. Osud erodovaného, přemístěného a deponovaného SOC je však v současnosti stále předmětem odborných debat. Dle Kuhna et al. (2012) či Doetterla et al. (2015a) je plné porozumění zatím nemožné vzhledem k nedostatku dat, která jsou k dispozici, obzvláště co se týče preferenčního působení eroze a procesů probíhajících při transportu organické hmoty, jakož i stability deponovaného materiálu.

Dle Lala (2005) existuje rozpor v názoru na bilanci organického uhlíku zejména mezi sedimentology a pedology (Obrázek 1). Tento rozpor není v současnosti stále plně dořešen, je značně diskutován a zatím mezi vědci nedošlo ke konsenzu (Kirkels et al., 2014; Doetterl et al., 2015a). Dle jedné teorie je SOC uložený se sedimenty fyzicky chráněn proti mineralizaci a ten redistribuovaný z erozních ploch je dynamicky nahrazovaný produkcí biomasy. Tento proces dle nich vede k sekvestraci (ukládání) uhlíku (Smith et al., 2001; Renwick et al., 2004; Van Oost et al., 2004; Smith et al., 2005a; Rosenbloom et al., 2006; Berhe et al., 2007; Quine a Van Oost, 2007; Ritchie et al., 2007; Van Oost et al., 2007; Quinton et al., 2010; Doetterl et al., 2012). Naopak dle druhé teorie velká část vodou transportovaného SOC zahrnuje labilní frakci, a tak vlivem eroze dochází k zvýšené mineralizaci dříve stabilní organické hmoty. Tento proces pak může

být zdrojem atmosférického CO<sub>2</sub> (Jacinthe et al., 2001; Lal, 2003; Lal et al., 2004a, 2004b).



Obrázek 1: Celkový vliv redistribuce půdy na cyklus uhlíku dle současných studií – převzato z Doetterl et al. (2015a).

Vzhledem k výše zmíněnému se výzkum v současné době ve větší míře obrátil na výzkum fungování procesů působících na organický uhlík v průběhu eroze a po ní. Kuhn et al. (2009) či Kirkels et al. (2014) například uvádějí, že perspektivou řešení rozdílných konceptů je eko-geomorfologický přístup zahrnující geomorfologický, pedologický a biologický výzkum faktorů spojených s erozí, transportem a sedimentací na širší časoprostorové bázi. Řada studií se zabývá např. půdní respirací respektive její variabilitou (Bajracharya et al., 2000; Berhe et al., 2008; Dlugosz, 2011; Fiener et al., 2012) či stabilitou a osudem půdních agregátů v průběhu eroze (Ayoubi et al., 2012; Hu a Kuhn, 2014; Wang et al., 2014a; Chaplot a Cooper, 2015). Dosažené výsledky jsou však zatím neprůkazné a často se výrazně liší v závislosti na zájmové lokalitě. Navíc jejich

prostorové a časové omezení komplikuje hodnocení zásob SOC na úrovni povodí, krajiny i na globální úrovni (Yadav a Malanson, 2009; Kirkels et al., 2014).

Erozně-akumulační procesy postihují organický uhlík zejména redistribucí po ploše (laterální tok), sedimentací v depresních místech a na plochách, kde klesá sklon, nebo transportem do jiných (např. vodních) ekosystémů a ovlivněním procesu mineralizace a vertikálních toků v různých fázích erozního a sedimentačního procesu (Chaopricha a Marín-Spiotta, 2014). Množství a kvalita SOC je ovlivněna transportními procesy selektivní eroze (vodní, větrná) a neselektivní eroze (zpracováním půdy) a jeho distribuce je tak úzce svázána s odtokovými podmínkami a topografickou pozicí (Kirkels et al., 2014).

### 2.3.1 Vodní eroze

---

Půdní organická hmota je lehká a má nízkou objemovou hmotnost (Starr et al., 2000; Lal, 2003), což pravděpodobně vede k preferenčnímu odstranění SOC během erozních procesů. Nicméně míra preferenčního odnosu a obohacení sedimentů o SOC se výrazně liší v závislosti na půdních podmínkách (menší u jílovitých půd) a charakteristikách erozní události (Hu et al., 2013; Müller-Nedebock a Chaplot, 2015). Míra a způsob redistribuce SOC závisí na nosné kapacitě transportního média (Morgan, 2005), v tomto případě vody. Větší obohacení sedimentů je tak vázané spíše na menší erozní události charakteru plošné či mezirýhové eroze (Wang et al., 2014a; Fiener et al., 2015). Tento typ eroze je však v redistribuci sedimentů objemově významný spíše lokálně než v globálním a regionálním měřítku (Kuhn, 2007; Kuhn et al., 2009; Wang et al., 2010a; Kuhn et al., 2012; Fiener et al., 2015). Dle Kuhna et al. (2009) není organický uhlík transportovaný vlivem mezirýhové eroze přemísťován na velké vzdálenosti a je ukládán na depozičních plochách v povrchových vrstvách a je tak vystaven atmosférickým vlivům. Jak uvádějí Jacinthe et al. (2004), uhlík mobilizovaný během méně intenzivních erozních událostí může být až 2,5krát labilnější oproti velkým událostem. Při větších událostech však dochází k redistribuci podstatně většího množství SOC, byť je v sedimentech v menší koncentraci (Martínez-Mena et al., 2012).

Erozní procesy spojené s rýhovou a výmolovou erozí jsou svou povahou neselektivní vůči SOC (Van Oost et al., 2004). Výsledné sedimenty mají tedy obdobné charakteristiky jako půdy na erozních plochách (Kuhn et al., 2012). Je však potřeba brát v úvahu jistou diferenciaci sedimentů v závislosti na procesu sedimentace. Koncentrace SOC

v sedimentech se v důsledku rychlejší sedimentace těžších částic může zvyšovat s rostoucí vzdáleností od zdrojových ploch (Kuhn et al., 2009), což vede k zvýšenému obsahu v rozpuštěných sedimentech (Quine a Van Oost, 2007; Wang et al., 2010b). Dle Lala (2003) je navíc na větší vzdálenost transportována lehčí frakce zahrnující labilní složku SOC. Podíl organické hmoty exportované do vodních ekosystémů a sedimentované na ploše je však poměrně nejasný a řada autorů upozorňuje na vlivy, které mohou podhodnotit nebo naopak přecenit tento podíl (Kuhn et al., 2009; Hu a Kuhn, 2014).

#### 2.3.1.1 Erozní části svahu

Na erozních částech svahu jsou zásoby SOC vodní erozí snižovány v závislosti na charakteru erozní události, sklonitosti, délce svahu a konvexitě reliéfu. Fyzické odstranění aktivní složky SOC může být doprovázeno zvýšením úrovně mineralizace vlivem změn oxidačního potenciálu, změn teplotních a vlhkostních podmínek spojených s obnažením hlubších vrstev půdy. Zároveň může docházet k snížení produkce biomasy a tedy k nižším vstupům organické hmoty do půdy (Yadav a Malanson, 2009; Quinton et al., 2010). Nicméně může být zvýšen i potenciál sekvestrace SOC vlivem obnažení vrstev, které mají menší nasycení SOC (Kirkels et al., 2014).

V případě, že na erozních plochách nedochází k dynamickému nahrazování SOC ve stejné úrovni jako k jeho úbytku, může časem docházet ke změnám SOC v erozních sedimentech jak kvantitativním (úroveň obsahu SOC v sedimentech), tak kvalitativním (poměr stabilní a labilní složky). Tento proces je spojen s obnažením spodních vrstev půdy na erodovaných plochách, které mají nižší obsah SOC a obsahují více labilní složky SOC. Úbytek SOC na erozních plochách a emise CO<sub>2</sub> mohou být tedy v průběhu času nižší (Liu et al., 2003; Van Oost et al., 2005). Úroveň dynamického nahrazování SOC na erodovaných plochách a jeho vliv na cyklus uhlíku jsou však v současnosti předmětem diskuzí mezi dvěma výše prezentovanými skupinami, přičemž obecné závěry zřejmě zatím není možné vyjádřit. Úroveň nahrazování SOC je tak zřejmě specifická dle lokálních podmínek v závislosti na úrovni erozních procesů a podmínek pro primární produkci organické hmoty (přírodní podmínky a lidská aktivita) (Dlugosz et al., 2012).

Obdobné dilema je prezentováno v souvislosti se změnami mineralizace SOC na erozních plochách. Mineralizace může být zvýšena vlivem změny podmínek - vyšší teplota, menší vlhkost (Jacinthe et al., 2001; Lal, 2003; Lal et al., 2004b) nebo naopak snížena vlivem



menší dostupnosti SOC v souvislosti s jeho úbytkem (Liu et al., 2003; Quinton et al., 2010). Míra mineralizace může být také ovlivněna redistribucí půdních mikroorganismů vlivem erozních procesů (Huang et al., 2013).

#### 2.3.1.2 Transportní části svahu

SOC odstraněný vlivem eroze je dále redistribuován v krajině prostřednictvím transportních procesů. Vlivem rozrušování a transportu dochází k rozpadu půdních agregátů, což vede k obnažení dříve fyzicky chráněného SOC a vystavení vlivům mineralizace mikrobiálními procesy. Stupeň mineralizace během transportu je v současnosti opět předmětem vědecké diskuze. Jak uvádí Kirkels et al. (2014), studií zabývajících se mineralizací SOC během transportu je zatím relativně málo. Lal (1995) a další navazující práce (Jacinthe et al., 2001; Lal et al., 2004b) uvádějí, že ztráty SOC mineralizací během transportu mohou dosáhnout až 20 %. Práce Quinton et al. (2010); Renwick et al. (2004); Van Oost et al. (2007) naopak uvádějí, že podíl mineralizovaného SOC je minimální. Dle Kirkelse et al. (2014) navíc mineralizace během transportu závisí na typu a délce transportní dráhy a následných podmínkách depozice (selektivní či neselektivní), tedy na faktorech, které jsou v současnosti stále nedostatečně zhodnocené.

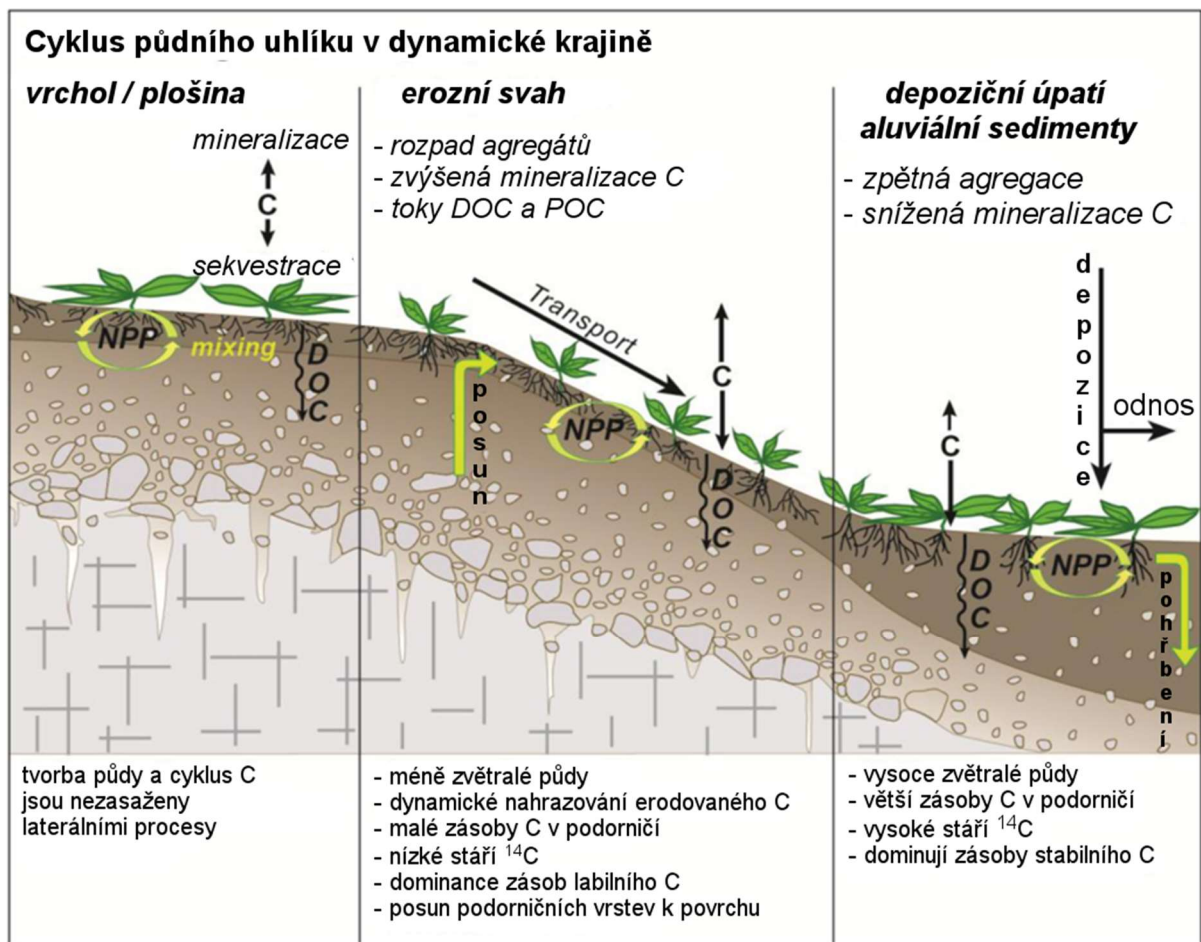
#### 2.3.1.3 Akumulační části svahu

Redistribuce SOC vede k jeho koncentraci na depozičních plochách, přičemž k depozici může dojít v prostředí koluvií, aluvií, případně ve vodním prostředí a na zamokřených plochách. SOC na depozičních plochách je ovlivňován řadou komplexních procesů zahrnujících změny v míře mineralizace, produkce biomasy či pohřbení SOC. Mechanismus pohřbení SOC popisuje jeho přesun z aktivní zásoby SOC, která interaguje s biosférou, do pasivní zásoby, kde je relativně dobře chráněn proti mineralizaci (McCarty a Ritchie, 2002; Van Oost et al., 2005; Berhe et al., 2007; Wang et al., 2014b; VandenBygaart et al., 2015). Pohřbený SOC může představovat značnou zásobu uhlíku (Van Oost et al., 2005; Zádorová et al., 2011, 2015).

Osud erodovaného SOC je závislý na několika faktorech, zejména na podmínkách depozice (pohřbení, odhalení SOC) ovlivňujících potenciál mineralizace a stability SOC a povaze stabilizačních mechanismů (Nadeu et al., 2012). Podmínky na depozičních plochách jsou také výrazně ovlivňovány frekvencí a povahou (velikostí) erozních a sedimentačních procesů, které ovlivňují dobu expozice či pohřbení SOC (Kirkels et al., 2014; Fiener et al., 2015).

Změny míry mineralizace vlivem depozičních procesů jsou opět předmětem odborných debat zejména mezi skupinami Lal a kolegové versus Van Oost a další (viz výše). Zatímco Lal (2003) a Lal et al. (2004b) argumentují větší přítomností labilního SOC v sedimentech, která může povzbudit mikrobiální a biologickou aktivitu a tedy zvýšení mineralizace, druhá skupina (Van Oost et al., 2004, 2005; Berhe et al., 2007; Van Hemelryck et al., 2010, 2011) argumentuje snížením míry mineralizace vlivem změny podmínek v pohřbených sedimentech (menší teplota, aerace apod.). Navíc na depozičních plochách mohou být lepší podmínky pro tvorbu agregátů (vyšší koncentrace organické hmoty a jílu) zvyšující fyzikální a chemickou ochranu SOC. Jak uvádějí např. Quinton et al. (2010); Van Hemelryck et al. (2010) či Van Hemelryck et al. (2011), SOC uložený v blízkosti povrchu ukazuje vyšší míru mineralizace pouze krátkodobě, což dle autorů nepředstavuje podstatný objem toků uhlíku na úrovni krajiny.

Dle Kirkelse et al. (2014) jsou hlavními mezerami v povědomí o dynamice SOC na depozičních plochách zejména omezené výzkumy hodnotící akumulaci sedimentů, dlouhodobou stabilitu SOC na těchto plochách a míru mineralizace v závislosti na velikosti a kvalitě SOC. Aldana-Jague et al. (2016) dále vidí mezeru v poznání v řídkém a nespojitém mapování vertikální distribuce SOC (s malým rozlišením, obvykle v jedné či málo vrstvách) oproti mapování horizontální variability s vysokým rozlišením.



Obrázek 2: Přehled cyklu uhlíku v dynamické erozní krajině a klíčové mechanismy sekvestrace a uvolňování uhlíku z půdy – převzato z Doetterl et al. (2015a). NPP = čistá primární produkce biosféry (*net primary production*), DOC = rozpuštěný organický uhlík (*dissolved organic carbon*), POC = nerozpuštěný organický uhlík (*particulate organic carbon*)

### 2.3.2 Eroze zpracováním půdy

Eroze zpracováním půdy (*tillage erosion*) označuje pohyb půdních částic po svahu vlivem působení zemědělské mechanizace při zpracování půdy. Redistribuce půdy vlivem tohoto procesu má za následek tedy i redistribuci SOC. Míra redistribuce je závislá na použité technologii zpracování půdy (Morgan, 2005; Quinton et al., 2006), půdních vlastnostech (Van Oost et al., 2009; Quinton et al., 2010) a vlastnostech terénu (Young et al., 2014). Redistribuce půdy a SOC erozí orbou obvykle působí ztráty na konvexních částech svahu a akumulaci v konkávních částech (Reicosky et al., 2005; Van Oost et al., 2009), přičemž nedochází k přímým ztrátám z pozemků. Dle van Oosta et al. (2005; 2009) je výsledná redistribuce vlivem zpracování půdy těžko rozlišitelná od vlivu přirozených

geomorfologických procesů, nicméně dobře odlišitelná od vlivu vodní eroze (Doetterl et al., 2012). Xiaojun et al. (2013) uvádějí, že eroze zpracováním půdy je v intenzivně obhospodařované krajině dominantní na příkřejších svazích, zatímco na mírnějších svazích je dominantním procesem redistribuce vodní eroze. Dále ve své studii ukázali, že eroze zpracováním půdy nemá na rozdíl od vodní eroze vliv na uhlík mikrobiální biomasy. Na rozdíl od vodní eroze se totiž nejedná o selektivní proces pohybu, a nedochází při něm k mineralizaci SOC vyvolané tímto pohybem (Van Oost et al., 2004).

### 2.3.3 Větrná eroze

Větrná eroze je degradační proces půdy, jehož kvantifikace je založená spíše na přibližných odhadech či modelování. Jedná se o proces, který se může odehrávat nepozorovaně, přičemž dle Chepila (1960) může jít o nepozorovatelnou a nezměřitelnou redistribuci půdního materiálu v řádu několika desítek  $t \cdot ha^{-1} \cdot rok^{-1}$ . Jelikož se jedná o prostorově neohrazený proces způsobující transport částic na dlouhé vzdálenosti a sedimentaci na rozsáhlých plochách, je velice těžké tento proces kvantifikovat, což přináší podstatné nejistoty do bilance uhlíkového cyklu. Redistribuce SOC vlivem větrné eroze není zahrnutá ve většině bilancí uhlíku, nicméně ve skutečnosti v nich může zahrnovat podstatnou část (Webb et al., 2012; Buschiazzo a Funk, 2015). Jak také uvádějí Webb et al. (2012), je v současnosti velice malé povědomí o typu a osudu větrem erodovaného SOC. Další výzkum k objasnění různého dopadu eolických procesů, transportu a depozice na SOC je zapotřebí s ohledem na míru mineralizace, ztráty SOC do atmosféry, obohacení eolických sedimentů a ztráty ve vodním prostředí.

Větrná eroze je selektivní proces, který v závislosti na síle větru preferenčně odnáší nejlehčí minerální částice a organickou hmotu. Obohacení eolických sedimentů o SOC bylo v různé míře prokázáno v několika studiích (např.: Buschiazzo et al., 2007; Hoffmann et al., 2008). Dle Buschiazzo a Funk (2015) jsou větší koncentrace SOC v erozních sedimentech sledovány po orbě, nicméně s časem se snižují vlivem nedostupnosti erozního materiálu. Jak dále popisují Buschiazzo a Funk (2015), zvýšený obsah SOC v erozních sedimentech může být popsán vlivem separace materiálu v závislosti na rozdílech objemové hmotnosti mezi lehčí organickou hmotou a těžšími minerálními částicemi, přestože aerodynamické parametry jsou stejné. Nicméně, jak upozorňuje Lal (2003), různé typy SOC jsou postiženy erozními procesy různě v závislosti na jejich velikosti, tvaru a hustotě.

Buschiazzo a Funk (2015) uvádějí, že na dlouhodobě sledovaných plochách v severním Německu mohou být s větrnou erozí spojeny ztráty SOC mezi roky 1990 – 2009 v rozsahu až 25 t.ha<sup>-1</sup>. V České republice je větrnou erozí potenciálně ohroženo 25,7 % výměry orné půdy (Výzkumný ústav meliorací a ochrany půdy, 2015). Antropogenní zásahy, které ovlivňují míru větrné eroze, a které v značné míře způsobují tento stav, spočívají zejména v odstraňování přirozených krajinných prvků a změně půdních podmínek narušujících vodní režim a agregátovou stabilitu.

## 2.4 Metody kvantifikace SOC a jeho redistribuce

### 2.4.1 Klasické metody

---

Klasickou metodou hodnocení redistribuce SOC je bodový odběr a analýza půdních vzorků. Analyzované vzorky mohou být odebrány v různé prostorové a časové struktuře v závislosti na zkoumaném jevu – příčině redistribuce. Kvantifikace SOC je obecně prováděna na půdních vzorcích přeseťých přes 2mm síto s vyloučením kořenů, nerozložených rostlinných zbytků a větší fauny. Obsah SOC či SOM může být odvozen metodou ztráty žiháním, elementární analýzou (*dry combustion*), často prováděnou pomocí automatických analyzátorů, nebo mokrou cestou titrací po oxidaci organických molekul chromsírovou směsí jako v klasické metodě Walkley-Black používané v anglosaských zemích či Tjurinově metodě a různých jejích modifikacích používané ve východoevropských zemích (Vindušková, 2013; Chenu et al., 2015). Tyto metody mají různou míru přesnosti a různá omezení (metodická, cenová, environmentální apod.), jak uvádí celá řada prací zabývajících se srovnáním jednotlivých metod s různými půdními vzorky (Sleutel et al., 2007; Meersmans et al., 2009; Sato et al., 2014). Jak uvádějí Goidts et al. (2009), hodnoty směrodatné odchylky se pohybují v rozmezí 1,2 – 15,8 % u ztráty žiháním, 1,6 - 4,2% u metody Walkley-Black a 1,3 - 7,1 % u elementární analýzy. V dnešní době jsou tak zavedeny víceméně přesné metody pro měření uhlíku v půdních vzorcích, nicméně jak uvádějí Conant et al. (2010), dokumentování celkových zásob SOC v půdě je obtížné vzhledem k prostorové variabilitě faktorů určujících tyto zásoby (obsah SOC, objemová hmotnost půdy, hloubka odběru vzorků a obsah skeletu). Nepřesnosti jsou pak zvyšovány přirozenou variabilitou těchto faktorů. Například nepřímé hodnocení objemové hmotnosti na základě pedotransferových funkcí může dle shrnutí v Goidts et al. (2009) vést k chybě odhadu zásob SOC v rozmezí 9 – 36 %.

Dalším způsobem odvození hodnot obsahu SOC v půdě jsou nepřímé metody využívající např. simulační modely nebo spektrální vlastnosti půd (například metody LIBS - Spektroskopie

laserem buzeného plazmatu - *Laser Induced Breakdown Spectroscopy*, DRIFTS - Difúzně-reflexní infračervená spektroskopie s Fourierovou transformací - *Diffuse Reflectance Fourier Transform Infrared Spectroscopy*, či INS - Neelastický rozptyl neutronů - *Inelastic Neutron Scattering*) (Izaurre et al., 2013).

Důležitým prvkem pro hodnocení variability obsahu SOC je také schéma vzorkování. Za prvé se jedná o hloubku vzorkování. Ta závisí na účelu vzorkování, nicméně ve většině studií je vzorkován orniční horizont do hloubky 30 cm, méně pak do 1 m. Vzorkování pod 1 m je spíše výjimečné (Minasny et al., 2013; Jandl et al., 2014). Návrh schématu odběrové sítě je pak důležitým krokem pro postižení co největší variability obsahu SOC a minimalizaci chyb plynoucích ze vzorkování. V tomto ohledu je třeba brát zřetel na přírodní podmínky zkoumaného území a jejich variabilitu a dostupné zdroje pro vzorkování a analýzu. Koncepty vzorkování lze rozdělit na vzorkování bez statistického určení v pravidelné síti nebo v náhodné síti, stratifikované vzorkování (Minasny et al., 2013) nebo hnízdovité vzorkování (*nested sampling*) se zvyšujícími se náklady a přesností v tomto pořadí (Jandl et al., 2014). Mezi využívanými metodami lze zmínit např. vzorkování pomocí redukční pravděpodobnostní metody podmíněných Latinských hyperkrychlí (cLHS - *Conditioned Latin hypercube sampling*) (Minasny a McBratney, 2006; Penížek et al., 2014), fuzzy shlukování metodou nejbližších středů - *fuzzy k-means clustering* (de Gruijter et al., 2010) apod. Batjes a Wesemael (2015) a Goidts et al. (2009) doporučují při výběru vhodné vzorkovací metody využít konceptu minimální detekované diference (*minimum detectable difference* – MDD), která umožňuje vyhodnotit vhodnost a přesnost zvolené metody. V rámci redukce chyb plynoucích z vysoké prostorové variability na malém prostoru se doporučuje využít směsných vzorků (Goidts et al., 2009). Nevýhodou směsných vzorků je ovšem poskytnutí průměrné informace z větší plochy, což může naopak vést k redukci získané informace.

#### 2.4.2 Pedometrické metody

---

Pro mapování plošné variability a vytvoření spojitých hodnot v prostoru lze využít pedometrické metody, jakožto soubor kvantitativních matematických a statistických metod aplikovaných na pedologické údaje. Bodové údaje ze vzorkování SOC jsou

pomocí různých interpolačních metod využívajících spojitost jevu či prostorovou závislost - autokorelaci (geostatistické modely) využity pro odvození hodnot v neměřených bodech. Vzhledem k vysoké variabilitě SOC ve vztahu k podmínkám území je pro interpolaci a odvození prostorové distribuce SOC z diskrétních bodů zapotřebí využít přesného popisu prostorové heterogenity různých environmentálních faktorů namísto použití pouze globálního prostorového trendu. Pro vytvoření plošných map a predikci hodnot v neměřených bodech je tak využíváno empirického přístupu, kdy data z omezeného počtu pozorování zkoumané veličiny jsou modelována pomocí dat prostorově rozložených proměnných při využití mnohorozměrných kalibračních metod. Rozvoj statistických nástrojů vytěžování dat (*data mining*), výpočetní síly počítačů a GIS a zvýšená dostupnost digitálních prostorových dat vedly na konci 20. století k formulaci principů tzv. digitálního půdního mapování (*Digital Soil Mapping - DSM*) (McBratney et al., 2003). DSM má tři hlavní komponenty – vstup (zahrnující použití stávajících dat a sběr nových dat pomocí statistických metod vzorkování), proces (zahrnující vytvoření matematického nebo statistického modelu popisujícího vztah mezi pozorováními a environmentálními proměnnými či faktory prostředí *scorpan*) a výstup (ve formě prostorového půdního informačního systému ve tvaru rastru/gridu predikovaných hodnot společně s vymezením nejistoty predikce) (Minasny a McBratney, 2015). Model predikce je obecně popisován jako prostorová predikční půdní funkce, respektive konceptuální model, např. *scorpan* (McBratney et al., 2003), případně model STEP-AWBH (Grunwald et al., 2015), odvozené ze známé Jennyho rovnice vývoje půdy CLORPT (Jenny, 1941). Model *scorpan* je používán pro kvantitativní predikci spojitých půdních vlastností nebo půdních tříd na základě empirického pozorování a je aplikován na environmentální data zahrnující jednotlivé funkční faktory (s - půda, c - klima, o - organismy, r - reliéf, p – půdotvorný substrát, a - věk, n - pozice v prostoru). Častými podpůrnými daty pro tvorbu predikčních modelů jsou pak také různé spektrální charakteristiky půd získané pomocí metod dálkového či pozemního průzkumu Země (Minasny a McBratney, 2015). Funkce popisující vztah mezi predikovanými půdními vlastnostmi a vysvětlujícími proměnnými pak může být ve formě jednoduchého lineárního modelu či komplikovanějšího nástroje vytěžování dat (Minasny et al., 2013).

Nejčastěji využívané vysvětlující proměnné využívané v modelech pro odvození distribuce SOC jsou terénní atributy, půdní typ, mateční substrát, typ využití půdy a klimatické faktory (Hancock et al., 2010; Doetterl et al., 2012; Minasny et al., 2013;

Grunwald et al., 2015), tedy logicky proměnné ovlivňující distribuci SOC v krajině. Každý z těchto faktorů ovlivňuje rozložení SOC v jiném měřítku. V prostředí erozního reliéfu v měřítku půdních bloků mohou být chápány jako hlavní řídicí faktor redistribuce SOC terénní vlastnosti, obzvláště v případě homogenního substrátu (Ritchie et al., 2007; Minasny et al., 2013; Zádorová et al., 2015). Terénní vlastnosti jsou obvykle odvozovány z digitálního modelu terénu s využitím nástrojů geografických informačních systémů (GIS). Tato data v různém stupni rozlišení umožňují odvození prostorově distribuované informace o charakteristikách reliéfu, přičemž pro potřeby precizního statistického vyhodnocení je zapotřebí využít modelu s relativně podrobným rozlišením (Hengl et al., 2004). Při modelování a predikci distribuce SOC, ale i jiných půdních vlastností, je v modelech používáno řady terénních atributů jakožto vysvětlujících proměnných. Lze využít jak primárních (nadmořská výška, sklonitost, expozice, zakřivení, sběrná plocha), tak odvozených charakteristik reliéfu (topografický index – TWI, index síly toku – SPI apod.). Přehled vybraných výzkumů využívajících terénní vlastnosti pro predikci SOC předkládá Tabulka 1 uvedená v příloze.

Celou řadu pedometrických metod využívaných v digitálním mapování půd je možno rozdělit do skupin metod statistických, geostatistických či hybridních (McBratney et al., 2000; Penížek, 2005; Grunwald, 2009). Mezi statistické metody využívané při predikci SOC můžeme zařadit např. klasifikační a regresní stromy (Bou Kheir et al., 2010; Martin et al., 2011), umělé neuronové sítě (Li et al., 2013; Tiwari et al., 2015) či obecné lineární a nelineární modely (Florinsky et al., 2002; Sleutel et al., 2007; Meersmans et al., 2012; Li et al., 2013), mezi geostatistické metody, vycházející z metody krigingu, běžný kriging – *ordinary kriging* (Wu et al., 2009; Brodský et al., 2011b; Długoń, 2011; Marchetti et al., 2012; Tiwari et al., 2015), univerzální kriging – *universal kriging* (Veronesi et al., 2014) či pravděpodobnostní kriging – *probability kriging* (Zhang et al., 2013a). Hybridní metody pak kombinují výše zmíněné statistické a geostatistické metody – *co-kriging* (Odeh et al., 1995; Wu et al., 2009) či regrese

kriging - *regression-kriging* (Odeh et al., 1995; Długoń, 2011; Li et al., 2013; Adhikari et al., 2014).

Dle Li et al. (2013) a Song et al. (2016) jsou nejčastěji používanými modelovými přístupy v predikci SOC vícenásobné lineární regrese, regrese kriging, regresní stromy – *regression trees* a umělé neuronové sítě – *artificial neural networks*. Nicméně různé



metody mají různé nevýhody a je tedy zapotřebí dbát na výběr správného modelu, případně otestovat modelů více. Metody lineární regrese například pracují s lineárními vztahy mezi veličinami, které nejsou obvykle v přírodě dosahovány. Nelineární a logistická regrese není naopak vhodná pro kategoriální proměnné. Umělé neuronové sítě pak neposkytují jednoduše pochopitelný a vysvětlitelný model. Metody neřízené klasifikace jako shlukové a faktorové analýzy zacházejí se všemi proměnnými stejně bez výjimky vysvětlované proměnné a predikují pouze spojité proměnné (Bou Kheir et al., 2010). Metody strojového učení (*machine learning*) překonávají nedostatky parametrických a neparametrických statistických metod, jako je prostorová autokorelace, nelinearita či přeučení (*overfitting*), což zvyšuje predikční schopnost prostorových modelů, nicméně vyžadují pokročilé znalosti a jejich využití je tak zatím sporadické (Were et al., 2015; Zádorová et al., 2015). Vzhledem k variabilitě modelů a vysvětlujících proměnných je tak třeba pro konkrétní účel nalézt nejvhodnější řešení, které není obvykle zobecnitelné.

Z rešerše Minasnyho et al. (2013), zabývající se studii digitálního mapování SOC, vyplývají některá zajímavá zjištění: Přesnost predikce stoupá logaritmičticky se zvyšující se hustotou vzorkování. V polovině studií nebyla provedena nezávislá validace, pouze křížová validace (*cross-validation*) či interní validace a většina studií neuvádí žádný odhad nejistoty predikce, s výjimkou geostatistického mapování.

### 2.4.3 Simulační modely

---

Při výzkumu redistribuce SOC je využíváno i různých simulačních modelů. Modely umožňují pokročilé analýzy dynamiky SOC pomocí modelování vertikálních toků uhlíku v půdě či simulací různých erozních scénářů a to v různém prostorovém a časovém rozlišení. V současnosti existuje celá řada těchto dynamických modelů. Bližší přehled předkládají např.: Shibu et al. (2006); Smith (2006); Plante a Parton (2007); Manzoni a Porporato (2009); Stockman et al. (2011); Batlle-Aguilar et al. (2011) či Parton et al. (2015). Vzhledem k velké variabilitě modelů jsou rozdělovány do několika skupin (Polyakov a Lal, 2004; Smith, 2006) – a) procesní modely (single nebo multi-kompartmentové<sup>1</sup>) zaměřené na procesy zprostředkovávající pohyb a transformaci látek

---

<sup>1</sup> Kompartment – morfologicky definovaná část celku se zřetelnou vnější hranicí, která selektivně ovlivňuje výměnu látek mezi vnějším a vnitřním prostorem. Určitá

a energie, b) modely orientované na organismy, simulující transfer uhlíku v rámci potravní sítě půdních organismů, c) kombinované modely předchozích dvou přístupů a d) kohortní modely, uvažující každý vstup rostlinné biomasy jako oddělenou skupinu (kohortu<sup>2</sup>), která se kontinuálně rozkládá (Smith, 2006). Většina modelů jsou multi-kompartimentové procesní modely (Polyakov a Lal, 2004). Dle Watsona et al. (2000) se některé modely zabývají jednotlivými ekosystémovými komponentami jako půda, např. model RothC (Ranatunga et al., 2001; Smith et al., 2005b; Barančíková et al., 2010; Eglin et al., 2010; Falloon et al., 2011), jiné simulují procesy v celých ekosystémech (např. model CENTURY – viz dále), zatímco některé jsou zaměřeny na úroveň biomů či globální úroveň (např. model OSCAR - Eglin et al. 2010). Tyto modely mají potenciál pro hodnocení jak přírodních, tak antropogenních změn v zásobách a dynamice SOC. Pomocí nich je možné také extrapolovat výsledky měření v čase i prostoru, nicméně by měly být nejprve kalibrovány na lokální podmínky a validovány na nezávislých datech. Dle Lia et al. (2003) či van Oosta et al. (2005) je zapotřebí do modelů lépe zakomponovat procesy redistribuce živin, změn mineralizace a časoprostorovou variabilitu SOC. Kuhn (2013) pak dále zdůrazňuje potřebu začlenění selektivní depozice sedimentovaného SOC. Tyto návrhy plynou zejména z výsledků, které ukazují významné rozdíly mezi simulacemi a přímým pozorováním. K tomuto problému přispívá i nedostatek kvantitativních dat pro validaci modelů (Van Oost et al., 2009).

Většina modelů je modulárních, takže umožňují flexibilní rozšíření, například o simulaci efektu různých typů eroze. Většina modelů však přímo nespecifikuje toky SOC vlivem eroze, ale umožňují je zahrnout. Obecný koncept a principy simulace dynamiky SOC v modelech široce popisují Polyakov a Lal (2004), stejně tak různé modely zahrnující erozní složku, jejich bližší popis, výhody a nevýhody jejich použití a potřebné vstupy do modelů. Obecně jsou simulační modely poměrně náročné na vstupní data zahrnující podrobné informace o půdních podmínkách, klimatických podmínkách a o způsobu

---

(koncepční) zóna daného systému, jejíž částice téhož typu jsou podrobeny působení týchž vlivů (procesů).

<sup>2</sup> Kohorta - soubor jedinců zrozených v určitém časovém úseku, sloužící ke stanovení struktury určité živočišné populace, stejnověká populace

managementu zemědělských ploch. Mezi modely, které zahrnují erozní komponentu a byly využity pro simulace toků SOC, patří především modely CENTURY (Pennock a Frick, 2001; Yadav a Malanson, 2009) či EPIC (Izaurre et al., 2001), případně modely použité pro specifické účely jako Bouwmanův model (Bouwman, 1989), REM (*Rehabilitation Ecosystem Model*) (West a Wali, 2002) či Modifikovaný VanVeenův model (Voroney et al., 1981). Redistribuce (respektive ztráta) SOC je v modelech obvykle hodnocena ve vztahu ke ztrátě půdy, nejčastěji vypočítávané pomocí empirických modelů založených na Univerzální rovnici ztráty půdy USLE (či jejich variant RUSLE, MUSLE) (Starr et al., 2000; Polyakov a Lal, 2004). Bohužel tento přístup se zabývá hlavně erozními procesy a není schopen řešit sedimentační procesy. Tento problém řeší např. model EDCM (*Erosion-Deposition-Carbon-Model*) (Liu et al., 2003). Nicméně podobné modely analyzují erozi a depozici odděleně a bodově. Z tohoto důvodu van Oost et al. (2003) vyvinuli distribuovaný model SPEROS-C, který je kombinací erozního modelu SPEROS a simulačního modelu dynamiky uhlíku ICBM (*Introductory Carbon Balance Model*) (Fiener et al., 2012, 2015). Tento model řeší jak vodní erozi, tak erozi zpracováním půdy (Dlugosz et al., 2012). Pro modelování redistribuce SOC vlivem eroze zpracováním půdy se v jiných modelech často využívá například modelu TEP (*Tillage Erosion Prediction*) (Lindstrom et al., 2000; Reicosky et al., 2005; Young et al., 2014).

#### 2.4.4 Spektroskopie

---

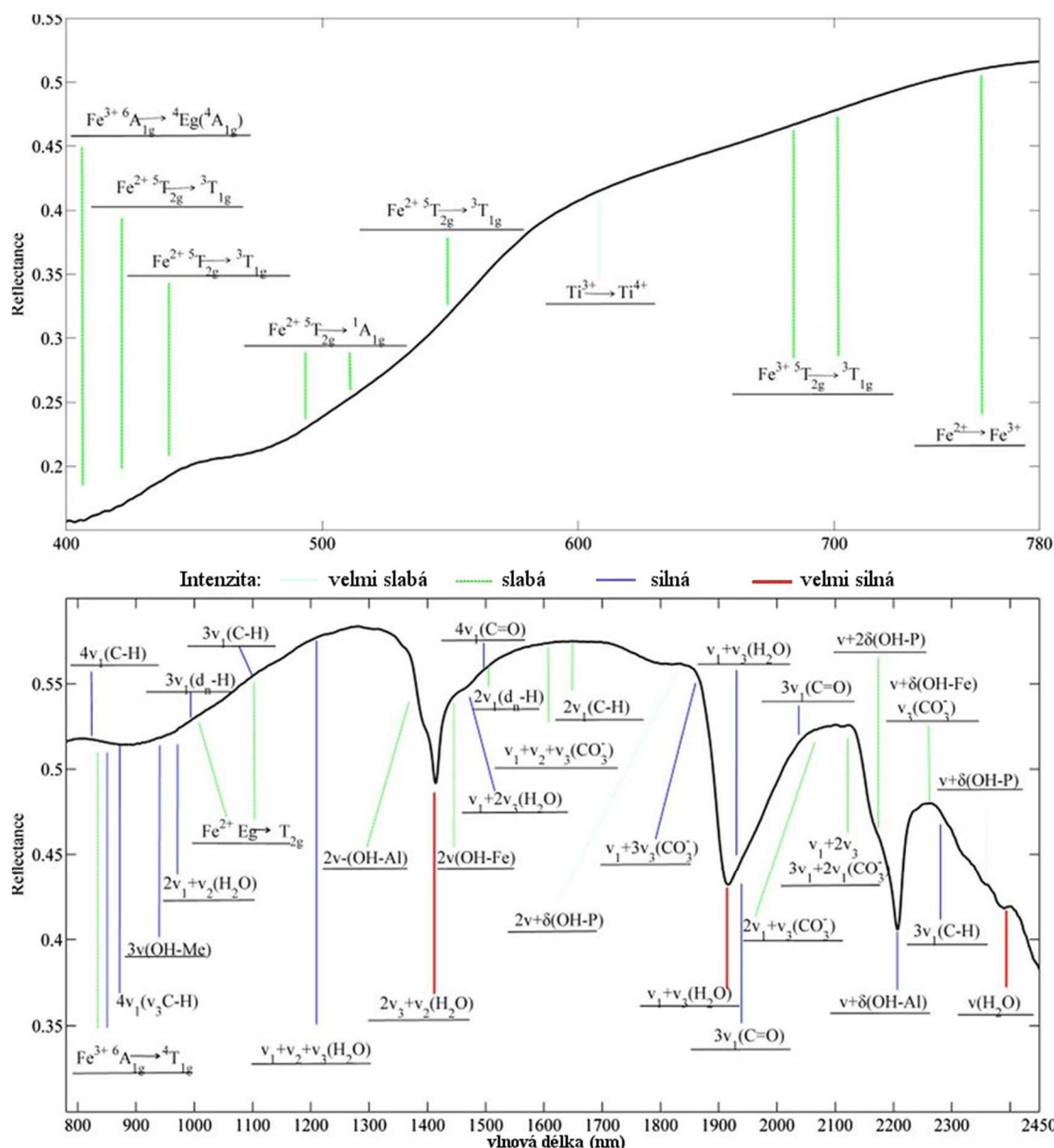
Dalšími progresivními výzkumnými metodami při sledování obsahu SOC a tedy i jeho dynamiky v přírodním prostředí jsou metody využívající spektrálních vlastností organické hmoty, ať už se jedná o měření pomocí bodové spektrometrie (jak laboratorně tak in situ), nebo o využití metod dálkového průzkumu Země (DPZ) a analýzy obrazových spektrálních dat leteckých a družicových snímků.

Jak uvádějí Bellon-Maurel a McBratney (2011), začátek výzkumu využití spektroskopie v pedologii sahá do 80. let 20. století, nicméně v posledních 10 letech zaznamenal tento obor značný nárůst pozornosti. Přehled literatury v této záležitosti lze najít v několika publikacích (Viscarra Rossel et al., 2006b; Kusumo et al., 2008; Cécillon et al., 2009; Du a Zhou, 2009; Ladoni et al., 2010; Reeves, 2010; Stenberg et al., 2010; Gholizadeh et al., 2013; Nocita et al., 2015).

Tak jako půdní organická hmota hraje hlavní roli ve vztahu k mnohým chemickým a fyzikálním procesům v půdním prostředí, tak také významně ovlivňuje tvar a podstatu spektrální křivky půdní odrazivosti (Ben-Dor et al., 1999). Organická hmota je zřejmě nejvíce studovanou půdní komponentou ve vztahu ke spektrální odrazivosti a zároveň nejlépe predikovatelnou půdní komponentou ze spektrálních dat ve spektru VNIR-SWIR (viditelné a blízké infračervené spektrum až krátkovlnné infračervené spektrum). Organická hmota je důležitou chromoforou v rámci celého tohoto spektra a v mnoha pracích byla prokázána významná korelace mezi jejím obsahem v půdě a hodnotami spektrální odrazivosti (Ben-Dor et al., 1999; Klement, 2014).

Jedním z indikátorů klasicky používaných pro mapování SOC je barva půdy specifikovaná spektrální odrazivostí ve viditelném spektru. Tmavé půdy obvykle obsahují více organické hmoty než světlé půdy. Toto ztmavení půdy s vyšším obsahem SOC je způsobeno vlivem organické hmoty a rozdílů ve skladbě a kvantitě černých huminových kyselin a půdní vlhkosti (Viscarra Rossel et al., 2006a). Tyto vztahy však nejsou dostatečně robustní pro praktické aplikace, zvláště v případě velké variability půd (Viscarra Rossel et al., 2006a).

Spektrum mezi 1650 – 2500 nm je obecně citováno jako nejrelevantnější pro měření SOC (Bellon-Maurel a McBratney, 2011). Půdní organická hmota však zahrnuje mnoho komponent a tak může být zjišťována v různorodých částech spektra (VIS-NIR-SWIR-MIR). Základními komponentami organické hmoty jsou sloučeniny jako lignin (spektrální projev např. v pásmu 2050 a 2351 nm), celulóza (např. 1370, 1725 a 2347 nm), pektin (např. 1320, 1582, 1761, a 2111 nm) a huminové kyseliny (např. 1929 a 1932 nm), které jsou opticky aktivní ve zmíněných spektrálních oblastech, přičemž se tyto regiony mohou navzájem překrývat (Summers et al., 2011). Spektrální odezva organické hmoty je nicméně ovlivňována také stupněm jejího rozkladu. Vzhledem k poměrně velké variabilitě složení organické hmoty a existenci řady spektrálně aktivních funkčních skupin v organické hmotě existuje v rámci spektra celá řada absorpčních pásem pro tuto půdní komponentu. Některé z nich jsou uvedeny na obrázku (Obrázek 3).



Obrázek 3: Chromofory v půdách a horninách. Elektronové přechody, vyšší harmonické vibrační přechody (*overtones*) ve VIS-NIR spektru a vyšší vibrační přechody a současné vibrační přechody (*combination*) ve SWIR spektru (zdroj: Xu et al., 2018 podle Ben-Dor et al., 1999)

Mnoho laboratorních experimentů ukázalo, že organický uhlík neovlivňuje jen odrazivost v určitých částech spektra, ale obecně i tvar spektrální křivky. V případě nízké koncentrace organické hmoty má spektrální křivka v rozmezí vlnových délek 0,35 – 1,4  $\mu\text{m}$  spíše konvexní tvar. Organická hmota absorbuje energii v celém rozsahu těchto vlnových délek, čímž se snižuje celkové albedo, ale hlavně se mění celkový tvar spektrální křivky na více konkávní.

I když jsou vztahy mezi organickou hmotou a odrazivostí (tedy i barvou) poměrně dobře a dlouho známy, samotná kvantifikace SOC je složitá, protože půdní odrazivost je přímo ovlivňována dalšími chemickými a fyzikálními chromofory jako drsností povrchu, vlhkostí, obsahem železa nebo různých minerálů. Vztahy mezi obsahem organické hmoty a odrazivostí tak mohou být kvalitně popsány v případě, kdy půdní vlastnosti nejsou v prostoru příliš variabilní. V opačném případě mohou být odhady provedené na základě těchto vztahů značně nepřesné (Hill a Schütt, 2000).

Vzhledem ke komplexnosti půdního materiálu, projevující se například silnými chemickými interakcemi a vzájemným ovlivňováním mezi půdními složkami (oxidy železa, jíly, organická hmota apod.), nelze navíc při analýze půdního spektra použít jednoduchých postupů spektrální analýzy, či například modelů lineárního míšení základních elementárních prvků (*end members*), jako je tomu například v geologických aplikacích. Je tedy zapotřebí využití sofistikovaných analytických a statistických metod, například metod vícerozměrné analýzy (Ben-Dor et al., 2009).

Kvantitativní spektrální analýza půdy pomocí odrazové spektroskopie tedy vyžaduje sofistikované statistické techniky pro kvantitativní odvození půdních vlastností ze spektrálních charakteristik (Gomez et al., 2008; Ge et al., 2011). K tomu účelu jsou používány různé statistické metody. Nejčastěji používanými jsou zejména PLSR – regrese pomocí částečných nejmenších čtverců (*partial least-squares regression*) (Madari et al., 2006; Kusumo et al., 2008; Aïchi et al., 2009; Nocita et al., 2011) a dále např. SMLR – postupná vícenásobná lineární regrese (*stepwise multiple linear regression*), PCR – regrese hlavních komponent (*principal components regression*), RT – regresní stromy (*regression trees*) či RF - náhodné lesy (*random forests*). Vasques et al. (2008), stejně jako Croft et al. (2012) jejich vhodnost použití ohodnotili ve výše zmíněném pořadí. V poslední době se také objevuje využití metod aplikujících principy strojového učení jako SVMR – regrese pomocí podpůrných vektorů (*support vector machine regression*) (Gholizadeh et al., 2013) či neuronových sítí (Nowkandeh et al., 2013; Tiwari et al., 2015). Vasques et al. (2008) a Ladoni et al. (2010) také provedli přehled studií zabývajících se odrazivou spektroskopií SOC, přičemž koeficient determinace  $R^2$  se pohyboval mezi hodnotami 0,45 – 0,98 (většinou více než 0,8), což ukazuje dobrou využitelnost zmiňovaných metod v predikci obsahu organického uhlíku v půdách. Bartholomeus et al. (2008) nicméně nevýhodu těchto metod (predikčních

modelů) vidí v jejich komplexnosti a problému s přesunem na jiné senzory vlivem různých spektrálních charakteristik (pozice vlnových délek, počet pásem) a na jiné lokality. Transfer modelů pro využití na jiných lokalitách může být komplikovaný i vlivem nejasnosti, zda model predikuje na základě absorpce organické hmoty nebo nepřímo na základě absorpce dalšími půdními složkami, jako jsou oxidy železa či jílové minerály, s kterými obsah organické hmoty může korelovat (Bartholomeus et al., 2008). Nocita et al. (2015b) uvádějí, že přestože je půdní spektroskopie ve světě široce studována a je mnoho studií, které ukazují její potenciál, existuje jen relativně málo příkladů jejího rutinního užití. Největší překážku pak vidí v problémech s užitím standardních protokolů a propojením spektrálních knihoven.

Budování spektrálních knihoven půd je pro budoucí využití spektroskopie v pedologii důležitým prvkem (Gholizadeh et al., 2013). Spektrální knihovny jsou databáze naměřených půdních spekter a půdních vlastností, které, pokud jsou robustní (dostatečný počet dat z široké škály půd), mohou sloužit ke kalibraci modelů pro odvození půdních vlastností ze spektrálních dat bez nutnosti pořízení množství referenčních dat ze studovaných lokalit (Cécillon et al., 2009; Viscarra Rossel, 2009; Bellinaso et al., 2010; Brodský et al., 2011a; Das et al., 2015; Shi et al., 2015). Jak se prokazuje, lepší výsledky jsou dosahovány s lokálními robustními knihovnami než s využitím rozsáhlých knihoven (Gholizadeh et al., 2013; Stevens et al., 2013). Popisem existujících spektrálních knihoven půd se ve své doktorské práci zabývá Klement (2014).

#### 2.4.4.1 Bodová spektroskopie

Značné množství prací bylo v minulosti zaměřeno na predikci obsahu SOC pomocí difúzní spektrometrie v laboratorních podmínkách, kdy jsou vzorky upraveny (vysušeny, rozmělněny) a následně je měřena jejich spektrální odrazivost (Ben-Dor et al., 1997; Brown et al., 2006; Madari et al., 2006; Aïchi et al., 2009; Ladoni et al., 2010; Brodský et al., 2011b; Gholizadeh et al., 2013; Aldana-Jague et al., 2016). Tento přístup umožňuje sledování spektrálních charakteristik různých půdních sloučenin bez narušení vnějšími vlivy. O'Rourke a Holden (2011) porovnávali klasické analytické metody kvantifikace SOC s metodami optické a chemometrické analýzy a konstatují, že spektrometrické metody jsou v případě většího množství vzorků levnější a časově méně náročnou metodou, nicméně není jimi dosahovaná taková analytická přesnost jako v případě stanovení pomocí elementární analýzy (*dry combustion*). Velmi dobrou predikční

schopnost odrazové spektrometrie při mapování SOC uvádějí také např. Brodský et al. (2013), kteří se zabývali nejistotami při použití této metody. Srovnáním různých spektrometrů se zabývali Ge et al. (2011), přičemž uvádějí, že druh spektrometru a měřicí metoda ovlivňují naměřené půdní spektrum a kalibrační modely tedy nelze přenášet z jednoho zařízení na druhé. Při měření spektrometrem existují totiž dva druhy chyb, které znesnadňují porovnávání spekter naměřených v různých podmínkách a různými přístroji. Jedná se o systematické ovlivnění (kalibrace spektrometru či geometrie snímání) a nesystematické ovlivnění (nestabilita spektrometru, nestabilita světelného zdroje, ovlivnění atmosférou, zkušenost uživatele). Aby bylo možno různě naměřená spektra porovnávat a přenášet (využívat v jednotných spektrálních knihovnách), je třeba pro odstranění těchto vlivů využít standardních protokolů měření (Ben-Dor et al., 2015) a interního půdního standardu (Pimstein et al., 2011; Kopačková a Ben-Dor, 2016).

V případě bodového měření pomocí spektrometrů in-situ je nutné počítat s vlivy různé půdní vlhkosti, drsnosti povrchu, různých světelných podmínek, vegetačního krytu apod., které zanášejí do měření šum a komplikují tak použití této technologie (Chabrillat et al., 2003; Kusumo et al., 2008; Vasques et al., 2008; Nocita et al., 2011; Rienzi et al., 2014; Ji et al., 2015). Ji et al. (2015) však ukazují, že efekt environmentálních faktorů na pořizované spektrum lze do jisté míry odstranit pomocí algoritmů standardizace, například metodami DS – přímá standardizace (*direct standardization*) či PDS – částečná přímá standardizace (*piecewise direct standardization*) a dosáhnout tak výrazné zlepšení predikční schopnosti in-situ spektrometrie. Obdobně s různou úspěšností lze využít další techniky předzpracování spekter jako metody MSC – vícenásobná korekce rozptylu (*multiplicative scatter correction*), SNV - standardní transformace normálního rozdělení četností (*standard normal variate*), odstranění kontinua, derivace spektra či algoritmus Savitzky–Golay (Gholizadeh et al., 2013). Zpřesnění predikce SOC z in-situ měření ukazují dále např. Nocita et al. (2013), kteří navrhují využití normalizovaného indexu půdní vlhkosti - NSMI (*Normalised soil moisture index*) pro odstranění vlivu vlhkosti půdy. Další využití představují např. Noon et al. (2014), kteří využili nástrojů spektroskopie pro identifikaci a kvantifikaci jednotlivých frakcí půdní organické hmoty, nebo Ben-Dor et al. (2008a), kteří vyvinuli sondu pro měření spektrálních vlastností v celém půdním profilu.



Přehled literatury využívající spektroskopických metod v NIR a MIR oblasti spektra při hodnocení půdního uhlíku a jejich kritické zhodnocení předkládají Bellon-Maurel a McBratney (2011) a nověji pak Gholizadeh et al. (2013). Z jejich závěrů lze vyzdvihnout zejména tyto poznatky:

- a. Při měření na stejných vzorcích lze dosáhnout lepších výsledků při využití spekter MIR oproti NIR. Při měření v oblasti MIR je nicméně důležitější úprava vzorků a proto je jeho použití problematictější při měření in situ.
- b. S rostoucí rozlohou a heterogenitou zkoumaného území dochází ke zvyšování chyby predikce.
- c. Křížová validace pomocí metody *leave-one-out* (opakované vynechání jednoho měření) provedená na závislých vzorcích, obzvláště v případě jejich malého počtu, vede k příliš optimistickým výsledkům.
- d. Analýza SOC z neupravených vzorků (nevysušené a nepřesáté) může dosáhnout uspokojivých výsledků.
- e. Kalibrační modely založené na vybraných vlnových délkách mají uspokojivé výsledky, z čehož vyplývá perspektiva pro budoucí vývoj levnějších senzorů pro stanovení organického uhlíku.

Přehled studií využívajících bodovou spektroskopii při hodnocení SOC a charakteristiky jejich úspěšnosti nabízejí např. publikace Stevens et al. (2006); Viscarra Rossel et al. (2006b); Bellon-Maurel a McBratney (2011); O'Rourke a Holden (2011). Přehled vybraných novějších studií v obdobné struktuře nabízí Tabulka 2 uvedená v příloze.

#### 2.4.4.2 Obrazová spektroskopie

V posledních letech je ve výzkumu půdních vlastností, včetně analýzy distribuce SOC, čím dál více využíváno i obrazové spektroskopie, jakožto prostředku pro sledování spektrálních charakteristik v prostorové doméně. Obrazová spektroskopie může být použita v rozličných měřítkách od snímků pořízených satelitními senzory až po laboratorní snímky. Tato metoda má nicméně svá specifika a je zapotřebí využití řady nástrojů pro obrazovou analýzu (Ben-Dor et al., 2009; Cécillon et al., 2009). S vývojem senzorů (lepší radiometrické i prostorové rozlišení) a vývojem analytických metod se možnosti využití obrazové spektroskopie zvyrazňují.

Jelikož je půdní organická hmota koncentrována hlavně ve svrchních vrstvách půdy, které jsou vystaveny slunečnímu záření, je to vlastnost, která je vhodná pro hodnocení pomocí této metody (Ben-Dor et al., 2009). Zatím však nebylo publikováno mnoho prací, které by se zabývaly použitím leteckých nebo satelitních obrazových dat pro hodnocení SOM, a to hlavně proto, že v mnoha půdách je nízký obsah SOM. Tyto studie se objevují až v posledních letech. V často citované práci Baumgardner et al. (1970) autoři uvádějí, že při obsahu organické hmoty menším než 2 % jsou spektrální charakteristiky půdy více ovlivňovány dalšími půdními složkami, jako například oxidy železa, a vliv organické hmoty je tedy obtížné určit. Nicméně řada studií dochází k dobré predikci i při malém obsahu SOC.

Při odhadu SOC pomocí obrazové spektroskopie je zapotřebí mít na paměti, že stav povrchu půdy může ovlivnit spektrální signál. Může být ovlivněn jak v čase, tak i v prostoru například různou texturou, vlhkostí, drsností povrchu, vegetačním pokryvem či stupněm tvorby škraloupu (jakožto výsledek dopadu vodních kapek). Tyto faktory pak ovlivňují i spektrální odezvu SOC. Vypořádání se s některými z těchto vlivů je však potenciálně možné. Jak ukázali například Bartholomeus et al. (2011), odstranění vlivu řídké vegetace je možné pomocí metod oddělení spekter (*spectral unmixing*), přičemž výsledná predikční schopnost modelu PLSR při využití reziduálního půdního spektra dosahovala přesnosti jako ve studiích s holou půdou. Nicméně jak uvádějí Hbirkou et al. (2012), další výzkum metod na odstranění vlivu vegetace a rostlinných zbytků je zapotřebí. Denis et al. (2014) například dospěli k lepším výsledkům predikce z obrazových spektrálních dat pomocí metody korekce efektu relativního zastínění půdy. Ebengo et al. (2018) dále například využili pro zpřesnění predikce SOC ze satelitních optických dat informace o drsnosti povrchu získané z radarových satelitních dat.

Přesnost predikce může být zároveň ovlivněna radiometrickými a atmosférickými příčinami či vlivem spektrálního a prostorového rozlišení pořízených dat. V případě využití satelitních dat DPZ je také nutné počítat s nižším poměrem úrovně signálu a šumu (SNR - *signal-to-noise ratio*), tedy velkým ovlivněním šumem u pořízených dat vlivem krátkého pořizovacího času nad zkoumanou lokalitou (Ben-Dor et al., 2008b; Gomez et al., 2008; Grunwald et al., 2015). Vystává tak otázka, zda budou sledované rozdíly v obsahu SOC větší než nepřesnost analýzy. Croft et al. (2012) vidí metody predikce obsahu SOC pomocí metod DPZ jako metody, které jsou stále ve vývoji a nemají zatím

potřebnou přesnost. Navrhují však metody, které by mohly predikci obsahu SOC zlepšit – např. kombinace využití dat DPZ a některého erozního modelu, kombinace s geostatistickými metodami či využití spektrálních knihoven.

Zvýšená prostorová variabilita půdních vlastností může být dalším problémem pro potenciální využití obrazové spektroskopie. Gomez et al. (2012) například uvádějí, že právě vysoká variabilita půdních vlastností vedla k velice nízké predikční schopnosti jejich modelu založeném na hyperspektrálních datech oproti jiným studiím (Selige et al., 2006; Stevens et al., 2006, 2010). V případě vysoké variability půdních podmínek a větší studované plochy je tak zapotřebí pro vyšší predikční schopnost počítat s větším množstvím analyzovaných půdních vzorků. Stevens et al. (2012) ve své studii provedli zhodnocení různých metod validace spektrálních modelů a konstatují, že většina využívaných metod křížové validace silně podhodnocuje chybu validace, obzvláště na větších studovaných plochách. Autoři proto doporučují předchozí analýzu spektrální variability v obrazových spektrálních datech před uskutečněním vzorkování. Tento postup umožní nalezení lepšího vzorkovacího schématu, které lépe charakterizuje spektrální variabilitu, a proto může zlepšit kalibrační modely.

Predikce SOC pomocí metod DPZ je většinou založena na celkovém snížení odrazivosti ve viditelné a blízké infračervené části spektra (Chen et al., 2000), nicméně pro tuto predikci jsou hodnotné i další vlnové délky (Chen et al., 2008; Stevens et al., 2008). Korelace může být nalezena i v měřených agregovaných širokých spektrálních pásech jako např. u družice Landsat, což prokázal již například Da Costa (1979). Spektrální rozlišení ovšem výrazně ovlivňuje kvalitu predikce SOC (Castaldi et al., 2016). Pro přesné odhady SOC je proto zapotřebí využít data s vhodným spektrálním rozlišením pořízená v celé šíři oblasti VNIR-SWIR (Ben-Dor et al., 1999). V odborných studiích tak byla demonstrována schopnost určení SOC spíše pomocí leteckých hyperspektrálních senzorů (Ben-Dor et al., 2002; Selige et al., 2006; Stevens et al., 2006, 2010, 2012, 2015) než pomocí satelitních dat (např.: Gomez et al. 2008). Jelikož však satelitní data nabízejí široký prostorový záběr a možnosti častého pořízení snímků, jsou i satelitní hyperspektrální data využitelná pro predikci SOC (Wang et al., 2010a; Anne et al., 2014). V současné době jsou tyto zdroje dat otázkou vývoje, nicméně jejich vypuštění je plánováno v nejbližších letech. Na oběžnou dráhu se tak mohou brzy dostat hyperspektrální senzory s poměrně vysokým SNR a prostorovým rozlišením od jedné do

několika desítek metrů. Mezi ně patří německý Environmental Mapping and Analysis Program (EnMAP), italský Hyperspectral Precursor of the Application Mission (PRISMA), satelit vyvíjený americkou NASA Hyperspectral Infra-Red Imager (HyspIRI), japonský Hyperspectral Imager Suite (HISUI), francouzský HypXIM, izraelsko-italský Spaceborne Hyperspectral Applicative Land and Ocean Mission (SHALOM) nebo čínský TianGong-1.

V případě potřeby mapování a kvantifikace obsahu SOC na velké ploše bez plošně rozsáhlé kalibrace pomocí půdních vzorků by dle Mulder et al. (2011) dále mohlo být řešením použití spektrálních indexů založených na absorpčních prvcích jednotlivých biochemických složek organické hmoty. Tento přístup je založen na detekci jednotlivých složek SOM: celulóza, škrob, lignin a humusové látky. Přesné vztahy byly nalezeny např. pro indexy založené na viditelné oblasti spektra a absorpčních znacích spojených s celulózou (okolo 2100 nm). Nejpřesnější modely založené na indexech byly srovnatelné s výsledky s použitím regresních metod (PLSR) (Bartholomeus et al., 2008). Ačkoli se použití indexů zdá být slibné, je ještě potřeba je testovat na satelitních senzorech, které mají nižší SNR (Mulder et al., 2011).

Některé studie tedy ukázaly, že existuje potenciál spektrálně detekovat SOM při využití obrazové spektroskopie, nicméně tento potenciál stále daleko zaostává za optimálním stavem vhodným pro využití v praxi (Ben-Dor et al., 2009; Das et al., 2015). Výzkumy, které využily obrazovou spektroskopii při predikci obsahu organického uhlíku a nastínily tak možnosti této techniky, uvádí podrobněji Tabulka 3 uvedená v příloze.

### 3 Vědecká hypotéza

---

Redistribuce organického uhlíku v území ovlivněném půdní erozí úzce souvisí s parametry reliéfu a ovlivňuje optické vlastnosti půdy. Mapování redistribuce organických látek je tak možné provést na základě analýzy spektrálních obrazových dat a modelu terénu s využitím metod digitálního mapování půd.

### 4 Cíle práce

---

Cílem disertační práce je analyzovat možnosti predikce a mapování přesunů půdního organického uhlíku v územích ovlivněných půdní erozí v podmínkách České republiky pomocí progresivních distančních metod výzkumu a metod digitálního mapování půd. V rámci práce je možno vydělit několik dílčích cílů:

1. Pomocí detailního terénního průzkumu vybrat a zmapovat zájmové erozně ovlivněné lokality s různými dominantními půdními jednotkami a variabilitou půdních vlastností.
2. S využitím analýzy leteckých obrazových a bodových hyperspektrálních dat testovat způsoby vymezení obsahu organické hmoty ve svrchních vrstvách půdy a ohodnotit využitelnost satelitních dat pro tento účel.
3. Na základě využití terénních a laboratorních metod, technik dálkového průzkumu Země, zejména obrazové a spektrální analýzy, definovat vztahy mezi spektrálními vlastnostmi půdy, erozním poškozením půd, terénními parametry reliéfu a obsahem organické hmoty v půdě.
4. S využitím metod digitálního mapování půd vytvořit a ověřit modely predikce množství organické hmoty v půdě v závislosti na topografické charakteristice území a spektrálních vlastnostech půd.

## 5 Publikované práce

---

### 5.1 Assessment of Soil Degradation by Erosion Based on Analysis of Soil Properties Using Aerial Hyperspectral Images and Ancillary Data, Czech Republic

---

- **Žížala, D.**, Zádorová, T., Kapička, J., 2017. Assessment of Soil Degradation by Erosion Based on Analysis of Soil Properties Using Aerial Hyperspectral Images and Ancillary Data, Czech Republic. *Remote Sensing*. 9 (1). 28 [doi: 10.3390/rs9010028]

Article

# Assessment of Soil Degradation by Erosion Based on Analysis of Soil Properties Using Aerial Hyperspectral Images and Ancillary Data, Czech Republic

Daniel Žížala <sup>1,2,\*</sup>, Tereza Zádorová <sup>2</sup> and Jiří Kapička <sup>1</sup>

<sup>1</sup> Research Institute for Soil and Water Conservation, Žabovřeská 250, Prague CZ 156 27, Czech Republic; kapicka.jiri@vumop.cz

<sup>2</sup> Department of Soil Science and Soil Protection, Faculty of Agrobiolgy, Food and Natural Resources, Czech University of Life Sciences Prague, Kamýcká 29, Prague CZ 165 00, Czech Republic; zadorova@af.czu.cz

\* Correspondence: zizala.daniel@vumop.cz; Tel.: +42-02-5702-7232

Academic Editors: José A.M. Demattê, Clement Atzberger and Prasad S. Thenkabail

Received: 28 October 2016; Accepted: 28 December 2016; Published: 1 January 2017

**Abstract:** The assessment of the soil redistribution and real long-term soil degradation due to erosion on agriculture land is still insufficient in spite of being essential for soil conservation policy. Imaging spectroscopy has been recognized as a suitable tool for soil erosion assessment in recent years. In our study, we bring an approach for assessment of soil degradation by erosion by means of determining soil erosion classes representing soils differently influenced by erosion impact. The adopted methods include extensive field sampling, laboratory analysis, predictive modelling of selected soil surface properties using aerial hyperspectral data and the digital elevation model and fuzzy classification. Different multivariate regression techniques (Partial Least Square, Support Vector Machine, Random forest and Artificial neural network) were applied in the predictive modelling of soil properties. The properties with satisfying performance ( $R^2 > 0.5$ ) were used as input data in erosion classes determination by fuzzy C-means classification method. The study was performed at four study sites about 1 km<sup>2</sup> large representing the most extensive soil units of the agricultural land in the Czech Republic (Chernozems and Luvisols on loess and Cambisols and Stagnosols on crystalline rocks). The influence of site-specific conditions on prediction of soil properties and classification of erosion classes was assessed. The prediction accuracy ( $R^2$ ) of the best performing models predicting the soil properties varies in range 0.8–0.91 for soil organic carbon content, 0.21–0.67 for sand content, 0.4–0.92 for silt content, 0.38–0.89 for clay content, 0.73–0.89 for Fe<sub>ox</sub>, 0.59–0.78 for F<sub>ed</sub> and 0.82 for CaCO<sub>3</sub>. The performance and suitability of different properties for erosion classes' classification are highly variable at the study sites. Soil organic carbon was the most frequently used as the erosion classes' predictor, while the textural classes showed lower applicability. The presented approach was successfully applied in Chernozem and Luvisol loess regions where the erosion classes were assessed with a good overall accuracy (82% and 67%, respectively). The model performance in two Cambisol/Stagnosol regions was rather poor (51%–52%). The results showed that the presented method can be directly and with a good performance applied in pedologically and geologically homogeneous areas. The sites with heterogeneous structure of the soil cover and parent material will require more precise local-fitted models and use of further auxiliary information such as terrain or geological data. The future application of presented approach at a regional scale promises to produce valuable data on actual soil degradation by erosion usable for soil conservation policy purposes.

**Keywords:** soil erosion; imaging spectroscopy; hyperspectral image; soil properties

## 1. Introduction

Soil erosion is one of the most significant and widespread forms of soil degradation in Europe [1]. In the Czech Republic, soil erosion of different types (water, wind, and tillage) is identified as the most severe type of soil degradation [2], which significantly affects soil functions, production of agricultural crops and the quality of water resources. The degradation risk by erosion is currently relatively well known at both local and regional scale due to evaluation using erosion models [3]. According to these calculations, nearly 50% of arable land in the Czech Republic is endangered by water erosion and about 10% by wind erosion [4]. Nevertheless, the widely applied erosion models (mostly based on USLE/RUSLE models) only provide the estimation of potential erosion. The calculation of the actual soil losses due to soil erosion and estimation of real long-term soil degradation are still insufficiently developed in spite of being essential for policy and management purposes [5,6].

Currently, the assessment of soil degradation by erosion is solved mainly at a local scale using different methods, e.g., direct field monitoring, observations and measurements obtained from distributed point datasets (identification of erosion features and soil profile truncation, assessment of Caesium-137, risk elements and other relevant soil properties) [7–11]. At a regional or global scale, information on the level of soil degradation by erosion is often based on expert knowledge approach consisting in the extrapolation of acquired local data using ancillary data. This is due to the lack of reliable methods, since detailed soil mapping is not financially feasible and it is extremely difficult particularly at this scale [12]. Nevertheless, estimates based on the physical evidence are much required [5,13].

Application of remote sensing represents a possible solution in the assessment of soil degradation by erosion at a regional and global scale. The main advantage of remote sensing methods consists in the possibility of rapid data acquirement from large areas in a detailed spatial resolution. However, its potential has not been fulfilled and there are still many theoretical and technical gaps and unanswered questions [13,14]. Continual progress in measurement techniques, image processing algorithms, development of computation models, new sensors and new satellite missions have brought new data and methods. Use of hyperspectral data in the erosion assessment represents a promising method, particularly in the context of the expectations forthcoming spaceborne hyperspectral sensors with high signal-to-noise ratio (SNR) and pixel size from one to several tens of metre, such as German Environmental Mapping and Analysis Program (EnMAP), Italian Hyperspectral Precursor of the Application Mission (PRISMA), NASA's Hyperspectral Infra-Red Imager (HypIRI), Japanese Hyperspectral Imager Suite (HISUI), French HypXIM, israel-italian Spaceborne Hyperspectral Applicative Land and Ocean Mission (SHALOM) [15] or Chinese TianGong-1 [16].

Land degradation by soil erosion can be assessed directly using different remote sensing methods [14,17,18]: (i) spatial delineation of degraded land and erosion features (rills, gullies, and sediment depositions) using visual interpretation of aerial images [19], computer pre-processing [20–22] or automatic classification methods [23–25]; (ii) soil loss measurement methods based on digital elevation models (DEM) comparison (laser altimetry or radar interferometry); and (iii) assessment of soil degradation stages and monitoring of soils affected by soil erosion and their properties. These methods are based on classification techniques or use different mathematical and statistical procedures to assess the correlation between erosion signs and their spectral reflectance [15,26,27]. Soil erosion and accumulation affect chemical and physical properties of upper layer of soils; thus, spectral reflectance is changed and eroded soils have different spectral response from non-eroded “healthy” soils [28–34].

Soil properties with direct relation to the spectral signature and with the best prediction performance on one hand and a high variability due to erosion-accumulation processes on the other hand include soil organic carbon (SOC) concentration, particle size distribution (particularly clay content), CaCO<sub>3</sub> concentration, Fe and Al oxides ratio and water content [15,35–40]. Other soil properties used for determination of erosion-affected areas are soil colour, pH, structure or coarse fragments content [41–45].



Imaging spectroscopy or generally analysis of soil spectral characteristics has a great potential for soil erosion assessment [36,46], as the hyperspectral data, thanks to their high spectral resolution, allows for more efficient quantification of spectral features in comparison with, e.g., multispectral data. Thus far, only few studies have employed this method in soil erosion assessment [47–49], a majority of them in semi-arid conditions [30,33,45,50–52]. Several studies dealt with the monitoring of specific soil properties related to soil erosion, such as development of soil crust [50] or changes in soil moisture [47,48]. Hyperspectral data have scarcely been used for distinguishing soils influenced by soil erosion. Hill et al. [51,52] used linear spectral mixture analysis and k-means clustering for classification of erosion stages based on skeleton content determination. Schmid et al. [33] distinguished erosion classes using support vector machine classification method and development of image-derived endmembers for each erosion class. Lin and Zhou [31,45] have analysed a spectral response of different eroded soils in subtropical China. They have compared a direct identification of erosion stages by analysing laboratory hyperspectral data and an indirect identification using prediction of soil properties; the latter performed better due to mixing and crossover effect among erosion groups.

However, there are still many limitations in the use of the image hyperspectral data for soil erosion assessment. On one hand, there are restraints connected to data collecting, such as atmospheric attenuation, signal-to-noise ratio, image resolution and, above all, the Bidirectional Reflectance Distribution Function (BRDF) effect [36]. On the other hand, the limitations are often caused by surface characteristics making the direct soil assessment impossible or difficult (soil covered with vegetation, litter, dust or soil crust). Moreover, the spectral information is considerably influenced by soil properties (soil moisture, soil roughness, soil texture or size of soil aggregates) and heterogeneity of environmental settings. This is valid mainly in an erosion relief, where the combination of soil loss and redeposition may lead to similar soil surface properties in eroded and accumulated soils [52,53]. A successful application of hyperspectral data then requires a very thorough planning of flight campaigns, precise image corrections and a sufficient amount of reference soil data. In temperate climate, a multi-temporal approach must be considered when assessing larger areas, as in each period some of the soils are covered with vegetation.

In spite of the progress in knowledge and algorithms (especially in terms of atmospheric correction), more studies are needed for refinement of this method and widening its application.

The aim of this study is to analyse the possibilities of imaging spectroscopy using aerial hyperspectral data for the assessment of soil degradation by erosion on arable land in temperate agriculture regions with different dominant soil unit. The specific objectives of this work were to: (1) quantify the prediction performance of selected soil surface properties derived from hyperspectral data in context of various soil environment, spectral pre-processing methods and regression methods; and (2) determine erosion classes that represent soils differently impacted by soil redistribution by applying the predicted soil surface properties as site-specific indicators and input data in classification models of erosion classes distinguishing.

## 2. Materials and Methods

### 2.1. Regional Settings

Four study sites representing the most extensive soil units of agricultural land in the Czech Republic were chosen. Soil regions are represented by Chernozems and Luvisols on loess and Cambisols and Stagnosols on crystalline and sedimentary rocks. Locations of the study sites are depicted in Figure 1. Sites are similar in terms of terrain characteristics (dissected relief including a set of following terrain units: side valley, toe-slope, plateau and back-slope), land management (long-term tillage, no conservation practices, plough depth 25 cm, 5–6 course rotation based on the Norfolk system) and climatic conditions (rain erosivity). All study sites are located within regions with high rates of both potential and actual degradation by erosion according to Maps of long-term average annual soil loss by water erosion [3] and database of Monitoring of soil erosion on agricultural

land [8]. The types of erosion influencing the soil redistribution include mainly sheet and rill erosion and tillage erosion. Wind erosion is presumed to have a minor impact at the Chernozem site (Šardice). Environmental settings and details of each locality are given in Table 1.

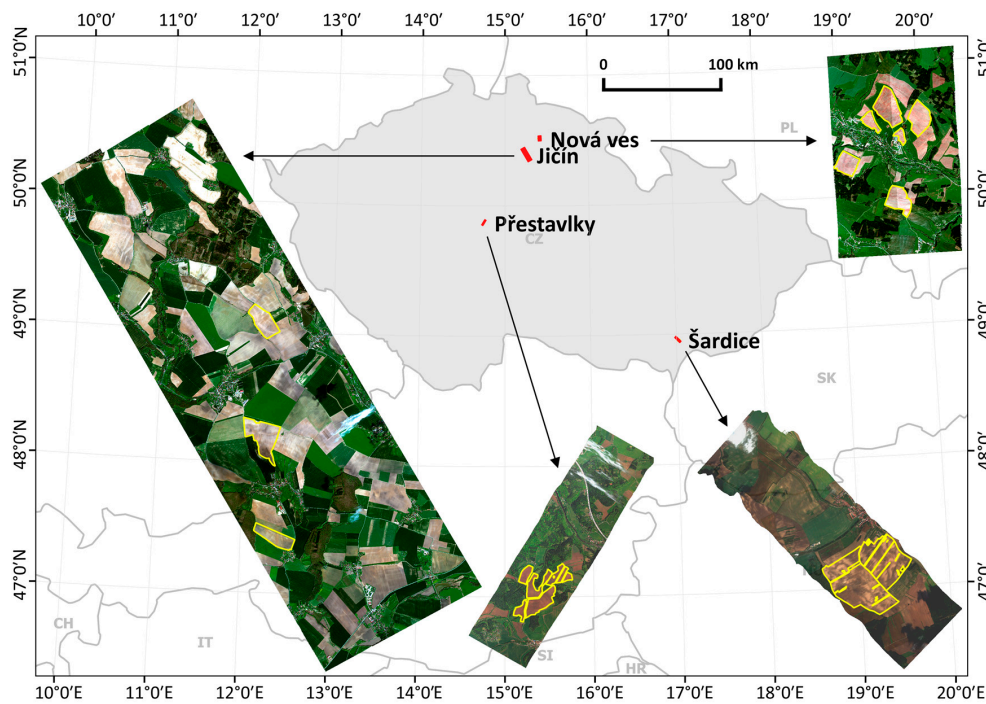


**Figure 1.** Location of the study sites (yellow border) with position of hyperspectral images.

**Table 1.** Study sites and their characteristics.

Site	Area <sup>1</sup>	Dominant Soil Unit (WRB 2014)	Bedrock/Parent Material	MA <sup>2</sup>	MAP <sup>3</sup>	MAT <sup>4</sup>	R <sup>5</sup>	Soil Loss <sup>6</sup>
Přestavlky	0.73	Haplic Stagnosol, Haplic and Stagnic Cambisol, Leptosol	Complex of Proterozoic and Paleozoic rocks (schist, granodiorite)	403	650	7–8	46	10 (0–106)
Šardice	1.45	Calcic Chernozem	Pleistocene loess	218	550	9–10	49	29 (0–370)
Nová Ves	1.17	Haplic Cambisol	Permian–Carboniferous rocks (sandstone, siltstone)	471	750	6–7	54	8 (0–89)
Jičín	1.34	Luvic Chernozems, Albic Luvisols, Luvisols	Pleistocene loess	298	650	7–8	47	11 (0–185)

<sup>1</sup> Area in km<sup>2</sup>; <sup>2</sup> mean altitude in m.a.s.l.; <sup>3</sup> mean annual precipitation in mm; <sup>4</sup> mean annual temperature in °C; <sup>5</sup> factor of rainfall erosivity in MJ·ha<sup>-1</sup>·cm·h<sup>-1</sup>; <sup>6</sup> average annual soil loss by USLE in t·ha<sup>-1</sup>·year<sup>-1</sup> (mean and range).

## 2.2. Flight Campaign (Imaging Spectroscopy) and Image Pre-Processing

Four image scenes were acquired during four flight campaigns from the VNIR (visible and near-infrared) sensor—Compact Airborne Spectrographic Imager (CASI1500; 370–1040 nm) and SWIR (short-wavelength infrared) sensor—Shortwave infrared Airborne Spectrographic Imager (SASI600; 960–2440 nm). Both sensors are developed by Itres Ltd. (Calgary, AB, Canada). The sensors are pushbroom sensors with a Field Of View of 40°. Sensors acquired data in 72 spectral bands in the VNIR with a full width at half maximum (FWHM) of 10 nm (CASI) and 100 bands in the SWIR with FWHM  $\approx$  15 nm (SASI). Sensors were mounted on Cessna 208B Grand Caravan aircraft. The flight campaigns took place during dry conditions (minimum of five days after last rain), and study fields were prepared for seeding—ploughed and harrowed without vegetation or litter. Details of individual flight campaigns are given in Table 2.

**Table 2.** Details of individual aerial hyperspectral campaigns.

Site	ToA <sup>1</sup>	SZ <sup>2</sup>	SA <sup>3</sup>	FA <sup>4</sup>	Atmospheric Condition	N. of Strips	HF <sup>5</sup>	SR <sup>6</sup>
Přestavlky	7 May 2015 10:23	45°	131°	218°	Slightly cloudy (cumulus) visibility 40 km	1	~2060	1, 2
Šardice	21 September 2015 10:52	54°	144°	143°	Slightly cloudy (cumulus) visibility 40 km	1	~2575	1.2, 3.1
Nová Ves	22 April 2016 11:45	49°	153°	185°	Slightly cloudy (cumulus), visibility 30 km	2	~2266	1, 2.7
Jičín	22 April 2016 11:15	47°	142°	159°		3	~2266	1, 2.7

<sup>1</sup> date and time of acquisition (local time); <sup>2</sup> solar zenith; <sup>3</sup> solar azimuth; <sup>4</sup> flight azimuth; <sup>5</sup> height of flight in m above ground; <sup>6</sup> spatial resolution in m (CASI, SASI).

Data acquisition and pre-processing (geometrical and atmospheric corrections) were realized by the Flying Laboratory of Imaging Systems (FLIS) [54,55] operated by Global Change Research Institute CAS (Brno, Czech Republic). The radiometric correction was performed using the RadCorr Ver. 9.2.6.0 (Itres Ltd.) and by means of calibration parameters obtained in laboratory. Data output was given in radiometric units ( $\mu\text{W}\cdot\text{cm}^{-2}\cdot\text{sr}^{-1}\cdot\text{nm}^{-1}$ ). Atmospheric correction was applied to remove the effect of atmospheric influences and convert radiance values into at-surface reflectance. MODTRAN radiative transfer model incorporated into the program ATCOR-4 ver. 7.0 was used for this purpose. Algorithm BREFCOR was used for BRDF effect reduction. The geometric correction and geo-referencing of images was performed using the Geocor tool (Itres Ltd.), based on data recorded by the on-board GPS/IMU sensors and digital elevation model. Image data were resampled by nearest neighbour method and transformed into the UTM map projection.

Image data were masked by bare soil mask (by means of knowledge of study sites and NDVI computing) and resampled to 6-metre spatial resolution (due to random noise reduction in data and corresponding to the size of sampling plots) before processing. Spectral bands highly influenced by the absorption in the atmosphere and bands on the edge of spectra influenced by noise were removed from the dataset. The data finally include 49 bands for CASI (400–750 and 770–880 nm) and 53 bands for SASI (1000–1080, 1200–1300, 1490–1770, 2060–2370 nm). Spectral data extraction from data cubes, as well as other data manipulation, was done using the R software [56].

### 2.3. Data Collection and Soil Analysis

Soil sampling was carried out during four field campaigns following each flight campaign. Fifty samples were taken from each site in an optimized network of borings fashioned using cLHS (conditioned Latin hypercube sampling [57]) stratified random strategy. Terrain attributes and spectral data obtained within hyperspectral campaign were used as feature space variables. This approach ensures the cover of maximal variation of each variable. Exact position of sampling sites was measured by GPS Trimble GeoXM receiver, with a post-processing accuracy of approximately 1m. Soil unit, profile stratigraphy, soil depth, and thickness of horizons were determined by description of gouge auger core. The composite soil samples for analysis of SOC, texture classes,  $\text{CaCO}_3$  and Fe oxides content were taken from each site at 0–10 cm depth.

The soil samples were air-dried, ground and sieved using 2 mm sieve (ISO 11464: 2006). The basic chemical and physical soil properties were obtained using standard laboratory procedures. Soil particle size distribution (5 fractions: less than 0.002; 0.002–0.01; 0.01–0.05; 0.05–0.25; 0.25–2 mm) was obtained by the pipette method (ISO 11277:2009). SOC was determined as total oxidized carbon and measured using wet oxidation (ISO, 14235:1998).  $\text{CaCO}_3$  content was determined volumetrically after soil reaction with HCl (ISO 10693, 1995). the amount of oxalate extractable Fe ( $\text{Fe}_{\text{ox}}$ ) by acid ammonium oxalate extraction [58] and dithionite extractable Fe ( $\text{Fe}_{\text{d}}$ ) was extracted by citrate-bicarbonate-dithionite extraction [59].

#### 2.4. Statistical Analysis of Soil Properties

Different multivariate regression methods were used to establish relationships between image spectral data and soil properties. Different pre-treatment and regression methods were tested. Selected soil properties data were used in regression models as response variables, and spectral reflectance data (transformed spectra) as predictors. Terrain derivatives were used for A horizon thickness establishing. The best resulting regression models were then applied on all the image data with the aim of predict spatial variability of particular soil surface properties and create maps. All spectroscopic and statistical analyses were implemented in R environment [56].

##### 2.4.1. Pre-Processing

Before performing statistical analyses, mathematical pre-treatments were applied to adjust raw reflectance spectra. These transformations were performed to improve the prediction accuracy by noise reduction and mitigation of influence of environment and sensing properties. Continuum removal (CR), Savitzky-Golay filter (third order polynomial smoothing and 5 bands window widths) with first (SG 1st) and second derivatives (SG 2nd) [60] and standard normal variate transformation (SNV) were applied. Reflectance was transformed into absorbance ( $\log(1/R)$ ) as well. Transformation of CASI and SASI spectra were carried out separately as spectra was not acquired with same bandwidth. Bands on the edge of spectra affected by pre-treatment due to moving window averaging were removed from final dataset. R package Prospectr [61] was used for spectra pretreatment.

##### 2.4.2. Calibration and Validation

The dataset was divided into training set used for fitting models and validation set used for assessing the prediction accuracy of each model. Dividing in a 3:1 ratio was performed by random stratified sampling. The procedure of prediction modelling was carried out using caret package [62] of the R software. In the first step, the training set was used for fitting the model. Model performance was assessed through 5-fold cross-validation of the training set. Random search method generated by caret package, providing the automatic search of parameter values, was used for selecting the best parameters of models. Single model with yielding smallest root mean squared error of cross validation ( $RMSE_{CV}$ ) value was selected for subsequent validation on the validation set. The final prediction accuracy was assessed with root mean squared error of prediction ( $RMSE_P$ ) and coefficient of determination ( $R^2$ ). The ratio of standard deviation to standard error of prediction (RPD) was also calculated alternatively to  $R^2$ . Goodness of fit was visually inspected through a plot depicting the observed values against the predicted values.

##### 2.4.3. Multivariate Techniques

Different multivariate techniques successfully used in soil imaging spectroscopy were selected for testing their ability of soil properties prediction. The tested methods included Partial Least Square Regression (PLSR) [63], Support Vector Machine Regression (SVMR) [64–66] (using different kernel functions—linear, polynomial and radial), random forest (RF) [67] and artificial neural network (ANN) [68]. More information can be found in Heung et al. [69], Vasques et al. [70] or Gholizadeh et al. [27].

#### 2.5. Assessment of Soil Erosion Classes

Assessment of the different erosion classes on the study sites was performed in several steps: (1) definition of groups of site-specific erosion classes based on soil data from field campaigns; (2) assessment of soil properties for distinguishing erosion classes; (3) classification of spatial data into erosion classes; and (4) validation of results based on comparison with point soil data. Flowchart of the whole process is depicted in Figure 2.

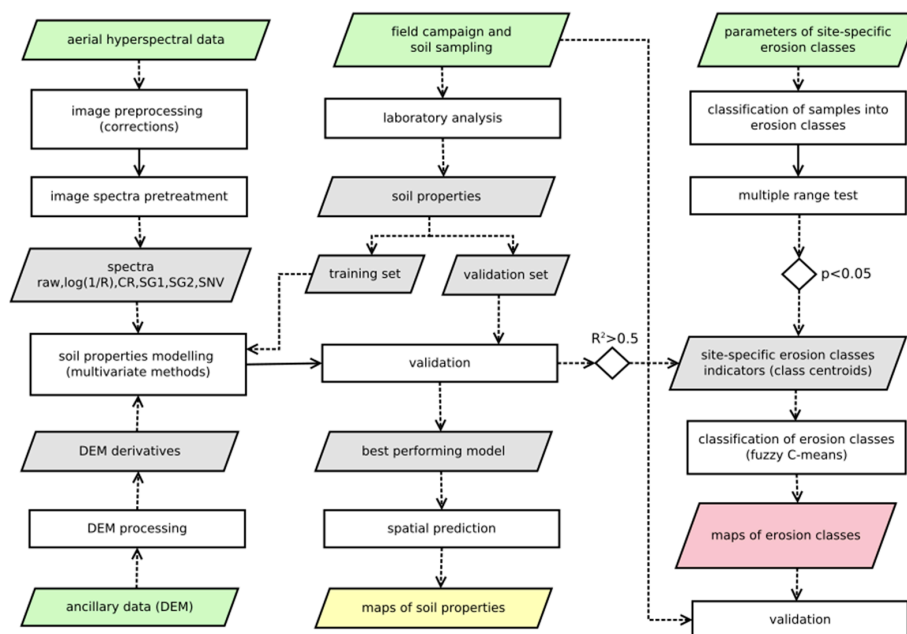


Figure 2. Scheme of the method for soil erosion assessment.

### 2.5.1. Definition of Groups of Site-Specific Erosion Classes

Soil samples data were classified into groups based on description of soil profiles (soil profile stratigraphy, soil depth or A horizon thickness), field observation (evidence of erosion such as ploughed subsoil, increase in skeleton content) and expert knowledge of soil erosion evidences in different pedological conditions on study sites. Setting of defining parameters of each class is site-specific depending on soil type and parent material. The quantitative setting of each erosion stage at individual study sites was based on previously performed regional studies [71,72]. Four groups (erosion classes of soils) were established at each study site (see Table 3):

Non-eroded soils (NE)—unchanged autochthon soils with no or negligible evidence of material removal or accumulation;

Eroded soils with various stage of degradation—moderately eroded (ME) and strongly eroded (SE) soils—soil profiles with evidence of material removal and soil profile truncation; and

Accumulated soils (AC) formed by material re-deposition in concave parts of relief—soil profiles with evidences of accumulation of new material manifested by increased thickness of A horizon or burial of former surface horizons.

Table 3. Erosion classes distinguished at each site according to soil profile stratigraphy and thickness of A horizon.

Site	EC <sup>1</sup>	Profile Stratigraphy	SD <sup>2</sup>	AHT <sup>3</sup>	WRB <sup>4</sup>
Přestavky	AC	Ap-A-Bw(g)-C		>40	Haplic Cambisol (Colluvic), Stagnic Cambisol (Colluvic), Haplic Stagnosol (Colluvic)
	NE	A-Bw(g)-(B/C)-C	>50		Haplic Cambisol, Stagnic Cambisol, Haplic Stagnosol
	ME	Ap-Bw(g)-B/C-C	35–50		Haplic Cambisol, Stagnic Cambisol, Haplic Stagnosol
	SE	Ap-(B/C)-C	<35		Skeletal Cambisol, Cambic Leptosol

Table 3. Cont.

Site	EC <sup>1</sup>	Profile Stratigraphy	SD <sup>2</sup>	AHT <sup>3</sup>	WRB <sup>4</sup>
Šardice	AC	Ap-A-A/C-Ck		>80	Calcic Chernozem (Colluvic), Calcic Kastanozem (Colluvic)
	NE	Ap-A-A/C-Ck		50–80	Calcic Chernozem
	ME	Ap-A/C-Ck		30–50	Calcic Chernozem, Calcic Kastanozem
	SE	Ap-Ck		<30	Haplic Calcisol, Calcic Kastanozem
Nová Ves	AC	Ap-A-Bw-C		>40	Haplic Cambisol (Colluvic)
	NE	Ap-Bw-(B/C)-C	>50		Haplic Cambisol
	ME	Ap-(Bw)-B/C-C	35–50		Haplic Cambisol
	SE	Ap-(B/C)-C	<35		Skeletal Cambisol, Cambic Leptosol
Jičín	AC	Ap-A-Bt-C		>50	Haplic Luvisol (Colluvic), Luvic Kastanozem (Colluvic), Luvic Phaeozem (Colluvic)
	NE	Ap-A-Bt-(B/C)-C	>60		Haplic Luvisol, Luvic Kastanozem
	ME	Ap-Bt-(B/C)-C	40–60		Haplic Luvisol
	SE	Ap-(B/C)-C	>40		Haplic Calcisol

<sup>1</sup> erosion class (AC—accumulated soils, NE—non-eroded soil, ME—moderately eroded soils, SE—severely eroded soils); <sup>2</sup> soil depth in cm; <sup>3</sup> A horizon thickness in cm; <sup>4</sup> World reference base for soil resources 2014.

### 2.5.2. Assessment of Soil Properties for Erosion Classes Distinguishing

Each of erosion classes was consequently characterized by a range of values of distinctive soil surface properties (soil erosion indicators, [30]) having specific spectral reflectance characteristics that can be obtained using imaging spectroscopy (SOC, texture classes, CaCO<sub>3</sub> and iron oxides). We presume that in ME and SE, the removal of topsoil and its mixture with subsoil leads to qualitative and quantitative changes in surface soil properties manifested in spectral reflectance characteristics [30,33,41,42,73]. However, the soil properties of deposited material can vary significantly (both topsoil and subsoil material can be accumulated), strongly depending on site-specific conditions (topography, parent material, soil properties of parental soil, type, intensity and frequency of erosion events). This fact can significantly influence the information value of surface soil properties and the corresponding reflectance data and their applicability in defining the AC class [71,73]. For this purpose, thickness of A horizon was used as an additional indicator for the definition of this class. The thickness was spatially predicted using the data from borings and derivatives of DEM (altitude, slope, curvatures, catchment area, and topographic wetness index). The 5 × 5 m<sup>2</sup> resolution DTM (DMR 4G<sup>®</sup>) distributed by Czech Office for Surveying, Mapping and Cadaster—ČÚZK, obtained using laser scanning with a total mean height error of 0.3 m was used.

Soil properties applicability to distinguish individual erosion classes was analysed using multiple range test (parametric and non-parametric, depending on statistics of normality and variability in the set). Only the properties that showed significant differences in at least two erosion classes (by means of unique confidence interval) were used for distinguishing the erosion classes. Soil properties which achieved low prediction accuracy using hyperspectral image processing ( $R^2 < 0.5$ ) were not used as defining parameters.

### 2.5.3. Classification of Spatial Data into Erosion Classes

Classification of erosion stages was carried out using fuzzy C-means (FCM) clustering algorithm [74]. C-means function from R package e1071 [75] was used for clustering execution. The method creates partitioning of dataset in multivariate space by maximizing similarity between samples within the same cluster and dissimilarity among different clusters. The probability of cluster membership of samples is computed. Final classification into classes is based on the highest probability.

Spatial data of previously selected soil properties derived from hyperspectral images and DEM were used as input data layers. Initial cluster centres were determined as means of soil properties values for defined erosion classes.

### 2.5.4. Validation of Results

Summarizing the validation of results was performed by confusion matrix. Overall and individual class accuracy was obtained for all study sites. Since the independent samples were not available, point data classes determined under the field campaign were used for the validation.

## 3. Results and Discussion

### 3.1. Descriptive Statistics of Soil Samples

Summary statistics and correlation matrix for the soil samples from the study sites are shown in Tables 4 and 5. The SOC content analysis in topsoil has revealed differences among the study sites. Low contents were observed at Jičín site (Luvisols), where values ranged from 0.7% to 1.41% (mean 1.03%), the highest variability and low to high contents were observed at Šardice site (range 0.84%–2.62%, mean 1.44%). On the other sites (Cambisols) Nová Ves (range 0.56%–1.44%, mean 1.07%) and Přestavlky (range 0.61%–1.88%, mean = 1.19%), the content of SOC is low to medium. The soil texture analysis has revealed silt loam (partially silty clay loam) at Jičín site, prevalence of loamy soils at Šardice site (locally more sandy or clayey), sandy loam and loam at Nová Ves and silt loam and loam at Přestavlky. CaCO<sub>3</sub> content was analysed only on sites with loess parent material. At Jičín site, presence of CaCO<sub>3</sub> was identified only in 3 topsoil samples (~0.1%). At Šardice site, CaCO<sub>3</sub> content varies from 0% to 10%. Fe oxides in soils extracted by two reagents (Fe<sub>ox</sub> and Fe<sub>dith</sub>) were analysed only on Cambisols sites. The content of both was identified higher at Přestavlky site (Fe<sub>ox</sub> mean 0.77%; Fe<sub>dith</sub> mean 3.59%) than at Nová Ves site (Fe<sub>ox</sub> mean 0.21%; Fe<sub>dith</sub> mean 1.24%).

**Table 4.** Descriptive statistics of soil properties measured in collected soil samples.

Site		SOC (%)	Sand (%)	Silt (%)	Clay (%)	Fe <sub>ox</sub> (%)	Fe <sub>d</sub> (%)	CaCO <sub>3</sub> (%)
Přestavlky <i>n</i> = 45	Mean	1.19	38.12	49.63	12.26	0.77	3.59	
	Min	0.61	26.2	30.6	7.5	0.20	1.37	
	Max	1.88	59.0	61.5	20.1	2.19	7.38	
	SD	0.25	8.37	7.17	3.22	0.51	1.81	
Šardice <i>n</i> = 50	Mean	1.44	38.91	38.49	22.6			4.07
	Min	0.84	15.2	27.5	14.2			0
	Max	2.62	58.3	49.1	48.3			10.0
	SD	0.39	8.34	4.67	6.80			3.34
Nová Ves <i>n</i> = 50	Mean	1.07	51.24	37.59	11.16	0.21	1.24	
	Min	0.56	29.8	15.9	6.7	0.11	0.63	
	Max	1.44	77.2	56.6	24.7	0.60	2.37	
	SD	0.17	12.32	9.95	3.57	0.10	0.36	
Jičín <i>n</i> = 50	Mean	1.03	12.24	66.12	21.64			0.01
	Min	0.70	7.7	52	14.2			0
	Max	1.41	18.2	75.0	32.5			0.1
	SD	0.15	2.41	5.56	5.14			0.03

**Table 5.** Correlation matrix of soil properties.

Site		SOC	Sand	Silt	Clay	Fe <sub>ox</sub>	Fe <sub>d</sub>
Přestavlky	SOC						
	Sand	<b>−0.51 ***</b>					
	Silt	<b>0.61 ***</b>	<b>−0.93 ***</b>				
	Clay	−0.04	<b>−0.54 ***</b>	0.18			
	Fe <sub>ox</sub>	<b>0.6 ***</b>	<b>−0.52 ***</b>	<b>0.55 ***</b>	0.13		
	Fe <sub>d</sub>	<b>0.58 ***</b>	<b>−0.3 *</b>	<b>0.39 **</b>	−0.07	<b>0.73 ***</b>	
Šardice	SOC						
	Sand	−0.26					
	Silt	<b>−0.28 *</b>	<b>−0.58 ***</b>				
	Clay	<b>0.51 ***</b>	<b>−0.83 ***</b>	0.02			
	CaCO <sub>3</sub>	<b>−0.74 ***</b>	−0.17	<b>0.33 *</b>	−0.02		
Nová Ves	SOC						
	Sand	<b>−0.45 **</b>					
	Silt	<b>0.45 **</b>	<b>−0.97 ***</b>				
	Clay	<b>0.3 *</b>	<b>−0.75 ***</b>	<b>0.57 ***</b>			
	Fe <sub>ox</sub>	<b>0.37 **</b>	<b>−0.65 ***</b>	<b>0.57 ***</b>	<b>0.67 ***</b>		
	Fe <sub>d</sub>	0.18	<b>−0.53 ***</b>	<b>0.43 **</b>	<b>0.61 ***</b>	<b>0.39 **</b>	
Jičín	SOC						
	Sand	0.2					
	Silt	−0.2	<b>−0.39 **</b>				
	Clay	0.13	−0.05	<b>−0.9 ***</b>			
	CaCO <sub>3</sub>	0.01	0.12	<b>−0.31 *</b>	<b>0.28 *</b>		

\* correlation is significant at the 0.05 level; \*\* correlation is significant at the 0.01 level; \*\*\* correlation is significant at the 0.001 level; non-signed values are non-significant.

### 3.2. Prediction of Soil Properties by Imaging Spectroscopy

Different multivariate techniques (ANN, PLS, RF, SVM) were used to predict soil properties spatial distribution using raw spectroscopic data and data adjusted by different pre-treatment methods (log, SG 1st, SG 2nd, CR and SNV). The results of multivariate modelling indicate different prediction accuracy according to soil properties, number of soil samples used for calibration, study sites, used multivariate technique and pre-treatment methods. Table 6 summarizes the results of calibration and validation by prediction models with the highest accuracy according to lowest RMSE<sub>p</sub> values. Values of R<sup>2</sup> and RMSE in training and validation sets for all models and different types of pre-treatment are shown in Figure S1 (in supplementary material). Plots of measured vs. predicted soil parameters for the validation datasets are given in Figure 3.

In summary, the best prediction accuracy was achieved for SOC content, where R<sup>2</sup> value in the validation set ranged for the best models within sites between 0.8 and 0.91. Consequently, these models yielded RMSE<sub>p</sub> between 0.07% and 0.12%. SOC is the most frequently predicted soil property using hyperspectral imaging data. Reported values of R<sup>2</sup> and RMSE for SOC prediction from previous works are highly variable [37] and depend on many local conditions and used techniques (type of sensors, corrections, site conditions, size of study area, number of samples etc.). Nevertheless, the prediction of SOC distribution is generally successful thanks to good spectral response of SOC and the values reported in similar studies (R<sup>2</sup><sub>p</sub> ranged between 0.65 and 0.96) are comparable to our results [76–79].

Prediction accuracy of textural classes is highly variable among study sites and more variable than in SOC prediction. R<sup>2</sup><sub>p</sub> and RMSE<sub>p</sub> values vary between 0.21–0.67 R<sup>2</sup><sub>p</sub> and 2.49%–9.04% RMSE<sub>p</sub> for sand content, 0.4–0.92 R<sup>2</sup><sub>p</sub> and 2.75%–7.06% RMSE<sub>p</sub> for silt content and 0.38–0.89 R<sup>2</sup><sub>p</sub> and 1.47%–2.88% RMSE<sub>p</sub> for clay content. In general, lower value of R<sup>2</sup><sub>p</sub> for certain textural class was achieved at the sites where its content is low. This is, for example, the case of Jičín site where a very low prediction accuracy of sand (R<sup>2</sup><sub>p</sub> 0.21) was assessed. Alternatively, the prediction accuracy of sand and silt which are not spectrally active in VNIR-SWIR region can be influenced by a correlation between these



properties and spectrally active properties (SOC, clay, CaCO<sub>3</sub> and Fe forms). This is probable at Jičín site where a good model performance for silt ( $R^2_p$  0.92) can be given by its strong correlation with clay ( $R^2_p$  0.89) or at Šardice site where sand ( $R^2_p$  0.67) is highly negative correlated with clay ( $R^2_p$  0.89) (Table 5). Another factor influencing the variability of the prediction accuracy can be a different level of BRDF effect caused by diverse hyperspectral sensing conditions. This is valid for Přestavlky and Nová Ves sites where the BREFCOR corrections have not led to full elimination of BRDF effect. A high variability of model performances was reported in several studies dealing with texture prediction by RS [80–85].

**Table 6.** Accuracy of the best prediction models (the best performing model according to lowest RMSE<sub>P</sub> values).

Site		SOC	Sand	Silt	Clay	Fe <sub>ox</sub>	Fe <sub>d</sub>	CaCO <sub>3</sub>
Přestavlky $n^1 = 36/8$ (44)	BM <sup>2</sup>	SVM.l SG (2nd)	ANN log	SVM.p SG (1st)	SVM.r log	SVM.p log	SVM.p log	-
	$R^2_{cv}$	0.92	0.88	0.88	0.91	0.99	0.63	-
	RMSE <sub>cv</sub>	0.08	2.92	2.78	1.34	0.05	1.10	-
	$R^2_p$	0.83	0.61	0.40	0.38	0.73	0.78	-
	RMSE <sub>P</sub>	0.12	5.87	5.05	1.96	0.44	1.10	-
	RPD	2.08	1.42	1.42	1.64	1.16	1.65	-
$n^1 = 36/12$ (48)	BM <sup>1</sup>	SVM.p SG (1st)	PLS SG (2nd)	SVM.l SG (1st)	PLS cr	-	-	ANN log
	$R^2_{cv}$	0.87	0.80	0.53	0.90	-	-	0.84
	RMSE <sub>cv</sub>	0.17	3.55	3.08	1.90	-	-	1.32
	$R^2_p$	0.80	0.67	0.49	0.89	-	-	0.82
	RMSE <sub>P</sub>	0.16	5.06	3.82	2.88	-	-	1.48
	RPD	2.43	1.65	1.22	2.36	-	-	2.26
Nová Ves $n^1 = 29/8$ (37)	BM <sup>1</sup>	SVM.l SG (2nd)	ANN raw	SMV.l log	ANN SG (1st)	SVM.r log	SVM.r raw	-
	$R^2_{cv}$	0.79	0.95	0.89	0.99	0.90	0.72	-
	RMSE <sub>cv</sub>	0.08	3.31	3.23	0.01	0.04	0.20	-
	$R^2_p$	0.80	0.41	0.69	0.41	0.89	0.59	-
	RMSE <sub>P</sub>	0.11	9.04	7.06	1.47	0.11	0.29	-
	RPD	1.55	1.36	1.41	2.43	0.91	1.24	-
Jičín $n^1 = 36/14$ (50)	BM <sup>1</sup>	SVM.p SG (2nd)	SVM.p raw	SVM.l snv	SVM.p raw	-	-	-
	$R^2_{cv}$	0.90	0.01	0.89	0.98	-	-	-
	RMSE <sub>cv</sub>	0.05	2.38	1.79	0.63	-	-	-
	$R^2_p$	0.91	0.21	0.92	0.89	-	-	-
	RMSE <sub>P</sub>	0.07	2.49	2.75	1.92	-	-	-
	RPD	2.14	0.96	2.02	2.67	-	-	-

<sup>1</sup> number of samples used for calibration and validation; <sup>2</sup> best performing model including multivariate technique and preprocessing method.

Models dealing with iron oxides and CaCO<sub>3</sub> content performed with  $R^2_p$  0.73–0.89 for Fe<sub>ox</sub>, 0.59–0.78 for Fe<sub>d</sub> and 0.82 for CaCO<sub>3</sub> (only at site Šardice). Fe<sub>ox</sub>, Fe<sub>d</sub> (iron oxides in general) and CaCO<sub>3</sub> are only rarely studied soil properties by imaging spectroscopy. The high to moderate prediction accuracy for Fe<sub>ox</sub>, Fe<sub>d</sub> and CaCO<sub>3</sub> is similar [84] or even better [86,87] in comparison to other studies.

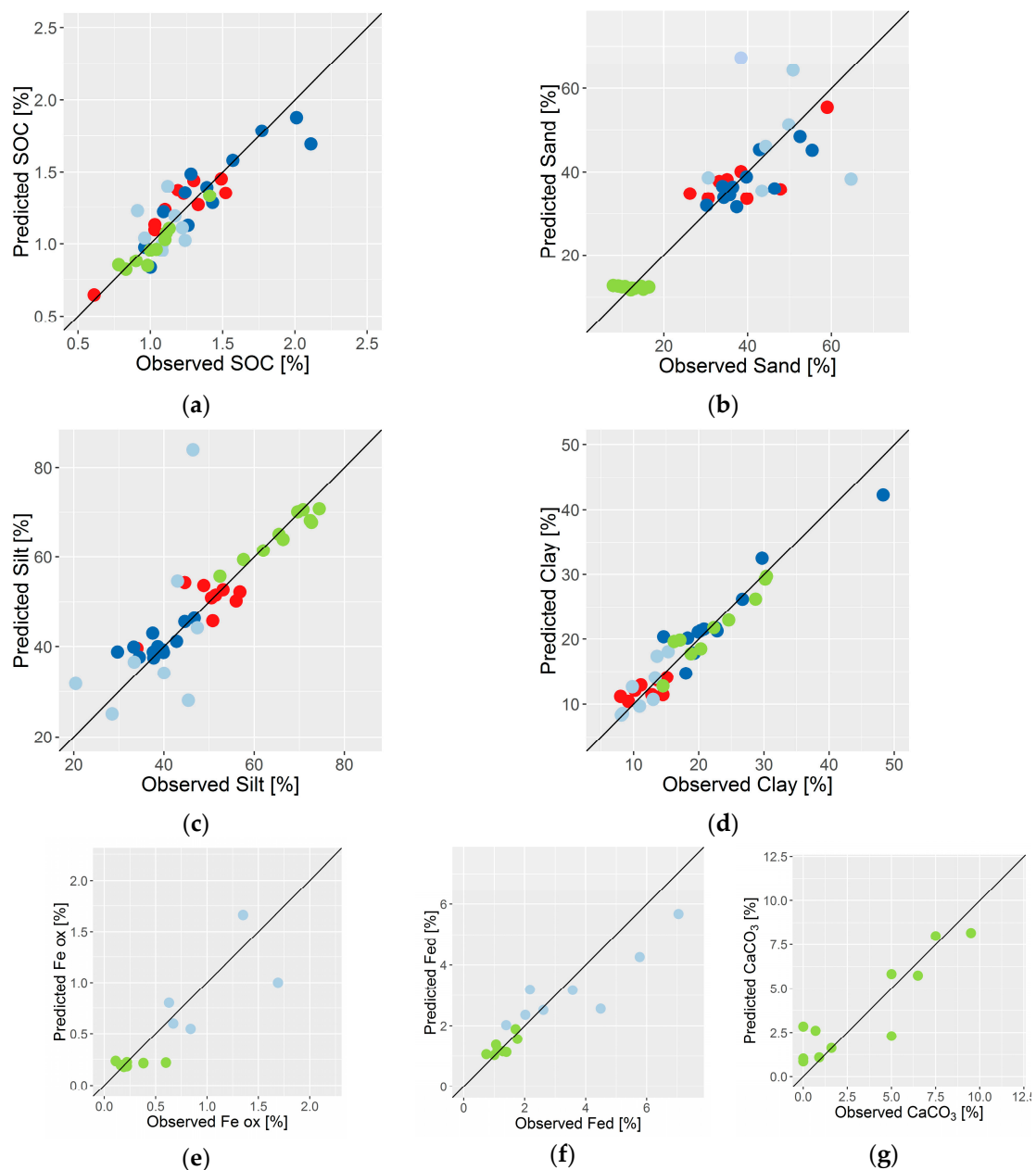


**Figure 3.** Comparison of predicted and observed values in the validation set of sampling points: (a) SOC; (b) sand; (c) silt; (d) clay; (e) Fe<sub>ox</sub>; (f) Fe<sub>d</sub>; and (g) CaCO<sub>3</sub>. Colour of the points identifies the study site: (red) Přestavlky; (dark blue) Šardice; (light blue) Nová Ves; (green) Jičín.

In conclusion, the analysis showed that the distribution of soil properties in eroded landscapes can be successfully predicted using the spectroscopic data. The prediction accuracy is adequate in majority of sites and predicted properties; however, a significant worsening in the model performance was observed in case of properties with low content [36]. Moreover, the presented models are locally-trained (for few field blocks in maximum) which increase their prediction capability in comparison with similar regional models [76].

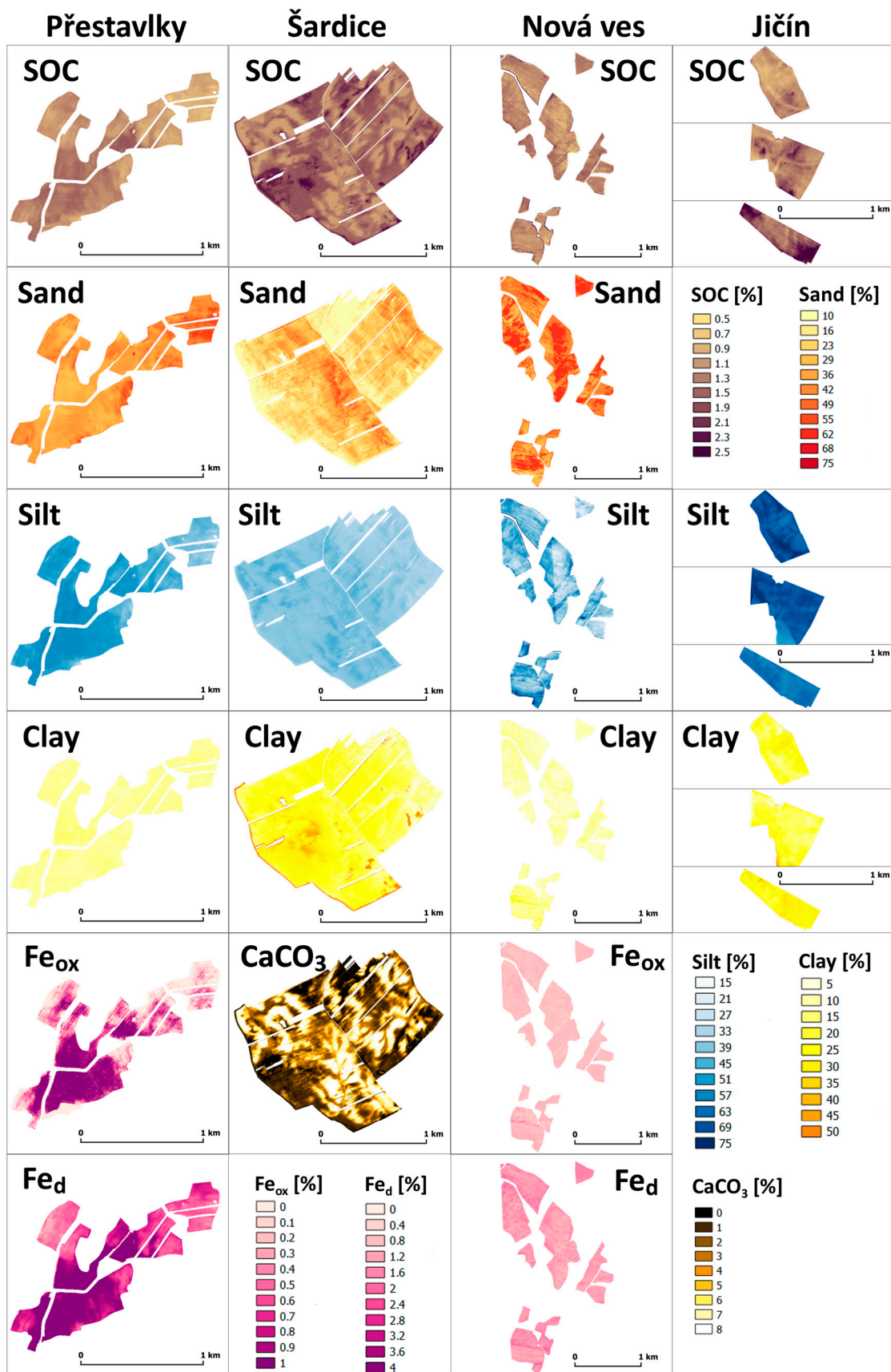


**Figure 4.** Spatial distribution of soil properties at the study sites based on multivariate prediction using the best performing model.

Methods of machine learning SVM (71% of cases) and ANN (19%) showed the best prediction accuracy. At Šardice site, the PLS model (10%) showed the best accuracy for two textural classes (similar to machine learning models). PLS technique has been traditionally used in many studies dealing with soil spectroscopy and its ability to prediction of soil properties from spectral data was proven, but with varying accuracy [36]. In this study, PLS models reveal slightly lower accuracy than other methods, however not significantly worse. More recently, machine learning techniques have been used in imaging spectroscopy [30,76,88–91]. Whereas ANN method is not so frequently used due to the need of a large training dataset, training demands and a tendency to over-fitting, the SVM has become the most frequent method overcoming the difficulties of the ANN technique [27]. Contrarily to the mentioned ANN shortcomings, the tendency to over-fitting by ANN was not fully proven in our study. The problem with over-fitting was observed in RF in all cases. This finding is in contrast to Viscarra Rossel and Behrens [92] and it is most probably influenced by insufficient optimization of model parameters by random search method for automatic search of parameter values. General applicability of SVM as a robust model with low sensitivity to noise in data [76,89] and its ability to predict soil properties across hyperspectral images with small amount of samples was proven in our study as the SVM was the method of the first choice in the majority of predicted properties at the study sites.

Regarding the spectra pre-treatment methods, significant differences of prediction accuracy were not observed. The majority of the best performing models (33%) used the techniques of absorbance transformations. Raw data (reflectance), SG (1st), and SG (2nd) were used in 19%, CR and SNV in 5% of the finally selected models. The methods of pre-treatment performed better (according to  $R^2$ ) than reflectance and absorbance data in case of SOC and  $Fe_{ox}$  prediction at Přestavlky and Nová Ves sites, where the conditions of hyperspectral data acquisition were less favourable, which led to stronger influence of BRDF effect. This effect can be highlighted at these sites by cementing effect of iron oxides correlated to soil aggregation [36,93].

In case of other properties, the relationship between prediction ability and the use of a pre-treatment method was not observed. Spatial distribution of all predicted soil properties for all sites is shown in Figure 4.

### 3.3. Assessment of Soil Erosion Classes

Four erosion classes were distinguished on the study sites. The highest number of profiles was identified as non-eroded (11 at Šardice, 29 at Přestavlky, 30 at Jičín and 40 at Nová Ves) except for the Chernozem site Šardice where 23 profiles were classified as strongly eroded soils. Moderately eroded soils were identified in 5–8 cases at each site. Accumulated soil class was identified only at Šardice (9) and Jičín (12) sites.

#### 3.3.1. Assessment of Soil Properties for Erosion Classes Distinguishing

Results of selection and assigning soil properties to each erosion class are shown in the Table 7. The table shows selected soil properties and their centres (means) used for erosion classes classification. The performance and suitability of different properties for erosion classes' classification are highly variable at the study sites. In summary, the SOC content is applicable at every site except for Jičín, where the difference in the values among erosion classes was not significant. At three study sites (except for Jičín), SOC can be used for distinguishing of NE and SE class with significantly the highest and lowest SOC content, respectively. Potential of SOC for ME classification is low. In contrast to Schmid et al. [30] a Hill and Schütt [42] who assessed the erosion stages in semi-arid climate, our study showed difficulties in distinguishing the AC class using SOC content in topsoil. At Šardice site, the SOC content in topsoil decreases in AC class. This is due to an advanced stage of erosion degradation at the study site when loess is exposed in eroded parts of slopes and redeposited in the accumulation positions [53,72]. Zádorová et al. [94] described this process as a retrograde soil development typical for the most vulnerable loess regions with dissected relief. Moreover, the combination of preferential

(interill erosion) and non-preferential (rill and tillage erosion) removal of soil material influences the resulting variability of SOC distribution in topsoil [95–97].

**Table 7.** Class centres used for determination of erosion classes by fuzzy C-means method.

Site		A Thick.	SOC	Sand	Silt	Clay	Fe <sub>ox</sub>	Fe <sub>d</sub>	CaCO <sub>3</sub>
Přestavlky	NE	*	<b>1.22</b> SE	<b>35</b> SE	* SE	* SE	-	-	-
	ME	*	<b>1.17</b>	<b>37</b> SE	* SE	* SE	-	-	-
	SE	*	<b>1.10</b> NE	<b>51</b> NE,ME	* NE,ME	* NE,ME	-	-	-
Šardice	AC	<b>87</b> NE,ME,SE	<b>1.32</b> ME,NE	* ME,NE	*	<b>17</b> NE	-	-	<b>4.6</b> ME,NE
	NE	<b>62</b> AC,ME,SE	<b>1.94</b> AC,SE	* AC	*	<b>26</b> AC	-	-	<b>0.2</b> AC,SE
	ME	<b>31</b> AC,NE	<b>1.65</b> AC,SE	* AC	*	<b>23</b>	-	-	<b>1.1</b> AC,SE
	SE	<b>26</b> AC,NE	<b>1.18</b> ME,NE	* AC	*	<b>23</b>	-	-	<b>6.6</b> NE,ME
Nová ves	NE	*	<b>1.11</b> SE	* ME,SE	<b>41</b> ME,SE	* ME,SE	<b>0.23</b> SE	<b>1.3</b> ME	-
	ME	*	<b>0.95</b>	* NE	<b>26</b> NE	* NE	<b>0.14</b>	<b>0.96</b> NE	-
	SE	*	<b>0.89</b> NE	* NE	<b>23</b> NE	* NE	<b>0.13</b> NE	<b>1.01</b>	-
Jičín	AC	<b>80</b> NE,ME,SE		*	<b>68</b> ME	<b>20</b> ME	-	-	-
	NE	<b>38</b> AC		* SE	<b>66</b> ME	<b>21</b> ME	-	-	-
	ME	<b>31</b> AC		*	<b>63</b> AC,NE	<b>26</b> AC,NE	-	-	-
	SE	<b>31</b> AC		* NE	<b>65</b>	<b>27</b>	-	-	-

AC,NE,ME,SE class with significantly different mean values in indicated erosion classes (Multiple Range Test Method: 95.0% LSD); \* soil properties with prediction accuracy from hyperspectral data  $R^2 < 0.5$ ;—not analysed; bolded values were used for erosion classes classification.

In case of texture, the classification potential of at least one textural class was proven at all the study sites. However, the accuracy of prediction model for these properties did not reach required limit of  $R^2$ ; therefore, only sand at Přestavlky, silt at Nová Ves and Jičín and clay at Jičín were used for classification. At Přestavlky site, SE was significantly different from NE and ME in sand content. This result can be expected at sites with high sand content where the fine particles are selectively removed from the eroded soils. At Nová Ves, high silt content can be used for distinguishing NE class. AC class was significantly distinguishable from NE at Šardice site by clay content. Iron oxides applicability was observed only at Nová Ves site.

CaCO<sub>3</sub> content was analysed only at Šardice site (only negligible amount was observed at Jičín site), where it showed a good potential to distinguish AC class from NE and ME class. The AC and SE classes were not significantly different, as the CaCO<sub>3</sub> content is similarly high due to truncation of soil profile and admixture of loess in the plough layer in case of SE class and accumulation of CaCO<sub>3</sub>-rich material in case of AC class. The study showed that the CaCO<sub>3</sub> content can be used as an erosion classes indicator only in regions with CaCO<sub>3</sub>-rich subsoil that is exposed at soil surface due to A horizon removal or tillage, similarly to [30,33].

Due to poor results of tested soil properties in AC class distinguishing, we used A horizon thickness as an auxiliary indicator at Šardice and Jičín sites, where the AC class was identified. The A horizon thickness prediction using DEM modelling was previously successfully used in Zádorová et al. [71,72] for identification of deep colluvial soils. In our study, the A horizon thickness showed very good potential in AC distinguishing at both sites. It was also significant for NE class in Šardice; at Jičín site, it did not differ significantly in any other class except for AC.

### 3.3.2. Classification of Spatial Data into Erosion Classes

Results of classification based on FCM and previously determined class centres are shown in Figure 5. In total, 1.24 km<sup>2</sup> of strongly eroded soil was classified. This class is arranged in descending order; 32.9% at Nová Ves, 29.1% at Šardice, 23.3% at Jičín and 16.9% at Přestavlky. At Přestavlky site, the NE class (46.2%) followed by ME class (36.8%) cover the rest of the area. At Nová Ves site, the area of moderately eroded soil (35.4%) exceeded the area of non-eroded soils (31.7%). At both localities, SE class can be found only on the most exposed terrain position (in context of both water and tillage erosion). The pattern of different erosion classes is more complex at Šardice and Jičín sites. The AC

class is present mainly in the terrain concavities (side valleys) closely neighbouring to strongly and moderately eroded soils at the back slopes (20.7% at Šardice; 13.6% at Jičín). Non-eroded soils were classified in flat and nearly flat relief (plateaus) (22.0% at Šardice; 40.5% at Jičín). These findings are in accordance with previous studies performed in regions with similar conditions. Zádorová et al. [94], Schmitt and Rodzik [98] or Terhorst [99] observed a high heterogeneity of soil cover, depth and SOC stocks and a significant area covered by strongly eroded soils in Chernozem and Luvisol loess regions. The Cambisol regions on crystalline rocks were typical in terms of less pronounced erosion evidences with lower incidence of both accumulated soils and soils with severe erosion removal [71].

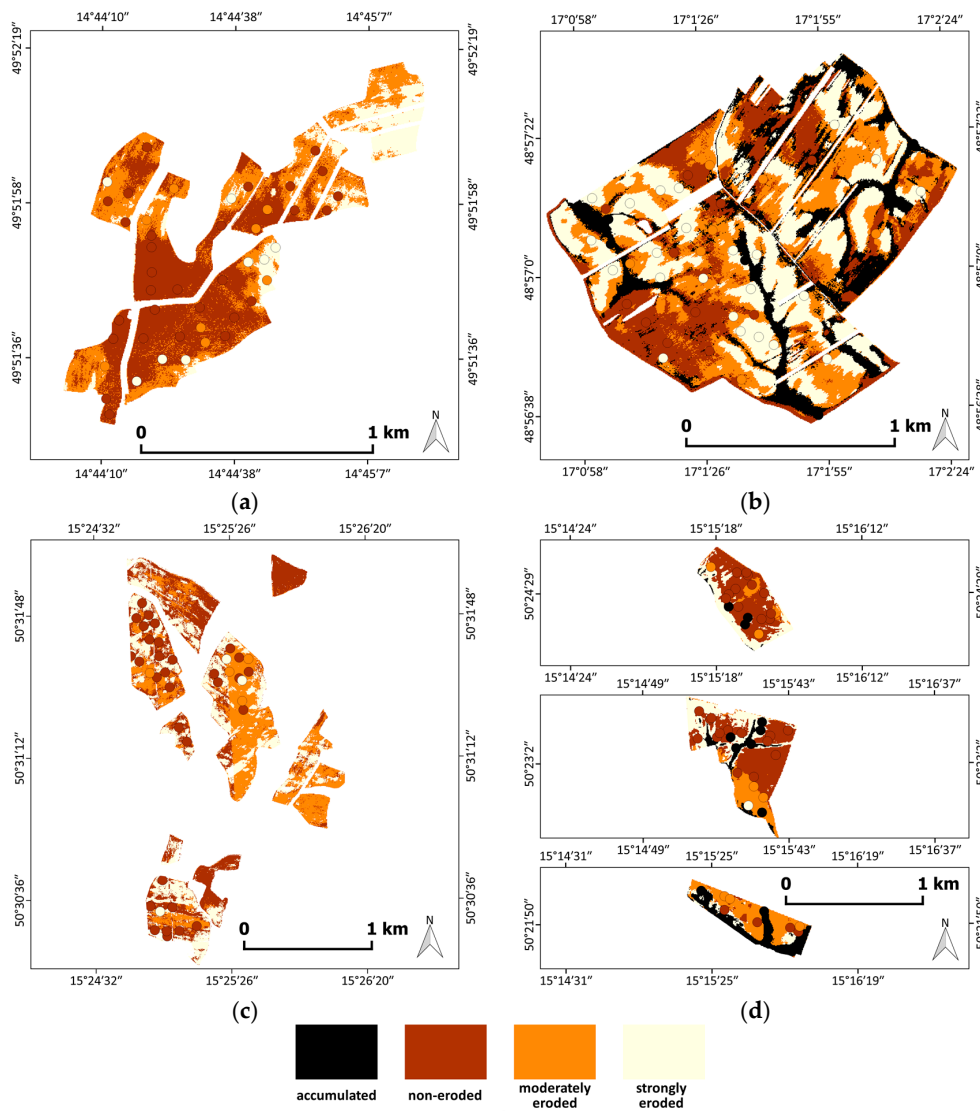


**Figure 5.** Maps of erosion classes at the study sites as derived by means of fuzzy C-means method using the mean values of selected soil properties as class centres: (a) Přestavlky; (b) Šardice; (c) Nová Ves; and (d) Jičín.

### 3.3.3. Validation of Results

The overall accuracy of erosion classes' classification varies across the sites (Table 8). High accuracy was obtained in Šardice site (82%), moderate accuracy was obtained in Jičín site (67.3%). Přestavlky and Nová Ves achieved 51.1% and 52.6%, respectively. This is regarded as a low accuracy. Significant deficiencies of the spectral modelling were expressed in case of classification of two classes of eroded soils (SE and ME). The most frequent classification error is in all sites linked with

misclassification of moderately eroded class to non-eroded or to strongly eroded class or vice versa. In general, the moderately eroded class achieved lowest values of both producer and user accuracy. This problem was also reported in Schmid et al. [30] who identified the majority of misclassifications in the moderately eroded class. According to the results of classes' separability and model validation, distinguishing two classes of eroded soils shows to be too detailed and classification of one class of eroded soil would be sufficient as the two classes overlap in a number of soil properties. Distinguishing transitional classes can be performed using the fuzzy classification and comparison of membership in non-eroded and eroded classes. However, distinguishing of different classes of eroded soils can be reasonable and bring good results (77% in overall accuracy) in certain conditions as was proven by Schmid et al. [30] in a large, severely degraded semi-arid region on CaCO<sub>3</sub>-rich parent material. Zádorová et al. [94] reported similar degree of misclassification in case of slightly and strongly accumulated soils at a Chernozem study site. The slightly accumulated soils showed the lowest overall accuracy due to aggregating the properties of other classes.

**Table 8.** Confusion matrix of the erosion stages classification.

Site	Predicted	Observed				Producer Accuracy (%)	User Accuracy (%)	Overall Agreement Rate
		AC	NE	ME	SE			
Přestavlky	AC	-	-	-	-	-	-	51.1%
	NE	-	17	5	2	58.6	70.8	
	ME	-	12	2	2	25	12.5	
	SE	-	0	1	4	50	80	
Šardice	AC	8	1	0	0	88.8	88.9	82%
	NE	0	10	1	0	90.9	90.9	
	ME	0	0	6	6	85.7	50	
	SE	1	0	0	17	73.9	94.4	
Nová Ves	AC	-	-	-	-	-	-	52.6%
	NE	-	16	0	0	55.2	100	
	ME	-	11	4	3	100	22.2	
	SE	-	4	0	0	0	0	
Jičín	AC	6	0	0	0	50	100	67.3%
	NE	1	23	3	0	76.7	85.2	
	ME	0	6	4	1	57.1	36.4	
	SE	5	1	0	0	0	0	

At Přestavlky site, two SE samples were classified as NE. The profiles are situated on the slope with high amounts of rock fragments on the surface (up to 20%) and evidence of erosion features; the misclassification to NE class is evident. At Nová Ves site, 4 NE soil profiles were classified as SE. The pattern of eroded and non-eroded soils is very complex at this site, strongly depending on the tillage erosion. The site is distinctive by abrupt change of soil depth within short distances. Misinterpretation of erosion classes at this site can be therefore associated to an insufficient spatial accuracy of input data (GNSS, hyperspectral, DEM) for the exact delineation of the soil variability at short distances.

Few misclassifications between SE and AC classes were observed at Šardice (1) and Jičín (5) sites. The misclassified points were situated near the inflex points of the slope where removal, transport and sedimentation can act in dependence to the intensity and the type of erosion. The resulting surface soil properties correspond to such a complex process and can overlap in the studied classes. This fact is proven by the fuzzy membership that is evenly distributed to more erosion classes. Two samples in the north part of Jičín site identified as AC were predicted as SE. This error can be again explained by the mixed effect; the points are situated in the narrow transitional strip between Luvisol and gleyic Chernozem nearby the stream.

The validation of results showed high to moderate potential of used methods for erosion classes' classification. In our study, the high applicability of spectral data is restricted to Chernozem and Luvisol loess study sites (Šardice and Jičín). This can be attributed to two facts. The first is the homogeneity of parent material and soil properties of former dominant soil cover at these sites, now changed by erosion. The observed differences in the soil properties are then closely linked to erosion processes and thus well performing in the prediction models. In contrast, the variability of soil properties at the sites on heterogeneous crystalline and sedimentary rocks with more heterogeneous soil cover (Přestavlky and Nová Ves) is a result of more co-acting processes and local conditions and is not necessarily linked to the soil erosion. The second factor is the intensity of the soil cover change due to erosion processes. Erosion leads to extreme (Šardice) and significant (Jičín) redistribution of soil material at the loess sites and results in development of severely degraded soils with truncated soil profile on one hand and several metres deep colluvial soils on the other hand [53]. The particular erosion classes are then very distinctive and form a specific soil mosaic. The intensity of soil erosion at Cambisol study sites is less pronounced; the accumulation class has not been identified and SE class covers marginal areas. Thus, the soil properties variability given solely by soil erosion is presumably less significant and the soil pattern driven by erosion material transport is less evident. Similar results were reported by [71] who compared the soil units and SOC stock prediction DEM based models in Chernozem, Luvisol and Cambisol study sites with similar area. They reported a very good model performance in Chernozem and Luvisol sites and a poor performance at the Cambisol site. The studies from semiarid regions dealing with soil erosion stages prediction using spectral data [30,33] showed high accuracy of the model, similar to the results at Šardice site. However, the comparison is not fully relevant according to differences in site area and conditions.

#### 4. Conclusions

The study demonstrates the potential of different soil properties predicted using hyperspectral data for the assessment of soil degradation by erosion at four pedologically different study sites influenced by soil redistribution due to accelerated erosion. The erosion impact at the study sites was evaluated by distinguishing four erosion classes representing different stages of soil redistribution by erosion.

The study showed that: (i) soil properties prediction can be successfully performed using spectral data and adequate prediction method; and (ii) selected soil properties are applicable for the assessment of soil degradation by erosion. The selected predictive properties, best performing predictive methods and classification models accuracy differed in the study sites. The accuracy of classification models was influenced by variability of soil units and parent material. The presented approach was successfully applied in Chernozem and Luvisol loess regions where the erosion classes were assessed with good overall accuracy (82% and 67%, respectively). The model performance in two Cambisol regions was rather poor (51%–52%). At study sites with less pronounced soil degradation, the restriction of the erosion classes from four to three can bring better results. However, at severely degraded sites, the limited number of classes may lead to a significant loss of information and decrease in models' applicability in conservation management. The sites with heterogeneous soil properties and parent material will require more precise local-fitted models and use of further auxiliary information such as terrain or geological data.

The key requirement for a successful use of hyperspectral data in soil predictive modelling is the application of high quality input spectral data with precisely performed corrections and limited influence of physical factors. The approach presented in the study can be applied exclusively on bare soil. Thus, the direct observation is in case of temperate agricultural regions limited to periods with minimum vegetation cover. More images from different periods are needed to cover wider areas. The study sites selected for the study and the periods of viewing were chosen with aim to minimize the roughness, wetness and non-photosynthetic vegetation cover. Further research is needed to find effective methods to filter out these factors and facilitate the use of hyperspectral imaging at



regional scale, especially in context of increased use of no tillage farming. Implementation of satellite hyperspectral sensors as well as further research on application of multi- and super-spectral sensors represent other effective tools in application of presented approach.

The applicability of the presented approach at the global scale has considerable limitations. To develop and apply a global model of a reasonable accuracy, utilizable for management purposes, similar conditions (atmospheric, surface roughness etc.) within the flight campaigns or a very precise image pre-processing (namely the elimination of the BRDF effect) are needed. Thus, regional models performed at a watershed scale or at a level of a geologic/pedologic/agricultural region represent, from the practical point of view, a more applicable option as a reasonable accuracy of the models can be provided more easily.

The presented approach promise, mainly at the local a regional scale, to produce valuable data on actual soil degradation, present structure of soil cover and redistribution of soil properties due to soil erosion, that will be usable for soil conservation policy purposes. The acquired data can be directly used by farmers for adjustment of management practices according to the level of soil degradation by erosion. At present, such information on real erosion impact on different soils is not available in the required detail and quality.

**Supplementary Materials:** The following are available online at [www.mdpi.com/2072-4292/9/1/28/s1](http://www.mdpi.com/2072-4292/9/1/28/s1), Figure S1: R2 and RMSE of prediction models for training and validation datasets by study site, multivariate technique and pre-treatment method.

**Acknowledgments:** This work was supported by the Ministry of Agriculture of the Czech Republic under grant number NAZV QJ QJ1330118—“Using remote sensing for monitoring of soil degradation by erosion and erosion evidence”.

**Author Contributions:** Daniel Žížala and Tereza Zádorová designed the workflow and conceived the methods. The methods were performed by Daniel Žížala (field work, data-preprocessing, predictive modeling, fuzzy classification) and Jiří Kapička (field work, data-preprocessing). Daniel Žížala and Tereza Zádorová wrote the paper.

**Conflicts of Interest:** The authors declare no conflict of interest.

## References

1. Panagos, P.; Borrelli, P.; Poesen, J.; Ballabio, C.; Lugato, E.; Meusburger, K.; Montanarella, L.; Alewell, C. The new assessment of soil loss by water erosion in Europe. *Environ. Sci. Policy* **2015**, *54*, 438–447. [[CrossRef](#)]
2. Dostál, T.; Janeček, M.; Kliment, Z.; Krása, J.; Langhammer, J.; Vrána, K. Czech Republic. In *Soil Erosion in Europe*; Boardman, J., Poesen, J., Eds.; John Wiley & Sons: Chichester, UK, 2007; pp. 107–116.
3. Novotný, I.; Žížala, D.; Kapička, J.; Beitlerová, H.; Mistr, M.; Kristenová, H.; Papaj, V. Adjusting the CP max factor in the Universal Soil Loss Equation (USLE): Areas in need of soil erosion protection in the Czech Republic. *J. Maps* **2016**, *12*, 1–5. [[CrossRef](#)]
4. Janeček, M.; Dostál, T.; Kozlovsky-Dufková, J.; Dumbrovský, M.; Hůla, J.; Kadlec, V.; Konečná, J.; Kovář, P.; Krása, J.; Kubátová, E.; et al. *Ochrana Zemědělské Půdy Před Erozí Protection of Agricultural Soils from the Soil Erosion*; Powerprint: Praha, Czech Republic, 2012.
5. Gobin, A.; Jones, R.; Kirkby, M.; Campling, P.; Govers, G.; Kosmas, C.; Gentile, A.R. Indicators for pan-European assessment and monitoring of soil erosion by water. *Environ. Sci. Policy* **2004**, *7*, 25–38. [[CrossRef](#)]
6. Van der Knijff, J.M.; Jones, R.J.A.; Montanarella, L. *Soil Erosion Risk Assessment in Europe*; Space Applications Institute: Penteli, Greece, 2000.
7. Watson, A.; Evans, R. A comparison of estimates of soil erosion made in the field and from photographs. *Soil Tillage Res.* **1991**, *19*, 17–27. [[CrossRef](#)]
8. Žížala, D.; Kapička, J.; Novotný, I. Monitoring soil erosion of agricultural land in Czech Republic and data assessment of erosion events from spatial database. In *Proceedings of the International Conference Soil—The Non-Renewable Environmental Resource*, Brno, Czech Republic, 7–9 September 2015; pp. 354–370.
9. Prasuhn, V. Soil erosion in the Swiss midlands: Results of a 10-year field survey. *Geomorphology* **2011**, *126*, 32–41. [[CrossRef](#)]

10. Hoper, H.; Meesenburg, H. Tagungsband 20 Jahre Bodendauerbeobachtung in Niedersachsen. *GeoBerichte* **2012**, *23*, 6–18.
11. Poreba, G.J. Caesium-137 as a soil erosion tracer: A review. *Geochronometria* **2006**, *25*, 37–46.
12. Vandekerckhove, L.; Arnoldussen, A.; Bazzoffi, P.; Böken, H.; Castillo, V.; Crescimanno, G.; Düwel, O.; Esteve, J.F.; Imeson, A.; Jarman, R.; et al. Working Group on Soil Erosion Task Group III on Impacts of Soil Erosion. Available online: [http://s3.amazonaws.com/academia.edu.documents/40429096/finalreporttg3.pdf?AWSAccessKeyId=AKIAJ56TQJRTWSMTNPEA&Expires=1483088793&Signature=mO3jNVZxvex1o3slqWwMgAc7fDQ%3D&response-content-disposition=inline%3B%20filename%3DWorking\\_Group\\_on\\_Soil\\_Erosion\\_Task\\_Group.pdf](http://s3.amazonaws.com/academia.edu.documents/40429096/finalreporttg3.pdf?AWSAccessKeyId=AKIAJ56TQJRTWSMTNPEA&Expires=1483088793&Signature=mO3jNVZxvex1o3slqWwMgAc7fDQ%3D&response-content-disposition=inline%3B%20filename%3DWorking_Group_on_Soil_Erosion_Task_Group.pdf) (accessed on 30 December 2016).
13. Vrieling, A. Satellite remote sensing for water erosion assessment: A review. *Catena* **2006**, *65*, 2–18. [[CrossRef](#)]
14. Shoshany, M.; Goldshleger, N.; Chudnovsky, A. Monitoring of agricultural soil degradation by remote-sensing methods: A review. *Int. J. Remote Sens.* **2013**, *34*, 6152–6181. [[CrossRef](#)]
15. Demattê, J.A.M.; Morgan, C.L.S.; Chabrilat, S.; Rizzo, R.; Franceschini, M.H.D.; Terra, F.D.; Vasques, G.M.; Wetterlind, J. Spectral sensing from ground to space in soil science: State of the art, applications, potential and perspectives. In *Land Resources Monitoring, Modeling, and Mapping with Remote Sensing*; Thenkabail, P.S., Ed.; CRC Press: Boca Raton, FL, USA, 2015; pp. 661–732.
16. Li, X.; Wu, T.; Liu, K.; Li, Y.; Zhang, L. Evaluation of the Chinese fine spatial resolution hyperspectral satellite TianGong-1 in urban land-cover classification. *Remote Sens.* **2016**, *8*, 438. [[CrossRef](#)]
17. Vrieling, A. *Mapping Erosion from Space*; Wageningen University: Wageningen, The Netherlands, 2007.
18. Luleva, M.I. Tracing Soil Particle Movement. Towards A Spectral Approach to Spatial Monitoring of Soil Erosion. Ph.D. Dissertation, University of Twente, Enschede, The Netherlands, 2013.
19. Fadul, H.M.; Salih, A.A.; Ali, I.A.; Inanaga, S. Use of remote sensing to map gully erosion along the Atbara River, Sudan. *Int. J. Appl. Earth Obs. Geoinf.* **1999**, *1*, 175–180. [[CrossRef](#)]
20. Fulajtár, E. Identification of severely eroded soils from remote sensing data tested in Riš ň ovce, Slovakia. In *Sustaining the Global Farm. Selected Papers from the 10th International Soil Conservation Organization Meeting, Held 24–29 May 1999*; Stott, D.E., Mohtar, R.H., Steinhardt, G.C., Eds.; Purdue University and the USDA-ARS National Soil Erosion Research Laboratory: West Lafayette, Indiana, 2001; pp. 1075–1081.
21. Šarapatka, B.; Netopil, P. Erosion processes on intensively farmed land in the Czech Republic: Comparison of alternative research methods. In *Proceedings of the 2010 19th World Congress of Soil Science, Soil Solutions for a Changing World, Brisbane, Australia, 1–6 August 2010*; pp. 47–50.
22. Kolejka, J.; Manakos, J. Integrate dat DPZ a GIS při identifikaci erozního poškození půdy. In *Sborník Příspěvků z Konference s Mezinárodní Účastí. GIS . . . Ostrava 2000*; VŠB: Ostrava, Czech Republic, 2000; p. 15.
23. Alatorre, L.C.; Beguería, S. Identification of eroded areas using remote sensing in a badlands landscape on marls in the central Spanish Pyrenees. *Catena* **2009**, *76*, 182–190. [[CrossRef](#)]
24. Mohammadi, T.A.; Nikkani, D. Methodologies of preparing erosion features map by using RS and GIS. *Int. J. Sediment Res.* **2008**, *23*, 130–137. [[CrossRef](#)]
25. Martínez-Casasnovas, J.A. A spatial information technology approach for the mapping and quantification of gully erosion. *Catena* **2003**, *50*, 293–308. [[CrossRef](#)]
26. Warner, T.; Foody, G.; Nellis, M. Remote sensing of soils. *Remote Sens. Soils* **2014**, *1*, 1–71.
27. Gholizadeh, A.; Luboš, B.; Saberioon, M.; Vašát, R. Visible, near-infrared, and mid-infrared spectroscopy applications for soil assessment with emphasis on soil organic matter content and quality: State-of-the-art and key issues. *Appl. Spectrosc.* **2013**, *67*, 1349–1362. [[CrossRef](#)] [[PubMed](#)]
28. Demattê, J.A.M.; Focht, D. Detecção de solos erodidos pela avaliação de dados espectrais. Detection of soil erosion by spectral reflectance. *Braz. J. Soil Sci.* **1999**, *3*, 401–413.
29. Schmid, T.; Palacios-Orueta, A.; Chabrilat, S.; Bendor, E.; Plaza, A.; Rodriguez, M.; Huesca, M.; Pelayo, M.; Pascual, C.; Escribano, P.; et al. Spectral characterisation of land surface composition to determine soil erosion within semiarid rainfed cultivated areas. In *Proceedings of the 2012 IEEE International Geoscience and Remote Sensing Symposium, Munich, Germany, 22–27 July 2012*; pp. 7082–7085.
30. Schmid, T.; Rodriguez-Rastrero, M.; Escribano, P.; Palacios-Orueta, A.; Ben-Dor, E.; Plaza, A.; Milewski, R.; Huesca, M.; Bracken, A.; Cicuendez, V.; et al. Characterization of soil erosion indicators using hyperspectral data from a Mediterranean rainfed cultivated region. *IEEE J. Sel. Top. Appl. Earth Obs. Remote Sens.* **2016**, *9*, 845–860. [[CrossRef](#)]

31. Lin, C.; Zhou, S.; Wu, S.; Zhu, Q.; Dang, Q. Spectral response of different eroded soils in subtropical china: A case study in Changting County, China. *J. Mt. Sci.* **2014**, *11*, 697–707. [[CrossRef](#)]
32. Conforti, M.; Buttafuoco, G.; Leone, A.P.; Aucelli, P.P.C.; Robustelli, G.; Scarciglia, F. Studying the relationship between water-induced soil erosion and soil organic matter using VIS-NIR spectroscopy and geomorphological analysis: A case study in southern Italy. *Catena* **2013**, *110*, 44–58. [[CrossRef](#)]
33. Chabrilat, S.; Milewski, R.; Schmid, T.; Rodriguez, M.; Escibano, P.; Pelayo, M.; Palacios-Orueta, A. Potential of hyperspectral imagery for the spatial assessment of soil erosion stages in agricultural semi-arid Spain at different scales. In Proceedings of the 2014 IEEE Geoscience and Remote Sensing Symposium, Quebec City, QC, Canada, 13–18 July 2014; pp. 2918–2921.
34. Chappell, A.; Zobeck, T.M.; Brunner, G. Using on-nadir spectral reflectance to detect soil surface changes induced by simulated rainfall and wind tunnel abrasion. *Earth Surf. Process. Landf.* **2005**, *30*, 489–511. [[CrossRef](#)]
35. Viscarra Rossel, R.A.; Behrens, T.; Ben-Dor, E.; Brown, D.J.; Demattê, J.A.M.; Shepherd, K.D.; Shi, Z.; Stenberg, B.; Stevens, A.; Adamchuk, V.; et al. A global spectral library to characterize the world's soil. *Earth Sci. Rev.* **2016**, *155*, 198–230. [[CrossRef](#)]
36. Ben-Dor, E.; Demattê, J.A.M. Remote sensing of soil in the optical domains. In *Land Resources Monitoring, Modeling, and Mapping with Remote Sensing*; Thenkabail, P.S., Ed.; CRC Press: Boca Raton, FL, USA, 2015; pp. 733–787.
37. Nocita, M.; Stevens, A.; Van Wesemael, B.; Aitkenhead, M.; Bachmann, M.; Barth, B.; Csorba, A.; Dardenne, P.; Demattê, J.A.M.; Genot, V. Soil spectroscopy: An alternative to wet chemistry for soil monitoring. *Adv. Agron.* **2015**, *132*, 1–21.
38. Ben-Dor, E.; Irons, J.R.; Epema, G.F. Soil reflectance. In *Manual of Remote Sensing: Remote Sensing for Earth Science*; Rencz, A.N., Ryerson, R.A., Eds.; John Wiley & Sons: Hoboken, NJ, USA, 1999; Volume 3, pp. 111–187.
39. Stenberg, B.; Viscarra Rossel, R.A.; Mouazen, A.M.; Wetterlind, J. Visible and near infrared spectroscopy in soil science. In *Advances in Agronomy*; Academic Press: Cambridge, MA, USA, 2010; Volume 107, pp. 163–215.
40. Chabrilat, S.; Ben-Dor, E.; Rossel, R.A.V.; Dematt, J.A.M. Quantitative soil spectroscopy. *Appl. Environ. Soil Sci.* **2013**, *2013*, 4–6. [[CrossRef](#)]
41. Chabrilat, S. Land Degradation Indicators: Spectral indices. *Ann. Arid Zone* **2006**, *45*, 331–354.
42. Hill, J.; Schütt, B. Mapping complex patterns of erosion and stability in dry mediterranean ecosystems. *Remote Sens. Environ.* **2000**, *74*, 557–569. [[CrossRef](#)]
43. Schmid, T.; Koch, M.; Gumuzzio, J.; Medel, I. Field and Imaging spectroscopy to determine soil degradation stages in semi-arid terrestrial ecosystems. In Proceedings of the 4th EARSeL Workshop on Imaging Spectroscopy. New Quality in Environmental Studies, Warsaw, Poland, 26–29 April 2005; Zagajewski, B., Sobczak, M., Wrzesien, M., Eds.; EARSeL and Warsaw University: Warsaw, Poland, 2005.
44. Mathieu, R.; Cervelle, B.; Rémy, D.; Pouget, M. Field-based and spectral indicators for soil erosion mapping in semi-arid mediterranean environments (Coastal Cordillera of central Chile). *Earth Surf. Process. Landf.* **2007**, *32*, 13–31. [[CrossRef](#)]
45. Lin, C.; Zhou, S.L.; Wu, S.H. Using hyperspectral reflectance to detect different soil erosion status in the Subtropical Hilly Region of Southern China: A case study of Changting, Fujian Province. *Environ. Earth Sci.* **2013**, *70*, 1661–1670. [[CrossRef](#)]
46. Ben-Dor, E.; Chabrilat, S.; Demattê, J.A.M.; Taylor, G.R.; Hill, J.; Whiting, M.L.; Sommer, S. Using Imaging Spectroscopy to study soil properties. *Remote Sens. Environ.* **2009**, *113*, S38–S55. [[CrossRef](#)]
47. Haubrock, S.; Chabrilat, S.; Kaufmann, H. Application of hyperspectral imaging and laser scanning for the monitoring and assessment of soil erosion in a recultivation mining area. In *Remote Sensing and GIS for Environmental Studies: Applications in Geography*; Erasmi, S., Cyffka, B., Kappas, M., Eds.; Göttinger Geographische Abhandlungen: Göttingen, Germany, 2004; pp. 230–237.
48. Haubrock, S.; Chabrilat, S.; Kaufmann, H. Application of hyperspectral imaging for the quantification of surface soil moisture. In Proceedings of the 4th EARSeL Workshop on Imaging Spectroscopy. New Quality in Environmental Studies, Warsaw, Poland, 26–29 April 2005; Zagajewski, B., Sobczak, M., Wrzesień, M., Eds.; EARSeL and Warsaw University: Warsaw, Poland, 2005; pp. 163–171.
49. Chabrilat, S.; Kaufmann, H.; Merz, B.; Mueller, A.; Bens, O.; Lemmnitz, C. Development of relationships between reflectance and erosion modelling: Test site preliminary field spectral analysis. In Proceedings of the 3rd EARSeL Workshop on Imaging Spectroscopy, Herrsching, Germany, 13–16 May 2003; pp. 13–16.

50. Ben-Dor, E.; Goldshleger, N.; Braun, O.; Kindel, B.; Goetz, A.F.H.; Bonfil, D.; Margalit, N.; Binaymini, Y.; Karnieli, A.; Agassi, M. Monitoring infiltration rates in semiarid soils using airborne hyperspectral technology. *Int. J. Remote Sens.* **2004**, *25*, 2607–2624. [[CrossRef](#)]
51. Hill, J.; Mehl, W.; Altherr, M. Land degradation and soil erosion mapping in a Mediterranean ecosystem. In *Imaging Spectrometry—A Tool for Environmental Observations*; Hill, J., Mégier, J., Eds.; Kluwer Academic Publishers: Dordrecht, The Netherlands, 1994; pp. 237–260.
52. Hill, J.; Mégier, J.; Mehl, W. Land degradation, soil erosion and desertification monitoring in Mediterranean ecosystems. *Remote Sens. Rev.* **1995**, *12*, 107–130. [[CrossRef](#)]
53. Zádorová, T.; Penížek, V.; Šefrna, L.; Drábek, O.; Mihaljevič, M.; Volf, Š.; Chuman, T. Identification of Neolithic to Modern erosion-sedimentation phases using geochemical approach in a loess covered sub-catchment of South Moravia, Czech Republic. *Geoderma* **2013**, *195–196*, 56–69. [[CrossRef](#)]
54. Hanuš, J.; Fabiánek, T.; Kaplan, V.; Homolová, L. Flying Laboratory of Imaging Systems (FLIS) at CzechGlobe. In *Proceedings of the SGEM2014 Conference Proceedings*, Albena, Bulgaria, 7–26 June 2014; STEF92 Technology: Sofia, Bulgaria, 2014; pp. 177–182.
55. Hanuš, J.; Fabiánek, T.; Fajmon, L. Potential of airborne imaging spectroscopy at Czechglobe. In *The International Archives of the Photogrammetry, Remote Sensing and Spatial Information Sciences*; World Forensic Festival: Prague, Czech Republic, 2016; Volume XLI-B1, pp. 15–17.
56. R Core Team. *R: A Language and Environment for Statistical Computing*; R Foundation for Statistical Computing: Vienna, Austria, 2016.
57. Minasny, B.; McBratney, A.B. A conditioned Latin hypercube method for sampling in the presence of ancillary information. *Comput. Geosci.* **2006**, *32*, 1378–1388. [[CrossRef](#)]
58. Tamm, O. Eine Methode zur Bestimmung der anorganischen Komponenten des Gelkomplexes in Boden. *Medd. Från Statens Skogförsöksanstalt* **1922**, *19*, 385–404.
59. Coffin, D.E. A method for the determination of free iron in soils and clays. *Can. J. Soil Sci.* **1963**, *43*, 7–17. [[CrossRef](#)]
60. Savitzky, A.; Golay, M.J.E. Smoothing and differentiation of data by simplified least squares procedures. *Anal. Chem.* **1964**, *36*, 1627–1639. [[CrossRef](#)]
61. Stevens, A.; Ramirez-Lopez, L. An Introduction to the Prospectr Package 2013. Available online: [https://www.researchgate.net/publication/255941339\\_An\\_introduction\\_to\\_the\\_prospectr\\_package](https://www.researchgate.net/publication/255941339_An_introduction_to_the_prospectr_package) (accessed on 30 December 2016).
62. Kuhn, M.; Wing, J.; Weston, S.; Williams, A.; Keefer, C.; Engelhardt, A.; Cooper, T.; Mayer, Z.; Kenkel, B.; Benesty, M.; et al. caret: Classification and Regression Training. Available online: <http://adsabs.harvard.edu/abs/2015ascl.soft05003K> (accessed on 30 December 2016).
63. Wold, S.; Sjöström, M.; Eriksson, L. PLS-regression: A basic tool of chemometrics. *Chemom. Intell. Lab. Syst.* **2001**, *58*, 109–130. [[CrossRef](#)]
64. Vapnik, V.N. *The Nature of Statistical Learning Theory*; Springer: New York, NY, USA, 1995.
65. Schölkopf, B.; Smola, A.J. *Learning with Kernels: Support Vector Machines, Regularization, Optimization, and Beyond*; MIT Press: Cambridge, MA, USA, 2001.
66. Cristianini, N.; Shawe-Taylor, J. *An Introduction to Support Vector Machines: And Other Kernel-Based Learning Methods*; Cambridge University Press: New York, NY, USA, 2000.
67. Breiman, L. Random Forests. *Mach. Learn.* **2001**, *45*, 5–32. [[CrossRef](#)]
68. Behrens, T.; Förster, H.; Scholten, T.; Steinrücken, U.; Spies, E.-D.; Goldschmitt, M. Digital soil mapping using artificial neural networks. *J. Plant Nutr. Soil Sci.* **2005**, *168*, 21–33. [[CrossRef](#)]
69. Heung, B.; Ho, H.C.; Zhang, J.; Knudby, A.; Bulmer, C.E.; Schmidt, M.G. An overview and comparison of machine-learning techniques for classification purposes in digital soil mapping. *Geoderma* **2016**, *265*, 62–77. [[CrossRef](#)]
70. Vasques, G.M.; Grunwald, S.; Sickman, J.O. Comparison of multivariate methods for inferential modeling of soil carbon using visible/near-infrared spectra. *Geoderma* **2008**, *146*, 14–25. [[CrossRef](#)]
71. Zádorová, T.; Penížek, V.; Vašát, R.; Žížala, D.; Chuman, T.; Vaněk, A. Colluvial soils as a soil organic carbon pool in different soil regions. *Geoderma* **2015**, *253–254*, 122–134. [[CrossRef](#)]
72. Zádorová, T.; Žížala, D.; Penížek, V.; Čejková, Š. Relating extent of colluvial soils to topographic derivatives and soil variables in a Luvisol Sub-Catchment, Central Bohemia, Czech Republic. *Soil Water Res.* **2014**, *9*, 47–57.

73. Brodský, L.; Zádorová, T.; Klement, A.; Jakšík, O.; Borůvka, L. Utilization of VNIR diffuse reflectance spectroscopy to map soil erosion Study on two arable fields. In *The Second Global Workshop on Proximal Soil Sensing*; Adamchuk, V.I., Viscarra Rossel, R.A., Eds.; McGill University: Montreal, QC, Canada, 2011; pp. 84–87.
74. Bezdek, J.C.; Ehrlich, R.; Full, W. FCM: The fuzzy c-means clustering algorithm. *Comput. Geosci.* **1984**, *10*, 191–203. [[CrossRef](#)]
75. Dimitriadou, E.; Hornik, K.; Leisch, F.; Meyer, D.; Weingessel, A. e1071: Misc Functions of the Department of Statistics (e1071), TU Wien. Available online: <https://www.r-project.org/> (accessed on 30 December 2016).
76. Stevens, A.; Miralles, I.; van Wesemael, B. Soil Organic Carbon Predictions by Airborne Imaging Spectroscopy: Comparing Cross-Validation and Validation. *Soil Sci. Soc. Am. J.* **2012**, *76*, 2174. [[CrossRef](#)]
77. Denis, A.; Stevens, A.; van Wesemael, B.; Udelhoven, T.; Tychon, B. Soil organic carbon assessment by field and airborne spectrometry in bare croplands: Accounting for soil surface roughness. *Geoderma* **2014**, *226–227*, 94–102. [[CrossRef](#)]
78. Hbirkou, C.; Pätzold, S.; Mahlein, A.K.; Welp, G. Airborne hyperspectral imaging of spatial soil organic carbon heterogeneity at the field-scale. *Geoderma* **2012**, *175–176*, 21–28. [[CrossRef](#)]
79. Hively, W.D.; McCarty, G.W.; Reeves, J.B.; Lang, M.W.; Oesterling, R.A.; Delwiche, S.R. Use of airborne hyperspectral imagery to map soil properties in tilled agricultural fields. *Appl. Environ. Soil Sci.* **2011**, *2011*, 1–13. [[CrossRef](#)]
80. Casa, R.; Castaldi, F.; Pascucci, S.; Palombo, A.; Pignatti, S. A comparison of sensor resolution and calibration strategies for soil texture estimation from hyperspectral remote sensing. *Geoderma* **2013**, *197–198*, 17–26. [[CrossRef](#)]
81. Garfagnoli, F.; Ciampalini, A.; Moretti, S.; Chiarantini, L. Mapping of soil properties from hyperspectral remote sensing: The DIGISOIL strategy for soil processes modelling. In *Geophysical Research Abstracts*; EGU: Wien, Austria, 2011; Volume 13, p. 7120.
82. Gerighausen, H.; Menz, G.; Kaufmann, H. Spatially explicit estimation of clay and organic carbon content in agricultural soils using multi-annual imaging spectroscopy data. *Appl. Environ. Soil Sci.* **2012**, *2012*, 868090. [[CrossRef](#)]
83. Gomez, C.; Lagacherie, P.; Coulouma, G. Continuum removal versus PLSR method for clay and calcium carbonate content estimation from laboratory and airborne hyperspectral measurements. *Geoderma* **2008**, *148*, 141–148. [[CrossRef](#)]
84. Gomez, C.; Lagacherie, P.; Coulouma, G. Regional predictions of eight common soil properties and their spatial structures from hyperspectral VIS-NIR data. *Geoderma* **2012**, *189–190*, 176–185. [[CrossRef](#)]
85. Selige, T.; Böhner, J.; Schmidhalter, U. High resolution topsoil mapping using hyperspectral image and field data in multivariate regression modeling procedures. *Geoderma* **2006**, *136*, 235–244. [[CrossRef](#)]
86. Bartholomeus, H.; Epema, G.; Schaepman, M. Determining iron content in Mediterranean soils in partly vegetated areas, using spectral reflectance and imaging spectroscopy. *Int. J. Appl. Earth Obs. Geoinf.* **2007**, *9*, 194–203. [[CrossRef](#)]
87. Lagacherie, P.; Baret, F.; Feret, J.B.; Madeira Netto, J.; Robbez-Masson, J.M. Estimation of soil clay and calcium carbonate using laboratory, field and airborne hyperspectral measurements. *Remote Sens. Environ.* **2008**, *112*, 825–835. [[CrossRef](#)]
88. Nocita, M.; Stevens, A.; Noon, C.; van Wesemael, B. Prediction of soil organic carbon for different levels of soil moisture using VIS-NIR spectroscopy. *Geoderma* **2013**, *199*, 37–42. [[CrossRef](#)]
89. Ballabio, C.; Panagos, P.; Montanarella, L. Predicting soil organic carbon content in Cyprus using remote sensing and earth observation data. *Proc. SPIE* **2014**, *9229*, 9229-0–9229-9.
90. Stevens, A.; Udelhoven, T.; Denis, A.; Tychon, B.; Liou, R.; Hoffmann, L.; van Wesemael, B. Measuring soil organic carbon in croplands at regional scale using airborne imaging spectroscopy. *Geoderma* **2010**, *158*, 32–45. [[CrossRef](#)]
91. Tiwari, S.K.; Saha, S.K.; Kumar, S. Prediction Modeling and mapping of soil carbon content using artificial neural network, hyperspectral satellite data and field spectroscopy. *Adv. Remote Sens.* **2015**, *4*, 63–72. [[CrossRef](#)]
92. Viscarra Rossel, R.A.; Behrens, T. Using data mining to model and interpret soil diffuse reflectance spectra. *Geoderma* **2010**, *158*, 46–54. [[CrossRef](#)]

93. Kodešová, R.; Vignozzi, N.; Rohošková, M.; Hájková, T.; Kočárek, M.; Pagliai, M.; Kozák, J.; Šimůnek, J. Impact of varying soil structure on transport processes in different diagnostic horizons of three soil types. *J. Contam. Hydrol.* **2009**, *104*, 107–125. [[CrossRef](#)] [[PubMed](#)]
94. Zádorová, T.; Penížek, V.; Šefrna, L.; Rohošková, M.; Borůvka, L. Spatial delineation of organic carbon-rich Colluvial soils in Chernozem regions by Terrain analysis and fuzzy classification. *Catena* **2011**, *85*, 22–33. [[CrossRef](#)]
95. Hu, Y.; Fister, W.; Kuhn, N. Temporal variation of SOC enrichment from interrill erosion over prolonged rainfall simulations. *Agriculture* **2013**, *3*, 726–740. [[CrossRef](#)]
96. Müller-Nedebock, D.; Chaplot, V. Soil carbon losses by sheet erosion: A potentially critical contribution to the global carbon cycle. *Earth Surf. Process. Landf.* **2015**, 3758. [[CrossRef](#)]
97. Chaplot, V.; Abdalla, K.; Alexis, M.; Bourennane, H.; Darboux, F.; Dlamini, P.; Everson, C.; Mchunu, C.; Muller-Nedebock, D.; Mutema, M.; et al. Surface organic carbon enrichment to explain greater CO<sub>2</sub> emissions from short-term no-tilled soils. *Agric. Ecosyst. Environ.* **2015**, *203*, 110–118. [[CrossRef](#)]
98. Schmitt, A.; Rodzik, J.; Zgłobicki, W.; Russok, C.; Dotterweich, M.; Bork, H.R. Time and scale of gully erosion in the Jedliczny Dol gully system, south-east Poland. *Catena* **2006**, *68*, 124–132. [[CrossRef](#)]
99. Terhorst, B. The influence of pleistocene landforms on soil-forming processes and soil distribution in a loess landscape of Baden-Wurttemberg (south-west Germany). *Catena* **2000**, *41*, 165–179. [[CrossRef](#)]



© 2017 by the authors; licensee MDPI, Basel, Switzerland. This article is an open access article distributed under the terms and conditions of the Creative Commons Attribution (CC-BY) license (<http://creativecommons.org/licenses/by/4.0/>).

## 5.2 Soil organic carbon and texture retrieving and mapping using proximal, airborne and Sentinel-2 spectral imaging

---

- Gholizadeh, A., **Žižala, D.**, Saberioon, M., Borůvka, L. (a.d.) Soil organic carbon and texture retrieving and mapping using proximal, airborne and Sentinel-2 spectral imaging. *Remote sensing of environment* – v recenzním řízení.

# Soil organic carbon and texture retrieving and mapping using proximal, airborne and Sentinel-2 spectral imaging

Asa Gholizadeh<sup>a,\*</sup>, Daniel Žižala<sup>a,b</sup>, Mohammadmehdi Saberioon<sup>c</sup>, Luboš Borůvka<sup>a</sup>

<sup>a</sup>*Department of Soil Science and Soil Protection, Faculty of Agrobiolgy, Food and Natural Resources, Czech University of Life Sciences, 16521 Prague, Czech Republic*

<sup>b</sup>*Research Institute for Soil and Water Conservation, 15627 Prague, Czech Republic*

<sup>c</sup>*Institute of Complex Systems, South Bohemian Research Centre of Aquaculture and Biodiversity of Hydrocenoses, Faculty of Fisheries and Protection of Waters, University of South Bohemia in České Budejovice, 37333 Nové Hradky, Czech Republic*

\*Correspondence E-mail: gholizadeh@af.czu.cz

## ABSTRACT

Soil Organic Carbon (SOC) is a useful representative of soil fertility and an essential parameter in controlling the soil dynamics of various agrochemicals. Soil texture is also used to calculate soil ability to maintain water for plant growth. SOC and soil texture are important parameters of agricultural soils and need to be monitored. Optical satellite remote sensing is a well-suited technique for surveying large areas and monitoring soil attributes at a high spatial and temporal interval. The recently-operated Sentinel-2 freely provides the possibility of useful and routine land observation with the combination of high resolution, novel spectral capabilities and wide coverage. This study examined the capability of Sentinel-2 in SOC, clay, silt and sand monitoring and digital mapping to compare to the results obtained from airborne hyperspectral and lab spectroscopy over the bare soils of four agricultural sites in the Czech Republic. Soil samples were scanned with an ASD FieldSpec spectroradiometer in the laboratory. Hyperspectral data from CASI/SASI sensors were also acquired over the study areas. Smoothing, pre-processing, modelling, validation and final prediction performance assessment of the datasets were determined. Two cloud-free Sentinel-2 images were atmospherically corrected and resampled. Combination of 10 extracted bands of the Sentinel-2 and 18 spectral indices as independent variables were used to train the model. Prediction models of the soil attributes were developed and validated. Additionally spatial distribution maps of the attributes were produced. The results showed that the prediction accuracy based on lab spectroscopy, CASI/SASI airborne and Sentinel-2 in the majority of the sites was adequate for SOC and fair for clay. However, the Sentinel-2 capability was not satisfactory for silt and sand assessment. Comparing the SOC and clay maps derived from the airborne and spaceborne datasets showed a relatively similar trend at both platforms. The SOC maps confirmed that in areas with high levels of SOC, Sentinel-2 was able to create the SOC map even more precisely than the airborne sensors. In general, Sentinel-2 showed a slight decrease of model performances compared to lab spectroscopy and airborne imagery, but it offers large spatial coverage and more frequent revisit-time, which will considerably influence obtainment of high-quality soil data.

**Keywords:** Agricultural soil; Spectroscopy; Hyperspectral data; Superspectral sensor; Digital soil mapping.

## 1. Introduction



Understanding variability of soil attributes allows the improvement of environmental and agricultural management as well as a more effective usage of resources. The qualitative information of available soil maps is often not adequate for site-specific management of water and fertilizers (Castaldi et al., 2016). For these purposes, the quantitative assessment and mapping of important soil attributes such as soil texture, Soil Organic Carbon (SOC), soil Nitrogen (N) and soil Moisture Content (MC) over the field is essential.

The emersion of proximal and remote sensing techniques has been documented as efficient detection methods for assessing and mapping soil attributes (Ben-Dor et al., 2002a; Viscarra Rossel et al., 2006). Proximal sensing is defined as the use of different sensors to obtain signals from the object when the sensor's receiver is in contact with or close to (within 2 m) the object (Viscarra Rossel et al., 2010). However, remote sensing has been explained as using electromagnetic radiation in order to acquire information about an object or phenomenon without physical contact (Elachi and Van Zyl, 2006). The spectral resolution of the aforementioned optical sensors largely depend on the numbers, sampling and position of bands. The multispectral sensors offer 3 to 7 bands, the superspectral sensors offer 7 to 20 bands, the hyperspectral sensors offer from 20 to 500 bands and the ultraspectral sensors offer more than 1000 bands. Laboratory Visible-Near Infrared-Short Wave Infrared (VIS-NIR-SWIR) spectroscopy using ultraspectral sensors proved to be a suitable alternative substitute for conventional laboratory analysis of soil chemical parameters including SOC (Ji et al., 2015), N, Phosphorus (P), Potassium (K), Cation Exchange Capacity (CEC), pH (Viscarra Rossel et al., 2006) and some physical parameters such as soil structure, bulk density and texture (Bellon-Maurel et al., 2010; Gholizadeh et al., 2014). Several researchers have also studied the potential of hyperspectral airborne sensors to attain quantitative assessment of soil parameters. Some have used the HyMap sensor to predict SOC content

(Selige et al., 2006) and soil texture (Gomez et al., 2008). For this purpose, other hyperspectral airborne sensors such as DAIS-7915 (Ben-Dor et al., 2002b), AHS-160 (Stevens et al., 2010), MIVIS (Casa et al., 2013), CASI and SASI (Zizala et al., 2017) have also been employed.

The application of multispectral and superspectral satellite remote sensing data into soil monitoring and digital mapping have advantages over proximal and airborne hyperspectral remote sensing including improvement of Signal to Noise Ratio (SNR), availability of high-quality temporal images, comprehensive monitoring of large-scale sites, better classification of results and data reduction (Gianinetto and Lechi, 2004; Yokoya et al., 2016). Over the last several years, analysis of data obtained from optical spaceborne techniques derived from various hyperspectral, multispectral and superspectral sensor imagery has proven to be an efficient way to assess surface soil characteristics (Castaldi et al., 2016; Danoedoro and Zukhrufiyati, 2015; Gomez et al., 2018; Vagen et al., 2016; Zhang et al., 2013). The large frequent data streams provided by spaceborne sensors enables the development of soil monitoring and mapping techniques from the local to the regional scale in an effective, fast, frequent and economical way for vast areas (Berger et al., 2012; Malenovsky et al., 2012). However, the use of satellite data in quantitative soil estimation is still challenging due to considerable limitations of some of these sensors. For example, Hyperion data suffer due to the very low SNR in the SWIR region especially around 2200 nm, where the spectral features of clay minerals are located (Castaldi et al., 2016) or Landsat-8 has low temporal resolution that brings inefficiency with regard to providing optimal acquisition time images and time-series studies (Immitzer et al., 2016).

The recently-operated European Space Agency (ESA) superspectral Sentinel-2A was successfully launched on 23 June, 2015. Sentinel-2 offers exceptional perspectives on land

with a combination of wide coverage (swath width of 290 km), spatial resolution (10-60 m), and minimum five-day global revisit-time (with twin satellites in orbit) (Drusch et al., 2012; Immitzer et al., 2016). Sentinel-2 produces useful information for a wide range of land applications (Malenovsky et al., 2012). Some simulation studies have been conducted to explore the potential of Sentinel-2 for a variety of land surface parameter estimations. For instance, Van der Meer et al. (2014) assessed the potential of Sentinel-2 for geological mapping by simulating a dataset from HyMap airborne hyperspectral image using Sentinel-2 band characteristics. They confirmed the capability of Sentinel-2 for presenting data endurance for ASTER in terms of generating reproducible and consistent data, which can differentiate surface mineralogy. Mielke et al. (2014) studied the potential of OLI, synthesized Sentinel-2 and then synthesized EnMap data for mapping the mining areas. They proved that these data had potential for soil monitoring and mapping. However, these findings need to be confirmed by real data. Castaldi et al., (2016) used simulated Sentinel-2 data to estimate and compare SOC and soil texture prediction models with Hyperion, HypsIRI, EnMAP, PRISMA, Landsat-8 and ALI retrieved models. They showed that Sentinel-2, Hyperion and Landsat-8 provided higher accuracies than the other sensors. The experiment conducted by Van der Werff and Van der Meer (2016) in southeast Spain was a pioneering study in terms of using Sentinel-2 actual data, which showed that the Sentinel-2 mission could provide data continuity for Landsat-8 OLI, when exploring mineralogy at the Earth's surface.

Clearly, using Sentinel-2 real data requires to be expended in order to prove its capability for various soil attributes monitoring and mapping worldwide. To this end, the main objectives of the current study on the superspectral Sentinel-2 actual data for soil parameters prediction and mapping in central Europe are assessment of Sentinel-2 capability in SOC and soil

texture monitoring and mapping and comparison of the accuracy of the spaceborne results with results obtained from other domains, laboratory spectroscopy and airborne hyperspectral. We strongly expect that this direction will pave the way for using remote sensing technology from orbit for frequently monitoring soil properties over vast areas.

## **2. Materials and methods**

### *2.1. Study sites*

Four study sites, Přestavlky, 0.73 km<sup>2</sup> (49°51' N; 14°44' E), Šardice, 1.76 km<sup>2</sup> (48°56' N; 17°1' E), Nová Ves, 1.17 km<sup>2</sup> (50°31' N; 15°24' E) and Jičín, 0.93 km<sup>2</sup> (50°21' N; 15°15' E), demonstrate the most extensive soil units of agricultural lands in the Czech Republic and were chosen for this study (Figure 1). The areas are primarily rural and devoted to winter and spring cereals, oilseed rape, maize and potatoes. The selected sites were representative of soilscapes, which were homogenous and similar in terms of terrain characteristics, land management and the climatic conditions (Buol et al., 1973; Schmidt et al., 2010). They were also characterized by dissected relief with side valleys, toe-slopes, plateaus and back-slopes. Land management included long-term tillage, no conservation practices, plough depth of 25 cm and 5 to 6 courses rotation based on the Norfolk system.

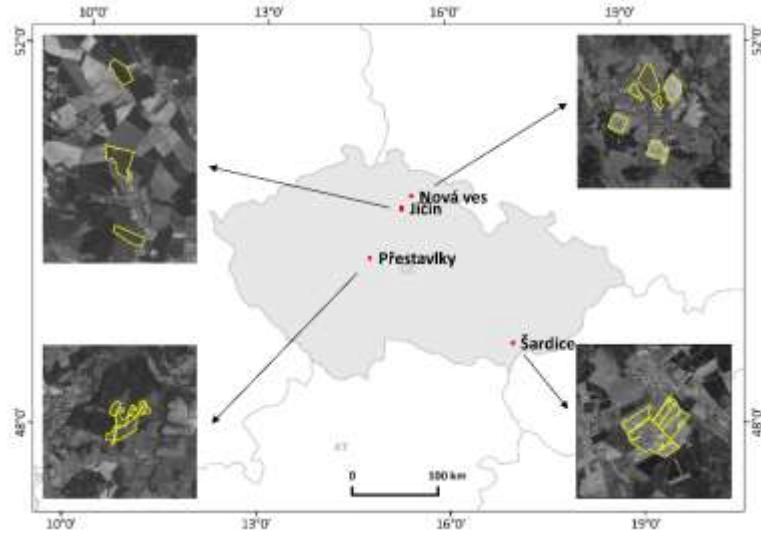


**Figure 1.** Location of the study areas (yellow borders)

According to the World Reference Base (WRB) for soil resources (IUSS Working Group WRB, 2014), soils of these regions were characterized mainly as Chernozems and Luvisols on loess, Cambisols and Stagnosols on crystalline and sedimentary rocks. Table 1 shows the study sites and data collection details.

**Table 1.** Study sites and data collection details

Site	Area (km <sup>2</sup> )	Dominant Soil Unit	Parent Material	Samples (no.)	Soil Sampling	Airborne Imaging	Superspectral Sentinel-2
Přestavlky	0.73	Haplic Stagnosol, Haplic and Stagnic Cambisol, Leptosol	Complex of Proterozoic and Paleozoic rocks (schist, granodiorite)	50	6.11.2015	7.5.2015	27.3.2016
Šardice	1.76	Calcic Chernozem	Pleistocene loess	50	6.4.2016	21.9.2015	27.3.2016
Nová Ves	1.17	Haplic Cambisol	Permian-Carboniferous rocks (sandstone, siltstone)	50	26.5.2016	22.4.2016	6.5.2016
Jičín	0.93	Luvisol, Albic Luvisol, Luvic Chernozem	Pleistocene loess	50	5.5.2016	22.4.2016	6.5.2016

## 2.2. Ground sampling and soil measurements

Two-hundred soil samples were collected using conditioned Latin Hypercube Sampling (cLHS) stratified random strategy (Minasny and McBratney, 2006). Regarding field size and

the chosen sampling and analysing algorithms (Kuang and Mouazen, 2012; Ramirez Lopez et al., 2014), the selected sample size had sufficient coverage of the predictor space and was a suitable indicator for the population in which the models were applied. The position of each sampling point was recorded by a GeoXM (Trimble Inc., Sunnyvale, California, USA) receiver with accuracy of 1 m. The soil samples were taken at 0-10 cm depth as composite samples over an area of 6 x 6 m, air-dried, ground and sieved ( $\leq 2$  mm) and thoroughly mixed before analyzing (ISO 11464:2006). SOC was measured as total oxidized carbon using wet oxidation (ISO 14235:1998). Additionally, soil particle size distribution was obtained by the pipette method (ISO 11277:2009).

### *2.3. Laboratory reflectance measurements*

Spectral reflectance was calculated across the 350-2500 nm wavelength range using an ASD FieldSpec III Pro FR spectroradiometer (ASD Inc., Denver, Colorado, USA) with a high intensity contact probe. The spectral resolution of the spectroradiometer was 2 nm for the region of 350-1050 nm and 10 nm for the region of 1050-2500 nm. Moreover, the radiometer bandwidth from 350-1000 nm was 1.4 nm while it was 2 nm from 1000-2500 nm. The instrument ran for about 30 minutes to allow the spectrometer and lamp to warm. Soil samples were placed in 9 cm diameter petri dishes and formed 2 cm layers of soil. This was done to avoid beam reflectance from the bottom of the dish due to down-welling solar and sky radiation penetrating into the soil at approximately  $1/2$  the wavelength (Jensen, 2007), which could have an unwanted effect for modifying the soil spectra. Samples were levelled off using a stainless steel blade to guarantee a flat surface flush with the top of the petri dish as a smooth soil surface ensures maximum light reflection and a high SNR (Mouazen et al., 2005). We measured all spectral readings in the centre of the samples (3 replications each)

in a dark room to avoid interference from stray light. The spectroradiometer was optimized using a white Spectralon™ (Lab-sphere, North Sutton, New Hampshire, USA) prior to the first scan and after every six measurements (Shi et al., 2016). For each soil measurement, 30 spectra were averaged to improve SNR.

#### 2.4. Hyperspectral airborne imaging spectrometers data acquisition and pre-processing

Hyperspectral data from VIS-NIR (370-1040 nm) CASI (Itres Ltd., Calgary, Canada) and SWIR (960-2440 nm) SASI (Itres Ltd., Calgary, Canada) sensors were acquired over the study area. The Field-Of-View (FOV) for both sensors was 40°. Sensors collected data in 72 spectral bands in the VIS-NIR with a Full Width at Half Maximum (FWHM) of 10 nm (CASI) and 100 bands in the SWIR with FWHM of 15 nm (SASI). The flight campaigns employing Cessna 208B Grand Caravan aircraft took place on bare soil during dry conditions (minimum of five days after the last rain). The soils of the study areas were ploughed and harrowed before seeding and were without vegetation or litter. Details of individual flight campaigns can be seen in Table 2.

**Table 2.** Individual aerial hyperspectral campaigns

Site	ADT	SZ	SA	FA	N. of Strips	FH	SR
Přestavlky	7.5.2015 10:23	45°	131°	218°	1	~ 2060	1 / 2
Šardice	21.9.2015 10:52	54°	144°	143°	1	~ 2575	1.2 / 3.1
Nová Ves	22.4.2016 11:45	49°	153°	185°	2	~ 2266	1 / 2.7
Jičín	22.4.2016 11:15	47°	142°	159°	3	~ 2266	1 / 2.7

ADT: Acquisition Date and Time (GMT+1), SZ: Solar Zenith, SA: Solar Azimuth, FA: Flight Azimuth, FH: Flight Height above ground (m), SR: Spatial Resolution of CASI/SASI (m).

Flying Laboratory of Imaging Systems (FLIS) was operated by Global Change Research Institute of the Czech Academy of Science located in Brno, Czech Republic and conducted

the data acquisition and pre-processing (atmospheric and geometrical corrections) (Hanus et al., 2014, 2016). The radiometric correction was carried out by calibration parameters obtained in the laboratory using the RadCorr (Itres Ltd., Calgary, Canada). To remove the noisy effects introduced by atmospheric influences and to convert the radiance units to reflectance units, the MODTRAN Radiative Transfer Model (RTM) incorporated into the program ATCOR-4 (ReSe Applications Schlapfer Inc., Zurich, Switzerland) was employed. Algorithm BREFCOR was chosen as a way to decrease the effects of the Bidirectional Reflectance Distribution Function (BRDF) (Schlapfer et al., 2014). The geometric correction and geo-referencing of images were performed using the Geocor (Itres Ltd., Calgary, Canada) based on the recorded data by the on-board GPS/IMU sensors and Digital Elevation Model (DEM-DMR 4G<sup>®</sup> with 5 x 5 m<sup>2</sup> resolution). Before processing, images were resampled to 6 m spatial resolution. To isolate the bare soil areas, Normalized Difference Vegetation Index (NDVI) was used to mask with threshold of 0.2. Moreover, noisy or troublesome spectral bands on the edge of spectra were also removed. Therefore, 49 bands for CASI (400-750 nm and 770-880 nm) and 53 bands for SASI (1000-1080 nm, 1200-1300 nm, 1490-1770 nm and 2060-2370 nm) were retained. Spectral data extraction from data cubes as well as other data manipulation were obtained using the R software (R Development Core Team, Vienna, Austria).

### *2.5. Superspectral satellite data pre-processing and indices retrieval*

Two cloud-free Sentinel-2 images (Level-1C processing) were downloaded from ESA Sentinels Scientific Data Hub according to the closest dates for field samplings (Table 1).

The processing Level-1C includes geometric and radiometric corrections with subpixel accuracy (European Space Agency, 2015). The Sentinel-2 Level-1C was atmospherically



corrected with ESA's Sen2Cor processor, which was integrated in the Sentinel Application Platform (SNAP) tool (Shoko and Mutanga, 2017). As Vuolo et al. (2016) described, Sen2Cor correction is based on the application of Look Up Tables (LUTs), which were pre-calculated using the libRadtran radiative transfer routines (European Space Agency, 2016). The nearest neighbor resampling was used since it is computationally efficient and preserves the input image pixel values (Roy et al., 2016) from the original Bottom of Atmospheric (BoA) 20 m spatial resolution to the 10 m resolution of Sentinel-2 bands.

Analysis was performed using two sets of remote sensing variables including 10 extracted bands of Sentinel-2, which are widely used to assess soil properties (Elhag and Bahrawi, 2017; Grinand et al., 2017; Maynard and Levi, 2017; Sanchez et al., 2015) and 18 calculated spectral indices as covariates, which are expected to improve the prediction capability. Soil optical properties are mainly influenced by four major factors in remote sensing, which includes mineral composition, soil moisture, organic matter content and soil texture. Therefore, in order to indirectly retrieve variables through inter-correlation between target variables, different groups of spectral indices including vegetation indices (which are sensitive to organic matter content), water indices (which are sensitive to soil moisture) and bright-related indices (which are sensitive to soil texture) were calculated (Ben-Dor et al., 2002b). The employed spectral indices were Normalized Differences Vegetation Index (NDVI), Transformed Vegetation Index (TVI), Enhanced Vegetation Index (EVI), Soil Adjusted Total Vegetation Index (SATVI), Soil-Adjusted Vegetation Index (SAVI), Moisture Stress Index (MSI), Green Normalized Difference Vegetation Index (GNDVI), Green-Red Vegetation Index (GRVI), Land Surface Water Index (LSWI), Transformed Soil Adjusted Vegetation Index (TSAVI), Modified Soil Adjusted Vegetation Index (MSAVI), the Second Modified Soil Adjusted Vegetation Index (MSAVI2), Weighted Difference

Vegetation Index (WDVI), Brightness Index (BI), the Second Brightness Index (BI2), Redness Index (RI), Colour Index (CI) and Vegetation (V). The formulas to derive these indices are shown in Table 3, details of the Sentinel-2 bands used in this study can also be seen in Table 4. SNAP was used to extract the values of bare soil pixels at the sampling locations.

**Table 3.** Derived indices detail

Index	Definition	Definition based on Sentinel-2	Details	Reference
NDVI	$\frac{\rho NIR - \rho Red}{\rho NIR + \rho Red}$	$\frac{B8 - B4}{B8 + B4}$	-	Rouse et al. (1974)
TVI	$\left( \frac{\rho NIR - \rho Red}{\rho NIR + \rho Red} + 0.5 \right)^{1/2} \times 100$	$\left( \frac{B8 - B4}{B8 + B4} + 0.5 \right)^{1/2} \times 100$	-	Nellis and Briggs (1992)
EVI	$G \frac{\rho NIR - \rho Red}{\rho NIR + C1 \times \rho Red - C2 \times \rho Blue + L}$	$G \frac{B8 - B4}{B8 + C1 \times B4 - C2 \times B2 + L}$	G=2.5, C1=6, C2=7.5, L=1	Huete et al. (2002)
SATVI	$\frac{\rho SWIR_1 - \rho Red}{\rho SWIR_1 + \rho Red + L} \times (1 + L) - \frac{\rho SWIR_2}{2}$	$\frac{B11 - B4}{B11 + B4 + L} \times (1 + L) - \frac{B12}{2}$	L=1	Marsett et al. (2006)
SAVI	$\frac{(\rho NIR - \rho Red) \times (1 + L)}{\rho NIR - \rho Red + L}$	$\frac{(B8 - B4) \times (1 + L)}{B8 - B4 + L}$	L=0.5	Huete (1988)
MSI	$\frac{\rho SWIR_1}{\rho NIR}$	$\frac{B11}{B8}$	-	Rock et al. (1985)
GNDVI	$\frac{\rho NIR - \rho Green}{\rho NIR + \rho Green}$	$\frac{B8 - B3}{B8 + B3}$	-	Gitelson et al. (1996)
GRVI	$\frac{\rho Green - \rho Red}{\rho Green + \rho Red}$	$\frac{B3 - B4}{B3 + B4}$	-	Tucker (1979)
LSWI	$\frac{\rho NIR - \rho SWIR_1}{\rho NIR - \rho SWIR_1}$	$\frac{B8 - B11}{B8 - B11}$	-	Xiao et al. (2004)
TSAVI	$\frac{s(\rho NIR - s \times \rho Red - a)}{(a \times \rho NIR + \rho Red - a \times s + X \times (1 + s \times s))}$	$\frac{s(B8 - s \times B4 - a)}{(a \times B8 + B4 - a \times s + X \times (1 + s \times s))}$	a=Soil line intercept s=Soil line slope X=Adjustment factor to minimize soil noise	Baret and Guyot (1991)
MSAVI	$\frac{(1 + L)(\rho NIR - \rho Red)}{(\rho NIR + \rho Red + L)}$	$\frac{(1 + L)(B8 - B4)}{(B8 + B4 + L)}$	L=1-2×s×NDVI×WDVI	Qi et al. (1994a)
MSAVI2	$\frac{2 \times \rho NIR + 1 - \sqrt{(2 \times \rho NIR + 1)^2 - 8 \times (\rho NIR - \rho Red)}}{2}$	$\frac{2 \times B8 + 1 - \sqrt{(2 \times B8 + 1)^2 - 8 \times (B8 - B4)}}{2}$		Qi et al. (1994b)
WDVI	$\rho NIR - C \times \rho Red$	$B8 - C \times B4$	$C = \frac{B8}{B4}$	Clevers (1989)
BI	$\frac{\sqrt{(\rho Red \times \rho Red) + (\rho Green \times \rho Green)}}{2}$	$\frac{\sqrt{(B4 \times B4) + (B3 \times B3)}}{2}$	-	Escadafal (1989)
BI2	$\frac{\sqrt{(\rho Red \times \rho Red) + (\rho Green \times \rho Green) + (\rho NIR \times \rho NIR)}}{3}$	$\frac{\sqrt{(B4 \times B4) + (B3 \times B3) + (B8 \times B8)}}{3}$	-	Escadafal (1989)
RI	$\frac{\rho Red \times \rho Red}{\rho Green \times \rho Green \times \rho Green}$	$\frac{B4 \times B4}{B3 \times B3 \times B3}$	-	Pouget et al. (1990)
CI	$\frac{\rho Red - \rho Green}{\rho Red + \rho Green}$	$\frac{B4 - B3}{B4 + B3}$	-	Pouget et al. (1990)
V	$\frac{\rho NIR}{\rho Red}$	$\frac{B8}{B4}$	-	Hill (2013)

**Table 4.** Technical details of Sentinel-2 bands used in this study

Band	Spectral Range (nm)	Spectral Position (nm)	Bandwidth (nm)	Spatial Resolution (m)	SNR (at Lref)
B2	458-523	490	65	10	154
B3	543-578	560	35	10	168
B4	650-680	665	30	10	142
B5	698-713	705	15	20	117
B6	733-748	740	15	20	89
B7	773-793	783	20	20	105
B8	785-900	842	115	10	174
B8a	855-875	865	20	20	72
B11	1565-1655	1610	90	20	100
B12	2100-2280	2190	180	20	100

(European Space Agency, 2010)

## 2.6. Data pre-processing, modelling and prediction performance assessment

Analysis of relationships between spectral data and soil properties was performed using digital soil mapping method. Spectral reflectance data were used as predictors in multivariate regression models and selected soil properties data as response variables. One local prediction model per site was built to analyze the influence of site conditions to predict accuracy.

Data from laboratory and airborne imaging sensors were pre-processed before modelling. Murray (1988) mentioned that removing outliers improves prediction accuracy. Therefore, the outliers of the lab spectra were left out using the principle of Mahalanobis distance (H) (Gomez et al., 2012; Mark and Tunnell, 1985; Shenk and Westerhaus, 1991), applied on PCA-reduced data. The H statistic recognized outliers, whose spectra were different from other samples that made up the calibration set (Cozzolino and Moron, 2006). In the present study, the number of removed outliers from laboratory, airborne and spaceborne datasets were 0-1, 1-4 and 2-4, respectively (depending on the property). Before using the data in calibration models, the 1<sup>st</sup> derivative was used as a spectra pre-processing algorithm. The 1<sup>st</sup> derivative transformation is very effective for removing baseline offset. According to some researchers, the 1<sup>st</sup> derivative transformation gives the best results and

uppermost accuracy among other techniques (Duckworth, 2004; Gholizadeh et al., 2015a, 2015b). In this study, before all laboratory spectra treatments, the noisy portions between 350-399 nm and 2451-2500 nm were eliminated and the spectra were subjected to Savitzky-Golay smoothing with a second-order polynomial fit and 11 smoothing points (Ren et al., 2009; Song et al., 2012) in order to remove the artificial noise caused by the spectroradiometer.

Modelling, validation and final prediction performance assessments were conducted by applying the same methods for all domains. Spectral modelling was done using Support Vector Machine Regression (SVMR) with radial basis kernel. The concept of SVMR follows a different approach of supervised learning and its algorithm is based on the statistical learning theory (Vohland et al., 2011). It has been shown to strike the right balance between accuracy attained on a given finite amount of training patterns and an ability to generalize unseen data (Kovacevic, 2009). The techniques are able to approximate nonlinear functions between multidimensional spaces (Stevens et al., 2010). It also has the capability to derive a linear hyperplane as a decision function for nonlinear problems, which can be considered another reason for the method's selection (Araujo et al., 2014; Boser et al., 1992). Model performance was assessed through 5-fold cross-validation of the training set (75% of samples). Division of the training set was used for fitting models and a validation set was measured by random stratified sampling. The grid search method was employed for selecting the best parameters of models. A single model with the smallest Root Mean Squared Error ( $RMSE_{cv}$ ) value was chosen for subsequent confirmation of the validation set. The final accuracy prediction was determined using Root Mean Squared Error of Prediction ( $RMSE_p$ ) and Ratio of Performance to Deviation (RPD) (Castaldi et al., 2018). RPD is the ratio between the Standard Deviation (SD) of the reference method against that of the  $RMSE_p$  (Hbirkou et al., 2012; Stevens et al., 2008). In this study, the classification system below recommended by Chang et al. (2001) was used.  $RPD < 1.0$  shows a very poor model and it is not recommended while  $1.0 < RPD$

$< 1.4$  expresses a poor model, where only high and low values are detectable. On the other hand,  $1.4 < \text{RPD} < 1.8$  indicates a fair model, which may be used for evaluation and correlation. Additionally,  $1.8 < \text{RPD} < 2.0$  represents a good model, where quantitative predictions are possible and  $2.0 < \text{RPD} < 2.5$  displays a very good quantitative model while  $\text{RPD} > 2.5$  means an excellent prediction. For the spectra pre-processing, package *Prospectr*, and the prediction modelling procedure, *e1071* and *caret* packages of the R software (R Development Core Team, Vienna, Austria) were employed.

### 2.7. Soil attributes mapping

Once the models were validated, an important step was the spatial prediction of soil attributes using different datasets, which reflects important information of the soil condition. The obtained regression models were applied on all spatial data (mask by bare soil) with the purpose of predicting spatial variability of selected soil attributes and creating the geospatial raster dataset. Final maps of soil properties were produced using QGIS software (QGIS Development Team, 2009, QGIS Geographic Information System).

## 3. Results

### 3.1. Soil attributes descriptive statistics and correlations

General statistical results of soil properties from different study sites including mean, minimum, maximum, SD and Coefficient of Variation (CV) are shown in Table 5.

**Table 5.** Statistics description of soil properties

Parameter	SOC	Clay	Silt	Sand
	(%)			
	Přestavlky (n=45)			
Mean	1.19	12.26	49.63	38.12
Min	0.61	7.5	30.6	26.2

<b>Max</b>	1.88	20.1	61.5	59
<b>SD</b>	0.25	3.22	7.17	8.37
<b>CV (%)</b>	21	26	14	22
<b>Šardice (n=50)</b>				
<b>Mean</b>	1.44	22.6	38.49	38.91
<b>Min</b>	0.84	14.2	27.5	15.2
<b>Max</b>	2.62	48.3	49.1	58.3
<b>SD</b>	0.39	6.80	4.67	8.34
<b>CV (%)</b>	27	30	12	21
<b>Nová Ves (n=50)</b>				
<b>Mean</b>	1.07	11.16	37.59	51.24
<b>Min</b>	0.56	6.7	15.9	29.8
<b>Max</b>	1.44	24.7	56.6	77.2
<b>SD</b>	0.17	3.57	9.95	12.32
<b>CV (%)</b>	16	32	26	24
<b>Jičín (n=50)</b>				
<b>Mean</b>	1.03	21.64	66.12	12.24
<b>Min</b>	0.70	14.2	52	7.7
<b>Max</b>	1.41	32.5	75	18.2
<b>SD</b>	0.15	5.14	5.56	2.41
<b>CV (%)</b>	15	24	8	20

Study sites were significantly different in the case of SOC content of topsoil. Low SOC contents (mean = 1.03 %) were observed at Jičín site (Luvisols). However, the highest mean contents were seen at Šardice (mean = 1.44 %). On the Cambisols sites, Nová Ves (mean = 1.07%) and Přestavky (mean = 1.19%), the SOC contents were low to medium. The soil texture analysis showed silty-loam and loam at Přestavky, loamy soils at Šardice (locally sandier or clayey), sandy-loam and loam at Nová Ves and silty-loam (partially silty-clay-loam) at the Jičín site. The samples displayed a narrow range of silt, particularly in Jičín (52%-75%). However, they widely varied in the case of sand and clay content. A comparison of attributes' CV showed that among all parameters, clay had the highest CV, especially in the Nová Ves and Šardice sites, 32% and 30%, respectively. In contrast, sand in Jičín had the lowest CV (8%), which shows that its distribution is more homogenous than other parameters.

Matrix correlations were represented to obtain soil properties correlated to each other for every location (Table 6). Pearson's 2-tailed test for soil parameters correlations showed that SOC did not have any significant correlation with other soil properties in Jičín but it had a significant correlation with all other properties in Nová Ves. In this location (Nová Ves), significant correlation was seen

among all parameters. However, the interrelationship of sand with other parameters was negative. The highest correlation coefficient value of parameters was  $r = -0.97$  for the correlation of sand and silt in Nová Ves.

**Table 6.** Correlation matrix of soil properties

Site	Parameter	SOC	Clay	Silt	Sand
Přestavlky	SOC		-0.04 <sup>ns</sup>	0.61 <sup>***</sup>	-0.51 <sup>***</sup>
	Clay	-0.04 <sup>ns</sup>		0.18 <sup>ns</sup>	-0.54 <sup>***</sup>
	Silt	0.61 <sup>***</sup>	0.18 <sup>ns</sup>		-0.93 <sup>***</sup>
	Sand	-0.51 <sup>***</sup>	-0.54 <sup>***</sup>	-0.93 <sup>***</sup>	
Šardice	SOC		0.51 <sup>***</sup>	-0.28 <sup>*</sup>	-0.26 <sup>ns</sup>
	Clay	0.51 <sup>***</sup>		0.02 <sup>ns</sup>	-0.83 <sup>***</sup>
	Silt	-0.28 <sup>*</sup>	0.02 <sup>ns</sup>		-0.58 <sup>***</sup>
	Sand	-0.26 <sup>ns</sup>	-0.83 <sup>***</sup>	-0.58 <sup>***</sup>	
Nová Ves	SOC		0.3 <sup>*</sup>	0.45 <sup>**</sup>	-0.45 <sup>**</sup>
	Clay	0.3 <sup>*</sup>		0.57 <sup>***</sup>	-0.75 <sup>***</sup>
	Silt	0.45 <sup>**</sup>	0.57 <sup>***</sup>		-0.97 <sup>***</sup>
	Sand	-0.45 <sup>**</sup>	-0.75 <sup>***</sup>	-0.97 <sup>***</sup>	
Jičín	SOC		0.13 <sup>ns</sup>	-0.2 <sup>ns</sup>	0.2 <sup>ns</sup>
	Clay	0.13 <sup>ns</sup>		-0.9 <sup>***</sup>	-0.05 <sup>ns</sup>
	Silt	-0.2 <sup>ns</sup>	-0.9 <sup>***</sup>		-0.39 <sup>**</sup>
	Sand	0.2 <sup>ns</sup>	-0.05 <sup>ns</sup>	-0.39 <sup>**</sup>	

<sup>ns</sup> non-significant, <sup>\*</sup>correlation is significant at the 0.05 level, <sup>\*\*</sup>correlation is significant at the 0.01 level, <sup>\*\*\*</sup>correlation is significant at the 0.001 level

### 3.2. Soil variable prediction using laboratory data

The assessment of soil parameters using the laboratory spectroscopy provided good results. All soil properties (except silt in Šardice, SOC in Nová Ves and sand in Jičín) were predicted with RPD higher than 1.47 (Table 7), which are classified as fair to excellent (SOC and clay in Jičín with  $RPD > 2.5$ ) models. The statistical accuracy obtained using laboratory spectroscopy measurements indicated that, for the soil parameters under study, laboratory proximal level predictions could give a reasonable indicator based on spectra from soil samples. According to the criteria of minimal  $RMSE_p$  and maximal RPD, SOC and clay in Jičín with  $RMSE_p = 0.07$  and  $0.80$ , and  $RPD = 2.93$  and  $3.46$ , respectively, which were considered as the best predicted variables across the different



locations. Overall, the results gained in our lab proved the potential of spectral data for soil texture and SOC estimation in the examined regions.

**Table 7.** Performance of prediction at different domains

Site	Parameter	Laboratory				Hyperspectral Airborne				Superspectral Spaceborne			
		RMSE <sub>cv</sub>	RMSE <sub>p</sub>	RPD	bias	RMSE <sub>cv</sub>	RMSE <sub>p</sub>	RPD	bias	RMSE <sub>cv</sub>	RMSE <sub>p</sub>	RPD	bias
Přestavlky	SOC	0.12	0.14	1.77	0.03	0.12	0.12	2.05	-0.02	0.14	0.14	1.60	0.03
	Clay	1.93	2.20	1.47	1.16	1.24	1.56	2.05	-0.59	2.87	3.05	1.27	-0.44
	Silt	3.77	4.40	1.63	2.02	3.46	5.15	1.40	0.21	5.71	6.28	1.13	-1.89
	Sand	3.69	4.50	1.86	-0.60	3.82	6.35	1.32	-0.59	5.93	8.22	1.02	-0.95
Šardice	SOC	0.16	0.17	2.13	0.09	0.10	0.20	1.80	0.08	0.23	0.24	1.70	0.07
	Clay	1.21	2.35	2.05	-1.92	1.47	2.31	2.06	-0.67	3.37	3.47	1.05	-1.13
	Silt	3.74	3.77	1.24	-0.06	3.63	3.63	1.23	-0.59	4.27	4.31	1.14	-0.28
	Sand	4.07	4.09	2.04	1.92	3.17	3.20	2.50	-0.65	5.63	5.96	0.89	-0.75
Nová Ves	SOC	0.08	0.12	1.29	-0.02	0.11	0.13	1.26	0.02	0.08	0.09	1.73	0.01
	Clay	0.68	1.18	2.08	0.15	1.32	2.25	1.09	0.13	2.51	2.83	1.55	0.69
	Silt	3.56	5.57	1.78	-2.25	4.86	7.36	1.35	-2.44	7.01	8.46	1.10	-1.18
	Sand	3.77	6.92	1.78	-2.02	4.98	7.95	1.38	-1.28	7.28	9.15	1.14	-2.78
Jičín	SOC	0.07	0.07	2.93	0.01	0.06	0.09	1.78	0.03	0.08	0.08	1.92	0.02
	Clay	0.53	0.80	3.46	-0.31	1.66	1.98	1.77	-0.45	1.96	2.57	1.89	1.62
	Silt	1.68	2.48	2.25	1.02	2.26	2.41	2.40	0.81	3.68	3.90	1.43	-0.23
	Sand	4.64	6.11	1.10	0.38	4.93	6.58	1.03	0.42	5.33	7.54	0.91	0.94

### 3.3. Soil variable prediction using hyperspectral airborne data

Hyperspectral airborne data were used for predicting the selected soil properties (SOC, clay, silt and sand). The results of calibration and validation by prediction models with the highest accuracy according to the lowest RMSE<sub>p</sub> and the highest RPD values have been summarized in Table 7. Prediction for SOC and clay indicated good predictive models with values of RMSE<sub>p</sub> ranging from 0.09 to 2.98 and RPD ranged from 1.77 to 2.06 for all locations except Nová Ves, which was the only location with relatively low RPD. Compared to Šardice and Nová Ves, Přestavlky and Jičín indicated better results except for sand, which showed very low RPD values especially in Jičín. Generally, estimating soil characteristics from the hyperspectral airborne sensors indicated that

airborne systems with high spatial and spectral resolution were well-adapted to soil assessment applications in our study area.

#### *3.4. Soil variable prediction using superspectral satellite data*

Table 7 also presents the results of SVMR modelling of soil properties using superspectral Sentinel-2 data. The estimation of soil variables provided rather good results for SOC in all locations, which was predicted with  $RMSE_p < 0.24$  and  $RPD > 1.60$ . The statistical accuracy obtained for other parameters was lower compared to those obtained for SOC. In this case, the clay estimation model also showed satisfactory prediction accuracy in the Jičín site with Luvisol soil. Table 7 shows that with the exception of the model for silt prediction in Jičín from superspectral data, the estimation accuracy of silt and sand was very low in all locations. This highlights the fact that the superspectral data from Sentinel-2 were not appropriate for assessing silt and sand in the current study.

#### *3.5. Soil spectral reflectance pattern and models accuracy assessment using different platforms*

The average spectral responses of soil samples from three different platforms in all locations are presented in Figure 2. It can be clearly seen that the spectral shape and position at all three spectra did not show any noticeable difference. However, spectra based on the lab spectroscopy demonstrated apparently higher albedo intensity and reflectance values relative to the hyperspectral airborne and superspectral spaceborne reflectance based on measurement on dried and grounded samples. The difference between hyperspectral airborne and superspectral spaceborne reflectance was influenced by sensing slightly different surface conditions based on the dates of acquisition (Table 1). There were also some differences in reflectance values among study areas, due to the location's soil characteristics.

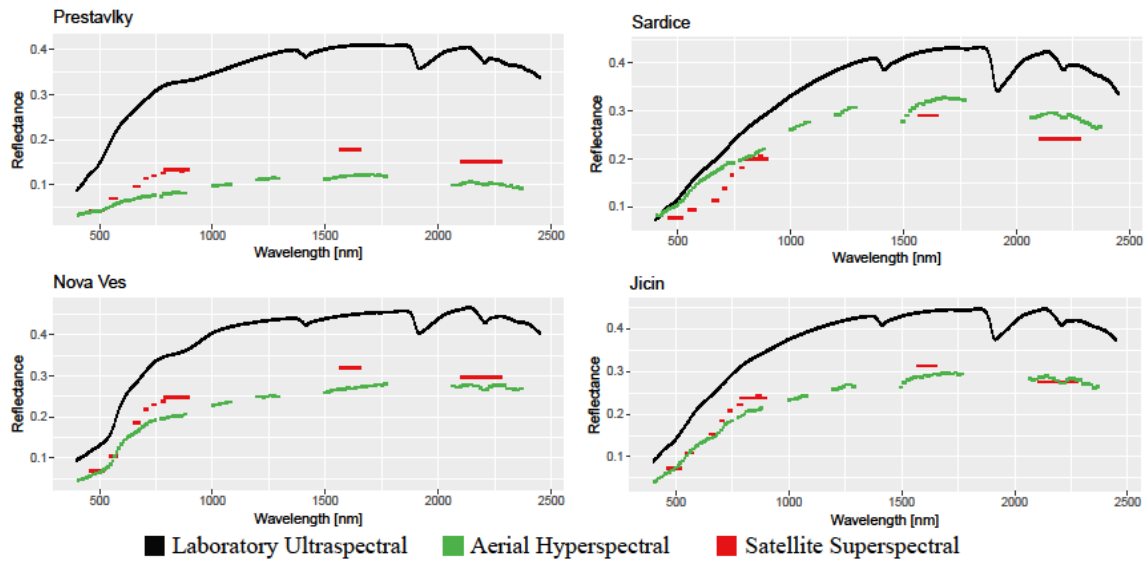


**Figure 2.** Average spectra of soil samples as measured by lab spectroscopy, hyperspectral airborne and supersepectral spaceborne at different locations

Scatterplots in Figure 3 show the results of predicted versus observed selected soil attributes using three platforms datasets over different locations. The difference in predicting SOC among various platforms in this study was not that obvious in different study areas (except slightly in Šardice, between the laboratory and other domains) based on all  $RMSEP_p$  and RPD parameters and scatterplots (Figure 3 and Table 7). Visually, a rather non-significant different pattern can be seen in clay prediction of Přestavlky and Nová Ves based on Figure 3. All platforms datasets for clay showed overall a similar and acceptable pattern. However, a relative difference is obvious between laboratory and Sentinel-2 data, which appeared in Šardice and Jičín. There were significantly more scatters in prediction of silt and sand, especially in Nová Ves and Jičín, when Sentinel-2 superspectral images were used. For the three studied datasets in the current study, the results improved with increased spectral resolution from the superspectral to the ultraspectral instruments.

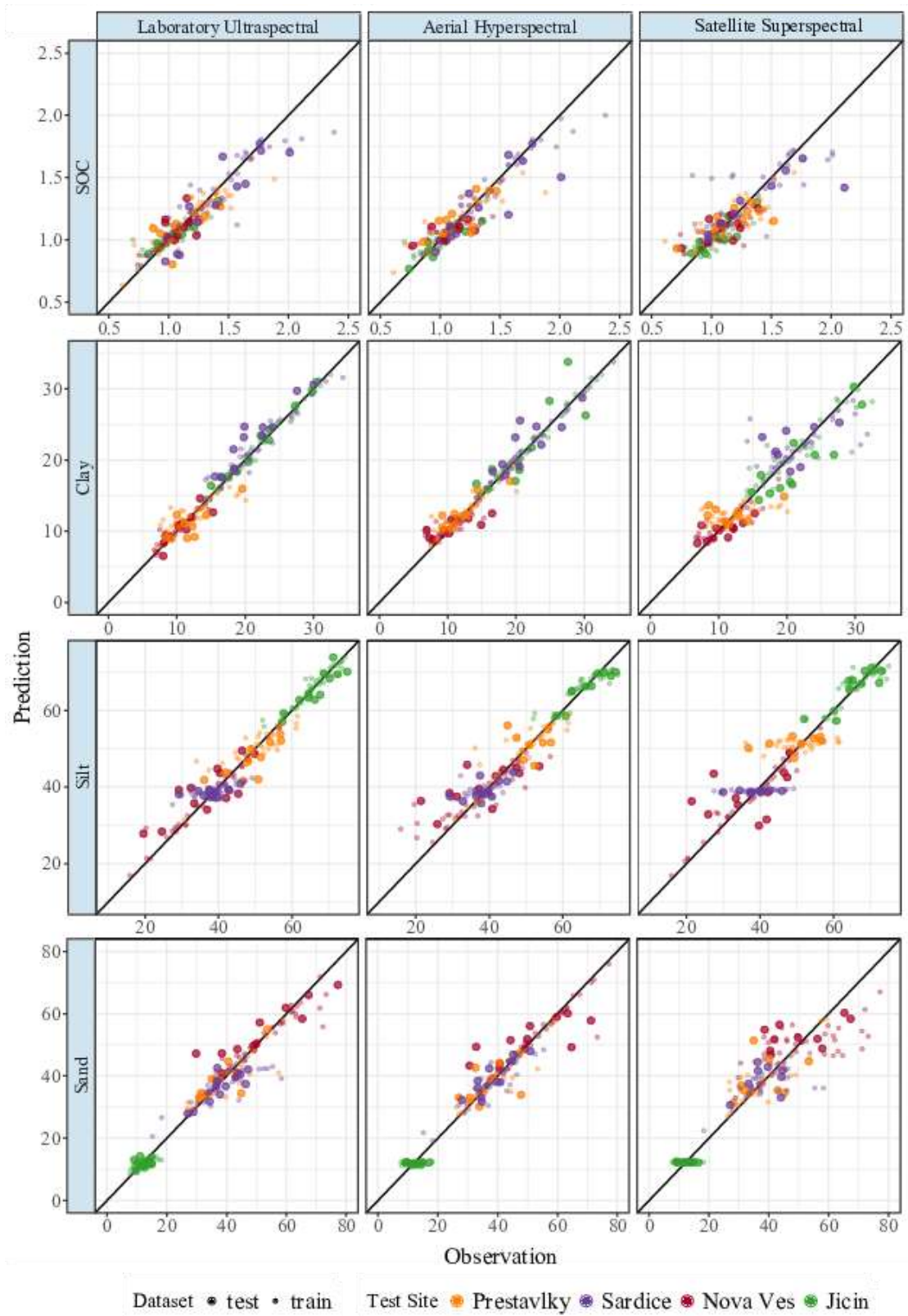


**Figure 3.** Predicted versus observed soil attributes using different platform data over different locations

### *3.6. Spatial distribution of SOC and clay using hyperspectral airborne and superspectral satellite data*

The resulting spatial distribution maps of SOC and clay (the properties with adequate prediction accuracy in this study) derived from the hyperspectral airborne and superspectral satellite data are illustrated in Figures 4 and 5. In general, from airborne to satellite data, the same tendency and a coherent spatial distribution were observed. Even the Sentinel-2 with lower spectral and spatial resolution clearly highlights the different values of SOC and clay contents.

Figure 4 shows that the maps based on Sentinel-2 data displayed low and minimum SOC values while also detecting the high and very high classes of SOC in Přestavlky and Šardice with higher SOC mean value (Table 5) in contrast to the CASI/SASI soil mapping. On the other hand, in Šardice the Sentinel-2 predicted higher values of SOC ( $> 2.3\%$ ) in the northern and western parts of the field, which could not be classified with airborne data. This trend did not work for clay maps in Šardice and did not work for Sentinel-2 nor for airborne CASI/SASI. Additionally, clay contents with more than 40% were not detectable using the data (Figure 5). However, the lowest predicted values of SOC as well as low and medium predicted clay contents showed a relatively similar trend at both platforms.

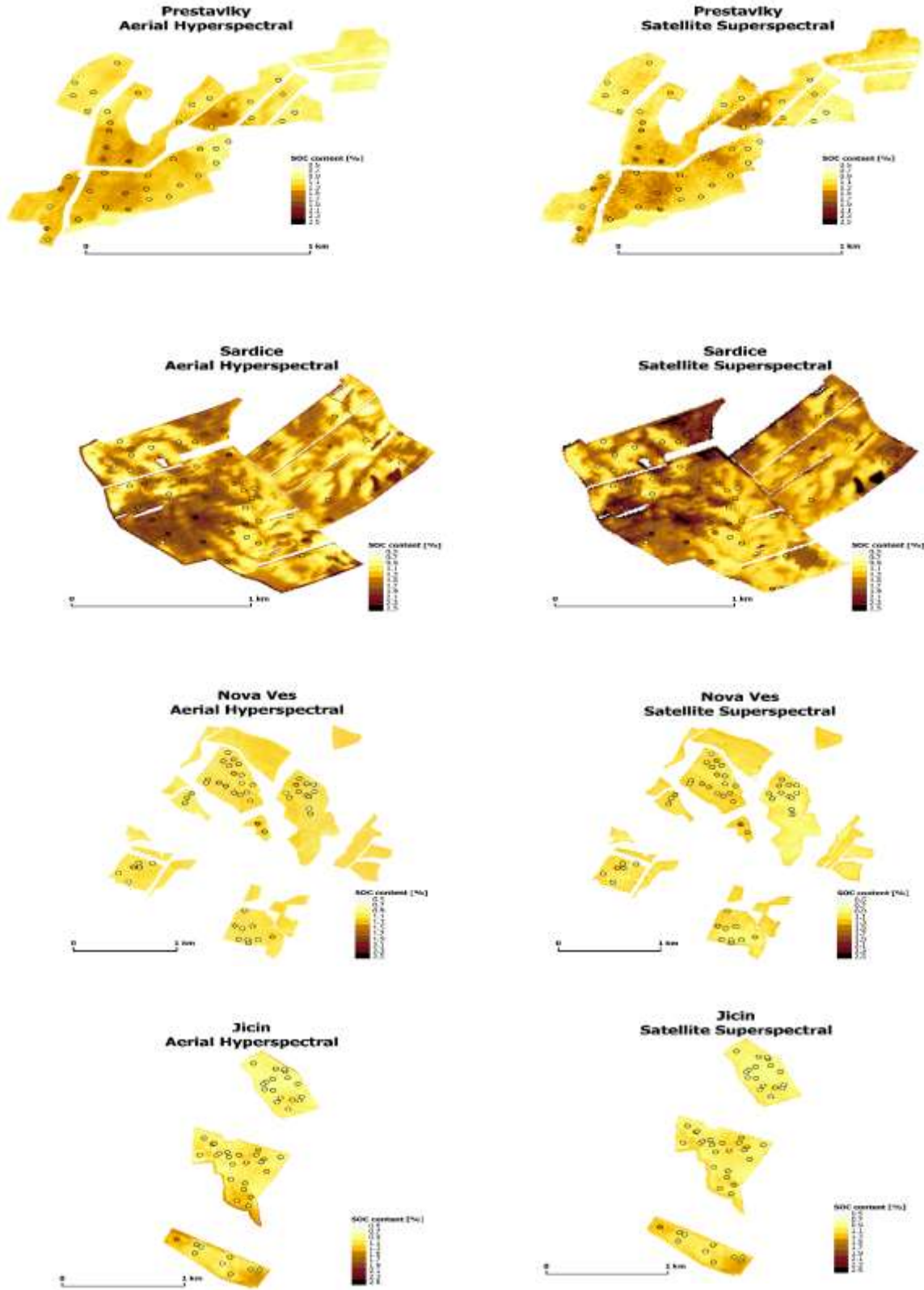


**Figure 4.** Spatial distribution of SOC at the study sites using hyperspectral airborne (left) and superspectral satellite data (right)

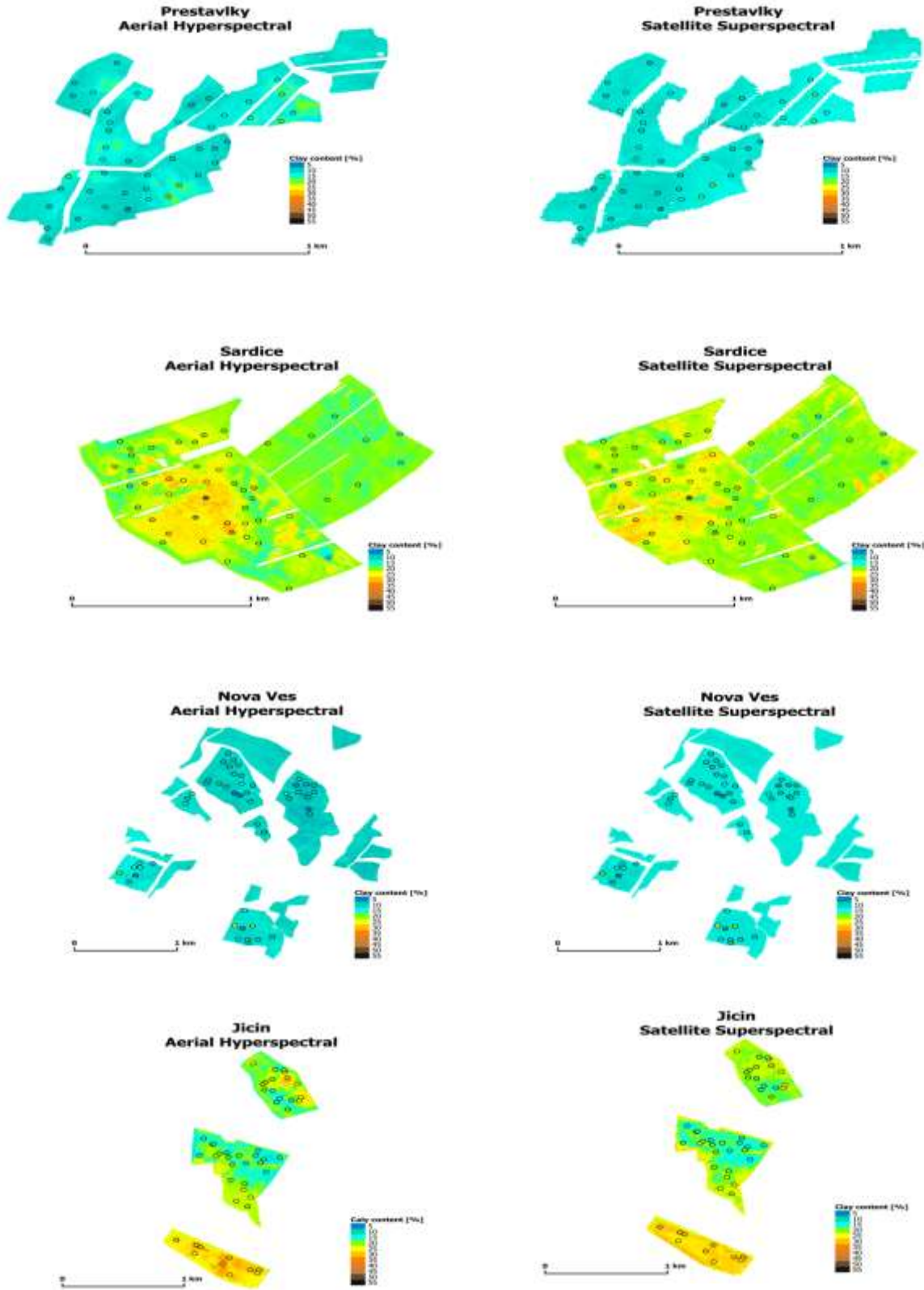


**Figure 5.** Spatial distribution of clay at the study sites using hyperspectral airborne (left) and superspectral satellite data (right)

According to the SOC maps developed from both airborne and spaceborne sensors at Nová Ves and Jičín (study sites with low mean values of SOC), the low range of 0.5% to 1.3% occupied the majority of the areas. The moderate values of SOC (1.5% to 1.7%) were detectable only in the map based on CASI/SASI airborne in Jičín, which were concentrated in small plots in the south of the site. On the other hand, both airborne and spaceborne sensors could detect the low SOC classes but Sentinel-2 failed to characterize high levels of SOC in sites with generally low SOC content. However, the general trends in spatial distribution of maps based on CASI/SASI and Sentinel-2 were still similar not only in SOC maps but also in clay maps. Therefore, Sentinel-2 was able to differentiate various classes of SOC and clay. Maps based on superspectral satellite data performed well and were reliable for SOC and clay mapping. However, in SOC maps based on Sentinel-2, maps were more consistent in areas with a high level of the soil attribute.

#### **4. Discussion**

Table 5 shows that soil texture influences the SOC content, which is in agreement with Schlecht-Pietsch et al. (1994) and Wang et al. (2010) results. Higher SOC contents can be seen in sites with higher clay amounts (except in Jičín) such that increased clay contents were related with increased aggregation or aggregate stability. This means that with increased soil aggregation, the storage of SOC is influenced by clay blocking organic materials and making them unreachable for degrading organisms (Plante et al., 2006). Saffih-Hdadi and Mary (2008) also mentioned that clay content can protect SOC from decomposition, which means higher clay contents may bring higher SOC concentrations. Nevertheless, other soil factors such as pH or nutrient content influences SOC content too. The samples showed a narrow range of silt particularly in Jičín (Table 5). Although, they widely varied in the case of sand and clay contents. The extensive range of clay can be related



to the high variability of the parent material in the region. Large differences were also noticed when looking at clay content as a function of soil type (Stevens et al., 2010).

Correlation of soil properties for every location (Table 6) were displayed among all locations and only in Nová Ves, each parameter had significant correlation with all the other properties. Relationships between SOC and soil texture have been widely studied (Konen et al., 2003; Wang et al., 2010). However, Goidts and Van Wesemael (2007) investigated the change of SOC during 50 years in agriculture and found soil texture did not correlate to SOC and was not the driving factor of SOC change. According to McLauchlan (2006), soil texture may not be significantly correlated to SOC accumulation rates after cessation of agronomic production. Generally, correlations between various soil properties can be explained as the combined effects of climate factors and pedological and lithology processes (Wang et al., 2010).

The prediction performance of ultraspectral laboratory spectroscopy for the studied parameters was promising (Table 7). Clay and SOC are the most frequently and successfully predicted soil properties using spectroscopy data (Gholizadeh et al., 2013; Gholizadeh et al., 2016; Wetterlind and Stenberg, 2010). Presented values of RMSE and RPD for SOC prediction performance from other studies are highly variable since they are collected with different protocols, sampling techniques, sample preparation, instrument specifications, spectral acquisition and analytical algorithms, which can severely affect spectroscopic models (Ben-Dor et al., 2015; Gholizadeh et al., 2017). Nonetheless, the clay distribution prediction is usually successful due to good spectral response of the parameter. Adeline et al. (2017) mentioned that the correlation of clay with iron, which is a parameter with very good prediction performance and an active spectral feature, likely plays an important role in maintaining acceptable prediction results. In addition, clay content is controlled by chemical (clay mineralogical abundance) and physical (clay granulometry) influences, which may help find more fundamental wavelengths in calibration (Adeline et al.,

2017). Prediction for SOC and clay using hyperspectral airborne data also indicated good predictive models (Table 7) except in Nová Ves, which can be related to the low mean value of SOC and clay particles. These are 1.07% and 11.16%, respectively, in the location (Table 5). The same RPD accuracy range for SOC predictions was found in the literature (Selige et al., 2006; Stevens et al., 2010; Uno et al., 2005). However, due to the large variation of SOC contents, RMSE<sub>p</sub> values were higher in our study. For instance, Stevens et al. (2010) obtained RMSE<sub>p</sub> as low as 1.7 for SOC measurement using Partial Least Square Regression (PLSR) algorithm and the AHS-160 (Caravan International Ltd., New York, USA) sensor in the 430-2450 nm range over an area in Belgian Lorraine, Luxembourg. Table 7 also showed that the prediction results of sand in Jičín was very weak, which may refer mainly to the low mean value of sand in this region. Therefore, a good prediction of sand seems rather difficult to obtain in this area with silty or silty-clay soils. In other words, a good local prediction is relatively problematic to gain in this area, where both silty and clay soils are found to have very different spectral characteristics (Table 5). Casa et al. (2013) explored the relationships between spectral data from corresponding pixels of MIVIS image and soil texture using PLSR model. The results provided a model with intermediate prediction accuracy ( $1.4 < \text{RPD} < 1.8$ ) for sand and clay using MIVIS with high spatial and spectral resolution. Since PLSR is a linear model and the relationship between soil parameter and reflectance is possibly non-linear, it is difficult to obtain a good calibration especially a global calibration. Yet such problems can be solved using the SVMR model, which has the capability to approximate a non-linear function between multidimensional spaces by utilizing their kernel-based approach (Stevens et al., 2010).

According to Table 7, the Sentinel-2 images provided relative satisfactory results for estimating SOC and clay in all locations. However, the silt and sand could not be effectively estimated based on the superspectral Sentinel-2 data. Castaldi et al. (2016) also investigated the potential of

Hyperion, Landsat-8 and Sentinel-2 satellite imagers for predicting SOC and soil texture from the European Land Use Cover Area frame Statistical Survey (LUCAS) spectral library and another dataset from central and southern Italy (PONMAC). The statistical accuracy attained using the LUCAS library was low and only the clay estimation model using Hyperion data showed suitable prediction accuracy with  $RMSE = 7.98$  and  $RPD = 1.62$ . However, in PONMAC dataset, Sentinel-2 simulated data provided the best results among the imagers for all properties except for silt. One of the parameters that affects prediction performance of soil attributes with weak or no spectral features is their correlation with spectrally active attributes. Therefore, the prediction accuracy of silt and sand, which are not spectrally active, are extremely dependent on their correlation with spectrally active parameters such as SOC and clay (Gholizadeh et al., 2016; Zizala et al., 2017). This is likely at the Jičín site, where weak model performance for sand can be related to non-significant correlation of this parameter with SOC and clay (Table 6). The low mean value of sand particles (12.24%) in this location can be an additional reason.

As can be seen in Figure 2, the average spectral responses of soil samples from three different platforms in all locations are characterized qualitatively by observing the positive and negative peaks, which occur at specific wavelengths. Due to the presence of the same spectrally active properties in all locations, the spectra of all soil samples were similar (Gholizadeh et al., 2015b). All sensors showed reflectance baseline values with absorption features at 1400 nm and 1900 nm, which may be due to the O-H of hygroscopic water. At 2300 nm, this can be assigned to clay minerals and organic matter (Araujo et al., 2014). However, some differences in reflectance values and albedo intensity of different sensors were obvious. According to Pimstein et al. (2011), differences in soil condition, particularly soil humidity status during the data acquisition in various domains might affect the spectral response. Soil moisture has a significant effect on the

composition and amount of reflected and emitted energy from a soil surface, which reduces the reflectance over the entire spectrum (Nocita et al., 2013).

The scatterplots in Figure 3 show that the differences in prediction capability of all platforms for SOC (except slightly in Šardice, between the laboratory and other domains) and clay (except in Šardice and Jičín between laboratory and Sentinel-2 data) was not that obvious. However, the sensors' performance in parameters prediction especially for silt and sand decreased in spectral resolution from the ultraspectral laboratory-based to the hyperspectral and superspectral remote measurements. The main reason can be attributed to the spectral information content of the sensors. Furthermore, according to Gomez et al. (2018), the differences between the laboratory spectroscopy and imaging data measurements including light sources, instrumental noise, spatial resolution, atmospheric condition and purity of the pixels may clarify these variations. In addition, since the actual remote sensing data are influenced by several factors including soil roughness, soil humidity and crop residues of various locations, this difference in predictions can be interpretable. In other words, imaging spectra may have turbulences, which alter the spectra quality and diminish the enactment of prediction when the spectral resolution is reduced (Gomez et al., 2018). For instance, Friedel et al. (2017) used reflectance spectroscopy and Hyperion satellite imagery for tropical soil estimates in Brazil. They proved that clay-rich soils monitoring was possible using both techniques even though some issues such as shadow existence limited the performance of satellite images. Peon et al. (2017) and Rocha Neto et al. (2017) obtained the same trend about the effect of sensors' spectral resolution for detecting of SOC and soil salinity, respectively. Moreover, Steinberg et al. (2016) compared the potential of HyMap airborne and simulated EnMap spaceborne. They confirmed that, even though both sensors reasonably predicted SOC and clay, the spaceborne compared to the airborne domain showed a slight decrease in prediction accuracy, which may be linked to atmospheric correction and spatial resolution. According to Ben-Dor et al.

(2009), Laghacherie et al. (2008) and Zhang and Zhou (2016), the lower prediction capability of satellite data is mostly associated with environmental conditions, the data collection situation and the different surface variables interpreted from satellite data at the temporal and spatial data scales. Laghacherie et al. (2008) stated that improvement in performance of airborne and spaceborne platforms could be seen in the future using superior techniques for radiometric and atmospheric corrections of the data.

The maps of SOC and clay created by hyperspectral airborne and superspectral satellite data in various study areas (Figures 4 and 5) showed generally similar trends in spatial distribution. The superspectral Sentinel-2 in Přestavky and especially in Šardice, which had higher levels of SOC contents, was capable of not only displaying low and minimum SOC values, but also detecting high and very high classes of SOC that could not be classified with airborne data. The averaging effect of a larger pixel size might be responsible for this trend (Steinberg et al., 2016). Conversely, in study sites with low mean values of SOC (Nová Ves and Jičín), both airborne and spaceborne sensors could predict low SOC levels. However, Sentinel-2 was unsuccessful at depicting high levels of SOC (Figure 4). This difference between aerial and satellite maps might be due to differences in acquisition date, existence of clouds, masking techniques or better masking effects (Immitzer et al., 2016; Steinberg et al., 2016) as well as uncertainties from atmospheric correction in spaceborne data (Richter et al., 2011). Nevertheless, the lowest predicted SOC contents as well as low and medium predicted clay values highlighted a reasonably similar pattern at both platforms. Better monitoring and mapping over bare soils, more reliable prediction performance and higher accuracies can be expected by optimum selection of image and by employing multi-temporal data (Castaldi et al., 2016; Li et al., 2015; Wulder et al., 2015). In general, estimating soil characteristics from the superspectral Sentinel-2 supported the validity of comparing Sentinel-2 models to the airborne models. These results can be interpreted if the SNR, which usually is lower in

hyperspectral sensors than superspectral ones, partly reimburses the disadvantage of the lower spectral resolution (Castaldi et al., 2016). Higher spatial resolution of airborne sensors is also considered a plus. However, the large spatial coverage and a frequent revisit-time of Sentinel-2 may compensate these limitations.

It should be noted that there are still some limitations in using spaceborne data, which are mainly associated with the data acquisition condition (e.g. atmospheric attenuation, vegetation-covered soils and plant litter), interpretation of different surface variables from satellite data at the temporal and spatial data scales (e.g. spectral mixing) and lack of standardization and an agreed-upon protocol. Therefore, further work is needed to deal with the abovementioned limitations and issues.

## **Conclusions**

In this study, the performances of lab spectroscopy along with airborne and spaceborne spectral imaging to derive selected soil parameters (SOC, clay, silt and sand) were analyzed and compared in agricultural sites of the Czech Republic. The main aim was to assess the potential of superspectral Sentinel-2 satellite for predicting and mapping the attributes. The prediction accuracy based on lab spectroscopy, airborne and spaceborne techniques in the majority of the sites was adequate for SOC and fair for clay. However, the prediction capability of the Sentinel-2 approach for silt and sand was not satisfactory. Laboratory and airborne data at a smaller scale and higher spectral resolution provided better results. Comparing the spatial distribution maps of SOC and clay derived from the airborne and spaceborne data showed a similar trend at both platforms. The SOC maps also confirmed that, in areas with a high level of SOC, Sentinel-2 was able to detect SOC more precisely than the airborne sensors. However, a decrease in the model and map performances was clear in the case of parameters with low contents. The findings of the current research showed that superspectral Sentinel-2 allows for the estimating and mapping SOC and clay.

The study also emphasized the importance of the superspectral Sentinel-2 data in soil characteristic assessments with a frequent revisit-time over larger areas than is currently done with laboratory and airborne instruments. Certainly, the repeatability of the Sentinel-2 products is still a work in progress and with the Sentinel-2B, a revisit-time of five-day and the temporal frequency of cloud-free acquisitions will be further increased. Accordingly, much more data will be freely available in the near future, which will have a significant influence obtaining high-quality soil data.

### **Acknowledgement**

The authors like to thank the partially financial support of the Ministry of Agriculture of the Czech Republic projects NAZV (project No. QJ1610289) and NAZV (project No. QK1720289). The authors also acknowledge the support of the Ministry of Education, Youth and Sport of the Czech Republic projects CENAKVA (project No. CZ.1.05/2.1.00/01.0024) and CENAKVA II (project No. LO1205 under the NPU I program). The support of the Czech Science Foundation (project No. 17-27726S) is also appreciated.

### **References**

- Adeline, K., Gomez, C., Gorretta, N., Roger, J.M., 2017. Predictive ability of soil properties to spectral degradation from laboratory Vis-NIR spectroscopy data. *Geoderma*. 288, 143-153.
- Araujo, S.R., Wetterlind, J., Dematte, J.A.M., Stenberg, B., 2010. Improving the prediction performance of a large tropical vis-NIR spectroscopic soil library from Brazil by clustering into smaller subsets or use of data mining calibration techniques. *Eur. J. Soil Sci.*, 65, 718-729.
- Baret, F., Guyot, G., 1991. Potentials and limits of vegetation indices for LAI and APAR assessment. *Remote Sens. Environ.* 35, 161-173.
- Bellon-Maurel, V., Fernandez-Ahumada, E., Palagos, B., Roger, J.M., McBratney, A., 2010. Critical review of chemometric indicators commonly used for assessing the quality of the prediction of soil attributes by NIR spectroscopy. *Trends Analyt. Chem.* 29(9), 1073-1081.
- Ben-Dor, E., 2002a. Quantitative remote sensing of soil properties. *Adv. Agron.* 75, 173-243.
- Ben-Dor, E., Chabrillat, S., Dematte, J.A., Taylor, G.R., Hill, J., Whiting, M.L., Sommer, S., 2009. Using imaging spectroscopy to study soil properties. *Remote. Sens. Environ.* 113, 38-55.
- Ben-Dor, E., Ong, C., Lau, I.C., 2015. Reflectance measurements of soils in the laboratory: Standards and protocols. *Geoderma*. 245-246, 112-124.

- Ben-Dor, E., Patkin, K., Banin, A., Karnieli, A., 2002b. Mapping of several soil properties using DAIS-7915 hyperspectral scanner data- A case study over clayey soils in Israel. *Int. J. Remote Sens.* 23, 1043-1062.
- Berger, M., Moreno, J., Johannessen, J.A., Levelt, P.F., Hanssen, R.F., 2012. ESA's sentinel missions in support of Earth system science. *Remote Sens. Environ.* 120, 84-90.
- Boser, B.E., Guyon, I.M., Vapnik, V.N., 1992. A training algorithm for optimal margin classifiers, in: Haussler, D. (Ed.), 5th annual ACM workshop on COLT. ACM Press: Pittsburgh, USA, pp. 144-152.
- Buol, S.W., Hole, F.D., McCracken, R.J., 1973. Soil genesis and classification. Univ. Press: Ames, USA.
- Casa, R., Castaldi, F., Pascucci, S., Palombo, A., Pignatti, S., 2013. A comparison of sensor resolution and calibration strategies for soil texture estimation from hyperspectral remote sensing. *Geoderma.* 197-198, 17-26.
- Castaldi, F., Chabrillat, S., Jones, A., Vreys, K., Bomans, B., Van Wesemael, B., 2018. Soil organic carbon estimation in croplands by hyperspectral remote APEX data using the LUCAS topsoil database. *Remote Sens.* 10, 153.
- Castaldi, F., Palombo, A., Santini, F., Pascucci, S., Pignatti, S., Casa, R., 2016. Evaluation of the potential of the current and forthcoming multispectral and hyperspectral imagers to estimate soil texture and organic carbon. *Remote Sens. Environ.* 179, 54-65.
- Chang, C.W., Laird, D.A., Mausbach, M.J., Hurburgh Jr., C.R., 2001. Near-infrared reflectance spectroscopy- Principal component analysis of soil properties. *Soil Sci. Soc. Am. J.* 65, 480-490.
- Clevers, J.G.P.W., 1988. The derivation of a simplified reflectance model for the estimation of leaf area index. *Remote Sens. Environ.* 25, 53-69
- Cozzolino, D., Moron, A., 2006. Potential of near-infrared reflectance spectroscopy and chemometrics to predict soil organic carbon fractions. *Soil Till. Res.* 85, 78-85.
- Danoedoro, P., Zukhrufiyati, A., 2015. Integrating spectral indices and geostatistics based on Landsat-8 imagery for surface clay content mapping in Gunung Kidul area, Yogyakarta, Indonesia. Proceedings of the 36<sup>th</sup> Asian Conference on Remote Sensing Fostering Resilient Growth. Manila, The Philippines.
- Drusch, M., del Bello, U., Carlier, S., Colin, O., Fernandez, V., Gascon, F., Hoersch, B., Isola, C., Laberinti, P., Martimort, P., Meygret, A., Spoto, F., Sy, O., Marchese, F., Bargellini, P., 2012. Sentinel-2: ESA's optical high-resolution mission for GMES operational services. *Remote Sens. Environ.* 120, 25-36.
- Duckworth, J., 2004. Mathematical data preprocessing, in: Roberts, C.A., Workman Jr. J., Reeves, J.B. III. (Eds.), Near-infrared spectroscopy in agriculture. ASA-CSSA-SSSA: Madison, WI, USA, pp. 115-132.
- Elachi, C., Van Zyl, J.J., 2006. Introduction to the physics and techniques of remote sensing, John Wiley & Sons, pp. 616.
- Elhag, M., Bahrawi, J.A., 2017. Soil salinity mapping and hydrological drought indices assessment in arid environments based on remote sensing techniques. *Geosci. Instrum. Method. Data Syst. Discuss.* 6, 149-158.
- Escadafal, R., 1989. Remote sensing of arid soil surface color with Landsat Thematic Mapper. *Adv. Space Res.* 9(1), 159-163.
- European Space Agency, 2010. GMES Sentinel-2 mission requirements document. Technical Report issue 2 revision 1.
- European Space Agency, 2015. Sentinel-2 user handbook. ESA Standard Document.



- European Space Agency, 2016. Sen2Cor 2.2.1-Software Release Note.
- Friedel, M.J., Buscema, M., Vicente, L.E., Iwashita, F., Koga-Vicente, A., 2017. Mapping fractional landscape soils and vegetation components from Hyperion satellite imagery using an unsupervised machine-learning workflow. *Int. J. Digit. Earth*. 2017, 1-21.
- Gholizadeh, A., Amin, M.S.M., Boruvka, L., Saberioon, M.M., 2014. Models for estimating the physical properties of paddy soil using visible and near infrared reflectance spectroscopy. *J Appl. Spectrosc.* 81(3), 534-540.
- Gholizadeh, A., Amin, M.S.M., Saberioon, M.M., Boruvka, L., 2013. Visible and near-infrared reflectance spectroscopy to determine chemical properties of paddy soils. *J. Food Agric. Environ.* 11(2), 859-866.
- Gholizadeh, A., Boruvka, L., Vasat, R., Saberioon, M.M., 2015a. Comparing different data preprocessing methods for monitoring soil heavy metals based on soil spectral features. *Soil Water Res.* 10(4), 218-227.
- Gholizadeh, A., Boruvka, L., Vasat, R., Saberioon, M.M., Klement, A., Kratina, J., Tejnecky, V., Drabek, O., 2015b. Estimation of potentially toxic elements contamination in anthropogenic soils on a brown coal mining dumpsite by reflectance spectroscopy: A case study. *PLoS One*. 10(2), e0117457.
- Gholizadeh, A., Carmon, N., Ben-Dor, E., Boruvka, L., 2017. Agricultural soil spectral response and properties assessment: Effects of measurement protocol and data mining technique. *Remote Sens.* 9, 1078.
- Gholizadeh, A., Saberioon, M.M., Boruvka, L., Vasat, R., 2016. A memory-based learning approach as compared to other data mining algorithms for the prediction of soil texture using diffuse reflectance spectra. *Remote Sens.* 8, 341.
- Gianinetto, M., Lechi, G., 2004. The development of superspectral approaches for the improvement of land cover classification. *IEEE Trans. Geosci. Remote Sens.* 42(11), 2670-2679.
- Gitelson, A.A., Kaufman, Y.J., Merzlyak, M.N., 1996. Use of a green channel in remote sensing of global vegetation from EOS-MODIS. *Remote Sens. Environ.* 58, 289-298.
- Goidts, E., Van Wesemael, B., 2007. Regional assessment of soil organic carbon changes under agriculture in southern Belgium (1955-2005). *Geoderma*. 141, 341-354.
- Gomez, C., Adeline, K., Bacha, S., Driessen, B., Gorretta, N., Lagacherie, P., Roger, J.M., Briottet, X., 2018. Sensitivity of clay content prediction to spectral configuration of VNIR/SWIR imaging data, from multispectral to hyperspectral scenarios. *Remote Sens. Environ.* 204, 18-30.
- Gomez, C., Lagacherie, P., Coulouma, G., 2012. Regional predictions of eight common soil properties and their spatial structures from hyperspectral Vis–NIR data. *Geoderma*. 189-190, 176-185.
- Gomez, C., Viscarra Rossel, R.A., McBratney, A.B., 2008. Soil organic carbon prediction by hyperspectral remote sensing and field Vis-NIR spectroscopy: An Australian case study. *Geoderma*. 146, 403-411.
- Grinand, C., Le Maire, G., Vieilledent, G., Razakamanarivo, H., Razafimbelo, T., 2017. Estimating temporal changes in soil carbon stocks at ecoregional scale in Madagascar using remote-sensing. *Int. J. Appl. Earth Obs. Geoinf.* 54, 1-14.
- Hanus, J., Fabianek, T., Fajmon, L., 2016. Potential of airborne imaging spectroscopy at CzechGlobe. *Int. Arch. Photogram. Remote Sens. Spat. Info. Sci.* XLI-B1, 15-17.
- Hanus, J., Fabianek, T., Kaplan, V., Homolova, L., 2014. Flying Laboratory of Imaging Systems (FLIS) at CzechGlobe. *Proceedings of the SGEM2014 Conference*. Sofia, Bulgaria.
- Hbirkou, C., Patzold, S., Mahlein, A.K., Welp, G., 2012. Airborne hyperspectral imaging of spatial soil organic carbon heterogeneity at field-scale. *Geoderma*. 175-176, 21-28.

- Hill, M.J., 2013. Vegetation index suites as indicators of vegetation state in grassland and savanna: An analysis with simulated SENTINEL 2 data for a north American transect. *Remote Sens. Environ.* 137, 94-111.
- Huete, A.R., 1988. A soil-adjusted vegetation index (SAVI). *Remote Sens. Environ.* 25, 295-309.
- Huete, A.R., Didan, K., Miura, T., Rodriguez, E.P., Gao, X., Ferreira, L.G., 2002. Overview of the radiometric and biophysical performance of the MODIS vegetation indices. *Remote Sens. Environ.* 83, 195-213.
- Immitzer, M., Vuolo, F., Atzberger, C., 2016. First experience with Sentinel-2 data for crop and tree species classifications in central Europe. *Remote Sens.* 8, 166.
- IUSS Working Group WRB. World Reference Base for Soil Resources 2014. International soil classification system for naming soils and creating legends for soil maps; World soil resources reports No. 106. FAO: Rome, Italy. Available online: <http://www.fao.org/3/a-i3794e.pdf> (accessed on 1 October 2015).
- Jensen, J.R., 2007. *Remote sensing of the environment: An Earth resource perspective*. Prentice Hall, Upper Saddle River: New Jersey, USA, 544.
- Ji, W., Viscarra Rossel, R.A., Shi, Z. 2015. Improved estimates of organic carbon using proximally sensed vis-NIR spectra corrected by piecewise direct standardization. *Eur. J Soil Sci.* 66(4), 670-678.
- Konen, M.E., Burras, C.L., Sandor, J.A., 2003. Organic carbon, texture, and quantitative color measurement relationships for cultivated soils in North Central Iowa. *Soil Sci. Soc. Am. J.* 67, 1823-1830.
- Kovacevic, M., Bajat, B., Trivic, B., Pavlovic, R., 2009. Geological units classification of multispectral images by using support vector machines, in: Badr, Y.K., Caballe, S., Xhafa, F., Abraham, A., Gros, B. (Eds.), *International conference on intelligent networking and collaborative systems*. IEEE: New York, USA, pp. 267-272.
- Kuang, B., Mouazen, A.M., 2012. Influence of the number of samples on prediction error of visible and near infrared spectroscopy of selected soil properties at the farm scale. *Eur. J. Soil Sci.* 63, 421-429.
- Lagacherie, P., Baret, F., Feret, J.B., Netto, J.M., Robbez-Masson, J.M., 2008. Estimation of soil clay and calcium carbonate using laboratory, field and airborne hyperspectral measurements. *Remote Sens. Environ.* 112(3), 825-835.
- Li, D., Ke, Y., Gong, H., Li, X., 2015. Object-based urban tree species classification using bi-temporal WorldView-2 and WorldView-3 images. *Remote Sens.* 7, 16917-16937.
- Malenovsky, Z., Rott, H., Cihlar, J., Schaepman, M., Garcia-Santos, G., Fernandes, R., Berger, M., 2012. Sentinels for science: Potential of sentinel-1, 2, and 3 missions for scientific observations of ocean, cryosphere, and land. *Remote Sens. Environ.* 120, 91-101.
- Mark, H.L., Tunnell, D., 1985. Qualitative near-infrared reflectance analysis using Mahalanobis distances. *Anal. Chem.* 57, 1449-1456.
- Marsett, R.C., Qi, J., Heilman, P., Biedenbender, S.H., Watson, M.C., Amer, S., Weltz, M., Goodrich, D., Marsett, R., 2006. Remote sensing for grassland management in the arid southwest. *Rangel. Ecol. Manag.* 59, 530-540.
- Maynard, J.J., Levi, M.R., 2017. Hyper-temporal remote sensing for digital soil mapping: Characterizing soil-vegetation response to climatic variability. *Geoderma.* 285, 94-109.
- McLauchlan, K.K., 2006. Effects of soil texture on soil carbon and nitrogen dynamics after cessation of agriculture. *Geoderma.* 136, 289-299.

- Mielke, C., Boesche, N.K., Rogass, C., Kaufmann, H., Gauert, C., de Wit, M., 2014. Spaceborne mine waste mineralogy monitoring in South Africa, applications for modern Push-Broom missions: Hyperion/OLI and EnMAP/Sentinel-2. *Remote Sens.* 6, 6790-6816.
- Minasny, B., McBratney, A.B., 2006. A conditioned Latin hypercube method for sampling in the presence of ancillary information. *Comput. Geosci.* 32, 1378-1388.
- Mouazen, A.M., de Baerdemaeker, J., Ramon, H. 2005. Towards development of on-line soil moisture content sensor using a fibre-type NIR spectrophotometer. *Soil Till. Res.* 80, 171-183.
- Murray, I., 1988. Aspects of interpretation of NIR spectra, in: Creaser, C.S., Davies, A.M.C. (Eds.), *Analytical application of spectroscopy*. Royal Society of Chemistry: London, UK, pp. 9-21.
- Nellis, M.D., Briggs, J.M., 1992. Transformed vegetation index for measuring spatial variation in drought impacted biomass on Konza Prairie, Kansas. *Trans. Kans. Acad. Sci.* (1903), 95, 93-99.
- Nocita, M., Stevens, A., Noon, C., Van Wesemael, B., 2013. Prediction of soil organic carbon for different levels of soil moisture using Vis-NIR spectroscopy. *Geoderma*, 199, 37-42.
- Peon, J., Fernandez, S., Recondo, C., Calleja, J.F., 2017. Evaluation of the spectral characteristics of five hyperspectral and multispectral sensors for soil organic carbon estimation in burned areas. *Int. J. Wildland Fire.* 26, 230-239.
- Pimstein, A., Ben-Dor, E., Notesko, G., 2011. Performance of three identical spectrometers in retrieving soil reflectance under laboratory conditions. *Soil Sci. Soc. Am. J.* 75, 110-174.
- Plante, A.F., Conant, R.T., Stewart, C.E., Paustian, K., Six, J., 2006. Impact of soil texture on the distribution of soil organic matter in physical and chemical fractions. *Soil Sci. Soc. Am. J.* 70, 287-296.
- Pouget, M., Madeira, J., Le Floch, E., Kamal, S., 1990. Caractéristiques spectrales des surfaces sableuses de la région cotée Nord-Ouest de l’Egypte: Application aux données satellitaires SPOT. 2eme Journées de T&D: Caractérisation et suivi des milieux terrestres en régions arides et tropicales. 4-6/12/1990. Ed. ORSTOM, Collection Colloques et Séminaires. Paris, France.
- Qi, J., Chehbouni, A., Huete, A.R., Kerr, Y.H., 1994a. Modified Soil Adjusted Vegetation Index (MSAVI). *Remote Sens. Environ.* 48, 119-126.
- Qi, J., Kerr, Y., Chehbouni, A., 1994b. External factor consideration in vegetation index development. *Proceeding of International Symposium on Physical Measurements and Signatures in Remote Sensing*. Val D’Isere, France.
- Ramirez-Lopez, L., Schmidt, K., Behrens, T., Van Wesemael, B., Dematte, J.A.M., Scholten, T., 2014. Sampling optimal calibration sets in soil infrared spectroscopy. *Geoderma*. 226-227, 140-150.
- Ren, H.Y., Zhuang, D.F., Singh, A.N., Pan, J.J., Qid, D.S., Shi, R.H., 2009. Estimation of As and Cu contamination in agricultural soils around a mining area by reflectance spectroscopy: A case study. *Pedosphere*. 19, 719-726.
- Richter, R., Schlapfer, D., Muller, A., 2011. Operational atmospheric correction for imaging spectrometers accounting for the smile effect. *IEEE Trans. Geosci. Remote Sens.* 49, 1772-1780.
- Rocha Neto, O.C., Santos Teixeira, A., Leao, R.A.O., Moreira, L.C.J., Galvao, L.S., 2017. Hyperspectral remote sensing for detecting soil salinization using ProSpec TIR-VS aerial imagery and sensor simulation. *Remote Sens.* 9, 42.
- Rock, B.N., Williams, D.L., Vogelmann, J.E., 1985. Field and airborne spectral characterization of suspected acid deposition damage in red spruce (*Picea rubens*) from Vermont. *Proceeding of Symposium on Machine Processing of Remotely Sensed Data*. West Lafayette, Indiana, USA.

- Rouse, J.W., Haas, J.R.H., Schell, J.A., Deering, D.W., 1974. Monitoring vegetation systems in the Great Plains witherts. Proceedings of the 3<sup>rd</sup> ERTS Symposium. Washington, USA.
- Roy, D.P., Li, J., Zhang, H.K., Yan, L., 2016. Best practices for the reprojection and resampling of Sentinel-2 Multi Spectral Instrument Level 1C data. *Remote Sens. Lett.* 7(11), 1023-1032.
- Saffih-Hdadi, K., Mary, B., 2008. Modeling consequences of straw residues export on soil organic carbon. *Soil Biol. Biochem.* 40, 594-607.
- Sanchez, N., Alonso-Arroyo, A., Martinez-Fernandez, J., Piles, M., Gonzalez-Zamora, A., Camps, A., Vall-Iloera, M., 2015. On the synergy of airborne GNSS-R and Landsat 8 for soil moisture estimation. *Remote Sens.* 7(8), 9954-9974.
- Schlapfer, D., Richter, R., Feingersh, T., 2014. Operational BRDF effects correction for wide-field-of-view optical scanners (BREFCOR). *IEEE Trans. Geosci. Remote Sens.* 53(4), 1855-1864.
- Schlecht-Pietsch, S., Wagner, U., Anderson, T.H., 1994. Changes in composition of soil polysaccharides and aggregate stability after carbonamendments to different textured soils. *Appl. Soil Ecol.* 1, 145-154.
- Schmidt, K., Behrens, T., Friedrich, K., Scholten, T., 2010. A method to generate soilsapes from soil maps. *J. Plant Nutr. Soil Sci.* 173(2), 163-172.
- Selige, T., Boehner, J., Schmidhalter, U., 2006. High resolution topsoil mapping using hyperspectral image and field data in multivariate regression modeling procedures. *Geoderma.* 136, 235-244.
- Shenk, J.S., Westerhaus, M.O., 1991. Population definition, sample selection, and calibration procedure for near infrared reflectance spectroscopy. *Crop Sci.* 31, 469-474.
- Shi, T., Wang, J., Chen, W., Wu, G., 2016. Improving the prediction of arsenic contents in agricultural soils by combining the reflectance spectroscopy of soils and rice plants. *Intl. J. Appl. Earth Obs. Geoinf.* 52, 95-103.
- Shoko, C., Mutanga, O., 2017. Examining the strength of the newly-launched Sentinel 2 MSI sensor in detecting and discriminating subtle differences between C3 and C4 grass species. *ISPRS J. Photogramm. Remote Sens.* 129, 32-40.
- Song, Y., Li, F., Yang, Z., Ayoko, G.A., Frost, R.L., Ji, J., 2012. Diffuse reflectance spectroscopy for monitoring potentially toxic elements in the agricultural soils of Changjiang river delta, China. *Appl. Clay Sci.* 64, 75-83.
- Steinberg, A., Chabrillat, S., Stevens, A., Segl, K., Foerster, S., 2016. Prediction of common surface soil properties based on Vis-NIR airborne and simulated EnMAP imaging spectroscopy data: Prediction accuracy and influence of spatial resolution. *Remote Sens.* 8, 613.
- Stevens, A., Udelhoven, T., Denis, A., Tychon, B., Liroy, R., Hoffmann, L., Van Wasemael, B., 2010. Measuring soil organic carbon in croplands at regional scale using airborne imaging spectroscopy. *Geoderma.* 158, 32-45.
- Stevens, A., Van Wasemael, B., Bartholomeus, H., Rosillon, D., Tychon, B., Ben-Dor, E., 2008. Laboratory, field and airborne spectroscopy for monitoring organic carbon content in agricultural soils. *Geoderma.* 144, 395-404.
- Tucker, C.J., 1979. Red and photographic infrared linear combinations for monitoring vegetation. *Remote Sens. Environ.* 8, 127-150.
- Uno, Y., Prasher, S.O., Patel, R.M., Strachan, I.B., Pattey, E., Karimi, Y., 2005. Development of field-scale soil organic matter content estimation models in Eastern Canada using airborne hyperspectral imagery. *Can. Biosys. Eng.* 47, 9-14.
- Vagen, T.G., Winowiecki, L.A., Tondoh, J.E., Desta, L.T., Gumbrecht, T., 2016. Mapping of soil properties and land degradation risk in Africa using MODIS reflectance. *Geoderma.* 263, 216-225.

- Van der Meer, F., Van der Werff, H., Van Ruitenbeek, F., 2014. Potential of ESA's Sentinel-2 for geological applications. *Remote Sens. Environ.* 148, 124-133.
- Van der Werff, H., Van der Meer, F., 2016. Sentinel-2A MSI and Landsat 8 OLI provide data continuity for geological remote sensing. *Remote Sens.* 8, 883.
- Viscarra Rossel, R.A., McBratney, A.B., Minasny, B., 2010. *Proximal soil sensing*, Springer, pp. 448.
- Viscarra Rossel, R.A., Walvoort, D.J.J., McBratney, A.B., Janikand, L.J., Skjemstad, J.O., 2006. Visible, near infrared, mid infrared or combined diffuse reflectance spectroscopy for simultaneous assessment of various soil properties. *Geoderma.* 131, 59-75.
- Vohland, M., Besold, J., Hill, J., Frund, H.C., 2011. Comparing different multivariate calibration methods for the determination of soil organic carbon pools with visible to near infrared spectroscopy. *Geoderma.* 166, 198-205.
- Vuolo, F., Zoltak, M., Pipitone, C., Zappa, L., Wenng, H., Immitzer, M., Weiss, M., Baret, F., Atzberger, C., 2016. Data service platform for Sentinel-2 surface reflectance and value-added products: System use and examples. *Remote Sens.* 8(11), 938.
- Wang, D.D., Shi, X.Z., Wang, H.J., Weindorf, D.C., Yu, D.S., Sun, W.X., Ren, H.Y., Zhao, Y.C., 2010. Scale effect of climate and soil texture on soil organic carbon in the uplands of northeast China. *Pedosphere.* 20(4), 525-535.
- Wetterlind, J., Stenberg, B., 2010. Near-infrared spectroscopy for within-field soil characterization: Small local calibrations compared with national libraries spiked with local samples. *Eur. J. Soil Sci.* 61, 823-843.
- Wulder, M.A., Hilker, T., White, J.C., Coops, N.C., Masek, J.G., Pflugmacher, D., Crevier, Y., 2015. Virtual constellations for global terrestrial monitoring. *Remote Sens. Environ.* 170, 62-76.
- Xiao, X., Zhang, Q., Braswell, B., Urbanski, S., Boles, S., Wofsy, S.C., Moore, B., Ojima, D., 2004. Modeling gross primary production of a deciduous broadleaf forest using satellite images and climate data. *Remote Sens. Environ.* 91, 256-270.
- Yokoya, N., Chan, J.C.W., Segl, K., 2016. Potential of resolution-enhanced hyperspectral data for mineral mapping using simulated EnMAP and Sentinel-2 images. *Remote Sens.* 8, 172.
- Zhang, D., Zhou, G., 2016. Estimation of soil moisture from optical and thermal remote sensing: A review. *Remote Sens.* 168(8), 1308.
- Zhang, T., Li, L., Zheng, B., 2013. Estimation of agricultural soil properties with imaging and laboratory spectroscopy. *J. Appl. Remote Sens.* 7, 073587.
- Zizala, D., Zadorova, T., Kapicka, J., 2017. Assessment of soil degradation by erosion based on analysis of soil properties using aerial hyperspectral images and ancillary data, Czech Republic. *Remote Sens.* 9, 28.

### 5.3 Mapping Soil Degradation using Remote Sensing Data and Ancillary Data - South-East Moravia, Czech Republic

---

- **Žížala, D.**, Juřicová, A., Zádorová, T., Zelenková, K., Minařík, R., 2018. Mapping Soil Degradation using Remote Sensing Data and Ancillary Data - South-East Moravia, Czech Republic. *European Journal of Remote Sensing*. [doi: 10.1080/22797254.2018.1482524]

## Mapping soil degradation using remote sensing data and ancillary data: South-East Moravia, Czech Republic

Daniel Žížala , Anna Juřicová , Tereza Zádorová<sup>b</sup>, Kateřina Zelenková  and Robert Minařík 

<sup>a</sup>Department of Soil Survey, Research Institute for Soil and Water Conservation, Prague, Czech Republic; <sup>b</sup>Department of Soil Science and Soil Protection, Czech University of Life Sciences Prague, Prague, Czech Republic; <sup>c</sup>Department of Physical geography and geocology, Charles University in Prague, Prague, Czech Republic

### ABSTRACT

Data on the real extent of soil that is degraded by erosion represent important information for the purposes of conservation policy. However, this type of data is rarely available for large areas. A remote-sensing-based method for identifying of eroded areas at the regional scale has been tested using a combination of time series of free access Sentinel-2 image data, airborne orthoimages and ground-truth data. The unsupervised classification ISODATA of the Sentinel-2A images has been performed. The minimum distance method has been applied for the assignment of unsupervised classes to four erosion classes using the ground-truth data. The automatic classification of eroded soils achieved an overall accuracy of 55.2% for three distinguished classes. An accumulated class has been eliminated as no unsupervised classes were assigned to this erosion class. A simplified classification of two classes (strongly eroded and other soils) reached an accuracy of 80.9%. The overall accuracy of the simplified classification increased to 86.9% after the visual refinement using orthoimages. This study shows the potential of the tested approach to produce valuable data on actual soil degradation by erosion. The limitations of the method are related to the soil cover variability, masking effect of clouds, vegetation or litter and the spectral separability of individual classes.

### ARTICLE HISTORY

Received 26 December 2017  
Revised 9 April 2018  
Accepted 27 May 2018

### KEYWORDS

Soil erosion; remote sensing; Sentinel-2; orthoimage; unsupervised classification; Chernozem

### Introduction

Soil erosion that causes the loss of a high-quality soil material is perceived as one of the most problematic and visible forms of soil degradation both in Europe (Boardman & Poesen, 2006; EEA & JRC, 2010; Grimm, Jones, & Montanarella, 2002; Panagos et al., 2016; Stolte et al., 2016) and on a global scale (FAO and ITPS, 2015). The total rate of actual soil erosion and the real extent of eroded areas, however, are often known only at the local scale based on the information from spatial limited field campaigns (Evans, 2013; Verheijen, Jones, Rickson, & Smith, 2009). At the regional and global scales, information on soil erosion is available only in the forms of potential erosion risk, expert-knowledge estimations or computations using empirical models of potential soil loss rates (Novotný et al., 2016; Panagos et al., 2015). The validation using field data is usually limited (Evans, 2013). According to the calculations of the potential erosion risk, water erosion threatens more than 50% of the arable land in the Czech Republic (Novotný et al., 2016). More than 10% of the arable soils are endangered by wind erosion (Podhrázká, Kučera, Chuchma, Středa, & Středová, 2013).

The erosion risk differs significantly in different soils and geological regions. Our study is located in the Chernozem region in southern Moravia, which is one of the most threatened areas in the Czech Republic (Novotný et al., 2016; Žížala, Kapička, & Novotný, 2016). Based on the empirical models, 84% of the arable land in this region is under threat from water erosion and approximately 86% is under threat from wind erosion. The first study on tillage erosion performed in the study area (Hrabalíková et al., 2016) also showed a significant impact of this form of erosion on the degradation of the soil cover.

Several studies based on field assessments and measurements of soil erosion indicate a discrepancy between modelled values and real field or plot data (Evans, 1998, 2013; Prasuhn, 2011; Žížala et al., 2016). The results point out considerable uncertainty in the quantification of real soil erosion. Moreover, the model-based approaches show a limited potential in the assessment of the erosion intensity and the spatial extent of degraded soils, namely, due to internal drawbacks of models and inaccuracy and uncertainty in the input data. However, despite a long-term criticism of empirical models by erosion scientists (Boardman, 2007; Evans & Boardman, 2016a,

2016b; Favis-Mortlock, Boardman, & MacMillan, 2001), their application is, due to the lack of reliable and accessible data on real erosion, currently essential for soil conservation policy purposes. Thus, applicable and cost-effective methods for real erosion assessment and monitoring are necessary. Methods based on remote sensing promise to be suitable for this purpose; the remote sensing represents a cost-effective tool applicable at the regional scale.

Remote sensing has been used in erosion studies for acquiring input data for erosion models, for an indirect assessment of soil erosion using the analysis of vegetation cover and for a direct identification of erosion features and soil degradation stages (Luleva, 2013; Shoshany, Goldshleger, & Chudnovsky, 2013; Vrieling, 2007). Indirect methods commonly provide input data for erosion models, whereas direct methods enable identification and delineation of individual erosion features (rills, gullies and sediment depositions) (Fadul, Salih, Imad-Eldin, & Inanaga, 1999; Martínez-Casasnovas, 2003), or eroded and accumulated areas (Alatorre & Beguería, 2009; Fulajtár, 2001; Kolejka & Manakos, 2000; Šarapatka & Netopil, 2010).

The basic principle of the identification of eroded and accumulated (AC) soils is based on the assumption that the spectral reflectance of eroded or AC soils has different attributes than non-eroded (NE) “healthy” soils. These differences are caused by changes in the chemical and physical properties of the upper layer of soils due to the processes connected with soil removal, soil transportation and accumulation (Chabrilat et al., 2014; Chappell, Zobeck, & Brunner, 2005; Conforti et al., 2013; Demattê & Focht, 1999; Lin, Zhou, Wu, Zhu, & Dang, 2014; Schmid et al., 2012, 2016; Žižala, Zádorová, & Kapička, 2017). Soil properties affected by erosion processes that have a spectral response in soil spectra at the same time can be identified as spectral soil erosion indicators. These properties are either affected by the preferential removal and transportation of light surface particles, such as soil organic matter content and soil texture (Schmid et al., 2016), or are related to the removal of topsoil and its mixture with subsoil, such as the content of carbonates (Curzio & Magliulo, 2010b; Žižala et al., 2017), content of iron oxides (Chabrilat, 2006; Frazier & Cheng, 1989; Lin et al., 2014; Mathieu, Cervelle, Rémy, & Pouget, 2007), or content of coarse fragments (Hill, Mégier, & Mehl, 1995; Hill, Mehl, & Altherr, 1994; Hill & Schütt, 2000). The possibility and accuracy of the delineation of eroded soils using spectral images is highly dependent on the intensity of the erosion processes on the one hand, and

on the corresponding changes in the spectral characteristic of disturbed soils on the other hand.

Remote sensing methods, traditionally used for the detection of eroded areas, include the visual interpretation of aerial images based on the interpretation of the soil colour and its changes related to the erosion processes (Fulajtár, 2001; Fulajtár, Jenčo, & Saksas, 2016; Servenay & Prat, 2003). Recently, the progress in satellite data and digital RS utilization, including computer pre-processing of images (Fulajtár, 2001; Kolejka & Manakos, 2000; Šarapatka & Netopil, 2010) and the development of automatic classification methods (Alatorre & Beguería, 2009; Curzio & Magliulo, 2010a; Martínez-Casasnovas, 2003; Mohammadi & Nikkami, 2008), has enabled the analyses of larger areas in a time-saving manner, and the quantification of the classifications’ accuracy. Spectra-based per-pixel classification methods are easily implemented (Li, Zang, Zhang, Li, & Wu, 2014). However, their application can be problematic in cases of a significant, within-class spectral variability and mixture effect of different surfaces, particularly in conditions of a highly heterogeneous soil cover. Fulajtár (2001) noted that additional ancillary data is needed for the classification of erosion patterns with required accuracy, and other authors have also recommended a combination of automatic classification approach and visual interpretation (Báčová & Krása, 2016; Pilesjoe, 1992; Šarapatka & Netopil, 2010; Smetanová, 2009). The application of the fuzzy classification (Meléndez-Pastor, Pedreño, Lucas, & Zorpas, 2017), the spectral mixture (sub-pixel) analysis (Haboudane, Bonn, Royer, Sommer, & Mehl, 2002; Rabah & Farah, 2016; Schmid et al., 2016) or the object classification (“spatio-contextual” image classification) (Mayr, Rutzinger, Bremer, & Geitner, 2016; Nobrega et al., 2006; Wang, Huang, Du, Hu, & Han, 2013) represents another solution to overcome the above mentioned difficulties related to the pixel-based methods (Li et al., 2014). Simultaneously, using higher resolution data in the spectral domain (hyperspectral data) promises an increase in the accuracy of the classification of erosion-degraded soils (Chabrilat et al., 2003, 2014; Haubrock, Chabrilat, & Kaufmann, 2004, 2005; Hill et al., 1994; Schmid et al., 2016; Žižala et al., 2017). The further development and wider application of this method can be expected with the forthcoming spaceborne hyperspectral sensors, such as German EnMAP, Italian PRISMA, Japanese HISUI, Israel-Italian SHALOM or Chinese TianGong-1 (Demattê et al., 2015). So far, multispectral Landsat series and SPOT data or high resolution data, such as IKONOS and QuickBird have been the most commonly used satellite data in soil erosion research (Luleva, Van Der Werff, Van Der Meer, & Jetten, 2012; Sepuru & Dube, 2017; Vrieling, 2006). Newly launched satellites, such as Landsat-8 and



Sentinel-2 with their improved spectral, radiometric and spatial characteristics provide freely available multi-temporal data suitable for soil erosion mapping. The verification of their applicability is currently required.

Despite the progress in the classification methods and development of new types of optical sensors, the still-existing gaps in our knowledge limit a regular use of these methods for the assessment of eroded soils.

Several main limitations can be distinguished: (i) Assessment of large areas with field plots characterized by varying soil conditions (soil moisture, soil roughness, soil covered with vegetation, litter, dust or soil crust). It is necessary to use a multi-temporal approach and methods enabling a reduction of these effects. So far, most of the studies have focused on local scale assessment (Sepuru & Dube, 2017), and a substantial progress at regional and global scaled research is needed. (ii) Indispensability of precise atmospheric corrections and masking of the clouds and their shadows. (iii) Heterogeneity of environmental settings, especially of the soil cover structure (occurrence of different soil types and parent material, historical human-induced disturbances (Zádorová, Penížek, Žížala, Matějovský, & Vaněk, 2018)). (iv) Specificities related to the erosion/accumulation process. Erosion and redeposition of soil material may lead to similar soil surface properties of eroded and AC soils (Zádorová et al., 2013, 2015). (v) Lack of historical data and related difficulties in the determination of original soil thickness, soil properties and erosion impact even at a local scale.

The aim of this study is to assess the potential of a combined use of time series of optical multispectral images from newly launched Sentinel-2 satellites, and time series of aerial orthoimages and field data for the (i) identification of the erosion spatial pattern at the regional scale and, (ii) delineation of the soils

impacted by soil erosion processes at the regional scale. This study presents a multi-temporal classification approach, assessing the erosion-related soil pattern at a larger spatial extent compared to previous studies. The presented approach promises to produce a practical method usable in a frequent monitoring of degradation of soils due to erosion in large agricultural areas.

### Regional settings

The study is located in the agricultural region in South-East Moravia, Czech Republic (Figure 1). The study area represents a region with the highest degradation risk by erosion on one the hand, and with some of the most fertile soils in the Czech Republic on the other hand. The area is delimited by longitudes 16.64 and 17.37E and latitudes 48.83 and 49.27N. The limits of the study area correspond with the occurrence of the Chernozem soil type and with boundaries of a region characterized by an undulating topography. The study area covers approximately 1,222 km<sup>2</sup>. Arable land covers 815 km<sup>2</sup> (66%) of the study area. The area has undulating relief with an elevation ranging between 163 m a.s.l. and 477 m a.s.l.; the mean slope at the arable land is 4.2° (with a standard deviation of 3.08°), but it reaches up to 20° in the steepest parts. The climate is characterized by a mean annual precipitation of 540 mm and a mean annual temperature of 8.4°C. The area is formed by upper Eocene molasse facies (sandstones, conglomerates and marls) and Oligocene sandstones covered by a Pleistocene loess layer with a variable depth ranging from several metres up to several tens of metres (Chlupáč, Brzobohatý, Kovanda, & Straník, 2002).

Calcic Chernozem on loess is the original dominant soil type in the study area. During the centuries of

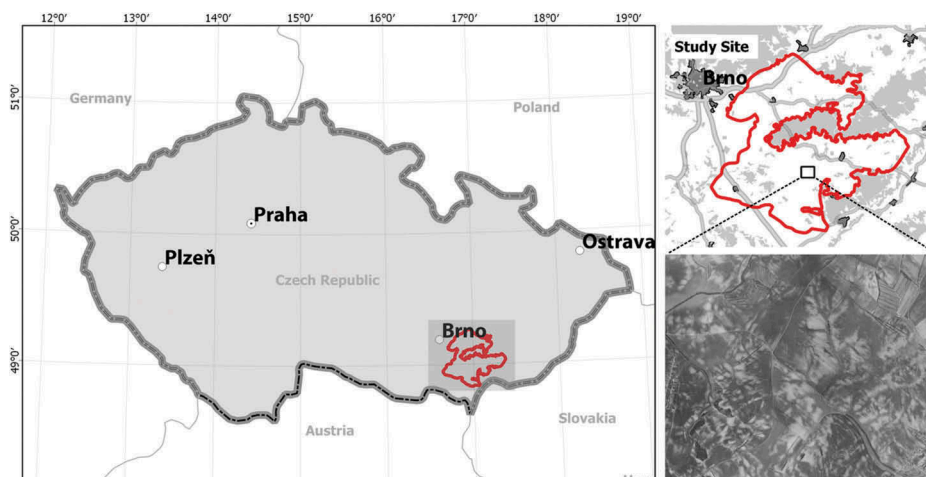


**Figure 1.** Location of the study site (red border) with position of tile satellite image and detail of the erosion pattern on arable land.

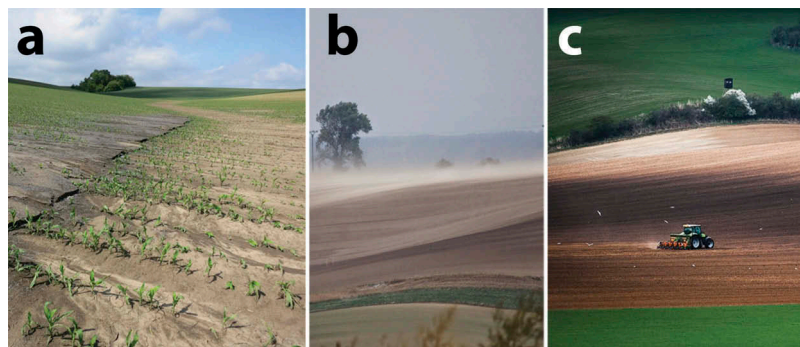


**Figure 2.** Impact of different types of erosion on the fields within the study area (a) water erosion, (b) wind erosion, (c) tillage erosion.

agricultural practices, the soil cover has been transformed into a diversified mosaic of different soil units along with variable erosion and deposition processes (Figure 2). In addition to the former Chernozems, which are currently preserved in places with minimal slope, Haplic Calcisols have developed on steep slopes and slope shoulders (Hrabovská, 2013; Vopravil et al., 2011; Zádorová, Penížek, Šefrna, Rohošková, & Borůvka, 2011). By contrast, deep colluvial soils have been formed in concave parts of the slopes (Zádorová et al., 2013, 2011; Zádorová et al., 2015). The intensive response to soil erosion can be attributed to several factors: a high erodibility of soils determined by their silty texture, a segmented landscape locally with high inclination, the excessive size of farmers' fields caused by forced collectivization of agricultural land in 1950s, an inappropriate management of arable land (intensive cultivation of crops susceptible to erosion, lack of manuring), and the destruction of landscape elements with an anti-erosion effects and unfavourable weather conditions (frequent episodes of drought) (Fukalová, Středová, & Vejtasová, 2014; Krása, Středová, Dostál, & Novotný, 2014).

## Materials and methods

### Soil data collection

The soil data contained in the datasets used for calibration and validation purposes originate from recently performed field campaigns carried out in the study area. The first part of the dataset is represented by the data acquired from field campaigns, where soil cover was surveyed in detail. All sites are characterized by high spatial variability of soil cover in response to soil erosion. Although the area is limited, all defined erosion and accumulation classes were found. This subset contains information from three local field campaigns:

- 50 samples from the site Sardice field survey performed in 2016 (Hrabalíková et al., 2016; Žížala et al., 2017),
- 75 samples filtered using stratified random sample selection from 600 samples acquired within

the detailed campaign at the site Poresice in 2009 (Brodský, Vašát, Klement, Zádorová, & Jakšík, 2013; Vašát, Kodešová, Klement, & Jakšík, 2015; Zádorová et al., 2011) and

- 78 samples from the site Oulehle surveyed in 2016.

This part of the dataset was used as a calibration set for the classification, or more precisely, as support data for supervised cluster categorization during post-processing after unsupervised classification. The second part of the dataset contains data from a sparse sampling campaign that was performed across the study area in 2016 and 2017. The sampling points' locations were selected from the database of an historical soil campaign, "Systematic soil survey of agricultural land in Czechoslovakia", carried out between 1960 and 1970 (Němeček, 1967; Zádorová & Penížek, 2011). The selection was performed using a stratified random strategy. The terrain attributes and spectral data were used as feature space variables for stratification. This part of the dataset, containing 115 samples, was used for validation purposes. The positions of all samples were measured by GNSS with a post-processing sub-meter accuracy. The information about soil profiles-soil unit, soil depth, profile stratigraphy and thickness of horizons was obtained by the description of a gouge auger core. The distribution of soil samples is depicted in Figure 3.

All soil samples from both datasets were classified into four classes with various stages of degradation by erosion. The determination of each class was based on the observation of soil erosion evidence on the sampling sites and the descriptions of the soil profiles. Four established classification classes consist of three erosion classes and one accumulation class. According to Žížala et al. (2017), the groups are defined as follows:

- NE soils – autochthon soils with a negligible evidence of soil loss or accumulation;
- Eroded soils with various stage of degradation – moderately eroded (ME) and strongly eroded (SE) soils – soil profiles with an evidence of soil loss and soil profile truncation; and

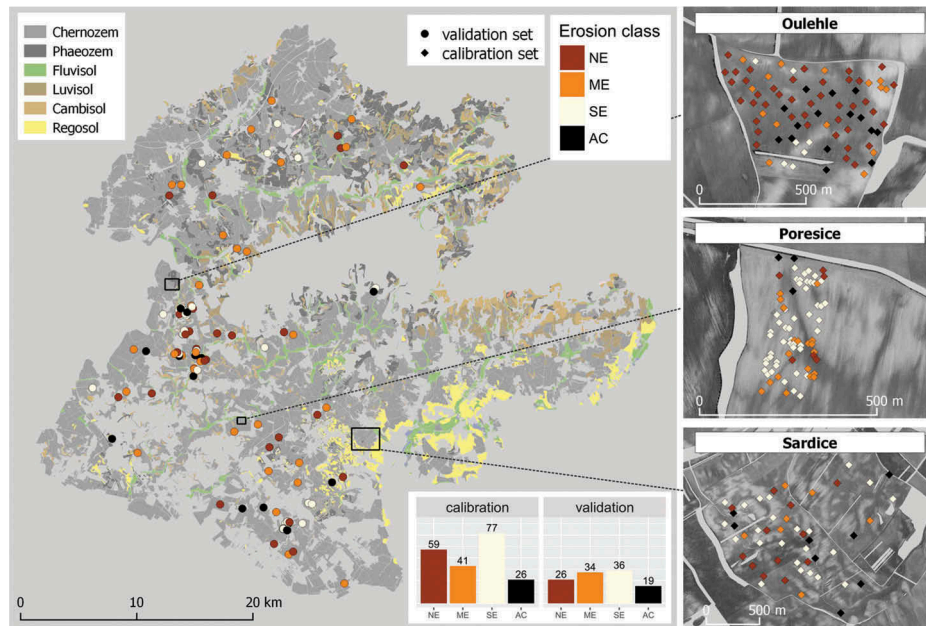


Figure 3. Soil samples distribution in study area.

- AC soils – soil profiles with an evidence of accumulation of new material and with increased thickness of the A horizon or burial of former surface horizons.

Soil samples were classified into erosion classes according to the description of soil profiles. The samples with the profile stratigraphy corresponding to the characteristics of the original Calcic Chernozems were classified as NE soils (59 samples in the calibration dataset and 26 samples in the validation dataset). These soils particularly cover the areas with minimal slope (0–2°). Calcic Chernozems occurring in the areas with increased slope and having significantly reduced thickness of A horizon were classified as ME (41 samples in the calibration dataset and 34 samples in the validation dataset). Soils with the truncated profiles were determined in the exposed areas with steep slopes (water erosion influence) and in the areas with high slopes gradients (tillage erosion influence). The profile stratigraphies of these soils corresponded to the Haplic Calcisol and were classified as SE soils (77 samples in the calibration dataset and 36 samples in the validation dataset). Deep colluvial soils with thick humus horizons were identified in the slope concavities, mainly in the toe-slopes, slope depressions and side valleys. These soils were

classified as AC (26 samples in the calibration dataset and 19 samples in the validation dataset).

### Images and image pre-processing

Sentinel-2 satellite images were used in the study. The time series of the seven Sentinel-2A MSI imagery (processing Level-1C) from 2015, 2016 and 2017 were downloaded from the Copernicus Open Access Hub (Table 1). The product Level 1C includes radiometric and geometric corrections with sub-pixel accuracy (European Space Agency, 2015). These data were processed to a Level-2A (atmospherically corrected) data product using Sentinel-2 Toolbox (Sentinel Application Platform, SNAP v5.0) with an integrated Sen2cor processor (Sentinel to Correction, v2.3.1).

All Level-2A data were pre-processed in Envi 5.4.1 to obtain a layer stack of 10 spectral bands (10 and 20 m resolution bands), resampled to the resolution of 10 m for all bands by the nearest neighbour method, and co-registered. The data from each image was masked as follows: the arable land mask, cloud cover mask and bare soil mask. The arable land mask was delimited by field boundary polygons obtained from the Land parcel identification system (LPIS – © Ministry of Agriculture of the

Table 1. Details of Sentinel-2 images.

No.	Tile	Sensing time	Sun zenith <sup>a</sup>	Sun azimuth <sup>a</sup>	Clouds [%] <sup>b</sup>	Thin cirrus [%] <sup>b</sup>	Cloud shadow [%] <sup>b</sup>	Bare soil [%] <sup>b</sup>
1	33UXQ	2015/08/30 10:05	41.21	162.92	4.90	12.90	0.05	27.99
2	33UXQ	2015/09/29 10:06	52.06	168.94	40.24	0.83	11.82	14.64
3	33UXQ	2016/05/23 9:54	30.22	155.73	2.04	17.54	0.05	10.72
4	33UXQ	2016/09/30 9:50	53.06	166.10	7.44	4.85	1.91	31.38
5	33UXQ	2017/03/29 9:50	47.32	159.70	6.66	5.73	0.73	58.44
6	33UXQ	2017/04/21 10:00	38.21	162.80	16.23	8.75	2.14	18.07
7	33UXQ	2017/05/18 9:50	31.22	156.46	8.90	7.73	0.05	13.58

<sup>a</sup>Mean sun angle.

<sup>b</sup>Based on L2A quality indicators

Czech Republic). The cloud mask was obtained from the scene classification maps of the L2A product. The classes of clouds (low, medium and high probability), thin cirrus, cloud shadows, dark areas, saturated pixels and defective pixels, were extracted and reclassified into one layer. For detecting the bare soils for each image scene, the “soil line” concept was implemented (Baret, Jacquemoud, & Hanocq, 1993a; Baret, Jacquemoud, & Hanocq, 1993b; Richardson & Wiegand, 1977), and the relationship between band 8 (Near-infra Red) and band 4 (Red) was explored. On the basis of the brightness detection, all

pixels marked in the scatter plot tool were detected and visualized in the image.

### Classification

A preliminary assessment of the spectral purity of the training samples showed very poor spectral separability of some classes based on the ground-truth training samples. The statistics and analysis of variance showed that the calibration set is inappropriate for supervised classification purposes (Figure 4). Therefore, an

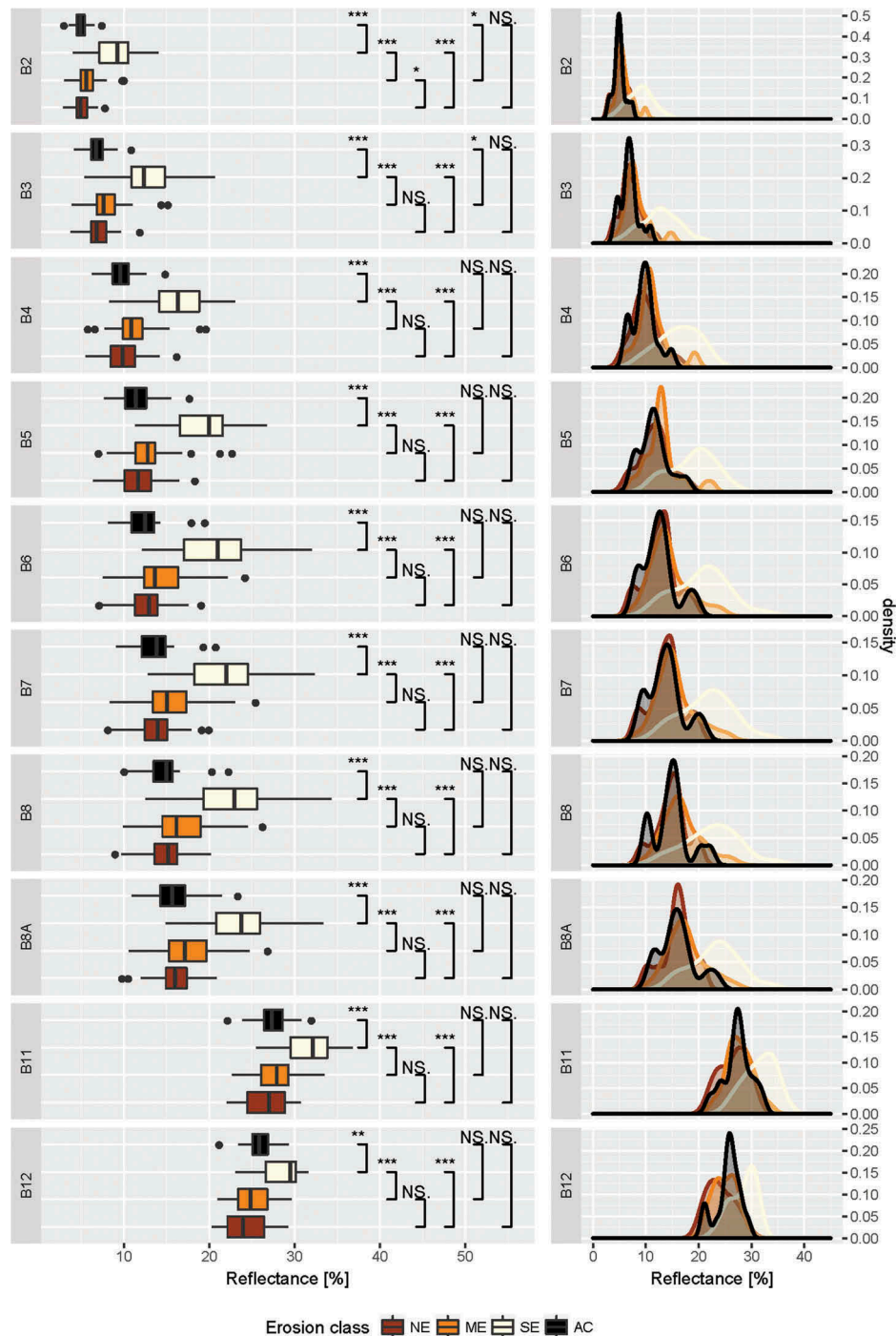


**Figure 4.** Spectral separability of erosion classes based on ground-truth training samples. B1 – B12 represents Sentinel2 spectral bands. \*, \*\*, \*\*\* indicates level of significance of difference of mean ( $*p \leq 0.05$ ,  $**p \leq 0.01$ ,  $***p \leq 0.001$ ), NS = non-significant difference.

unsupervised clustering algorithm ISODATA – Iterative Self-Organizing Data Analysis (Tou & Gonzalez, 1974) mixture with supervised cluster categorization Minimum Distance Method was used for the classification of the erosion classes. Due to possibly different soil conditions on each image, each satellite image was classified separately. All post-processed classified rasters were merged into one final classification synthesis using the recalculation according to the most frequent class value for each pixel of the classified area.

The main advantage of the automatic image classification is the speeding up of the data processing. It is a relatively simple, time-saving and inexpensive method that can be used for large areas (Gómez, White, & Wulder, 2016). In comparison with the supervised classifications that require a certain amount of representative training samples, the unsupervised classification algorithm is not dependent on training samples and their spectral separability (Sepuru & Dube, 2017). Moreover, unsupervised methods provide the opportunity to identify clusters that could not be identified with the training samples. It is guaranteed by internal algorithms in case of unsupervised classifiers.

The ISODATA clustering technique uses the minimum spectral distance measurements to form clusters in an image. Different numbers of temporal clusters were generated with the following modelling parameters: number of classes (min: 8; max: 12), maximum number of iterations (30), change threshold (5%), minimum number of pixels in a class (1,000), maximum class standard deviation (1), minimum class distance (5), and maximum number of merge pairs (2). Once this classification was completed, the automatic cluster categorization Minimum Distance Method, based on a calibration point dataset, was applied to the clusters to define the erosion classes (NE, ME, SE, AC).

### Refinement using aerial orthoimages

The time series of aerial survey orthoimages from years 2003, 2006, 2009, 2012 and 2015 (© Czech Office for Surveying, Mapping and Cadastre) were used for the refinement of the classification synthesis for the whole study area. The final classification raster was converted to a vector polygon layer. The area of 500 m<sup>2</sup> was set as the minimum mapped unit. On a scale of 1: 10,000, it is represented by a 5 × 1 mm<sup>2</sup> rectangle. It represents a trade-off compromise between the operational costs and the map informational requirement (resolution of map). Polygons with an area of less than 500 m<sup>2</sup> (5 pixels) were removed. These could be a product of noise generated during the classification process.

The classification assessment showed that the discrimination of the ME from other classes was not satisfactory (Figure 4 and Table 3). Accordingly, only the SE class was considered for the final identification of the eroded areas. On the basis of the visual inspection over multi-imagery scenes, individual polygons were modified and refined. The geometry of the features was adjusted according to the elements visible on orthoimages.

### Validation of results

An independent validation dataset comprising 115 soil samples distributed across the study area was used for validation. A confusion matrix was calculated for both the classification synthesis and visual refinement of the output using point soil data as a ground truth. The user's and producer's accuracy, the overall accuracy and kappa coefficient were calculated to evaluate the final classification synthesis.

The flowchart of the whole process is depicted in Figure 5.

### Results

Seven Sentinel-2A images were used for the classification. The images were masked by an arable soil layer, cloud non-affected pixels and bare soil pixels identified by the soil line concept. The extent of the bare soil for each image scene is depicted in Table 2. The maximum bare soil extent (53.4% from the total arable land) was obtained in September 2016; a significant extent of the bare soil was identified also in September 2015 and April 2017. The minimum bare soil extent (18.1% from the total arable land) occurred in May 2017. The final bare soil extent of the classification synthesis covered a total area of 733.6 km<sup>2</sup>, which was 90.1% of the total arable land of the study area.

The final synthesis map with erosion classes was produced using the ISODATA classification and cluster categorization Minimum Distance Method (MDM) performed on the Sentinel-2 images. Due to the high spectral heterogeneity of the AC soils and their very poor spectral separability from other classes (Figure 4), the AC was not assigned to any ISODATA class by the MDM. Therefore, only three eroded classes were determined (NE, ME, SE). In total, there are 6,711 arable land fields within the study area. The SE soils cover 18%, the ME soils cover 38% and the NE soils cover 44% of the total area.

Figure 6 shows the descriptive statistics of the classified erosion classes in respect to the spectral characteristics derived from the Sentinel-2 images. The overall values of the spectral data correspond to the general shape of the spectral curves of the

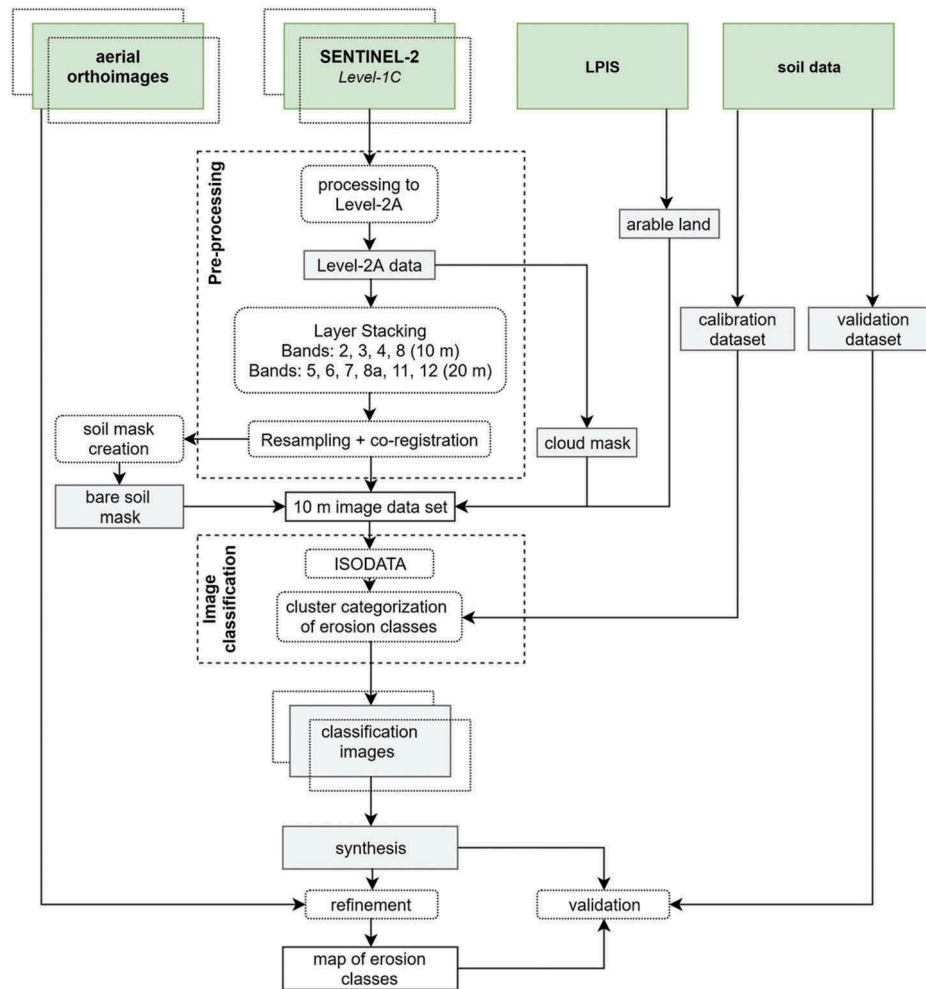


Figure 5. Flowchart of the processing images to eroded soil assessment.

Table 2. Bare soil masks description and classification results for Sentinel-2 image data set.

No.	Sensing time	Bare soil extent [km <sup>2</sup> ]	Bare soil extent from the total arable land [%]	Erosion classes representation (%)		
				NE	ME	SE
1	2015/08/30 10:05	249.3	30.6	58	26	16
2	2015/09/29 10:06	358.7	44.1	37	42	21
3	2016/05/23 9:54	117.1	14.4	40	38	21
4	2016/09/30 9:50	434.5	53.4	32	51	17
5	2017/03/29 9:50	345.7	42.5	57	28	15
6	2017/04/21 10:00	248.9	30.6	58	25	17
7	2017/05/18 9:50	147.4	18.1	43	44	12
<b>Final synthesis</b>		<b>733.6</b>	<b>90.1</b>	<b>44</b>	<b>38</b>	<b>18</b>

Chernozem soils. The results show low reflectance values in the visible wavelengths (B2, B3, B4 bands), with a gradual increased reflectance towards the infrared wavelengths (B5, B6, B7, B8

and B8A). The highest values were obtained from the SWIR region (B11 and B12). The NE soils have a lower reflectance than the ME and SE soils in every spectral band, except for the NE

Table 3. Confusion matrix of the erosion classes classification.

		Ground truth				Classification overall	Producer Accuracy (%)
		NE	ME	SE	AC		
Classifier results	<b>NE</b>	<b>22</b>	19	7	13	61	36.1
	<b>ME</b>	4	<b>11</b>	9	4	28	39.3
	<b>SE</b>	0	4	<b>20</b>	2	26	76.9
	<b>AC</b>	0	0	0	<b>0</b>	0	-
Truth overall		26	34	36	19	115	
User Accuracy		84.6	32.4	55.6			
Overall accuracy (%)		55.2					

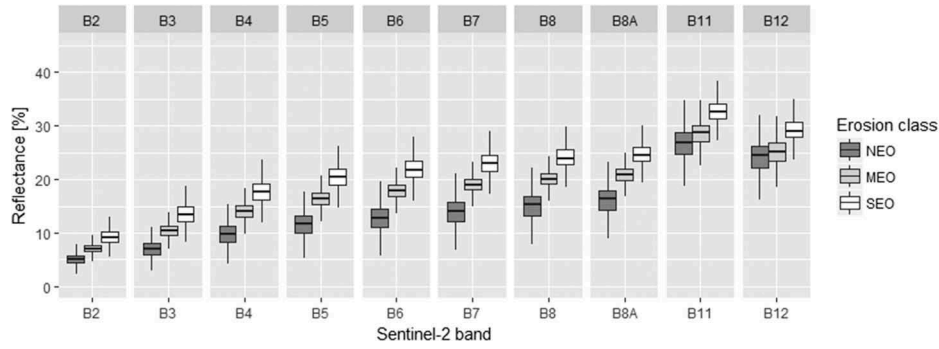


Figure 6. Descriptive statistics of reflectance values in the classified erosion classes.

and ME in the SWIR region where the difference is not significant.

The validation based on ground-truth data showed a low overall accuracy of the classification (see Table 3). It reached 55.2% (Kappa coefficient 0.34). The main misclassification is connected with an incorrect classification of ME to NE (19 cases). Other classification errors are represented by misclassifications between SE–NE (7 cases) and SE–ME (13 cases). The AC soils were classified mainly as NE soils (13 cases); in the six cases, they were assigned to eroded soils (ME and SE).

The overall accuracy increased significantly after an adjustment of the erosion classes. The performance of the classification scheme in distinguishing

two classes (SE and other soils) was satisfactory. The overall accuracy reached 80.9% (Kappa coefficient 0.52). When considering each single image, the images captured in early spring months – March and April – showed better overall accuracy (83.3–86.7%) than the images acquired in autumn (73.1–77.8%).

Finally, the samples-independent refinement of the SE was performed using orthoimages. The overall accuracy of the SE class classification reached 86.9%. Only one SE sample was misclassified into the other category and 10 samples of NE and ME were classified as SE (see Table 4). There were 4 from 19 AC samples that were located within the area of the SE class.

Table 4. Confusion matrix of the erosion stages classification based on refinement.

		Ground truth				Classification overall	Producer accuracy (%)
		NE	ME	SE	AC		
Orthophoto refinement results	SE	1	9	<b>35</b>	4	49	71.4
	Others	<b>25</b>	<b>25</b>	1	<b>15</b>	66	98.5
Truth overall		26	34	36	19	115	
User Accuracy		–	–	97.2	–		
Overall accuracy (%)		86.9					

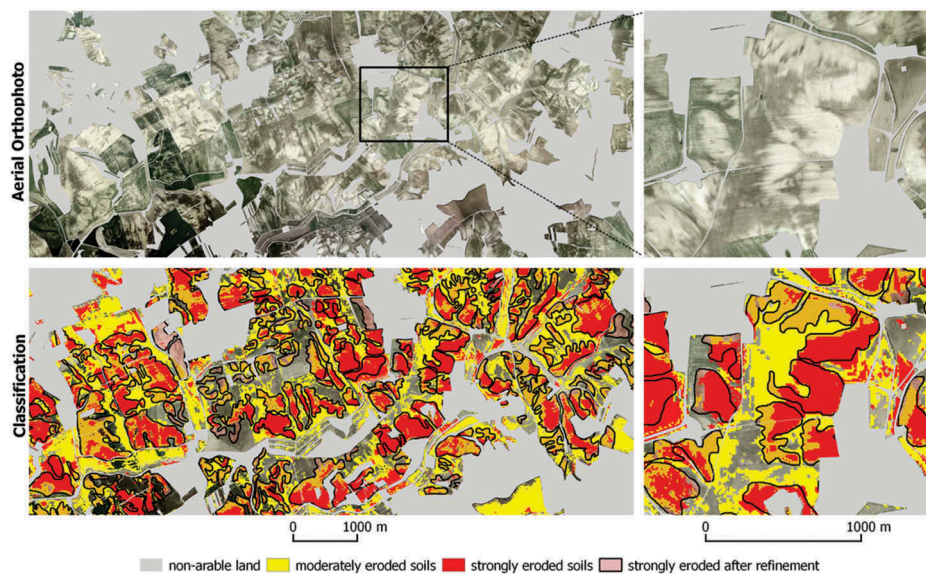


Figure 7. Delineation of eroded classes using the unsupervised classification and the refinement based on visual interpretation of orthoimages.

A delineation of erosion classes using the unsupervised classification and SE class refinement is shown in Figure 7. Generally, the classification shows that a highly diversified soil cover formed in the areas that were originally covered with Chernozems. In both cases, the SE class was distinguished on the most exposed terrain positions in terms of tillage and water erosion. The ME class was classified on the milder slopes and positions with lower slope gradients adjacent to the SE class. The NE class was distinguished on plateaus and low slopes up to 2°.

## Discussion

The main goal of this study was to analyse the possibilities of a direct delineation of eroded soil in agricultural land at a regional scale using optical multispectral images. Up to now, the majority of studies dealing with the direct delineation of eroded soils in agricultural land have been performed at a local scale, usually on small study sites consisting of one or few agriculture fields (Báčová & Krása, 2016; Fulajtár, 2001; Kolejka & Manakos, 2000; Šarapatka & Netopil, 2010; Smetanová, 2009). Other studies that have focused on the direct detection of eroded areas have delineated highly eroded non-agricultural areas characterized by bare soil or rock outcrops, such as badlands (Alatorre & Beguería, 2009; Beguería, 2006; Liberti et al., 2009; Pérez & García, 2017; Servenay & Prat, 2003). In these regions, different methods of eroded soils' delineation, based mainly on the land cover classification, have been applied.

The results of the unsupervised classification of three degradation stages of soils showed a low overall accuracy of up to 55.2%. The accuracy is lower than that observed in studies performed at a local scale. Floras and Sgouras (1999) used Landsat 5 images for a k-means supervised classification of land cover, including eroded soils in marls, and reached an overall accuracy of 83.94%. Fulajtár (2001) reached the accuracy of 60% of the unsupervised classification of eroded soils on loess using a SPOT panchromatic image at the local scale. Similarly, Šarapatka and Netopil (2010) used the unsupervised classification of aerial photographs for the delineation of eroded soils on loess at the local scale. Kolejka and Manakos (2000) used a single Landsat 7 image for the delineation of SE soils in different geosystems.

In the present study, the main source of the classification error is connected with the incorrect classification of the ME class. A similar problem of distinguishing more erosion classes, especially the transitional classes between the NE and SE classes, has been reported in the literature (Schmid et al., 2016; Zádorová et al., 2011; Žížala et al., 2017). The ME class has achieved the lowest values of both user and producer accuracy. The main

misclassification has been determined in the classification of ME to NE and vice versa. The results showed that distinguishing between these classes is very problematic using the present approach. The reasons for these inconclusive results lie in the character of the ME class. The ME class is characterized by a decrease of the A horizon thickness, but not under the depth of tillage. The tillage operations do not cause mixing of the humic A horizon with the contrasting subsoil (A/C horizon or loess). Thus, the properties of the topsoil are not significantly affected by soil removal, in contrast with SE soils, and the spectral differences of the NE and ME classes are observable with difficulties. The performance of the ME delineation can be potentially increased using fuzzy methods, object-oriented classification methods or data with a higher spectral resolution, such as hyperspectral data (Schmid et al., 2016; Žížala et al., 2017).

A preliminary assessment of the spectral purity of the training samples in this study showed very poor spectral separability of the classes based on ground-truth samples. According to Sepuru and Dube (2017), the low separability of classes limits the applicability of the supervised classification methods, particularly in spectrally complex erosion areas. The methods of machine learning, such as Support vector machine or the determination of a set of endmembers for different soil erosion and accumulation classes, represent a possible solution to overcome the limitations of the supervised classification methods (Schmid et al., 2016).

Despite the low accuracy of the automatic classification, the study showed a potential for the applied approach to distinguish SE soils from NE soils. Nevertheless, it still has many limitations. The use of refinement of the eroded classes based on the visual interpretation of time series of aerial orthoimages leads to the increase of the classification accuracy, as was shown in the present study. However, the visual interpretation represents a time-consuming and subjective method that is limited to the visible RGB spectra (Fulajtár, 2001; Šarapatka & Netopil, 2010). The main difficulty lies in the fact that the level of soil degradation changes gradually. However, the operator must assess the crisp boundaries of the erosion classes.

Moreover, the accuracy of the erosion classification may also be influenced by other factors. The pattern of the spectral reflectance differs due to not only the erosion processes but also the characteristics influencing the spectral response, which are soil moisture, the geometric properties of the soil surface (roughness) and the variability of other soil properties, such as soil texture, soil aggregate sizes or the presence of a soil crust (Ben-Dor & Dematté, 2015; Dematté et al., 2015; Goldshleger, Ben-Dor, Lugassi, & Eshel, 2010; Schmid et al., 2016). Additionally, spectral satellite



data are influenced by different light beam geometries according to the date of acquisition (solar zenith and azimuth). This joint effect cannot be completely eliminated by image corrections.

The multi-temporal approach represents a possible solution to map soil properties in temperate regions. First, the soil composite concept presented by Diek, Fornallaz, Schaepman, and de Jong (2017) or Rogge et al. (2018) can be applied. Second, each image can be processed separately to overcome the issue of different surface and geometry conditions. This approach was used successfully in this study. Nevertheless, a reference study is needed to compare both approaches.

The classification can be even more difficult in the case of the combined influence of more erosion and sedimentation processes. The study area is characterized by the combined effect of water, tillage and wind erosion. This combination of soil redistribution processes leads to a highly complex erosion pattern and, for example, similar soil surface properties of the eroded and AC soils (Hill et al., 1995; Zádorová et al., 2013; Žížala et al., 2017).

The variability of soil types is also an important restraint in the assessment of larger areas. The erosion processes ongoing in soils with different stratigraphy and properties can result in significantly different spectral properties of the soil surface (Šarapatka & Netopil, 2010; Schmid et al., 2016; Smetanová, 2009; Žížala et al., 2017). The present approach is therefore limited to pedologically homogeneous areas.

The direct classification approaches of arable soils can also be limited by the masking effects of vegetation, litter or cloud cover on images. Therefore, especially in the condition of a temperate climate, a multi-temporal approach must be applied to avoid problems related to masked surfaces in large areas (Gómez et al., 2016; Meléndez-Pastor et al., 2017; Topaloğlu, Sertel, & Musaoğlu, 2016). Our study confirmed that the use of periodically acquired images, such as time series of aerial orthoimages or satellite data with continuous acquisition of images from Sentinel-2 or Landsat satellites, is appropriate. In our study, the mask consisting of the LPIS, cloud mask, and bare soil mask was created. The main difficulty was associated with the bare soil mask. The spectral behaviour of the vegetation cover and the bare soil is, in some cases, very similar, and the distinguishing of the litter cover is also problematic (Šarapatka & Netopil, 2010). The time series of seven images covering the spring-autumn period were used. Then, it was possible to identify almost 90% of the area with bare soils by the concept of the bare soil line. Every single image was characterized by certain specifics in vegetation cover. The sparse vegetation cover often occurred in the spring (March, April, and May). Through the summertime (August), only a very small area was covered by the bare soil. The presence of crops

during the phase of harvesting (cereals, corn) was typical for September's images. These fields covered with ripened crops and stubble fields had the spectral characteristics similar to SE areas in the VIS/NIR domain and could not be identified by the soil line methods. They were removed manually. Therefore, a more complex approach is needed to increase the accuracy of the bare soils' identification (Richardson & Wiegand, 1977). Additionally, other more accurate methods (e.g. fmask – Zhu, Wang, & Woodcock, 2015) for the identification of the areas affected by clouds influence need to be tested.

## Conclusions

The present study tested the potential of the processing of time series of Sentinel-2 images and aerial orthoimages to assess the erosion stages of agricultural soils. The assessment has been performed at a regional scale, in a study area comprising hundreds of square kilometres. The impact of erosion at the study sites was evaluated by an unsupervised classification of satellite images combined with the visual interpretation of aerial images.

This study reveals that the applied approach enables the accurate distinction of NE and SE soils. However, the performance of method for more detailed classification of different erosion stages, including transitional classes (ME soils), was not satisfactory. An automatic unsupervised classification achieved an overall accuracy of 55.2% for distinguishing two eroded (strongly and moderately) and a NE class, and 80.9% for only one eroded class. The accuracy of the classification reached 86.9% after a visual refinement based on the orthoimages. Despite this high accuracy of the visual interpretation method, there are still many limitations, and more automatic and objective approaches need to be developed and tested. Moreover, some considerable limitations and gaps were identified in the automatic classification. The practical and routine implementation of this approach entails several problems related to soil cover variability, the masking effect of different objects (clouds, vegetation, litter), or the spectral separability of individual classes. Therefore, further research is required, especially in terms of the automatic selection and pre-processing of the images, reduce and overcome the negative effects of the masking properties, and a progressive statistical method should be applied in the classification process. The applicability of the presented approach is also limited to the pedologically and geologically homogeneous areas. A different approach, enabling the distinguishing of diverse spectral characteristics of degraded soil on different parent materials, should be adopted in heterogeneous areas.

Our study focused on the applicability of the presented multi-temporal approach at a larger spatial

extent compared to previous studies. Although the accuracy achieved by the automatic classification was not satisfactory and the method requires further testing and improvements, the presented approach promises to produce valuable data on the actual degradation of soils by erosion. This type of information, available at the regional scale, is strongly needed for conservation policy purposes, and therefore, further progress in improving this approach is required.

## Acknowledgments

This work was supported by the Ministry of Agriculture – National Agency for Agricultural Research (NAZV) under Grant QJ1520028; Grant QJ1610289; and Grant QK1720289.

## Disclosure statement

No potential conflict of interest was reported by the authors.

## Funding

This work was supported by the Ministry of Agriculture of the Czech Republic under grant number NAZV [QJ1520028, QJ1610289, QK1720289].

## ORCID

Daniel Žížala  <http://orcid.org/0000-0002-7685-7604>  
 Anna Juřicová  <http://orcid.org/0000-0001-9380-7986>  
 Kateřina Zelenková  <http://orcid.org/0000-0002-0848-0075>  
 Robert Minařík  <http://orcid.org/0000-0002-5654-1522>

## References

- Alatorre, L.C., & Beguería, S. (2009). Identification of eroded areas using remote sensing in a badlands landscape on marls in the central Spanish Pyrenees. *Catena*, 76(3), 182–190.
- Báčová, M., & Krása, J. (2016). Application of historical and recent aerial imagery in monitoring water erosion occurrences in Czech highlands. *Soil and Water Research*, 11(No. 4), 267–276.
- Baret, F., Jacquemoud, S., & Hanocq, J.F. (1993a). About the soil line concept in remote sensing. *Advances in Space Research*, 13(5), 281–284.
- Baret, F., Jacquemoud, S., & Hanocq, J.F. (1993b). The soil line concept in remote sensing. *Remote Sensing Reviews*, 7(1), 65–82.
- Beguería, S. (2006). Identifying erosion areas at basin scale using remote sensing data and GIS: A case study in a geologically complex mountain basin in the Spanish Pyrenees. *International Journal of Remote Sensing*, 27(20), 4585–4598.
- Ben-Dor, E., & Demattè, J.A.M. (2015). Remote sensing of soil in the optical domains. In P.S. Thenkabail (Ed.), *Land resources monitoring, modeling, and mapping with remote sensing* (Remote Sen, pp. 733–787). Boca Raton: CRC Press.
- Boardman, J. (2007). Soil erosion : The challenge of assessing variation through space and time. In A.S. Goudie & J. Kalvoda (Eds.), *Geomorphological variations* (pp. 205–220). Prague: P3K.
- Boardman, J., & Poesen, J. (2006). Soil erosion in Europe: Major processes, causes and consequences. In J. Boardman & J. Poesen (Eds.), *Soil erosion in Europe* (pp. 477–487). Chichester, UK: John Wiley & Sons, Ltd. doi:10.1002/0470859202.ch36
- Brodský, L., Vašát, R., Klement, A., Zádorová, T., & Jakšík, O. (2013). Uncertainty propagation in VNIR reflectance spectroscopy soil organic carbon mapping. *Geoderma*, 199, 54–63.
- Chabrillat, S. (2006). Land degradation indicators : Spectral indices. *Annals of Arid Zone*, 45(3–4), 331–354.
- Chabrillat, S., Kaufmann, H., Merz, B., Mueller, A., Bens, O., & Lemnitz, C. (2003, May 13–16). Development of relationships between reflectance and erosion modelling : Test site preliminary field spectral analysis. In *3rd EARSeL Workshop on Imaging Spectroscopy* (pp. 13–16). Herrsching: EARSeL.
- Chabrillat, S., Milewski, R., Schmid, T., Rodriguez, M., Escribano, P., Pelayo, M., & Palacios-Orueta, A. (2014). Potential of hyperspectral imagery for the spatial assessment of soil erosion stages in agricultural semi-arid Spain at different scales. In *2014 IEEE Geoscience and Remote Sensing Symposium* (pp. 2918–2921). IEEE. doi:10.1109/IGARSS.2014.6947087
- Chappell, A., Zobeck, T.M., & Brunner, G. (2005). Using on-nadir spectral reflectance to detect soil surface changes induced by simulated rainfall and wind tunnel abrasion. *Earth Surface Processes and Landforms*, 30(4), 489–511.
- Chlupáč, I., Brzobohatý, R., Kovanda, J., & Straník, Z. (2002). *Geologická minulost České republiky* [Geological history of the Czech Republic]. Prague, Czech Republic: Academia.
- Conforti, M., Buttafuoco, G., Leone, A.P., Aucelli, P.P.C., Robustelli, G., & Scarciglia, F. (2013). Studying the relationship between water-induced soil erosion and soil organic matter using Vis-NIR spectroscopy and geomorphological analysis: A case study in southern Italy. *Catena*, 110, 44–58.
- Curzio, S.L., & Magliulo, P. (2010a). Soil erosion assessment using geomorphological remote sensing techniques: An example from southern Italy. *Earth Surface Processes and Landforms*, 35(3), 262–271.
- Curzio, S.L., & Magliulo, P. (2010b). Soil erosion assessment using geomorphological remote sensing techniques: An example from southern Italy. *Earth Surface Processes and Landforms*, 35(3), 262–271.
- Demattè, J.A.M., & Focht, D. (1999). Detecção de solos erodidos pela avaliação de dados espectrais [Detection of soil erosion by spectral reflectance]. *Brazilian Journal of Soil Science*, 3, 401–413.
- Demattè, J.A.M., Morgan, C.L.S., Chabrillat, S., Rizzo, R., Franceschini, M.H.D., Terra, F.D., ... Wetterlind, J. (2015). Spectral sensing from ground to space in soil science: State of the art, applications, potential and perspectives. In P.S. Thenkabail (Ed.), *Land resources monitoring, modeling, and mapping with remote sensing* (pp. 661–732). Remote Sen. Boca Raton: CRC Press.
- Diek, S., Fornallaz, F., Schaepman, M.E., & de Jong, R. (2017). Barest pixel composite for agricultural areas using landsat time series. *Remote Sensing*, 9, 12.
- EEA, & JRC. 2010. *The European environment: State and outlook 2010*. In *Soil*. Luxembourg: Publications Office of the European Union. doi:10.2800/58866

- European Space Agency. (2015). *SENTINEL-2 user handbook*. GMES-S1OP-EOPG-TN-13-0001
- Evans, R. (1998). Field data and erosion models. In J. Boardman & D. Favis-Mortlock (Eds.), *Modelling soil erosion by water* (pp. 313–327). NATO ASI S. Berlin, Heidelberg: Springer. doi:10.1007/978-3-642-58913-3\_23
- Evans, R. (2013). Assessment and monitoring of accelerated water erosion of cultivated land - when will reality be acknowledged? *Soil Use and Management*, 29(1), 105–118.
- Evans, R., & Boardman, J. (2016a). A reply to panagos et al., 2016 (Environmental science & policy 59 (2016) 53–57. *Environmental Science and Policy*, 60, 63–68.
- Evans, R., & Boardman, J. (2016b). The new assessment of soil loss by water erosion in Europe. Panagos P. et al., 2015 Environmental science & policy 54, 438–447-A response. *Environmental Science and Policy*, 58, 11–15.
- Fadul, H.M., Salih, A.A., Imad-Eldin, A.A., & Inanaga, S. (1999). Use of remote sensing to map gully erosion along the Atbara River, Sudan. *International Journal of Applied Earth Observation and Geoinformation*, 1(3–4), 175–180.
- FAO and ITPS. (2015). Status of the world's soil resources (SWSR) – main report. *Food and Agriculture Organization of the United Nations and Intergovernmental Technical Panel on Soils, Rome, Italy*.
- Favis-Mortlock, D., Boardman, J., & MacMillan, V. (2001). The limits of erosion modeling. In R.S. Harmon & W.W. Doe (Eds.), *Landscape erosion and evolution modeling* (pp. 477–516). Boston, MA: Springer US. doi:10.1007/978-1-4615-0575-4\_16
- Floras, S.A., & Sgouras, I.D. (1999). Use of geoinformation techniques in identifying and mapping areas of erosion in a hilly landscape of central Greece. *International Journal of Applied Earth Observation and Geoinformation*, 1(1), 68–77.
- Frazier, B.E., & Cheng, Y. (1989). Remote sensing of soils in the eastern Palouse region with landsat thematic mapper. *Remote Sensing of Environment*, 28, 317–325.
- Fukalová, P., Středová, H., & Vejtasová, K. (2014). Development and prediction of selected temperature and precipitation characteristics in southern Moravia. *Acta Universitatis Agriculturae Et Silviculturae Mendelianae Brunensis*, 62(1), 91–98.
- Fulajtár, E. (2001). Identification of severely eroded soils from remote sensing data tested in Riš ň ovce, Slovakia. In D.E. Stott, R.H. Mohtar, & G.C. Steinhardt (Eds.), *Sustaining the Global Farm. Selected papers from the 10th International Soil Conservation Organization Meeting held May 24–29, 1999* (pp. 1075–1081). West Lafayette, IN: Purdue University and the USDA-ARS National Soil Erosion Research Laboratory.
- Fulajtár, E., Jenčo, M., & Saksa, M. (2016). Soil erosion mapping with the aid of aerial photographs tested at Pastovce, Ipel'ská pahorkatina. In M. Šulc Michalková, J. Miřijovský, D. Lóczy, & W. Zglobicki (Eds.), *Interdisciplinary studies of river channels and UAV mapping in the V4 region* (pp. 247–268). Bratislava: Comenius University in Bratislava.
- Goldshleger, N., Ben-Dor, E., Lugassi, R., & Eshel, G. (2010). Soil degradation monitoring by remote sensing: examples with three degradation processes. *Soil Science Society of America Journal*, 74(5), 1433–1445.
- Gómez, C., White, J.C., & Wulder, M.A. (2016). Optical remotely sensed time series data for land cover classification: A review. *ISPRS Journal of Photogrammetry and Remote Sensing*, 116, 55–72.
- Grimm, M., Jones, R., & Montanarella, L. (2002). *Soil erosion risk in Europe*. Italy. doi:10.1556/CRC.36.2008.Suppl.2
- Haboudane, D., Bonn, F., Royer, A., Sommer, S., & Mehl, W. (2002). Land degradation and erosion risk mapping by fusion of spectrally-based information and digital geomorphometric attributes. *International Journal of Remote Sensing*, 23(18), 3795–3820.
- Haubrock, S., Chabrillat, S., & Kaufmann, H. (2004). Application of hyperspectral imaging and laser scanning for the monitoring and assessment of soil erosion in a recultivation mining area. In S. Erasmí, B. Cyffka, & M. Kappas (Eds.), *Remote sensing and GIS for environmental studies: Applications in geography* (pp. 230–237). Göttinger. Goltze: Göttinger geographische Abhandlungen.
- Haubrock, S., Chabrillat, S., & Kaufmann, H. (2005). Application of hyperspectral imaging for the quantification of surface soil moisture. In B. Zagajewski, M. Sobczak, & M. Wrzesień (Eds.), *Proceedings of 4th EARSeL Workshop on Imaging Spectroscopy. New quality in environmental studies*. (pp. 163–171). Warsaw: EARSeL and Warsaw University.
- Hill, J., Mégier, J., & Mehl, W. (1995). Land degradation, soil erosion and desertification monitoring in mediterranean ecosystems. *Remote Sensing Reviews*, 12(1–2), 107–130.
- Hill, J., Mehl, W., & Altherr, M. (1994). Land degradation and soil erosion mapping in a mediterranean ecosystem. In J. Hill & J. Mégier (Eds.), *Imaging spectrometry — A tool for environmental observations* (pp. 237–260). Dordrecht: Kluwer Academic Publishers.
- Hill, J., & Schütt, B. (2000). Mapping complex patterns of erosion and stability in dry mediterranean ecosystems. *Remote Sensing of Environment*, 74(3), 557–569.
- Hrabalíková, M., Huislová, P., Ureš, J., Holubík, O., Žižala, D., & Kumhálová, J. (2016, August 22–26). Assessment of changes in topsoil depth redistribution in relation to different tillage technologies. In *3rd WASWAC Conference, Belgrade/Serbia*. Belgrade: The World Association of Soil and Water Conservation.
- Hrabovská, B. (2013). The intensity of water erosion on chernozems south Moravia. In P. Škarpa, P. Ryant, R. Cerkal, O. Polák, & J. Kovárník (Eds.), *MendelNet 2013. Proceedings of International PhD Students Conference* (pp. 301–307). Brno, Czech Republic: Mendel University in Brno.
- Kolejka, J., & Manakos, J. (2000). Integrate dat DPZ a GIS při identifikaci erozního poškození půdy [Integration of GIS and remote sensing for identification of soil degradation by erosion]. In *Sborník příspěvků z konference s mezinárodní účastí GIS... Ostrava 2000* (pp. 15). Ostrava. Retrieved from [http://gis.vsb.cz/GIS\\_Ostrava/GIS\\_Ova\\_2000/Sbornik/Kolejka/Referat.htm](http://gis.vsb.cz/GIS_Ostrava/GIS_Ova_2000/Sbornik/Kolejka/Referat.htm)
- Krása, J., Středová, H., Dostál, T., & Novotný, I. (2014, September 3–5). Rainfall erosivity research on the territory of the Czech Republic. In J. Rožnovský & T. Litschmann (Eds.), *Mendel a bioklimatologie, Brno* (p. 20). Brno: Mendel University in Brno, Czech Bioclimatological Society.
- Li, M., Zang, S., Zhang, B., Li, S., & Wu, C. (2014). A review of remote sensing image classification techniques: The role of spatio-contextual information. *European Journal of Remote Sensing*, 47(1), 389–411.
- Liberti, M., Simoniello, T., Carone, M.T., Coppola, R., D'Emilio, M., & Macchiato, M. (2009). Mapping badland areas using LANDSAT TM/ETM satellite imagery and morphological data. *Geomorphology*, 106(3–4), 333–343.

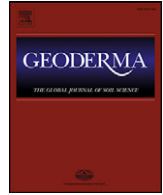
- Lin, C., Zhou, S., Wu, S., Zhu, Q., & Dang, Q. (2014). Spectral response of different eroded soils in subtropical china: A case study in Changting county, China. *Journal of Mountain Science*, 11(3), 697–707.
- Luleva, M.I. (2013). *Tracing soil particle movement. Towards a spectral approach to spatial monitoring of soil erosion Mila Ivanova Luleva PhD dissertation committee*. Enschede, The Netherlands: University of Twente.
- Luleva, M.I., Van Der Werff, H., Van Der Meer, F., & Jetten, V. (2012). Gaps and opportunities in the use of remote sensing for soil erosion. *Chemistry: Bulgarian Journal of Science Education*, 21(5), 748–764.
- Martínez-Casasnovas, J.A. (2003). A spatial information technology approach for the mapping and quantification of gully erosion. *Catena*, 50(2–4), 293–308.
- Mathieu, R., Cervelle, B., Rémy, D., & Pouget, M. (2007). Field-based and spectral indicators for soil erosion mapping in semi-arid mediterranean environments (Coastal cordillera of central Chile). *Earth Surface Processes and Landforms*, 32(1), 13–31.
- Mayr, A., Rutzinger, M., Bremer, M., & Geitner, C. (2016, July 12–19). Mapping eroded areas on mountain grassland with terrestrial photogrammetry and object-based image analysis. In *ISPRS Annals of the Photogrammetry, Remote Sensing and Spatial Information Sciences, XXIII ISPRS Congress* (Vols. 3–5, pp. 137–144). Prague, Czech Republic: International Society for Photogrammetry and Remote Sensing.
- Meléndez-Pastor, I., Pedreño, J.N., Lucas, I.G., & Zorpas, A.A. (2017). A model for evaluating soil vulnerability to erosion using remote sensing data and A fuzzy logic system. In S. Ramakrishnan (Ed.), *Modern fuzzy control systems and its applications* Rijeka: InTech. doi:10.5772/67989
- Mohammadi, T.A., & Nikkani, D. (2008). Methodologies of preparing erosion features map by using RS and GIS. *International Journal of Sediment Research*, 23(2), 130–137.
- Němeček, J. (1967). *Průzkum zemědělských půd ČSSR - Souborná metodika* [Soil survey of agricultural land in Czechoslovakia - aggregate methodology]. Prague, Czech Republic: Ministerstvo zemědělství a výživy [Ministry of Agriculture].
- Nobrega, R.A.A., O'Hara, C.G., Vijayaraj, V., Olson, G., Kim, S., Quintanilha, J.A., & Barros, M.T.L. (2006). Extracting and classifying bare soil erosion risk areas in a urban basin using object-oriented technologies, high resolution imagery and elevation data. In *Geographic Information Systems and Water Resources IV - AWRA Spring Specialty Conference*. Houston, Texas: AWRA
- Novotný, I., Žížala, D., Kapička, J., Beitlerová, H., Mistr, M., Kristenová, H., & Papaj, V. (2016). Adjusting the CPmax factor in the universal soil loss equation (USLE): Areas in need of soil erosion protection in the Czech Republic. *Journal of Maps*, 12(sup1), 58–62.
- Panagos, P., Borrelli, P., Poesen, J., Ballabio, C., Lugato, E., Meusburger, K., ... Alewell, C. (2015). The new assessment of soil loss by water erosion in Europe. *Environmental Science & Policy*, 54, 438–447.
- Panagos, P., Imeson, A., Meusburger, K., Borrelli, P., Poesen, J., & Alewell, C. (2016). Soil conservation in Europe: Wish or reality? *Land Degradation & Development*, 27(6), 1547–1551.
- Pérez, E., & García, P. (2017). Monitoring soil erosion by raster images: From aerial photographs to drone taken pictures. *European Journal of Geography*, 8(1), 117–129. Retrieved from <https://www.scopus.com/inward/record.uri?eid=2-s2.0-85013772734&partnerID=40&md5=64c0c4763393bbf6e34b17f79bcfe9e4>
- Pilesjoe, P. (1992). GIS and remote sensing for soil erosion studies in semi-arid environments. Estimation of soil erosion parameters at different scales. *Meddelanden Fraan Lunds Universitets Geografiska Institutioner. Avhandlingar* (Sweden). Lund University.
- Podhrázká, J., Kučera, J., Chuchma, F., Středa, T., & Středová, H. (2013). Effect of changes in some climatic factors on wind erosion risks - the case study of south moravia. *Acta Universitatis Agriculturae Et Silviculturae Mendelianae Brunensis*, 61(6), 1829–1837.
- Prasuhn, V. (2011). Soil erosion in the Swiss midlands: Results of a 10-year field survey. *Geomorphology*, 126 (1–2), 32–41.
- Rabah, Z.B., & Farah, I.R. (2016). Evaluation and predictability of water erosion based on spectral information analysis. In *2016 2nd International Conference on Advanced Technologies for Signal and Image Processing (ATSIP)* (pp. 533–536). IEEE. doi:10.1109/ATSIP.2016.7523157
- Richardson, A.J., & Wiegand, C.L. (1977). Distinguishing vegetation from soil background information. *Photogrammetric Engineering and Remote Sensing*, 43(12), 1541–1552.
- Rogge, D., Bauer, A., Zeidler, J., Mueller, A., Esch, T., & Heiden, U. (2018). Building an exposed soil composite processor (SCMaP) for mapping spatial and temporal characteristics of soils with Landsat imagery (1984–2014). *Remote Sensing of Environment*, 205, 1–17.
- Šarapatka, B., & Netopil, P. (2010, August 1–6). Erosion processes on intensively farmed land in the Czech Republic : Comparison of alternative research methods. In *2010 19th World Congress of Soil Science, Soil Solutions for a Changing World, Brisbane, Australia* (pp. 47–50). Brisbane: International Union of Soil Sciences.
- Schmid, T., Palacios-Orueta, A., Chabrilat, S., Bendor, E., Plaza, A., Rodriguez, M., ... Cicuendez, V. (2012). Spectral characterisation of land surface composition to determine soil erosion within semiarid rainfed cultivated areas. In *2012 IEEE International Geoscience and Remote Sensing Symposium* (pp. 7082–7085). IEEE. doi:10.1109/IGARSS.2012.6352031
- Schmid, T., Rodriguez-Rastrero, M., Escribano, P., Palacios-Orueta, A., Ben-Dor, E., Plaza, A., ... Chabrilat, S. (2016). Characterization of soil erosion indicators using hyperspectral data from a mediterranean rainfed cultivated region. *IEEE Journal of Selected Topics in Applied Earth Observations and Remote Sensing*, 9(2), 845–860.
- Sepuru, T.K., & Dube, T. (2017). An appraisal on the progress of remote sensing applications in soil erosion mapping and monitoring. *Remote Sensing Applications: Society and Environment*. doi:10.1016/j.rsase.2017.10.005
- Servenay, A., & Prat, C. (2003). Erosion extension of indurated volcanic soils of Mexico by aerial photographs and remote sensing analysis. *Geoderma*, 117(3–4), 367–375.
- Shoshany, M., Goldshleger, N., & Chudnovsky, A. (2013). Monitoring of agricultural soil degradation by remote-sensing methods: A review. *International Journal of Remote Sensing*, 34(17), 6152–6181.
- Smetanová, A. (2009). Bright patches on chernozems and their relationship to the relief. *Geografický Časopis/Geographical Journal*, 61(3), 215–227.
- Stolte, J., Tesfai, M., Øygarden, L., Kværnø, S., Keizer, J., Verheijen, F., ... Hessel, R. (2016). *Soil threats in Europe*. Luxembourg: European Union, Joint Research Centre. doi:10.2788/828742

- Topaloğlu, R.H., Sertel, E., & Musaoğlu, N. (2016). Assessment of classification accuracies of Sentinel-2 and Landsat-8 data for land cover/use mapping. *ISPRS - International Archives of the Photogrammetry, Remote Sensing and Spatial Information Sciences, XLI-B8*, 1055–1059.
- Tou, J.T., & Gonzalez, R.C. (1974). *Pattern recognition principles (Applied ma)*. London: Addison-Wesley Pub. Co.
- Vašát, R., Kodešová, R., Klement, A., & Jakšík, O. (2015). Predicting oxidizable carbon content via visible- and near-infrared diffuse reflectance spectroscopy in soils heavily affected by water erosion. *Soil and Water Research, 10*(2), 74–77.
- Verheijen, F.G.A., Jones, R.J.A., Rickson, R.J., & Smith, C.J. (2009). Tolerable versus actual soil erosion rates in Europe. *Earth-Science Reviews, 94*(1–4), 23–38.
- Vopravil, J., Khel, T., Vrabcová, T., Havelková, L., Procházková, E., Novotný, I., ... Hodek, T. (2011). *Vliv činnosti člověka na krajinu českého venkova s důrazem na vodní režim a zadržování vody v krajině* [Human influence to countryside landscape with respect to water regime and water retention]. Praha: VÚMOP, v.v.i.
- Vrieling, A. (2006). Satellite remote sensing for water erosion assessment: A review. *Catena, 65*(1), 2–18.
- Vrieling, A. (2007). *Mapping erosion from space*. Wageningen University. Retrieved from [http://library.wur.nl/sfx\\_local?sid=WUR%3ACLCLC&spage=&epage=&pages=NaN&pid=%3Cisn%3E1831221%3C%2Fisn%3E&genre=book&auinit=A&aulast=Vrieling&isbn=9789085045878&date=2007&title=Mappingerosionfromspace](http://library.wur.nl/sfx_local?sid=WUR%3ACLCLC&spage=&epage=&pages=NaN&pid=%3Cisn%3E1831221%3C%2Fisn%3E&genre=book&auinit=A&aulast=Vrieling&isbn=9789085045878&date=2007&title=Mappingerosionfromspace)
- Wang, L., Huang, J., Du, Y., Hu, Y., & Han, P. (2013). Dynamic assessment of soil erosion risk using Landsat TM and HJ satellite data in Danjiangkou Reservoir area, China. *Remote Sensing, 5*(8), 3826–3848.
- Zádorová, T., & Penížek, V. (2011). Problems in correlation of Czech national soil classification and world reference base 2006. *Geoderma, 167–168*, 54–60.
- Zádorová, T., Penížek, V., Šefrna, L., Drábek, O., Mihaljevič, M., Volf, Š., & Chuman, T. (2013). Identification of Neolithic to modern erosion-sedimentation phases using geochemical approach in a loess covered sub-catchment of South Moravia, Czech Republic. *Geoderma, 195–196*, 56–69.
- Zádorová, T., Penížek, V., Šefrna, L., Rohošková, M., & Borůvka, L. (2011). Spatial delineation of organic carbon-rich colluvial soils in Chernozem regions by terrain analysis and fuzzy classification. *Catena, 85*(1), 22–33.
- Zádorová, T., Penížek, V., Vašát, R., Žížala, D., Chuman, T., & Vaněk, A. (2015). Colluvial soils as a soil organic carbon pool in different soil regions. *Geoderma, 253–254*, 122–134.
- Zádorová, T., Penížek, V., Žížala, D., Matějovský, J., & Vaněk, A. (2018). Influence of former lynchets on soil cover structure and soil organic carbon storage in agricultural land, Central Czechia. *Soil Use and Management*, n/a-n/a. doi:10.1111/sum.12406
- Zhu, Z., Wang, S., & Woodcock, C.E. (2015). Improvement and expansion of the Fmask algorithm: Cloud, cloud shadow, and snow detection for Landsats 4–7, 8, and Sentinel 2 images. *Remote Sensing of Environment, 159*, 269–277.
- Žížala, D., Kapička, J., & Novotný, I. (2016). Monitoring soil erosion of agricultural land in Czech Republic and data assessment of erosion events from spatial database. In *Proceedings from International Conference Soil - the non-renewable environmental resource* (pp. 354–370). Brno, Czech Republic: Mendel University in Brno.
- Žížala, D., Zádorová, T., & Kapička, J. (2017). Assessment of soil degradation by erosion based on analysis of soil properties using aerial hyperspectral images and ancillary data, Czech Republic. *Remote Sensing, 9*(1), 28.

## 5.4 Colluvial soils as a soil organic carbon pool in different soil regions

---

- Zádorová, T., Penížek, V., Vašát, R., **Žížala, D.**, Chuman, T., Vaněk, A., 2015. Colluvial soils as a soil organic carbon pool in different soil regions. *Geoderma*. 253–254. p. 122–134. [doi: 10.1016/j.geoderma.2015.04.012]



## Colluvial soils as a soil organic carbon pool in different soil regions



Tereza Zádorová <sup>a,\*</sup>, Vít Penížek <sup>a</sup>, Radim Vašát <sup>a</sup>, Daniel Žížala <sup>a,b</sup>, Tomáš Chuman <sup>c</sup>, Aleš Vaněk <sup>a</sup>

<sup>a</sup> Department of Soil Science and Soil Protection, Faculty of Agrobiology, Food and Natural Resources, Czech University of Life Sciences Prague, Kamýcká 129, Praha 6, Czech Republic

<sup>b</sup> Research Institute for Soil and Water Conservation, Žabovřeská 250, 156 27 Praha 5, Zbraslav, Czech Republic

<sup>c</sup> Department of Physical Geography and Geoecology, Faculty of Science, Charles University in Prague, Albertov 6, Praha 2, Czech Republic

### ARTICLE INFO

#### Article history:

Received 10 January 2015

Received in revised form 25 March 2015

Accepted 10 April 2015

#### Keywords:

Soil organic carbon

Colluvial soil

Terrain attributes

Digital elevation model

Czech Republic

### ABSTRACT

Subsoil has been recognized as large reservoir of soil organic carbon in recent years. In our study, we investigated deep colluvial soils as a potentially important source of SOC due to high mass redistribution driven by soil erosion. Three agriculture plots from the Chernozem, Luvisol, and Cambisol regions were studied to assess the SOC storage in topsoil (0–25 cm), at 2 m depth (0–200 cm), and over the total soil depth (0–450 cm) as a function of relief. The study is based on 558 borings, and soil profile description and classification to facilitate the colluvial soil delineation. Among these locations, SOC content was measured at 230 sampling points. Prediction of the SOC stock for the plots was based on support vector machine algorithms using digital elevation model derivatives as predictors. Total SOC stock varied among the study plots. The highest relative SOC stock was measured in the Chernozem (CH) plot ( $144.7 \text{ t} \cdot \text{ha}^{-1}$ ), while at the Luvisol (LU) plot, it reached  $68.4 \text{ t} \cdot \text{ha}^{-1}$  and was  $73.4 \text{ t} \cdot \text{ha}^{-1}$  at the Cambisol (CM) plot. The role of colluvial soils regarding their spatial extent and SOC stock differs among the studied plots. Colluvial soils at the CH plot represent an important soil cover both spatially (13%) and by the volume of SOC stock (37%). A moderate importance of colluvial soils is determined for the LU plot (12% of SOC stock), and a low importance for the CM plot (5% of SOC stock). SOC stock contained in topsoil and subsoil differs in each plot. In the Luvisol and Cambisol plots, more than one half of SOC is retained in topsoil (53.4%, 60.3%). In contrast, more than two thirds of the SOC stock (73.1%) occurs in subsoil in the Chernozem plot. Moreover, 19.0% of the total SOC stock occurs at depths below 2 m. This finding indicates the importance of the incorporation of deep colluvial soil horizons in SOC stock estimations.

© 2015 Elsevier B.V. All rights reserved.

### 1. Introduction

The organic carbon stock in soils represents one of the largest terrestrial reservoirs of this substance (Chaopricha and Marín-Spiotta, 2014). Processes driving SOC flow in dynamic landscapes have been widely studied during the last two decades (Doetterl et al., 2012b; Polyakov and Lal, 2004; Van Oost et al., 2007). Some of the works have demonstrated that the SOC redistribution during erosion transport and the consequent terrestrial sedimentation play an important role in the global carbon cycle, and in the spatial variability of various physical and chemical soil features (Berhe and Kleber, 2013). Furthermore, soil erosion and deposition processes have significant implications for SOC persistence in the terrestrial biosphere (Berhe and Kleber, 2013; Van Hemelryck et al., 2010). Most of the understanding of the processes related to SOC storage and release is limited to the topsoil (0–30 cm) (Chabbi et al., 2009; Chaopricha and Marín-Spiotta, 2014). The dynamics and amount of SOC stored in deep soil horizons were not well understood and quantified for a long time. In recent years, subsoil and even

deep and buried soil horizons have been recognized as large reservoirs of carbon that are responsive to climatic–environmental processes (Chaopricha and Marín-Spiotta, 2014; Paul et al., 2006). The sensitivity of the subsoil carbon pool to land use changes was unknown until recently (Don et al., 2007). Studies from different environments show a dynamic response of deep SOC pools to land cover management (Devine et al., 2011; Harrison et al., 2011). Recent investigations of subsoil SOC have focused mainly on its chemical composition, persistence (Chabbi et al., 2009; Rumpel et al., 2004), bioturbation or burial, and its vertical transport through preferential flow-paths (Chaopricha and Marín-Spiotta, 2014; Wilkinson et al., 2009). Most of the studies assessing the spatial distribution of SOC stock in the landscape limit their computations to the topsoil, the upper 50 cm (Cambule et al., 2014; López-Fando and Pardo, 2011; Schwanghart and Jarmer, 2011; Simbahan et al., 2006), or the upper 100 cm (De Gryze et al., 2008; Don et al., 2007; Fang et al., 2012; Han et al., 2010; Khalil et al., 2013). Only a few studies have assessed the SOC stocks in deeper soil horizons, namely those situated in Chernozem regions, where deep A horizons are common (Kalinina et al., 2011; Liu et al., 2011; Vasques et al., 2010; Xi et al., 2011).

Deep SOC is often present in specific parts of the landscape where colluvial soils are formed. Colluvial soils form on concave slopes because

\* Corresponding author.

E-mail addresses: [zadorova@af.czu.cz](mailto:zadorova@af.czu.cz) (T. Zádorová), [zizala.daniel@vumop.cz](mailto:zizala.daniel@vumop.cz) (D. Žížala), [chumant@natur.cuni.cz](mailto:chumant@natur.cuni.cz) (T. Chuman).

of sedimentation of eroded topsoil material on agricultural land. Their soil profiles are characterized by the presence of a deep humus horizon (or less frequently of a horizon formed by slope sediment with varying SOC content) resulting from sedimentation of eroded topsoil from overlying soils in the landscape. The process of colluvial soil formation is a direct consequence of soil loss by water and tillage erosion conditioned by its position in the landscape. SOC storage in such deep colluvial humus-rich soils has not yet been studied (Zádorová et al., 2011b). Profile development and the thickness of colluvial soil depend on various factors, mainly on soil conditions and properties, the parent material, the source of colluvial material (rich in organic matter or SOC depleted), terrain character and land management (Zádorová et al., 2013). Colluvium several metres thick and rich in organic matter commonly occurs in loess regions and develops from humus-rich soils, mainly Chernozems (Poreba et al., 2011; Zádorová et al., 2011b, 2013; Zglobicki, 2013) and Luvisols (Fuchs et al., 2010; Kadereit et al., 2010; Lang and Hönscheidt, 1999; Rodzik et al., 2014). Shallower colluvial soils with a stratified profile have been reported from areas formed by Luvisol and Cambisols in the Czech Republic (Zádorová et al., 2014).

Techniques for SOC stock estimation can be divided into two groups (Cambule et al., 2014; Mishra et al., 2010): the traditional way of point SOC density measurement in a layer, and multiplying by the layer area. Recently, a landscape modelling approach analysing the spatial variability of SOC stocks with respect to variations in environmental co-variables has been applied in various studies at a local and regional scales (Cambule et al., 2014; Doetterl et al., 2012a; Simbahan et al., 2006). Environmental characteristics, such as terrain, geology, soil type, and land use and management are important variables when assessing and quantifying processes of soil erosion and deposition, and their impact on spatial variability of soil properties (e.g., De Gryze et al., 2008; Florinsky et al., 2002; McBratney et al., 2003). Predictors used as explanatory variables in SOC stock quantification most often comprise land use type, soil and parent material type, climatic factor (precipitation), terrain attributes, or soil reflectance (Cambule et al., 2014; Hancock et al., 2010; Van Oost et al., 2012). Each of the factors influences the soil mass redistribution at different scales. Terrain attributes can be considered as the main ruling factor at a plot scale, namely in tilled plots with homogenous parent material. Because of the lack of information on the relationship between terrain and deep humus-rich sediments, our study aims to:

- (i) assess and quantify the role of colluvial soils in SOC storage in three different soil regions; and
- (ii) estimate the potential use of topography as an explanatory factor in SOC stock modelling.

Our study is based on the following hypotheses: 1) quantitative terrain modelling can be applied for the SOC prediction and the colluvial soil delineation and 2) the proportion of SOC retained in colluvial soils will vary in different soil regions.

## 2. Regional setting

Three study plots, which represent the most extensive agricultural land soil units in the Czech Republic, were chosen. Their locations are depicted in Fig. 1. Plots that are similar in terms of terrain, land management and climatic conditions (rain erosivity) were selected to assess the influence of soil development and characteristics on soil mass redistribution. All of the plots are situated on arable land with analogous land management (long-term tillage, no conservation practices), plough depth (25 cm) and crop rotation (5–6 course rotation based on the Norfolk system). Plots were chosen with the aim of covering typical colluvial terrain positions (toe-slopes and side valleys). They are characterized by dissected relief and include the following set of terrain units: side valley, toe-slope, plateau and back-slope. Climatic conditions differ among the plots by annual precipitation rates and temperatures, but

belong to the same region in terms of rainfall erosivity factor (Janeček, 2012). Soils at all of the three plots have identical texture classes (silt loam). Each of the plots has homogenous geology and climatic conditions. Soil cover heterogeneity within the plot is according to erosion processes. The resulting erosion catena consists of unchanged autochthon soils, eroded soils in the steep parts of the landscape, and colluvial soils formed by sediment material in the lower parts of the plots (Fig. 2). Plot 1 (CH plot) is situated in the SE of the Czech Republic (48.967°N, 16.882°E). The area is covered by a Pleistocene loess layer with variable thickness (Chlupáč et al., 2002). Climate is characterized by a mean annual precipitation of 542 mm and a mean annual temperature of 8.4 °C. The research was carried out on an agricultural parcel (6 ha) that comprises a complex slope system with different terrain units: a plateau (slope 0–0.5°), a steep middle part (up to 19°) formed by a back-slope and a side valley, and a toe-slope. The mean slope of the plot is 7°. The side valley represents a major line of concentrated runoff emptying into a colluvial fan at the toe-slope. The back-slope is interrupted by a road that separates it from the floodplain. Plateau areas with no erosion are covered by Calcic Chernozem. Chernozems with a truncated mollic horizon cover areas with increasing slope (2–8°). Regosols (ploughed exposed loess material) cover the steepest parts of the slopes. Colluvial Chernozems and colluvial soils with deep A horizons are formed in concave parts of the landscape (Zádorová et al., 2011b). Colluvial soils with a 100–250 cm thick A horizon rich in organic matter have developed in the side valley, whereas the deepest colluvial profiles are formed by a mixture of loess and humus-rich material in the top 300 cm, and humus-rich material at 300–400 cm depth was found in the toe-slope.

Plot 2 (LU plot), which is represented by Luvisols, is situated in Central Bohemia (50.457°N, 14.509°E). The parent material is Pleistocene loess (Chlupáč et al., 2002). The mean annual precipitation is 588 mm and the mean annual temperature is 8.2 °C. The study plot (15 ha) is characterized by two perpendicular side valleys (north-south and east-west) connected in the south-west part of the plot. Adjacent slopes reach up to 17°. Large flat upper parts (0–0.5°) occur in the south, north-east and north-west sections of the plot. The mean slope of the plot is 5°. Haplic Luvisol is the dominant soil unit at the study plot. Regosols and Calcisols are formed in the steepest parts of the plot. Accumulated forms of Luvisol and colluvial soils with a maximum thickness of 100 cm have formed in the depositional areas of the landscape (Zádorová et al., 2014). A stagnic colour pattern at the bottom of the soil profile develops in the lowest part of the plot.

Plot 3 (CM plot; 33 ha) represents a Cambisol region (49.616°N, 14.367°E). The parent material is formed from Paleozoic contact metamorphic greywacke and siltstone (Chlupáč et al., 2002). The climate is cooler (7.1 °C), with higher annual precipitation (659 mm) than in the other two regions. The study plot is represented by a slope system with two side valleys divided by a distinct elevation. The plot has a marked north-south slope, with a maximal gradient of 20°. The flat parts (0–2°) are situated in the south part of the plot adjacent to a road. The mean slope of the plot is 7°. Cambisols cover both the flat parts and the lower and middle slopes. Leptic Cambisols and Leptosols are found on the steepest slopes. Colluvial soils with maximum depths of 100 cm form at the base of the accumulation positions. As in the LU plot, stagnic properties developed in the CM plot in the soils occurring at the confluence of the two side valleys.

Detailed information on terrain, climatic and soil characteristics of the three plots are shown in supplementary materials.

## 3. Methods

### 3.1. Terrain sampling and soil analyses

Soil sampling was conducted within two campaigns. The CH and CM study plots were sampled (Fig. 1) on an optimized network of borings and deep cores, projected using the conditioned Latin hypercube sampling (cLHS) approach (with terrain attributes as feature space



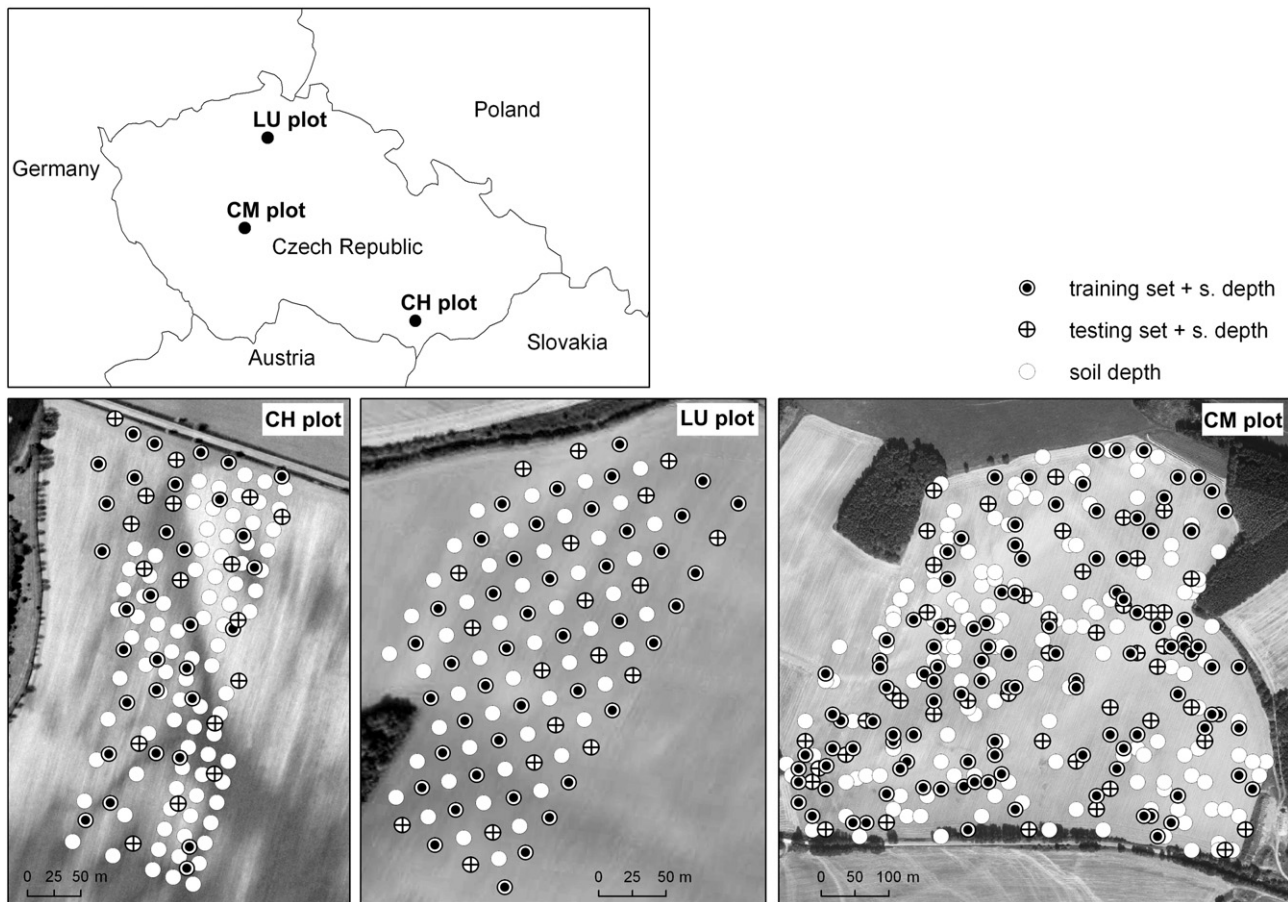


Fig. 1. Location and sampling scheme of the three study plots.

variables). A regular design ( $30 \times 30$  m) was used in the case of the LU plot. The marginal distribution of terrain attributes is well represented by all three sampling designs. For CH and CM plots, this is achieved by using cLHS which ensures full coverage of the range of each variable by maximally stratifying the marginal distribution. High density sampling is used at the LU plot. As documented by the probability distributions and box plots of the terrain attributes of initial and sampled locations, which are available as supplementary material, there is no clear difference between the three plots. Soil unit, profile stratigraphy, soil depth, and thickness of horizons were determined in each boring/core. For SOC analysis, samples were taken every 25 cm of the borings. Two hundred and thirty samplings were conducted (50 in CH, 67 in LU and 113 in CM). In addition, another 328 borings were made, and profiles were described to facilitate the colluvial soil delineation at the study plots. At each site, pits representing each soil unit were dug, and soil samples were taken from each 25 cm up to 150 cm for bulk density analysis.

Names of soil units used in this paper are based on the national classification Czech Taxonomic Classification System of Soils (CTCSS; Němeček et al., 2011). Soil units defined in the national classification better suit the description of soil cover structure after a long-term redistribution. The colluvial soil unit represents soil where the thickness of colluvial material exceeds 30 cm (CTCSS; Němeček et al., 2011). In reality, colluvial soil has an A horizon that is more than 30 cm thicker than the A horizon of soil with an unchanged soil profile. Correlation of studied soil units with the World Reference Base for Soil Resources 2006 (WRB 06; IUSS Working Group WRB, 2006) is described in Table 1. Zádorová and Penížek (2011a) provide detailed information about the correlation between CTCSS and WRB 06.

Soil organic carbon content was measured using wet oxidation (ISO, 14235:1998). Wet oxidation ( $K_2Cr_2O_7$ ) was followed by potentiometric

titration with ferrous ammonium sulphate. Bulk density was measured according to ISO, 11272:1998. All soil sample analyses were run as triplicates.

### 3.2. Digital elevation model assessment

The stereo-photogrammetry based DEM was provided as a  $1 \times 1$  m grid (provider Georeal Ltd.) and was smoothed and filtered using a Gaussian filter in SAGA GIS. Terrain attributes used in the analysis represent a standard set of morphometrical attributes, widely used in pedometrical studies of soil property prediction (e.g., Florinsky et al., 2002; McBratney et al., 2003; Zádorová et al., 2011b, 2014). Terrain attributes calculated from the DEM using integrated algorithms implemented in SAGA GIS (Fig. 3) include: altitude (ALT), slope (SLP), plane curvature (PLANC), profile curvature (PROFC), catchment area (CA), topographic wetness index (TWI), topographic position index (TPI) (Jenness, 2006; a relative measure of a cell's elevation in comparison to its neighbourhood), LS factor (LS), convergence index (CONVIN), and altitude above channel network (ALTCHN).

### 3.3. Colluvial soil delineation

Soil units (three at each plot – colluvial soil, non-eroded original soil and eroded soil) were determined at each sampling point of the original dataset. Spatial delineation of soil units was then modelled using the support vector machine (SVM) approach in classification mode. The support vector machine algorithm constructs a linear hyperplane or set of hyperplanes in a high- or infinite-dimensional feature space as the decision function for non-linear problems, and then applies a back-transformation in the non-linear space. In other words, it applies a simple linear method to the data but in a high-dimensional feature

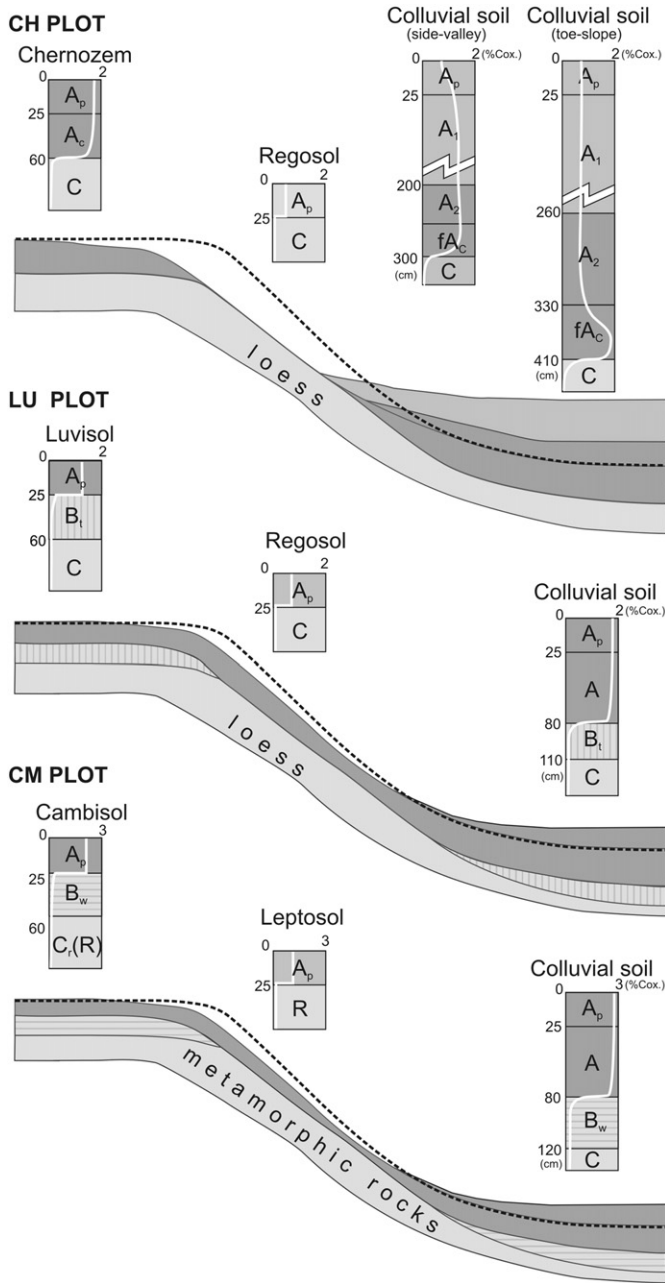


Fig. 2. Scheme of soil profile development and SOC concentration distribution at the studied plots. The white line indicates the SOC concentration (%) in the soil profiles.

space that is non-linearly related to the input space. Good separation is achieved by the hyperplane that has the largest distance to the nearest training data point of any class (the so-called functional margin)

because in general, the larger the margin, the lower the generalization error of the classifier. SVM can be used for classification, regression, or novelty detection tasks. For a detailed description, see Vapnik (1999) and Boser et al. (1992). To choose the most appropriate predictor variables (terrain attributes), we performed the best subset selection, which ensures that the very best combination of predictors is used. This consists of fitting separate SVM models for each possible combination of predictors, and selecting among them a single best model using 5-fold cross-validation (the best is defined as having the highest overall accuracy).

Finally, to assess the predictive ability of the single SVM model a test set validation is performed. It involves randomly dividing the available set of observations into two parts: a training set and a test set, in a 3:2 ratio. The model is fit to the training set, and the fitted model is then used to predict responses for the observations in the test set.

The prediction accuracy of the final model is expressed as the overall probability (%) that the classifier has labelled the image pixel into the true class (i.e., the probability of a reference pixel being correctly classified), and as Cohen's kappa coefficient ( $\kappa$ ), which is a statistical measure of inter-rater agreement that takes into account the possibility of agreement occurring by chance (Cohen, 1960).  $\kappa > 0.80$  represents strong agreement and good accuracy,  $0.40 < \kappa < 0.80$  represents middle accuracy, and  $\kappa < 0.40$  represents poor accuracy. In this study, we use a radial basis kernel contained in the e1071 R package for the SVM modelling (Meyer et al., 2012). Because SVM is very sensitive to proper settings of input parameters, each particular calibration was tuned for hyperparameters using the tune framework in e1071, i.e., by performing a grid search over specified parameter ranges.

### 3.4. Assessing SOC stock

SOC stock assessment comprised the following consecutive steps at each study plot:

- i. SOC stock assessment for sampling points
- ii. Prediction of the spatial distribution of SOC stock
- iii. Total SOC stock calculation
- iv. Assessment of the colluvial soil contribution to the total SOC stock.

#### 3.4.1. SOC stock assessment at the sampling points

SOC stock was assessed using the widely applied equation (e.g., Cambule et al., 2013; Wang et al., 2010):

$$SOC_{stock} = \sum (SOC \times \rho \times H \times 10^{-1})$$

where  $SOC_{stock}$  is the SOC stock at the sampling point ( $kg \cdot m^{-2}$ ),  $SOC$  is the SOC content (%) in different soil layers,  $\rho$  is the bulk density in different soil layers ( $g \cdot cm^{-3}$ ), and  $H$  is the soil layer thickness (cm).

SOC content was measured for each 25 cm thick layer, whereas bulk density was assigned to each 25 cm thick layer according to its presence within a given soil unit and soil depth. Bulk density measured in the 125–150 cm layer was also attributed to the layers below this depth,

Table 1  
Soil units distinguished at the plots and their correlation in WRB 06.

REGION	Soil unit	Count	Profile	Ap + A hor.depth (cm)	WRB 06
CH plot	Chernozem (CE)	33	Ap–A–Ck	30–80	Calcic Chernozem (Siltic)
	Colluvial soil (CO)	26	Ap–A–Ck	80–425	Colluvic Calcic Chernozem (Pachic, Siltic)
	Regosol (RG)	68	Ap–A–Ck	20–30	Haplic Calcisol (Siltic)
LU plot	Luvisol (LU)	73	Ap–Bt–C	25–50	Haplic Luvisol (Siltic)
	Colluvial soil (CO)	15	Ap–A–Bt–C	55–100	Luvic Phaeozem (Colluvic, Siltic)
	Regosol (RG)	24	Ap–C	25–50	Haplic Calcisol (Siltic) Haplic Regosol (Arenic)
CM plot	Cambisol (CA)	20	Ap–A–Bw–C	25–50	Haplic Cambisol (Siltic)
	Colluvial soil (CO)	206	Ap–A–(Bw)–C	55–100	Colluvic Regosol (Humic)
	Leptosol (LP)	93	Ap–A–C	25–50	Haplic Regosol (Skeletal)

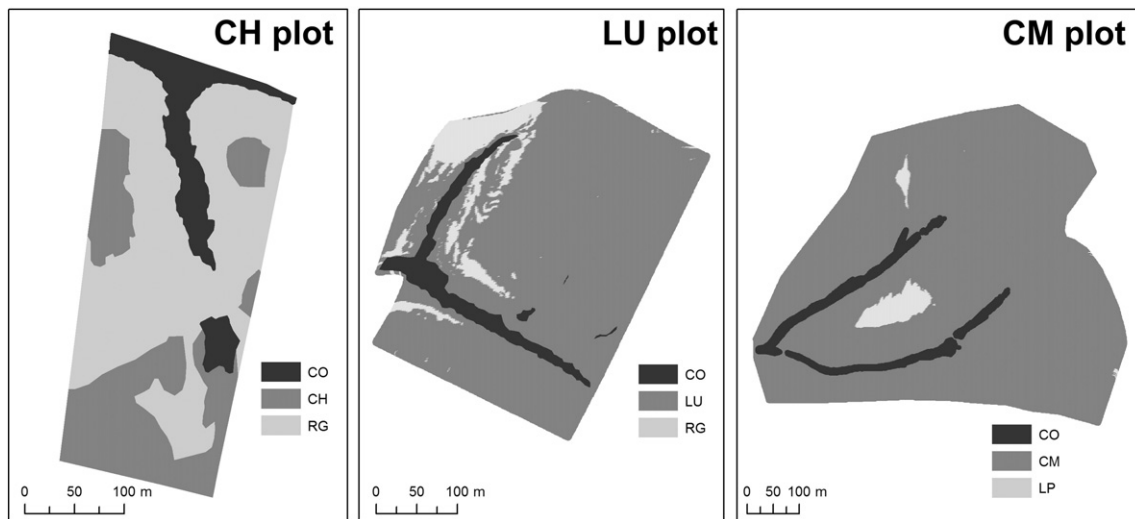


Fig. 3. Soil unit distribution at the three study plots (CH, LU and CM plots).

as the bulk density has constant values at 100–150 cm. SOC stock was assessed for the whole soil profile and for component depth intervals including topsoil (25 cm) and 200 cm.

Principal component analysis (PCA) was applied to show the structure of the dataset and reveal possible correlations between the variables.

#### 3.4.2. Prediction of the spatial distribution of SOC stock

The spatial distribution of SOC stock was converted to raster by support vector machines in regression mode using terrain attributes as predictor variables in the same way as previously performed with soil delineation (Section 3.3), i.e., by testing all possible combinations of predictors. Due to climatic, geological and land use homogeneity of the studied plots, only terrain attributes were considered. Each particular calibration was again tuned for optimal hyper-parameters using a grid search over specified parameter ranges. The best combination of predictors was selected by minimizing the root mean squared error (RMSE) of 5-fold cross-validation. To assess the predictive ability of the final model, an independent set of validation samples (Fig. 1) was used. The resulting prediction accuracy is given as the coefficient of determination ( $R^2_{\text{val}}$ ) and root mean squared error ( $\text{RMSE}_{\text{val}}$ ). To show what range of predicted values could be expected with a pre-defined probability, confidence intervals at the 95% confidence level were computed. These were computed by multiplying  $\text{RMSE}_{\text{val}}$  by 1.96 and first adding it to the estimates (upper 95% bound), and second subtracting it from the estimates (lower 95% bound). To visualize the goodness of fit, the observed values were plotted against the predicted values.

#### 3.4.3. Total SOC stock calculation

Total SOC stock was assessed by summing the grid cells from the prediction map for each study plot.

#### 3.4.4. Assessment of colluvial soil contribution to the total SOC stock

Assessment of the colluvial soil contribution to the total SOC stock was conditioned by their delineation. Colluvial soil delineation is described in Section 3.3. The SOC stock in colluvial soil as a percentage of the total SOC stock was computed by summing the grids appertaining to this soil unit.

Analyses were run in R software (R Development Core Team, 2014), and the final maps were prepared in ArcGIS 10.1.

## 4. Results and discussion

### 4.1. Delineation of colluvial soils

At each study plot, the area of colluvial soils was extracted from the maps of soil units constructed by the SVM algorithm. Table 2 shows the predictors used in the best performing model, the overall accuracy (%), and the overall accuracy corrected for agreement by chance ( $\kappa$ ), in addition to detailed model settings. TPI and LS were chosen in all three cases, while other predictors (ALTCHN, CONVIN, ALT and SLP) were used at two study plots. TWI and CA were not applied in any models.

The overall accuracy is good for all of the study plots (from 0.80% to 0.88%). However, the Cohen's kappa ( $\kappa$ ) indicates that the overall accuracy is rather moderate, but it still can be considered as good for the CH plot for which  $\kappa$  equals 0.80. According to  $\kappa$ , the best accuracy of classification (0.80) was achieved for the CH plot, and it was a bit worse for the LU (0.66) and CM plots (0.55).

Soil unit delineation is depicted in Fig. 3. In the CH plot, Regosols are the dominant soil unit, while Chernozems are present only in small areas at the plateau. In the LU and CM plots, the non-eroded or only slightly eroded soils prevail, and soils with a truncated profile (Regosols and Leptosols) cover only the steepest parts of the terrain. The area represented by colluvial soil is shown in Table 2. It reflects the erosion-sedimentation processes at the plots and counterweights the area of eroded soils. This area forms a significant part (13.45%) of the soil cover in the CH plot, whereas its area is moderate (8.78, 3.03%) in the LU and CM plots.

### 4.2. SOC stock assessment

#### 4.2.1. SOC stock at sampling points

Table 3 depicts the summary statistics of the SOC stock at the sampling points in the three study plots. The highest mean value of total SOC density was observed in the CH plot ( $19.60 \text{ kg} \cdot \text{m}^{-2}$ ) with a range of values from  $3.84 \text{ kg} \cdot \text{m}^{-2}$  to  $68.20 \text{ kg} \cdot \text{m}^{-2}$ . The LU and CM plots have similar total SOC stock values. Lower mean values ( $8.07 \text{ kg} \cdot \text{m}^{-2}$ ) were observed in the LU plot, despite having a thicker A horizon. The highest SOC topsoil stock values were determined in the CM plot ( $4.56 \text{ kg} \cdot \text{m}^{-2}$ ).

In the CH plot, the range of values is exceptionally broad if we take into account the small area of the study plot. This is due to the extreme diversity of the soil depth, which ranged from 25 cm down to 475 cm. Maximum SOC stock was observed in the deep colluvial soils situated

**Table 2**

SVM models for soil unit assessment: selected predictors, model settings, overall accuracy (%), and overall accuracy corrected for agreement by chance ( $\kappa$ ) and resulting area proportion of colluvial soils.

Plot	Predictors	Model settings (classification mode)					Prediction accuracy		CO (% of total area)
		Kernel	Gamma	Cost	Tolerance	Epsilon	Overall accuracy (%)	$\kappa$	
CH	ALTCHN CONVIN ALT LS PROFC TPI	Radial	1	100	0.001	0.1	0.88	0.80	13.45
LU	CONVIN ALT LS PLANC SLP TPI	Radial	0.1	10	0.001	0.1	0.84	0.66	8.78
CM	ALTCHN LS SLP TPI	Radial	0.1	10	0.001	0.1	0.80	0.55	3.03

at the toe-slope. Similar SOC stock in the LU and CM plots is caused by high SOC concentrations in CM topsoil. The lowest variability of values observed in the LU plot can be attributed to the absence of extremely deep or shallow profiles.

Fig. 4 shows the distribution of the dataset in the PCA biplot, reflecting the relationship between SOC stock, soil units and terrain attributes. The distribution of sampling points in the CH plot expressed by probability ellipsoids shows the isolated position of colluvial soils. The spatial distribution of colluvial soil is strongly negatively related to ALT, SLP and CONVIN, while their positive relationship with TWI and CA is weaker. SOC stock is negatively related to TPI, CONVIN, ALTCHN and SLP, while PROFC, PLANC and CA have very weak control on SOC stock distribution. There are slight differences between the SOC stock in topsoil, in the 200 cm interval, and in the whole profile. The weakest relationship with terrain was observed in topsoil that strongly negatively correlates only with SLP. SOC stock in the 200 cm depth interval is strongly negatively related to TPI and ALTCHN and is less strongly related to SLP and ALT. The relationship with SPL is more pronounced for SOC stock in the whole profile.

For the LU plot, PCA analysis showed different terrain control of the SOC stock and soil unit distribution. Colluvial soil again has a specific position, related to high values of CA and TWI, and low values of PLANC. SOC stock is correlated with the same attributes as colluvial soil. SLP, PROFC and ALT have weak relationships with SOC stocks.

In the CM plot, the position of colluvial soil is less isolated than in the other two plots. Their position is controlled mainly by PLANC, CA, TWI and CONVIN. SOC stock in topsoil is negatively related to SLP, although the total SOC stock is related mainly to CONVIN, PLANC, TWI and CA.

**Table 3**

SOC stock in the sampling points ( $\text{kg}\cdot\text{m}^{-2}$ ) in the three plots.

	Mean	Minimum	Maximum	Std. dev.	Coef. var.
25 cm					
CH plot	3.76a	1.79	6.41	1.15	30.66
LU plot	3.67a	2.56	5.11	0.53	14.34
CM plot	4.56b	1.43	9.77	0.94	20.63
Total					
CH plot	19.6a	3.84	68.20	18.44	94.12
LU plot	7.30b	3.77	14.56	2.25	30.90
CM plot	8.07b	1.43	19.53	3.99	49.43

(Mean values followed by the different letters (a, b, c) in the same column are significantly different at  $P < 0.05$  according to Multiple range test).

#### 4.2.2. SOC stock spatial distribution

The final models resulting from the selection of the best performing model are described in Table 4. These were further applied to the study plots to visualize the spatial distribution of SOC stock at different soil layers.

Performance of the models varies significantly among the plots and depth intervals. It is high in the CH and LU plots, but moderate or rather poor in the CM plot. In the CH plot, the model computing the total SOC stock explains 93% of the SOC stock distribution; coefficients in component depths are slightly lower. The best performance was obtained in the LU plot, where the prediction model explains 99% of the SOC stock variability in the whole profile and 83% in topsoil. The lowest prediction model performance was estimated in the CM plot. The model explains only 23% of topsoil SOC stock and 63% of total SOC stock. Prediction accuracy is visualized in Fig. 5 as a comparison of predicted and observed values in an independent set of sampling points. Significant differences in the prediction accuracy were determined in the three plots. The lowest  $\text{RSME}_{\text{val}}$  of total SOC stock ( $0.28 \text{ kg}\cdot\text{m}^{-2}$ , representing 4.09% of the mean) was reached in the LU plot. The highest  $\text{RSME}_{\text{val}}$  of total SOC stock was determined for the CH plot ( $2.85 \text{ kg}\cdot\text{m}^{-2}$ ), which represents a 19.35% proportion of the mean prediction. In the CM plot,  $\text{RMSE}_{\text{VAL}}$  is  $2.38 \text{ kg}\cdot\text{m}^{-2}$ , representing 32.42% of the mean.

The mean values of SOC stocks at given depths with confidence intervals of the best performing model are shown in Table 4. The studied plots do not significantly differ in terms of SOC stock in the topsoil. The highest SOC stock was found in the CM plot ( $4.21 \text{ kg}\cdot\text{m}^{-2}$ ). SOC stock differences among the studied plots are much more apparent with increasing soil depth compared with the SOC stock differences in the topsoil. The CH plot has double the total SOC stock ( $14.47 \text{ kg}\cdot\text{m}^{-2}$ ) compared to the other two localities ( $6.84 \text{ kg}\cdot\text{m}^{-2}$  in LU plot,  $7.34 \text{ kg}\cdot\text{m}^{-2}$  in CM plot).

Studies assessing the SOC stock in comparable environments generally have similar or slightly higher values for luvic and cambic soils. Studies from mollic soils on loess reported varying results, as the environment of these soils is highly variable. Xi et al. (2011) estimated the SOC density in deep soils (up to 1.8 m) in a loess plain in Northeast China at  $12.4\text{--}19.8 \text{ kg}\cdot\text{m}^{-2}$ , which is comparable to our results. However, SOC density in the deep Voronic Chernozems formed under typical steppe conditions is significantly higher. Kalinina et al. (2011) estimated the SOC density in the topsoil of such a Chernozem at  $7 \text{ kg}\cdot\text{m}^{-2}$ , and  $18.5 \text{ kg}\cdot\text{m}^{-2}$  in the first 50 cm. Yang and Wander (1999) estimated SOC density in a Luvic Phaeozem at  $9.3 \text{ kg}\cdot\text{m}^{-2}$  in the first 90 cm. Wiesmeier et al. (2013) present mean values of  $9.0 \text{ kg}\cdot\text{m}^{-2}$  for the whole soil profile in a large region of Bavaria covered by an association

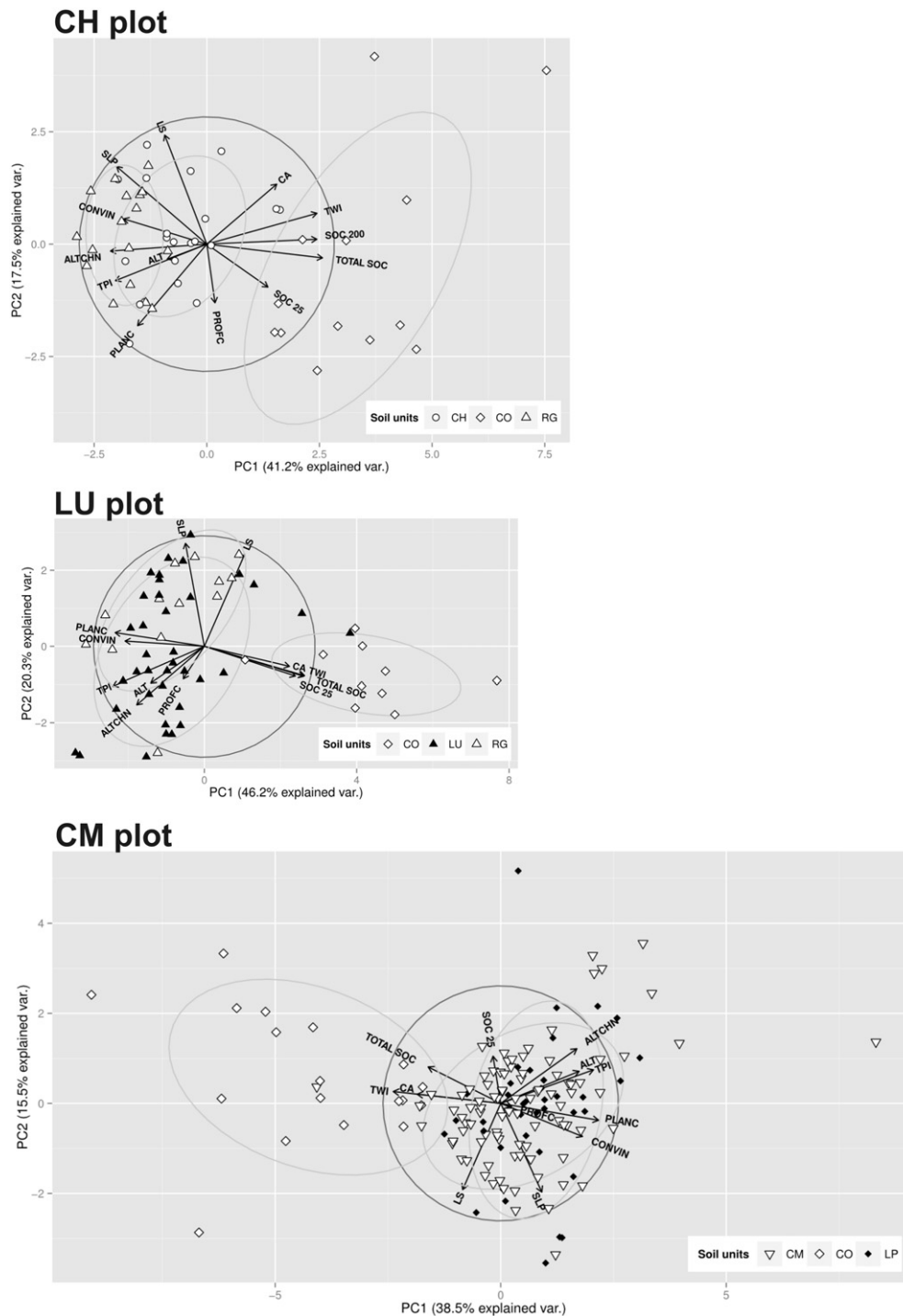


Fig. 4. PCA biplot of SOC stock, terrain attributes and soil units at the three study plots, with percentage of explained variance of principal components and normal probability ellipsoids.

of cambic/luvic/stagnic soils. Very similar results ( $9.4 \text{ kg} \cdot \text{m}^{-2}$  for clayey soils and  $11.3 \text{ kg} \cdot \text{m}^{-2}$  for loamy soils) were obtained by Doetterl et al. (2013) for the first 100 cm in a transect that is represented by Luvisols, Cambisols and Arenosols in Luxembourg. High SOC concentrations in A horizons in Cambisols can be attributed to less favourable conditions for soil organic matter mineralization, leading to the accumulation of humus. High SOC concentrations in Cambisol topsoil and even in cambic horizons have been described in large areas of the Czech uplands (Němeček and Tomášek, 1983).

In the LU plot, both the coefficient of determination (0.99) and prediction accuracy achieved convincing values, showing a high potential for usefulness of a model based on terrain predictors at this plot. A

broad range of values and lower density of testing profiles caused higher prediction errors in the CH plot. This is also expressed by a broad confidence interval of SOC stock means at the CH plot. The validation result in the CM plot can be considered as poor, and corresponds to the low explaining variance of the model, showing low potential for applying terrain attributes as model predictors at the CM plot. In most cases, studies discussing the reliability of SOC stock modelling, using  $RSME_{val}$  in proportion to mean values, are held in large areas and thus comparison is difficult (Cambule et al., 2013; Mishra et al., 2010). When comparing to studies performed at a detailed scale, our results appear better in the LU and CH plots, and similar or worse in the CM plot. Simbahan et al. (2006) estimated SOC stocks in Nebraska for fields of approximately 50

**Table 4**  
SVM models for SOC stock assessment: selected predictors, model settings and prediction accuracy.

Plot	SOC	Predictors	Model settings (regression mode)					Prediction accuracy			
			Kernel	Gamma	Cost	Tolerance	Epsilon	$R^2_{\text{val}}$	Mean (confidence intervals <sup>a</sup> ) ( $\text{kg}\cdot\text{m}^{-2}$ )	RMSE <sub>val</sub> ( $\text{kg}\cdot\text{m}^{-2}$ )	RMSE <sub>val</sub> (% of mean)
CH	0–25 cm	ALT ALTCHN CA PROFC SLP TWI	Radial	1	100	0.001	0.1	0.91	3.89 (3.16–4.64)	0.36	9.23
	25–200 cm	ALT PLANC TPI	Radial	0.01	100	0.001	0.1	0.85	13.59 (3.14–20.31)	2.77	20.39
	Total	ALT ALTCHN TPI	Radial	0.1	10	0.001	0.1	0.93	14.47 (6.03–22.15)	2.85	19.35
LU	0–25 cm	ALT CA CONVIN PLANC TWI	Radial	0.01	100	0.001	0.1	0.83	3.65 (3.32–3.99)	0.17	4.65
	Total	ALT CONVIN PLANC TWI	Radial	0.001	100	0.001	0.1	0.99	6.84 (6.05–7.54)	0.28	4.09
CM	0–25 cm	CA PROFC TPI TWI	Radial	0.1	1	0.001	0.1	0.23	4.21 (2.68–6.17)	0.89	21.14
	Total	CONVIN LS SLP TWI	Radial	0.1	10	0.001	0.1	0.62	7.34 (2.68–12.01)	2.38	32.42

<sup>a</sup> 95% confidence level.

to 65 ha using different geostatistical methods, with a resulting RSME<sub>val</sub> proportion of 17% to 30% of the mean. Minasny et al. (2006) assessed SOC stocks in the Loir Namoi Valley in Australia (1500 km<sup>2</sup>), with an estimated RSME<sub>val</sub> proportion to the mean of 30–140%.

Fig. 6 shows the SOC stock maps in the study plots for different soil depth intervals. We can assume that the largest SOC storage concentrates in the landscape positions defined by low slope (CH plot), concave curvature (LU plot), high values of hydrologic indexes indicating higher soil moisture (LU, CM plots), and low values of topographic indexes (ALTCHN and TPI) indicating strong geomorphic control of SOC storage (CH plot).

In the CH plot, maps of component depth intervals illustrate the consecutive filling of the side valley and the toe-slope with sediments. The highest SOC storage in topsoil is concentrated in the plateau with a non-eroded mollic horizon and low material removal. Topsoil of colluvial soils occurring in toe-slopes consists of a mixture of eroded A horizons and SOC-depleted material transported from truncated slopes. The SOC stock increase in the 200 cm depth interval is most significant in the side valley filled by material originating from an eroded mollic horizon. This trend is less pronounced in the toe-slope where the first 200 cm of the soil profile consists of sediments with a high proportion of eroded loess. The total SOC stock increases abruptly in the toe-slope, where the deepest colluvial soils occur. This distribution is supported by PCA analysis: total SOC is dependent on SLP, ALT and TPI, as the highest rates occur in the low flat positions in the toe-slope, although SOC stock in the 200 cm interval is more strongly related to TPI and less so to SLP. In the LU plot, the highest SOC stock in both the topsoil and in the total depth interval is concentrated in concave parts of the plot, represented by the two side valleys. The highest storage is evident in the joint of the drainage lines defined by the strongest sedimentation of material and the highest potential soil wetness. A strong relationship of SOC stocks with TWI and PLANC was also shown in PCA analysis. Similar to the CM plot, the total SOC stock in the LU plot corresponds to the two lines of concentrated runoff (high TWI), but the topsoil SOC stock does not relate significantly to the terrain units.

The high SOC stock is not necessarily connected only to colluvial soil but also occurs in Cambisols. This fact may correspond to locally increased SOC concentrations in topsoil out of the main accumulation area. Studies relating SOC storage with various environmental factors detected different variables explaining the spatial distribution and values of SOC density. Doetterl et al. (2013) showed the significance of curvature and TPI for subsoil SOC stock in loamy soils in Luxembourg, and relate this to steep and sloping terrain with very strong local geomorphic control. This is in accordance with our results from the CH plot, where the influence of TPI and ALTCHN on SOC density increased with increasing soil depth. Wiesmeier et al. (2013) showed a marked importance of soil moisture, represented by TWI, for the spatial distribution of SOC storage in Luvisol and Cambisol regions in southeast Germany. Furthermore, Doetterl et al. (2013) identified TWI as the most important factor in soils with higher clay contents. In our study, we also identified TWI as an important terrain attribute used in the prediction of SOC stock in LU and CM plots.

#### 4.3. Role of colluvial soils in SOC stock

Colluvial soils play a very different role in the SOC stock at the three plots (Tables 5a and 5b). In the CH plot, colluvial soil forms an important part of the soil cover. Comparing SOC stock among the soil units for topsoil, only Regosols differ significantly from the other soil units (3.4  $\text{kg}\cdot\text{m}^{-2}$ ). Mean SOC stocks in topsoil of CO and CH are practically identical (4.5  $\text{kg}\cdot\text{m}^{-2}$ ). More than 37% of total SOC stock is retained in colluvial soils that form 13.5% of the plot area. The mean total SOC stock in the CO is 40.4  $\text{kg}\cdot\text{m}^{-2}$ , while CH has 11.2 and RG only 10.4  $\text{kg}\cdot\text{m}^{-2}$ . SOC stock retained under 200 cm was estimated at 19%. In contrast with the CH plot, the increased SOC stock of CO soils is evident in the topsoil in the LU plot. The CO topsoil SOC stock (4.2  $\text{kg}\cdot\text{m}^{-2}$ ) statistically differs from both LU (3.6  $\text{kg}\cdot\text{m}^{-2}$ ) and RG (3.5  $\text{kg}\cdot\text{m}^{-2}$ ). Colluvial soil retains 12% of the total SOC stock, which is almost double that of the areal proportion of the soil unit. More than half (53.4%) of the total SOC stock is stored in topsoil. In the CM

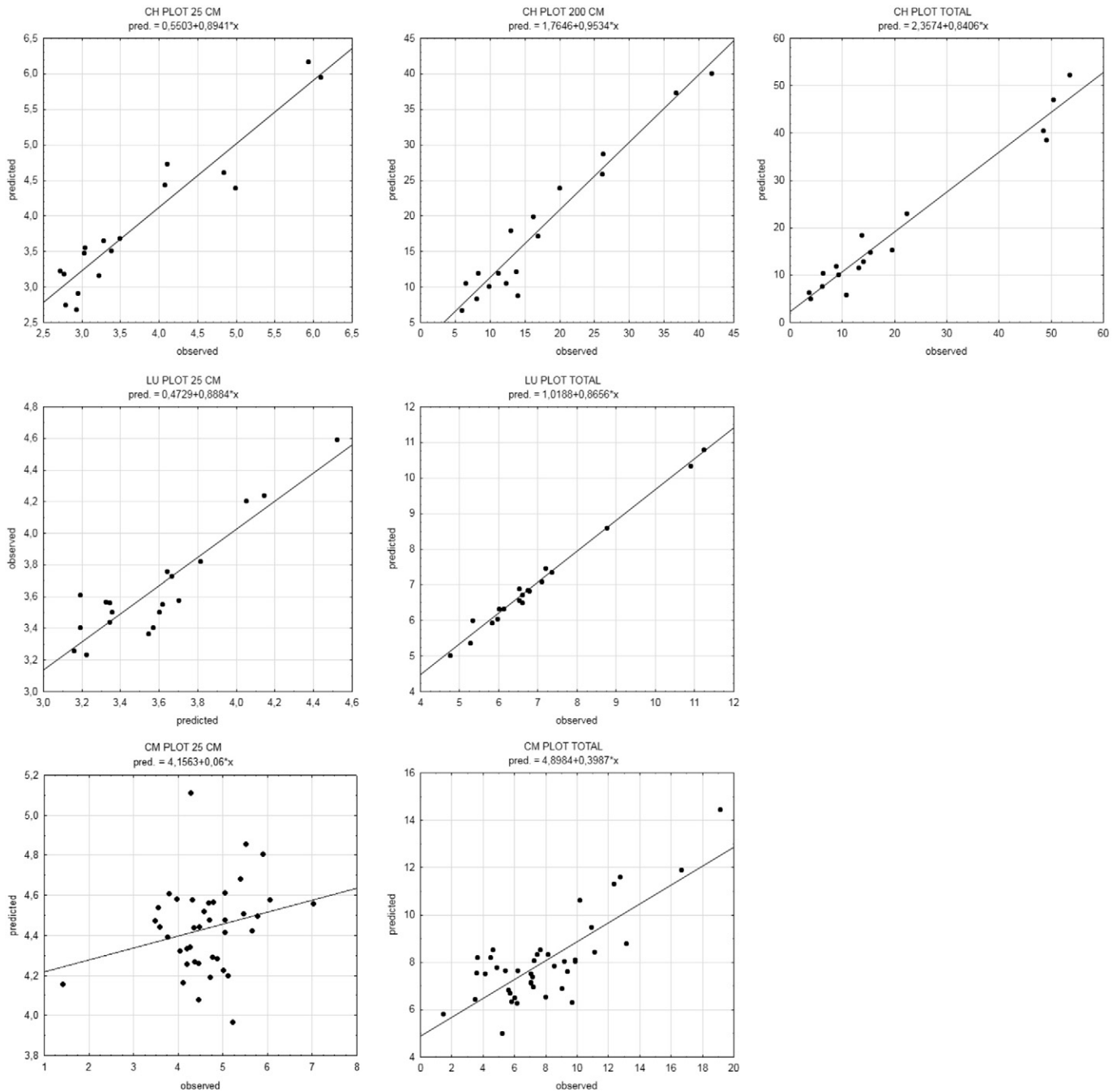


Fig. 5. Comparison of predicted and observed values in an independent set of sampling points.

plot, the topsoil SOC stock of CO soils ( $5.0 \text{ kg} \cdot \text{m}^{-2}$ ) is statistically higher than that the overall SOC stock in the CM ( $4.5 \text{ kg} \cdot \text{m}^{-2}$ ) and LP ( $4.4 \text{ kg} \cdot \text{m}^{-2}$ ) plots. Topsoil contains 60.3% of the SOC stock. Colluvial soils represent only a marginal soil unit, occupying 3% of the plot area, but represent 5.1% of the total SOC stock in the plot.

In all of the studied plots, significant differences in the SOC stock in colluvial, stable and erosional positions were estimated. Significant SOC density differences in erosional and depositional parts of the terrain have been analogously identified in several studies, mostly to the depth of 100 cm. Shukla and Lal (2005) studied differences in SOC stock (0–50 cm) in erosion, deposition and undisturbed positions on Luvisols in Ohio. They observed a significant SOC density decrease in eroded areas of the studied sites ( $4.0 \text{ kg} \cdot \text{m}^{-2}$ ) in comparison to stable ( $5.0 \text{ kg} \cdot \text{m}^{-2}$ ) and depositional areas ( $5.6 \text{ kg} \cdot \text{m}^{-2}$ ). Doetterl et al. (2013) identified a significant difference in SOC density between

erosional and depositional areas only in subsoil. De Gryze et al. (2008) measured a SOC density increase from  $3.8 \text{ kg} \cdot \text{m}^{-2}$  to  $6.9 \text{ kg} \cdot \text{m}^{-2}$  in erosional and depositional areas of a luvis/cambic soil cover. These evaluations correspond to the results obtained for the LU and CM plots. Values and differences among the three terrain positions identified in the first 100 cm of the CH plot ( $17.1 \text{ kg} \cdot \text{m}^{-2}$  for colluvial soils,  $9.8 \text{ kg} \cdot \text{m}^{-2}$  for Chernozems and  $5.4 \text{ kg} \cdot \text{m}^{-2}$  for Regosols) far exceed any of these estimations.

The mass of SOC stock retained in colluvial soil differs substantially in the studied plots. In the CH plot, the role of colluvial soils significantly increases with increasing depth. This is evident from both comparison of SOC stock among the soil units and from evaluations of total SOC stock in the plot. Due to their extreme depth, even higher SOC stock could be expected, but we must take into account that the top 100–200 cm of the deepest colluvial profiles is formed by mixed material

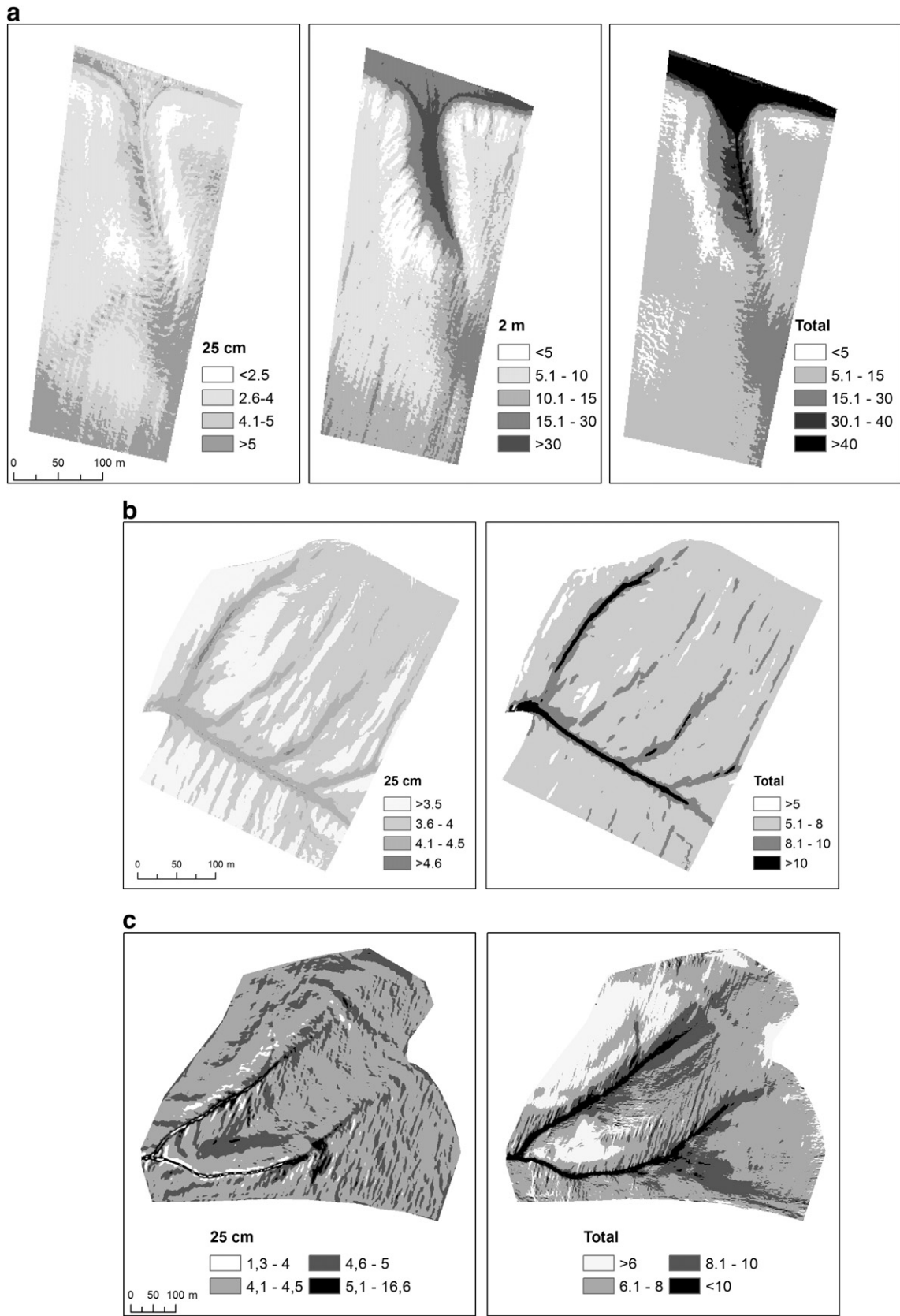


Fig. 6. Maps of the SOC stock distribution ( $\text{kg}\cdot\text{m}^{-2}$ ) at component soil depth intervals; a) CH plot, b) LU plot, c) CM plot.

from the original mollic horizon and loess material, which is relatively poor in organic matter. However, colluvial soil at the Chernozem plot represents a vast pool of organic matter, retaining a large amount of

SOC in very deep layers that are rarely included in the SOC stock estimations (Chaopricha and Marín-Spiotta, 2014). Note that almost one fifth of organic matter occurs under the depth of 2 m, which is widely



**Table 5a**  
Total and proportional SOC stock in the three plots in colluvial soil and in the component depth intervals.

	% from total SOC	% from total area	SOC stock (t·ha <sup>-1</sup> )
<i>CH plot</i>			
25 cm	26.9	100	39.0
200 cm	81.0	100	135.9
Total	100	100	144.7
Colluvial soil	37.6	13.5	404.0
<i>LU plot</i>			
25 cm	53.4	100	36.6
Total	100	100	68.4
Colluvial soil	12.0	8.8	93.2
<i>CM plot</i>			
25 cm	60.3	100	42.1
Total	100	100	73.4
Colluvial soil	5.1	3.0	122.8

considered as the lower limit of a soil profile definition (USDA, WRB). We came to the same conclusions as Chaopricha and Marín-Spiotta (2014), who refer to the importance of incorporating deeply deposited organic matter into SOC dynamics research, pointing out its large amounts and potential biological activity. Such high SOC stock beneath 2 m can be attributed to the deep colluvial horizon, with maximum SOC concentrations occurring under the depth of 2 m (Fig. 1). Zádorová et al. (2013) used detailed geochemical analysis to prove that this deep layer of high SOC content, occurring between 2 and 4.5 m, represents a buried mollic horizon of a former Chernozem, and thus the former soil surface. In addition, we must take into account that large amounts of material have been washed out from the plot during annual heavy rainfall events. Zádorová et al. (2013) averaged the sedimentation rate in the region over the last 200 years at 3 cm/year. This represents an order of magnitude difference from the sedimentation rates estimated in other studies from loess regions in central Europe (Zglobicki, 2013; Bluszczyk et al., 2007; Dotterweich et al., 2013). Reasons for such massive sediment transport can vary: the high erosion vulnerability of this Chernozem type (silty texture, rather low organic carbon content and weak soil structure due to intensive cultivation), and also the dissected, hilly terrain with steep slopes, numerous side valleys and terrain rills atypical of loess topography forming level relief (if not forming gully systems).

In the LU plot, the increased SOC content in the CO is evident even in topsoil, which is in contrast with the CH plot. This can be attributed to two processes: selective enrichment of SOC, and higher soil moisture in the concave part of the plot, leading to a decreased SOC mineralization rate (e.g., Doetterl et al., 2013). The difference in the CO SOC stock is more pronounced when considering the total SOC stock. Although the parent material is loess, as in the CH plot, erosion and deposition processes have not led to intensive soil material removal and subsequent formation of deep humus-rich colluvial profiles. The soil removal is limited mostly to topsoil. This is evident in the high SOC storage in topsoil, the small area covered with colluvial soils with depths reaching only to 70–100 cm, and the limited truncation of the Bt horizon in the steep parts of the plot. Zádorová et al. (2014) attribute this fact to the specific profile of Luvisols with an argic horizon, characterized by a developed and stable structure, representing a scarcely erodible layer protecting the underlying highly erodible loess material. Similarly,

Kodesova et al. (2009) studied the stability of soil structure in a Luvisol with similar soil properties, and reported a weak soil structure sensitive to intensive rainfall in the A horizon, and a well-developed soil structure with high aggregate stability in the argic (Bt) horizon.

In the CM plot, almost two thirds of the SOC stock is retained in topsoil, which is the highest proportion among the studied plots. This is due to generally high SOC content in the plough layer and the fact that the A horizon is predominantly limited to the plough layer (excluding CO soils). Colluvial soils represent only a marginal soil unit. The majority of the humus-rich profiles are concentrated in the side valleys, but their area is limited. As in LU, higher soil moisture in areas with colluvial soils causes increased SOC storage. Despite a markedly dissected relief and long and steep slopes, the soil pattern driven by erosional material transport is less evident than in the other two plots. It is debatable as to why the erosion effect is less intensive in the CM plot, which has the largest contributory area and the steepest slopes, particularly when we take into account the fact that other environmental factors are similar to those in the other two plots (e.g., soil texture, land use, climate). A possible explanation can be derived from its soil structure. Jirku et al. (2013) and Kodesova et al. (2009) found that the soil structure of Cambisols studied at an agricultural plot in Central Bohemia was stable even during intensive rainfall events. Kodesova et al. (2009) attribute this observation to a higher amount of organic matter and mostly to the presence of free iron oxides acting as cementing agents.

## 5. Conclusions

The study demonstrates how colluvial soils contribute to the total SOC stock at three pedologically different areas, which are influenced by soil redistribution due to accelerated erosion.

- The role of colluvial soils, with respect to their spatial extent and SOC stock, differs in the studied plots. The CO at the CH plots represents an important portion of the soil cover, both spatially (13%) and by volume of SOC stock (37%). CO has a moderate importance at the LU plot (12% of SOC stock) and a low importance at the CM plot (5% of SOC stock). The averaged SOC stock retained in colluvial soil significantly exceeds the mean SOC stock at each study plot. The SOC stock retained in colluvial soils and their spatial extent correspond to the intensity of soil mass redistribution. At the three plots with similar environmental settings (terrain, land management, climate), it is mostly soil characteristics and profile development, which are typical for each classification unit, that resulted in different degrees of importance of colluvial soil.
- SOC stock differs significantly for topsoil and subsoil in each plot. In Luvisol and Cambisol plots, more than one half of SOC is retained in topsoil and only marginal stock is contained below 50 cm, while more than two thirds of SOC stock occurs in subsoil in the Chernozem plot. Approximately 19% of the total SOC stock is below 2 m. This finding indicates the importance of the incorporation of deep and buried soil horizons in SOC stock estimations.
- The study demonstrated the high potential for the use of terrain variables as predictors in SOC stock modelling. However, significant differences in model performance have been identified among the studied plots. The best results were obtained in the LU plot, where both determination coefficients and prediction accuracy reached very good values. The model performance was also satisfactory in

**Table 5b**  
Mean SOC stock (t·ha<sup>-1</sup>) in different soil units at the three study plots.

	Soil unit	25 cm	Total		Soil unit	25 cm	Total		Soil unit	25 cm	Total
CH plot	CO	45.0a	404.0a	LU plot	CO	41.5a	93.2a	CM plot	CO	49.7a	122.8a
	CH	45.2a	112.0b		LU	36.2b	66.7b		CM	44.5b	72.0b
	RG	34.3b	103.7c		RG	35.0c	61.7c		LP	44.1c	66.2c

(Mean values followed by the different letters (a, b, c) in the same column are significantly different at  $P < 0.05$  according to Multiple range test).

the CH plot. The model showed its limitations in the CM plot, where a high uncertainty and low prediction accuracy resulted from a generally weak relationship between terrain and soil redistribution.

- PCA analysis and the use of predictors in prediction models revealed probable terrain attributes influencing the colluvial soil occurrence and SOC distribution in the plots. SOC stock in the highly dynamic environment of the Chernozem plot is driven mostly by intensive lateral sediment fluxes, indicated by terrain attributes such as slope and TPI. In Luvisol and Cambisol plots, the strong relationship with curvature and TWI corresponds to the combined process of sedimentation and soil moisture control on SOC concentration.

In summary, the results of the study revealed the significant influence of soil forming processes, resulting in different soil types, on the role of colluvial soil in total SOC stock, inter-site and in-depth variability, and topsoil/subsoil distribution of SOC stock at the three study plots. The results emphasize the importance of including deep soil sediments in total SOC stock estimation, mainly in plots with intensive soil mass redistribution. Our results suggest that the delineation of colluvial soils can identify areas with high potential deep organic carbon storage and thus improve the precision of our knowledge of SOC stock and its distribution in the agricultural landscape.

### Acknowledgements

The study was supported by grant nr. 13-07516P of the Czech Science Foundation and by grant nr. QJ1230319 of the Ministry of Agriculture. The authors thank Chris Ash for the language revision.

### Appendix A. Supplementary data

Supplementary data to this article can be found online at <http://dx.doi.org/10.1016/j.geoderma.2015.04.012>.

### References

- Berhe, A.A., Kleber, M., 2013. Erosion, deposition, and the persistence of soil organic matter: mechanistic considerations and problems with terminology. *Earth Surf. Process. Landf.* 38, 908–912.
- Bluszczyk, A., Poreba, G., Śnieżko, Z., 2007. The basis of the study of the age of the Holocene diluvium on loess areas of Polish highlands. *Geochronometria* 28, 61–66.
- Boser, B.E., Guyon, I.M., Vapnik, V.N., 1992. A training algorithm for optimal margin classifiers. In: Haussler, D. (Ed.), 5th Annual ACM Workshop on COLT. ACM Press, Pittsburgh, PA, pp. 144–152.
- Cambule, A.H., Rossiter, D.G., Stoorvogel, J.J., 2013. A methodology for digital soil mapping in poorly accessible areas. *Geoderma* 192, 341–351.
- Cambule, A.H., Rossiter, D.G., Stoorvogel, J.J., Smaling, E.M.A., 2014. Soil organic carbon stocks in the Limpopo National Park, Mozambique: amount, spatial distribution and uncertainty. *Geoderma* 213, 46–56.
- Chabbi, A., Kögel-Knabner, I., Rumpel, C., 2009. Stabilised carbon in subsoil horizons is located in spatially distinct parts of the soil profile. *Soil Biol. Biochem.* 41, 256–261.
- Chaopricha, N.T., Marín-Spiotta, E., 2014. Soil burial contributes to deep soil organic carbon storage. *Soil Biol. Biochem.* 69, 251–264.
- Chlupáč, I., Brzobohatý, R., Kovanda, J., Stranič, Z., 2002. *Geologická minulost České republiky* (in Czech). Academia, Praha.
- Cohen, J., 1960. A coefficient of agreement for nominal scales. *Educ. Psychol. Meas.* 20, 37–46.
- De Gryze, S., Six, J., Bossuyt, H., Van Oost, K., Merckx, R., 2008. The relationship between landform and the distribution of soil C, N and P under conventional and minimum tillage. *Geoderma* 144, 180–188.
- Devine, S., Markewitz, D., Hendrix, P., Coleman, D., 2011. Soil carbon change through 2 m during forest succession alongside a 30-year agroecosystem experiment. *For. Sci.* 57, 36–50.
- Doetterl, S., van Oost, K., Six, J., 2012a. Towards constraining the magnitude of global agricultural sediment and soil organic carbon fluxes. *Earth Surf. Process. Landf.* 37, 642–655.
- Doetterl, S., Six, J., et al., 2012b. Carbon cycling in eroding landscapes: geomorphic controls on soil organic C pool composition and C stabilization. *Glob. Change Biol.* 18, 2218–2232.
- Doetterl, S., Stevens, A., van Oost, K., Quine, T.A., van Wesemael, B., 2013. Spatially-explicit regional-scale prediction of soil organic carbon stock in cropland using environmental variables and mixed model approaches. *Geoderma* 204–205, 31–42.
- Don, A., Schumacher, J., Scherer-Lorenzen, M., Scholten, T., Schulze, E.-D., 2007. Spatial and vertical variation of soil carbon at two grassland sites — implications for measuring soil carbon stocks. *Geoderma* 141, 272–282.
- Dotterweich, M., Stankovič, M., Minar, J., Koco, S., Papco, P., 2013. Human induced soil erosion and gully system development in the Late Holocene and future perspectives on landscape evolution: the Myjava Hill Land, Slovakia. *Geomorphology* 201, 227–245.
- Fang, X., Xue, Z., Li, B., An, S., 2012. Soil organic carbon distribution in relation to land use and its storage in a small watershed of the Loess Plateau, China. *Catena* 88, 6–13.
- Florinsky, I.V., Eilers, R.G., Manning, G.R., Fuller, L.G., 2002. Prediction of soil properties by digital terrain modelling. *Environ. Model. Softw.* 17, 295–311.
- Fuchs, M., Fischer, M., Reverman, R., 2010. Colluvial and alluvial sediment archives temporally resolved by OSL dating: implications for reconstructing soil erosion. *Quat. Geochronol.* 5, 269–273.
- Han, F., Hu, W., Zheng, J., Du, F., Zhang, X., 2010. Estimating soil organic carbon storage and distribution in a catchment of Loess Plateau, China. *Geoderma* 154, 261–266.
- Hancock, G.R., Murphy, D., Evans, K.G., 2010. Hillslope and catchment scale soil organic carbon concentration: an assessment of the role of geomorphology and soil erosion in an undisturbed environment. *Geoderma* 155, 36–45.
- Harrison, R.B., Footen, P.W., Strahm, B.D., 2011. Deep soil horizons: contribution and importance to soil carbon pools and in assessing whole-ecosystem response to management and global change. *For. Sci.* 57, 67.
- ISO 11272:1998, 1998. Soil quality — determination of dry bulk density. Technical Committee ISO/TC 190.
- ISO 14235:1998, 1998. Soil quality — determination of organic carbon by sulfochromic oxidation. Technical Committee ISO/TC 190.
- IUSS Working Group WRB, 2006. World reference base for soil resources 2006. World Soil Resources Report No. 103. FAO, Rome.
- Janeček, M., 2012. *Protection of Agricultural Land Against Erosion*. MA CR, Prague.
- Jenness, J., 2006. Topographic Position Index (tpi\_jen.avx) Extension for ArcView 3.x, v. 1.2. available at: <http://www.jennessent.com/arcview/TP1.htm>.
- Jirku, V., Kodesova, R., Nikodem, A., Muhlhanselova, M., Zigova, A., 2013. Temporal variability of structure and hydraulic properties of topsoil of three soil types. *Geoderma* 204, 43–58.
- Kadereit, A., Kühn, P., Wagner, G.A., 2010. Holocene relief and soil changes in loess-covered areas of south-western Germany: the pedosedimentary archives of Bretten-Bauerbach (Kraichgau). *Quat. Int.* 222, 96–119.
- Kalinina, O., Krause, S.-E., Goryachkin, S.V., Karavaeva, N.A., Lyuri, D.I., Giani, L., 2011. Self-restoration of post-agrogenic chernozems of Russia: soil development, carbon stocks, and dynamics of carbon pools. *Geoderma* 162, 196–206.
- Khalil, M.I., Kiely, G., O'Brien, P., Müller, C., 2013. Organic carbon stocks in agricultural soils in Ireland using combined empirical and GIS approaches. *Geoderma* 193–194, 222–235.
- Kodesova, R., Vignozzi, N., Rohoskova, M., Hajkova, T., Kocarek, M., Pagliai, M., Kozak, J., Simunek, J., 2009. Impact of varying soil structure on transport processes in different diagnostic horizons of three soil types. *J. Contam. Hydrol.* 104, 107–125.
- Lang, A., Hönscheidt, S., 1999. Age and source of colluvial sediments at Vaihingen-Enz, Germany. *Catena* 38, 89–107.
- Liu, Z., Shao, M., Wang, Y., 2011. Effect of environmental factors on regional soil organic carbon stocks across the Loess Plateau region, China. *Agric. Ecosyst. Environ.* 142, 184–194.
- López-Fando, C., Pardo, M.T., 2011. Soil carbon storage and stratification under different tillage systems in a semi-arid region. *Soil Tillage Res.* 111, 224–230.
- McBratney, A.B., Santos, M.L.M., Minasny, B., 2003. On digital soil mapping. *Geoderma* 117, 3–52.
- Meyer, D., Dimitriadou, E., Hornik, K., Weingessel, A., Leisch, F., 2012. e1071: Misc Functions of the Department of Statistics (e1071). TU Wien.
- Minasny, B., McBratney, A.B., Mendonça-Santos, M.L., Odeh, I.O.A., Guyon, B., 2006. Prediction and digital mapping of soil carbon storage in the Lower Namoi Valley. *Aust. J. Soil Res.* 44, 233–244.
- Mishra, U., Lal, R., Liu, D., Van Meirvenne, M., 2010. Predicting the spatial variation of the soil organic carbon pool at a regional scale. *Soil Sci. Soc. Am. J.* 74, 906–914.
- Němeček, J., Tomášek, M., 1983. *Geography of Soils of Czechoslovakia*. Academia, Praha (in Czech).
- Němeček, J., Muhlhanselová, M., Macků, J., Vokoun, J., Vavříček, D., Novák, P., 2011. *Czech Taxonomic Classification System of Soils*. ČZU, Praha (in Czech).
- Paul, E.A., Morris, S.J., Conant, R.T., Plante, A.F., 2006. Does the acid hydrolysis-incubation method measure meaningful soil organic carbon pools? *Soil Sci. Soc. Am. J.* 70, 1023.
- Polyakov, V., Lal, R., 2004. Modeling soil organic matter dynamics as affected by soil water erosion. *Environ. Int.* 30, 547–556.
- Poreba, G., Śnieżko, Z., Moska, P., 2011. Some aspects of age assessment of Holocene loess colluvium: OSL and <sup>137</sup>Cs dating of sediment from Bia1a agricultural area, South Poland. *Quat. Int.* 240, 44–51.
- R Core Team, 2014. *R: A Language and Environment for Statistical Computing*. R Foundation for Statistical Computing, Vienna, Austria (URL <http://www.R-project.org/>).
- Rodzík, J., Mroczek, P., Wiśniewski, T., 2014. Pedological analysis as a key for reconstructing primary loess relief — a case study from the Magdalenian site in Klementowice (eastern Poland). *Catena* 117, 50–59.
- Rumpel, C., Eusterhues, K., Kögel-Knabner, I., 2004. Location and chemical composition of stabilized organic carbon in topsoil and subsoil horizons of two acid forest soils. *Soil Biol. Biochem.* 36, 177–190.
- Schwanghart, W., Jarmer, T., 2011. Linking spatial patterns of soil organic carbon to topography — a case study from south-eastern Spain. *Geomorphology* 126, 252–263.
- Shukla, M.K., Lal, R., 2005. Erosional effects on soil organic carbon stock in an on-farm study on Alfisols in west central Ohio. *Soil Tillage Res.* 81, 173–181.

- Simbahan, G.C., Dobermann, A., Goovaerts, P., Ping, J., Haddix, M.L., 2006. Fine-resolution mapping of soil organic carbon based on multivariate secondary data. *Geoderma* 132, 471–489.
- Van Hemelryck, H., Fiener, P., Van Oost, K., Govers, G., Merckx, R., 2010. The effect of soil redistribution on soil organic carbon: an experimental study. *Biogeosciences* 7, 3971–3986.
- Van Oost, K., Quine, T.A., Govers, G., Gryze, S.D., Six, J., Harden, J.W., Ritchie, J.C., McCarty, G.W., Heckrath, G., Kosmas, C., Giraldez, J.V., da Silva, J.R.M., Merckx, R., 2007. The impact of agricultural soil erosion on the global carbon cycle. *Science* 318, 626–629.
- Van Oost, K., Verstraeten, G., Doetterl, S., Notebaert, B., Wiaux, F., Broothaerts, N., Six, J., 2012. Legacy of human-induced C erosion and burial on soil-atmosphere C exchange. *Proc. Natl. Acad. Sci.* 109, 19492–19497.
- Vapnik, V., 1999. *The Nature of Statistical Learning Theory*. Springer-Verlag.
- Vasques, G.M., Grunwald, S., Comerford, N.B., Sickman, J.O., 2010. Regional modelling of soil carbon at multiple depths within a subtropical watershed. *Geoderma* 156, 326–336.
- Wang, Y., Fu, B., Lü, Y., Song, C., Luan, Y., 2010. Local-scale spatial variability of soil organic carbon and its stock in the hilly area of the Loess Plateau, China. *Quat. Res.* 73, 70–76.
- Wiesmeier, M., Hübner, R., Barthold, F., Spörlein, P., Geuß, U., Hangen, E., Reischl, A., Schilling, B., von Lütow, M., Kögel-Knabner, I., 2013. Amount, distribution and driving factors of soil organic carbon and nitrogen in cropland and grassland soils of southeast Germany (Bavaria). *Agric. Ecosyst. Environ.* 176, 39–52.
- Wilkinson, M.T., Richards, P.J., Humphreys, G.S., 2009. Breaking ground: pedological, geological, and ecological implications of soil bioturbation. *Earth Sci. Rev.* 97, 257–272.
- Xi, X., Yang, Z., Cui, Y., Sun, S., Yu, C., Li, M., 2011. A study of soil organic carbon distribution and storage in the Northeast Plain of China. *Geosci. Front.* 2, 115–123.
- Yang, X.-M., Wander, M.M., 1999. Tillage effects on soil organic carbon distribution and storage in a silt loam soil in Illinois. *Soil Tillage Res.* 52, 1–9.
- Zádorová, T., Penížek, V., 2011. Problems in correlation of Czech national soil classification and World Reference Base 2006. *Geoderma* 167–168, 54–60.
- Zádorová, T., Penížek, V., Šefrna, L., Rohošková, M., Borůvka, L., 2011. Spatial delineation of organic carbon-rich colluvial soils in Chernozem regions by terrain analysis and fuzzy classification. *Catena* 85, 22–33.
- Zádorová, T., Penížek, V., Šefrna, L., Drábek, O., Mihaljevič, M., Volf, Š., Chuman, T., 2013. Identification of Neolithic to Modern erosion–sedimentation phases using geochemical approach in a loess covered sub-catchment of South Moravia, Czech Republic. *Geoderma* 195–196, 56–69.
- Zádorová, T., Žižala, D., Penížek, V., Čejková, Š., 2014. Relating extent of colluvial soils to topographic derivatives and soil variables in a Luvisol sub-catchment, Central Bohemia, Czech Republic. *Soil Water Res.* 9, 47–57.
- Zglobicki, W., 2013. Present and past sedimentation rates in loess areas of the Lublin Upland (E Poland). *Géomorphol. Relief Process. Environ.* 1, 79–92.

## 5.5 Relating extent of colluvial soils to topographic derivatives and soil variables in a Luvisol sub-catchment, Central Bohemia, Czech Republic

---

- Zádorová, T., **Žížala, D.**, Penížek, V., Čejková, Š., 2014. Relating extent of colluvial soils to topographic derivatives and soil variables in a Luvisol sub-catchment, Central Bohemia, Czech Republic. *Soil and Water Research*. 9 (No. 2). p. 47–57. [doi: 10.17221/57/2013-SWR]

## Relating Extent of Colluvial Soils to Topographic Derivatives and Soil Variables in a Luvisol Sub-Catchment, Central Bohemia, Czech Republic

TEREZA ZÁDOROVÁ<sup>1</sup>, DANIEL ŽÍŽALA<sup>1,2</sup>, VÍT PENÍŽEK<sup>1</sup> and ŠÁRKA ČEJKOVÁ<sup>1</sup>

<sup>1</sup>Department of Soil Science and Soil Protection, Faculty of Agrobiological, Food and Natural Resources, Czech University of Life Sciences Prague, Prague, Czech Republic; <sup>2</sup>Research Institute for Soil and Water Conservation, Prague-Zbraslav, Czech Republic

### Abstract

ZÁDOROVÁ T., ŽÍŽALA D., PENÍŽEK V., ČEJKOVÁ Š. (2014): **Relating extent of colluvial soils to topographic derivatives and soil variables in a Luvisol sub-catchment, Central Bohemia, Czech Republic.** *Soil & Water Res.*, **9**: 47–57.

Colluvial soils, resulting from accelerated soil erosion, represent a significant part of the soil cover pattern in agricultural landscapes. Their specific terrain position makes it possible to map them using geostatistics and digital terrain modelling. A study of the relationship between colluvial soil extent and terrain and soil variables was performed at a morphologically diverse study site in a Luvisol soil region in Central Bohemia. Assessment of the specificity of the colluviation process with regard to profile characteristics of Luvisols was another goal of the study. A detailed field survey, statistical analyses, and detailed digital elevation model processing were the main methods utilized in the study. Statistical analysis showed a strong relationship between the occurrence of colluvial soil, various topographic derivatives, and soil organic carbon content. A multiple range test proved that four topographic derivatives significantly distinguish colluvial soil from other soil units and can be then used for colluvial soil delineation. Topographic wetness index was evaluated as the most appropriate terrain predictor. Soil organic carbon content was significantly correlated with five topographic derivatives, most strongly with topographic wetness index (TWI) and plan curvature. Redistribution of the soil material at the study site is intensive but not as significant as in loess regions covered by Chernozem. Soil mass transport is limited mainly to the A horizon; an argic horizon is truncated only at the steepest parts of the slope.

**Keywords:** digital elevation model; digital soil mapping loess; soil erosion; soil organic carbon

Colluvial soils form part of a mosaic of soil units in the soilscape, influenced by long-term erosion. Sedimentation of eroded humus-rich material forms deep fertile soils with more or less evident stratification of layers. Their close relationship with specific terrain units makes them a good object for digital soil mapping. Although their real spatial extent is not known, the ubiquitous occurrence of soil transport indicates that the extent of colluvial soils may be large (ZÁDOROVÁ *et al.* 2011). Formation of these soils is tightly connected with agricultural exploitation of the landscape and intensification of agriculture production. So far, a method for mapping of colluvial soil was developed

for small catchments in Chernozem regions (ZÁDOROVÁ *et al.* 2008, 2011), using geostatistics and fuzzy methods based on detailed terrain analysis. Colluvial soil mapping in loess-derived Luvisols is another step in the delineation of this soil unit and should be studied namely due to the large area of Luvisols and their generally high agricultural productivity. Luvisols, in comparison with e.g. loess-derived Chernozems, have a highly heterogeneous soil profile, namely in terms of the particle size distribution and soil structure. Thus, a different and more complex functioning of soil removal and sedimentation can be presumed. The presence of a dense, clay-rich argic horizon with highly

developed and stable soil structure can represent a significant threshold in erosive intensity and influence the resulting area and form of colluvial soils. The effect of soil aggregate stability, clay content, and soil organic matter on erosion vulnerability was studied by LE BISSONNAIS (1996), BRONICK and LAL (2005), CANTÓN *et al.* (2009). Aggregate stability is a critical component of soil erodibility since it controls the soil dispersion and surface seal development. The level of aggregation and stability of aggregates increases concurrent with increasing organic matter content, surface area of clay minerals, and cation exchange capacity (BRONICK & LAL 2005).

Soil organic carbon (SOC) distribution due to soil erosion is intensively studied (e.g. LAL 2001; RITCHIE *et al.* 2007). The general distribution of humus and its content in the colluvial profile reflects the specific sedimentation processes at the study plot. Increase in SOC in the colluvial horizon indicates preferential transport of material from A horizon. Decrease in SOC, on the other hand, indicates sedimentation of subsoil material and thus more intensive erosion (ZÁDOROVÁ *et al.* 2013).

Research on Central European loess colluvial soils is extensive. Soil redistribution in Luvisols as a result of erosion was described e.g. by TERHORST (2000), KLIMOWICZ and UZIAK (2001), or WOLF and FAUST (2013). Most of the studies concentrate on the structure of soil profiles along the studied transects. Other studies in Luvisol areas use colluvial soils as geoarchives due to their wide distribution and continuous presence for at least 7000 years (LANG & HÖNSCHIEDT 1999; LEOPOLD & VÖLKEK 2007; KADEREIT *et al.* 2010; KLIMEK 2010; POREBA *et al.* 2011).

Mapping of colluvial soils is based on topography and digital terrain modelling (ZÁDOROVÁ *et al.* 2011). Quantitative terrain data are widely applied in studies concerning how landscape position influences soil properties. Slope, curvature, catchment area, and topographic wetness index (TWI) are the most frequent variables. The various properties investigated include: soil depth (ODEH *et al.* 1995; PENÍŽEK & BORŮVKA 2006), thickness of horizons (FLORINSKY *et al.* 2002; VANWALLEGHEM *et al.* 2010), particle size distribution (ODEH *et al.* 1995; PENÍŽEK & BORŮVKA 2004), organic carbon content (SCHWANGHART & JARMER 2011), soil unit delineation (ZÁDOROVÁ *et al.* 2008, 2011). In Luvisols, few studies focus on soil depth and horizonation using terrain predictors. YOUNG and HAMMER (2000) studied a number of attributes and their relationship with the depth of Bt horizon in a loess-mantled landscape in Missouri.

The A horizon depth was studied by MOORE *et al.* (1993) or MARTIN and TIMER (2006). VANWALLEGHEM *et al.* (2010) studied the spatial variability of soil horizons in a natural forested area.

The presented study forms a part of a complex research concerning colluvial soil delineation in different soil and parent material conditions. This study directly continues from the study of a Chernozem region presented in ZÁDOROVÁ *et al.* (2011).

The particular objectives can be defined as follows: (i) to evaluate the relationship between the colluvial soil extent and selected topographic derivatives using different statistical methods, (ii) to define topographic derivatives with values specific for colluvial soils, which distinguish them from other soil units, and (iii) to assess the specificity of the colluviation process at the study plot with regard to profile characteristics of Luvisols. Soil profile structure and organic carbon distribution will be used for this aim.

## MATERIAL AND METHODS

**Study site.** The study was situated in Central Bohemia (Czech Republic), in the Pšovka River watershed (Figure 1). The wider area is underlain by Cretaceous sandstones covered by a Pleistocene loess layer (CHLUPÁČ *et al.* 2002). Haplic and Albic Luvisols are the original dominant soil units. Detailed research was carried out on a section of an agricultural parcel. The study plot is characterized by intensive topography dominated by two perpendicular side valleys (north-south and east-west) connected in the south-west part of the site (Figure 2). These two concave units

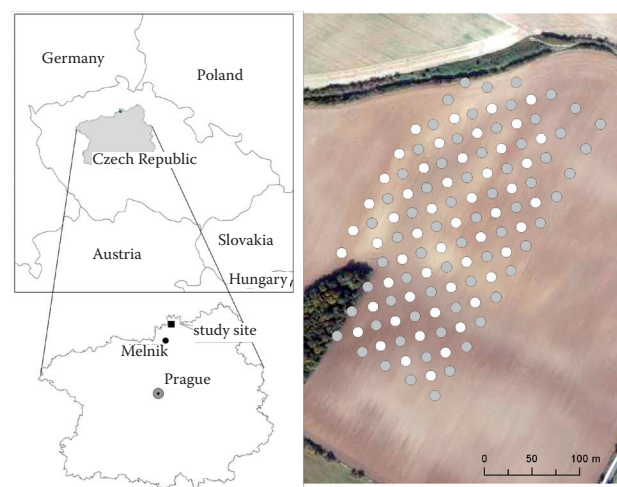


Figure 1. Localization of the study site (left) and the network of borings (white dots – soil profile description, grey dots – soil profile description and soil organic carbon analysis)

together with a significant rill in the east part of the plot represent the main accumulation positions at the plot. The adjacent slopes are relatively steep (up to 12°), while the south, north-east, and north-west parts of the plot are formed by flat terrain.

**Methods.** The study plot was investigated by soil sampling based on a regular grid (15 × 15 m) with 1 m deep auger observations (in total 119 bores) (Figure 1). The following soil characteristics were determined: soil unit, soil depth, soil profile stratigraphy. Samples for analysis of soil organic carbon content were taken from half of the borings (66 borings, grid 30 × 30 m).

The soil organic carbon content was measured using the dichromate redox titration method (SKJEMSTAD & BALDOCK 2008).

The topographic derivatives were obtained from the digital elevation model (DEM) derived from the airborne laser scanning procedure. The DEM was provided in 1 × 1 m point grid (provider GEODIS Ltd., Brno, Czech Republic), interpolated and filtered by Gaussian filter in SAGA GIS software. Computed topographic derivatives represent a standard set of terrain variables used for the soil-terrain mapping (MOORE *et al.* 1993; ODEH *et al.* 1995). The topographic derivatives were calculated using integrated algorithms implemented in SAGA GIS from the DEM: altitude (ALT), slope, plan, profile, and mean curvature (PLANC, PROF, MEANC), catchment area (CA), altitude above channel (ALTCHN), and topographic wetness index (TWI). Particular topographic derivatives were selected to be comparable with the study on colluvial soil delineation carried out in a Chernozem region (ZÁDOROVÁ *et al.* 2011).

Correlation between the soil characteristics and terrain derivatives was assessed by Pearson's (normal distribution variables) and Spearman's (other) coefficient. Multiple Range Test (parametrical and non-

parametrical) was used for all topographic derivatives to find out which of them are characteristic for the colluvial soil unit. It means that for colluvial soil there exists a unique confidence interval of topographic derivative value that significantly differentiates colluvial soil from other soil units. This analysis enabled the choice of a reasonable number of appropriate topographic derivatives to distinguish the colluvial soil from other units. Principal component analysis (PCA) was applied to display the structure of the data set and reveal possible inter-correlations between the variables. All statistical calculations were performed using the software R.

Names of soil units used in this paper are based on the national classification Czech Taxonomic Classification System of Soils (CTCSS; NĚMEČEK *et al.* 2011). Their correlation with World Reference Base for Soil Resources 2006 (WRB 06; IUSS Working Group WRB 2006) and CTCSS is described in Table 1. Detailed information on correlation between CTCSS and WRB 06 is given in ZÁDOROVÁ and PENÍZEK (2011). Soil units defined in the national classification are better suited for the soil cover pattern description after a long-term redistribution as they, opposite to the WRB, reflect the process of soil formation and can be used to differentiate particular erosion and accumulation stages of the soil profile.

## RESULTS AND DISCUSSION

**Soil cover pattern.** The soil cover pattern exists as a diverse mosaic of soil units due to intensive material redistribution caused by both water and tillage erosion. Five soil units, and/or subunits, were identified (Figure 3). Luvisols cover mainly the upper flat parts of the plot and lower slopes. The A horizon is restricted to the plough layer or reaches a maximum of 5–10 cm below. The eluvial horizon forms part of the plough layer. The argic horizon is well structured

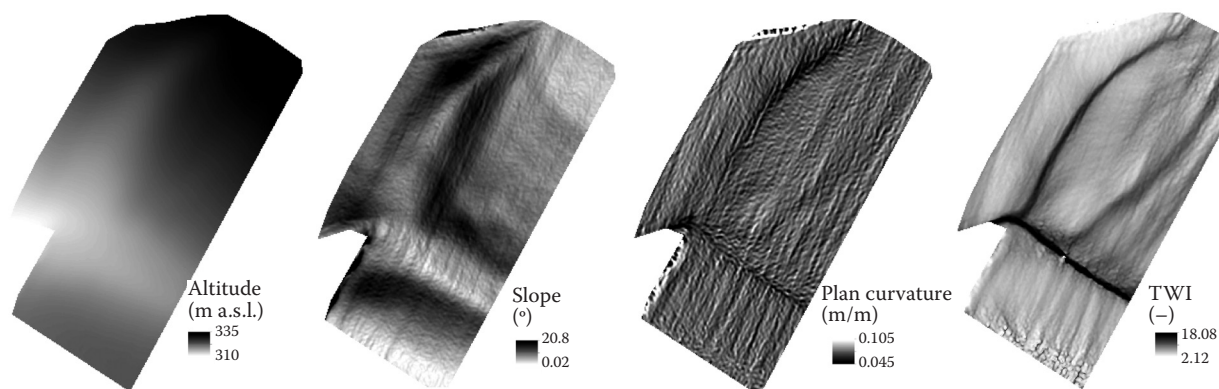


Figure 2. Digital elevation model and selected topographic derivatives; TWI – topographic wetness index

Table 1. Soil units names used in the paper and their correlation in World Reference Base for Soil Resources (WRB 06)

Soil unit	WRB 06	CTCSS	Profile	A horizon depth (cm)
LU	Haplic Luvisol	Hnědozem modální	A–Bt–C	A < 30
LUac	Luvic Phaeozem	Hnědozem modální akumulovaná	A–Bt–C	A > 30, < 60
CO	Luvic Phaeozem Colluvic	Koluvizem modální	A–Bt–C	A > 60
RG	Haplic Calcisol Haplic Regosol	Regozem modální	A–C	A < 30
RGac	Haplic Kastanozem	Regozem modální akumulovaná	A–C	A > 30, < 60

LU – Luvisol; LUac – accumulated Luvisol; CO – colluvial soil; RG – Regosol; RGac – accumulated Regosol; CTCSS – Czech Taxonomic Classification System of Soils

(polyhedral and prismatic structure) but its thickness varies significantly from 10 to 60 cm (Figure 4). Luvisols differ according to their accumulated forms in the concave parts of the terrain, mainly at the outer parts of the main side valleys. The A horizon is deeper (30–60 cm), but the eluvial horizon is not present. Colluvial soils develop exclusively in the bottom parts of the two side valleys. The A horizon exceeds 60 cm in thickness, in majority of profiles it is more than 80 cm thick (Figure 4). In a similar terrain arrangement, the thickness of colluvial horizons is fundamentally smaller than in Chernozems (ZÁDOROVÁ *et al.* 2011), namely because of generally shallower A horizons in Luvisols and the presence of a stable Bt horizon. Colluvial layers bury argic horizons indicating the original presence of Luvisols at the valley bottom. Steep slopes adjacent to the side valleys are covered by Regosols with an eroded profile. Regosols located close to the accumulation area have deep A horizons (up to 60 cm) but lack an argic horizon. This profile evolution corresponds

to the consecutive filling of the valleys bottom and accumulation of the soil matter at adjacent slopes. A strong influence of tillage erosion can be assumed in these profiles.

A very similar soil cover pattern was identified by TERHORST (2000) with Albic Luvisol at the flat-topped ridges, Regosols and Rendzinas at the slopes, and thick colluvial layers and buried Luvisols at the valleys bottom. KLIMOWICZ and UZIĄK (2001) estimated an average colluvial horizon thickness of 90 cm in the wider area of Polish loess-derived Luvisols. WOLF and FAUST (2013) reported severe truncation of Luvisol profiles at the slopes and colluvial sediment up to 1 m thick in accumulation positions. In contrast, at a comparable study site in a Chernozem region (ZÁDOROVÁ *et al.* 2011), the area with exposed parent material is negligible.

**Relationship between soil units and topographic derivatives.** Tables 2 and 3 show the relationship between each of the identified soil units and topographic derivatives. Results of PCA analysis are

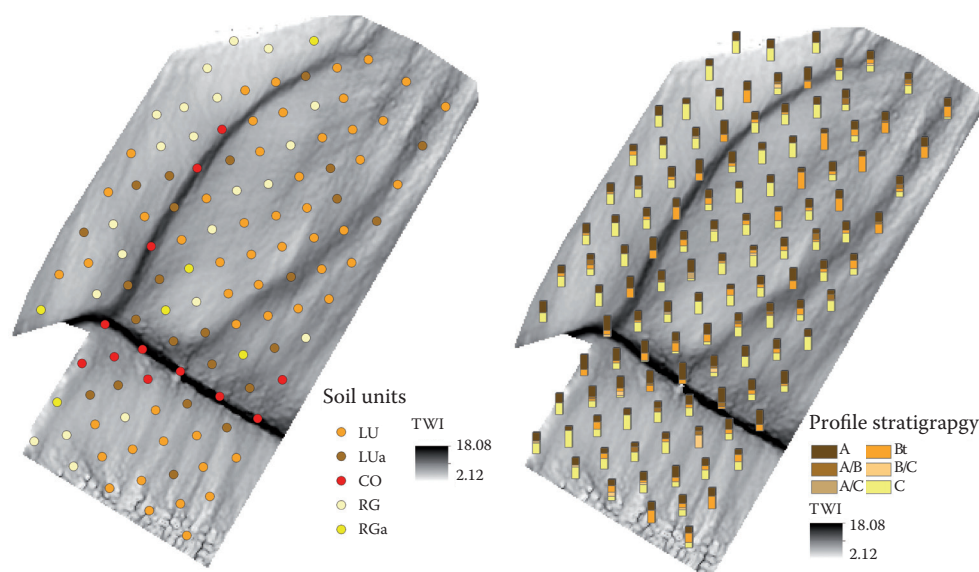


Figure 3. Soil units distribution at the study site (left) and soil profile stratigraphy (right)



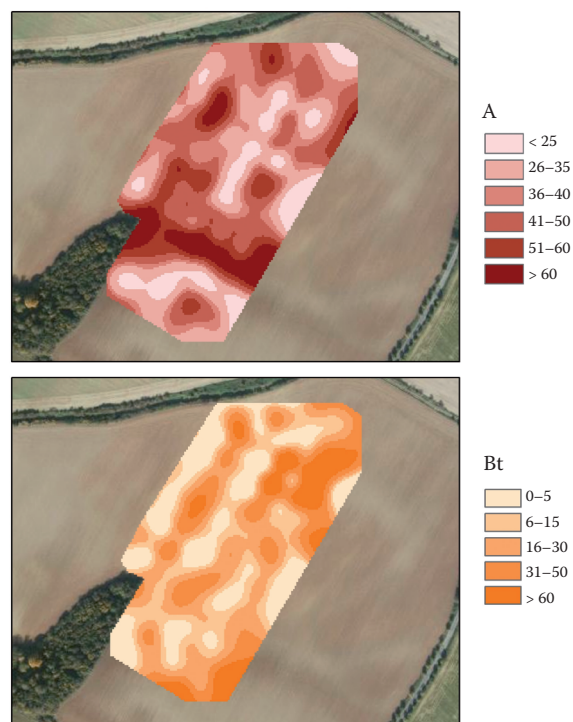


Figure 4. Interpolated soil horizons thickness (cm)  
A, Bt – soil profiles

depicted in Figure 5. Component 1 and component 2 explain 77% of the data variability. Mean values for each soil unit were generated for each involved topographic derivative (Table 2). In the majority of cases, mean values for colluvial soil lie in a different part of the interval than other soil units. This is noticeable in the case of ALT, slope, PLANC, CA, TWI, and ALTCHN (Figure 6). As the PCA analysis showed a strong inter-correlation of TWI and CA, only TWI will be used for the next analysis. Multiple range test for aggregated soil units (colluvial soil, Luvisol, and Regosol) proved significant differences between colluvial soil and other soil units in all of the above mentioned variables except for slope (Table 3). Colluvial soils can then be delineated using these

topographic variables. The most marked difference was determined in the case of TWI (Figure 6) This is an expected result as TWI has a high potential in the delineation of areas with different intake of sediments (FLORINSKY 2002; ZÁDOROVÁ *et al.* 2011). The significance of ALT and ALTCHN shows that the occurrence of colluvial soil is restricted to the lowest parts of the relief. PLANC also showed significant differences between colluvial soil and other soil units, indicating their development in the concave side valleys. PCA analysis also shows the isolated position of colluvial soils and their strong relationship with the above mentioned topographic derivatives. On the contrary, mean and profile curvature has no influence on the differentiation of soil units. With accumulated forms included, the differences were not significant for any of the derivatives (Table 3). This is caused mainly by the group of accumulated Luvisols having the properties typical of colluvial soil and Luvisol. PCA analysis shows this polarity as the profiles are aggregated in two distinct groups. Standardized means of topographic derivatives relevant for soil units can be compared with an analogous study conducted in a Chernozem region (ZÁDOROVÁ *et al.* 2011). In colluvial soil, the means of profile and mean curvature are very similar while the mean of slope is markedly lower in the case of the Luvisol area (0.38 in Luvisol area, 0.52 in Chernozem area) and the mean of TWI is higher in the Luvisol area (0.58 in Luvisol area, 0.44 in Chernozem area). The differences are caused mainly by different terrain configuration in both study sites when the colluvial soil in Chernozem region reaches up to the backslope positions with high slope. A relatively high value of slope in the case of Luvisol (0.59) proves that the extent of these soils is not limited to the flat areas and that the Luvisols are stable even at low and middle slopes (in contrast to Chernozems that are preserved exclusively at the flat positions). The MRT revealed

Table 2. Standardized means of topographic derivatives for each soil unit

Soil unit	ALT	SLOPE	MEANC	PLANC	PROFC	CA	TWI	ALTCHN
LU	0.593	0.513	0.378	0.344	0.575	0.001	0.248	0.206
LUac	0.428	0.495	0.323	0.302	0.625	0.007	0.340	0.084
CO	0.263	0.3848	0.365	0.275	0.506	0.149	0.585	0.040
RG	0.547	0.6428	0.432	0.412	0.514	0.001	0.196	0.216
RGac	0.344	0.706	0.425	0.367	0.592	0.001	0.226	0.117

LU – Luvisol; LUac – accumulated Luvisol; CO – colluvial soil; RG – Regosol; RGac – accumulated Regosol; ALT – altitude; SLOPE – slope; MEANC – mean curvature; PLANC – plan; PROFC – profile; CA – catchment area; TWI – topographic wetness index; ALTCHN – altitude above channel

Table 3. Differentiation of soil units based on topographic derivatives (Multiple Range Test Method: 95.0% LSD)

Soil unit	ALT	SLOPE	MEANC	PLANC	PROFC	CA	TWI	ALTCHN
<b>Aggregated soil units</b>								
LU	A	A	A	A	A	A	A*	A
CO	B*	A	A	B*	A	B*	B*	B*
RG	A	B*	A	AC	A	A	C*	A
<b>Soil units and subunits</b>								
LU	A	AB	A	AB	A	A	A	A
LUac	B	AB	A	A	A	B	AB	AB
CO	BC	A	A	A	A	B	B	B
RG	AB	B	A	B	A	A	AC	A
RGac	ABC	B	A	AB	A	AB	AC	AB

LU – Luvisol; LUac – accumulated Luvisol; CO – colluvial soil; RG – Regosol; RGac – accumulated Regosol; ALT – altitude; SLOPE – slope; MEANC – mean curvature; PLANC – plan; PROFC – profile; CA – catchment area; TWI – topographic wetness index; ALTCHN – altitude above channel; \*soil unit forms a distinguished group

the most important difference in the case of curvature (mean and profile); it was one of the most significant derivatives for the distinction of colluvial soils in the Chernozem region but it had a very low potential in the Luvisol area. Catchment area and TWI showed high potential for colluvial soil delineation in both study areas. Opposite from the Luvisol area, altitude was not a significant parameter in the Chernozem area where colluvial soils also reached higher parts of the study plot. In the Chernozem region, colluvial soil could be unified with accumulated Chernozem using some topographic derivatives and thus a wider accumulation area could be delineated. At the Luvisol study site, the colluvial soil and accumulated Luvisol

do not form a homogeneous group in any case. The wider accumulation area defined by colluvial soil and accumulated Luvisol cannot be properly defined using the topographic derivatives.

Not only the mean values but also the variability and range of the values of each soil unit are important. The variability of values in colluvial soils, Luvisols, and Regosols is rather low as these soil units are dependent on particular landform units. On the contrary, the accumulated sub-units have a high variability of terrain attributes as they occur in transitional positions where both mass transport and deposition can occur. Very similar results in variability have been reported from the Chernozem region (ZÁDOROVÁ *et al.* 2011).

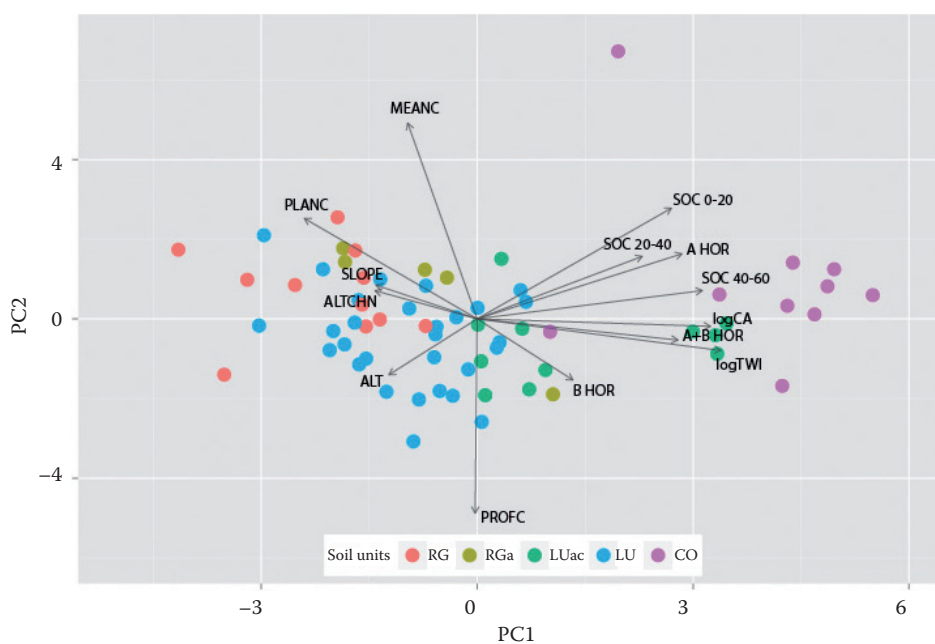


Figure 5. Principal component analysis biplot LU – Luvisol; LUac – accumulated Luvisol; CO – colluvial soil; RG – Regosol; RGac – accumulated Regosol; ALT – altitude; SLOPE – slope; PLANC – plan; PROFC – profile; MEANC – mean curvature; CA – catchment area; ALTCHN – altitude above channel; TWI – topographic wetness index; SOC – soil organic carbon

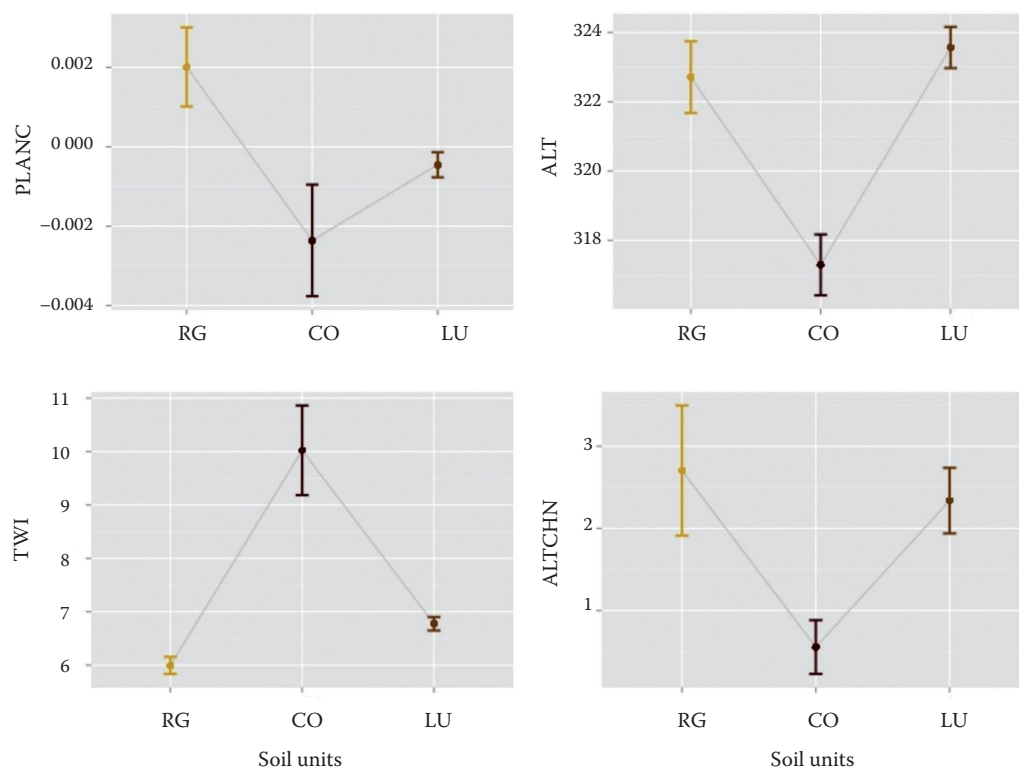


Figure 6. Mean values of selected topographic derivatives with confidence intervals for soil units (Multiple Range Test – LSD: 95% confidence interval)

LU – Luvisol; CO – colluvial soil; RG – Regosol; ALT – altitude; PLANC – plan; ALTCHN – altitude above channel; TWI – topographic wetness index;

Correlation of soil depth and horizon thickness with topographic derivatives was performed (Table 4). Soil depth and horizon thickness are closely linked with the soil unit. However, soil units with different erosional stages can have a similar thickness of some soil horizons; e.g. a deep A horizon is typical not only of colluvial soil and accumulated Luvisol, but also of accumulated Regosol. A shallow A horizon can occur not only in Regosol, but also in stable Luvisol. A horizon thickness significantly correlates with a number of topographic derivatives: ALT, PLANC, TWI, and ALTCHN. The strongest relationship in the case of ALTCHN ( $-0.47$ ) and TWI ( $0.38$ ) clearly shows the accumulation of humus material at the bottom of the side valleys. On the contrary, correlation of A horizon depth and slope is not significant. Such a weak correlation has been reported also in FLORINSKY *et al.* (2002) or ZÁDOROVÁ *et al.* (2011). A very weak relationship between MEANC ( $-0.14$ ) and PROFC ( $0.08$ ) and A horizon thickness is surprising and is in contrast with the findings of ZÁDOROVÁ *et al.* (2011). Thickness of B horizon correlates only with three topographic derivatives: TWI, PLANC, and slope. In this case, the closest correlation was found in the case of slope ( $-0.44$ ).

This can be explained by the presence of a deep undisturbed Bt horizon in the upper flat parts of the study plot covered by the most developed Luvisols. Lastly, soil depth is related significantly to PLANC, TWI, and slope. Low dependency on altitude and ALTCHN corresponds with the occurrence of deep soils both in the low parts of the valleys bottom and at the upper flat parts of the study plot.

The above-mentioned results confirmed known facts about topographic influence on the thickness of the horizons and soil depth at the agricultural areas (e.g. MOORE *et al.* 1993; FLORINSKY *et al.* 2002; ZÁDOROVÁ *et al.* 2011). The fact that the very close relationship between Luvisol profile stratification and topography is a specificity of agricultural land was reported by VANWALLEGHEM *et al.* (2010). Their research situated in a natural forest area showed that the dependence of soil depth on terrain units is very low and that the variability of soil horizon thickness is not related to the variability of topography.

**Soil organic carbon distribution.** The process of erosion and the following sedimentation of eroded material cause a significant redistribution of the organic carbon within the studied plot. The three maps (Figure 7) show the distribution of SOC content at

Table 4. Differentiation of soil units based on soil organic carbon (SOC) content at various depths (Multiple Range Test Method: 95.0% LSD)

Soil unit	SOC (depth, cm)		
	0–20	20–40	40–60
<b>Aggregated soil units</b>			
LU	A	A	A
CO	B*	B*	B*
RG	A	A	A
<b>Soil units and subunits</b>			
LU	A	A	A
LUac	AB	AB	AB
CO	B	B	B
RG	A	A	A
RGac	AB	AB	A

LU – Luvisol; LUac – accumulated Luvisol; CO – colluvial soil; RG – Regosol; RGac – accumulated Regosol; \*soil unit forms a distinguished group

three different soil depths. The highest SOC concentration at all of the three depths was observed in the two side valleys. However, differences can be seen in these two accumulation units. In the first 40 cm, high organic matter content (more than 2%) is described in

the majority of the north-south valley while the SOC content in the east-west valley is lower. At the depth of 60 cm and more, the SOC content is higher in the east-west valley proving the deeper A horizon in this part (shown also in Figure 4). Another isolated area of high SOC content is formed at the flat undisturbed part of the study plot. The soils covering steeper slopes have significantly lower SOC content in both topsoil and deeper horizons. The SOC distribution indicates the erosional-sedimentation processes at the study plot. Soil mass is primarily eroded from the slopes adjacent to the side valleys. The erosion is more intensive at the southern part of the plot; the soil profiles in the east-west valley are deeper and the plough layer contains less humus. In the late phase of erosion the colluvial horizon is built also by the material eroded from subsurface soil horizons poor in organic matter which are successively excavated by erosion. However, this process leading to retrograde soil development is weak in comparison with subsequent burying of A horizons known from Chernozem or Cambisol regions (ZÁDOROVÁ *et al.* 2008, 2011).

The relationship between SOC content, soil units, and topographic derivatives was statistically evaluated. Colluvial soil is distinguished by its SOC content at all three profile depths in the case of aggregated soil units. This means that the SOC content in colluvial

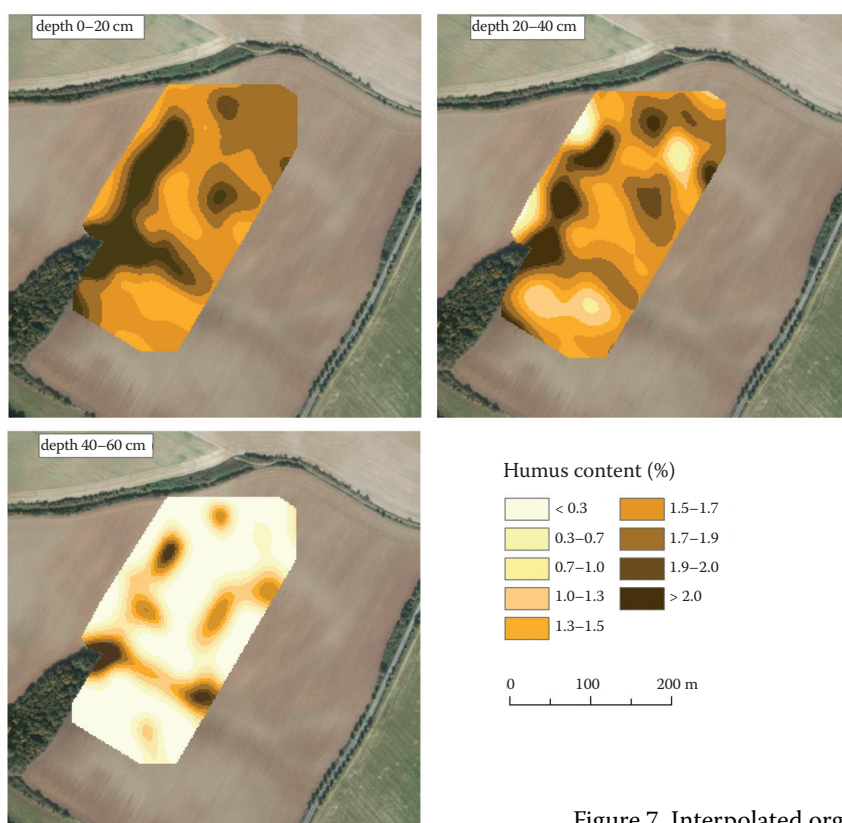


Figure 7. Interpolated organic matter content at various depths

Table 5. Correlation analyses between soil and topographic variables (Pearson's and/or Spearman's correlation coefficient)

	SOC (depth, cm)			HOR		ALT	MEANC	PLANC	PROFC	CA	TWI	ALTCNH	SLOPE
	0–20	20–40	40–60	A	B								
SOC (depth, cm)													
0–20		0.78**	0.56*	0.57**	0.49**	0.23	0.05	-0.47**	-0.15	0.43**	0.48**	-0.41**	-0.34*
20–40	0.78**		0.53**	0.50**	0.32*	0.10	-0.12	-0.43**	0.00	0.38*	0.47**	-0.40**	-0.32*
40–60	0.56**	0.53**		0.66**	0.58**	0.28	-0.28	-0.56**	0.05	0.56**	0.57**	-0.53**	-0.29
A	0.57**	0.50**	0.66**		0.49**	0.10	-0.14	-0.30**	0.08	0.36**	0.38**	-0.47**	-0.21
A + B	0.49**	0.32*	0.58**	0.49**		0.82**	-0.20	-0.39**	0.13	0.34**	0.51**	-0.28*	-0.50**
B	0.23	0.10	0.28	0.10	0.82**		-0.14	-0.29*	0.06	0.17	0.35**	-0.06	-0.44**
ALT	-0.19	-0.07	-0.25	-0.36**	-0.06	0.10	0.08	0.07	-0.04	-0.34**	-0.20	0.21	-0.14
MEANC	0.05	-0.12	-0.28	-0.14	-0.20	0.08		0.40**	-0.81**	-0.36**	-0.36**	0.25*	0.07
PLANC	-0.47**	-0.43**	-0.56**	-0.30**	-0.39**	0.07	0.40**		-0.24*	-0.65**	-0.65**	0.55**	0.07
PROFC	-0.15	0.00	0.05	0.08	0.13	0.06	-0.81**	-0.24*		0.18	0.20	-0.08	-0.05
CA	0.43**	0.38*	0.56**	0.36**	0.34**	0.17	-0.36**	-0.65**	0.18		0.88**	-0.73**	-0.04
TWI	0.48**	0.47**	0.57**	0.38**	0.51**	0.35**	-0.36**	-0.65**	0.20*	0.88**		-0.64**	-0.42**
ALTCNH	-0.41**	-0.40**	-0.53**	-0.47**	-0.28*	-0.06	0.25*	0.55**	-0.08	-0.73**	-0.64**		0.00
SLOPE	-0.34*	-0.32*	-0.29	-0.21	-0.50**	-0.44**	0.07	0.07	-0.05	-0.04	-0.42**	0.00	

SOC – soil organic contents; HOR – horizon; ALT – altitude; MEANC – mean curvature; PLANC – plan; PROFC – profile; CA – catchment area; TWI – topographic wetness index; ALTCNH – altitude above channel; SLOPE – slope; \*, \*\* $P < 0.05, 0.01$

soil is markedly higher than in other soil units (Table 4). This is in contradiction with findings from the Chernozem region, where the SOC content in the upper parts of the colluvial horizon was significantly lower than in the undisturbed Chernozem (ZÁDORO-VÁ *et al.* 2013). All units and subunits included, colluvial soil cannot be reliably distinguished as the accumulated Luvisol stands between colluvial soil and Luvisol.

SOC content is significantly correlated with several variables (Table 5). The strongest relationship was indicated between SOC content and A horizon thickness and soil depth. This is comprehensible as the greatest soil depth represents the accumulated soils. TWI and PLANC are positively correlated with the SOC content at all three depths while SLOPE and ALTCHN are negatively correlated.

The results showing SOC as a function of soil redistribution and topography correspond with long-term studies on SOC distribution in the landscape (e.g. RITCHIE *et al.* 2007). TWI showed the highest potential for the SOC mapping as it delineates areas with high potential accumulation and soil moisture. Findings of SCHWANGHART and JARMER (2011) and WIESMEIER *et al.* (2013) correspond with our results.

## CONCLUSION

The statistical relationship between colluvial soil extent and terrain and soil parameters was studied at a diversified study plot in a Luvisol region with the aim of finding topographic variables suitable for colluvial soil delineation.

Colluvial soils cover a significant part of the soil mosaic at the study site in the Luvisol area. Colluvial horizons reach a maximum thickness of 80 cm and their extent is limited to two perpendicular side valleys. Luvisols with a fully developed soil profile occur not only at the flat parts of the plot but also at low and middle slopes (up to 9°). The steepest parts of the plot are covered by Regosols.

Statistical analysis showed a significant relationship between colluvial soil extent and various terrain and soil variables. Multiple range test proved that four topographic derivatives (TWI, ALT, PLANC, ALTCHN) significantly distinguish colluvial soil from other soil units and can be then used for colluvial soil mapping. The most marked difference was determined in the case of TWI. TWI and ALTCHN also showed the strongest correlation with A horizon thickness and soil depth.

Soil organic matter redistribution is strongly dependent on erosion processes and shows a significant

relationship with numerous topographic derivatives (PLANC, TWI, ALTCHN, slope). SOC content distinguishes colluvial soil from other soil units proving intensive accumulation in the concave positions.

Redistribution of the soil material at the study site is intensive but not as pronounced as in Chernozem areas. The soil removal is limited mainly to the A horizon; the argic horizon is truncated only at the steepest parts of the slope where the parent material is exposed. This finding is supported by relatively shallow colluvial horizons, a high SOC content in the plough layer of colluvial soils meaning a weak admixture of mineral soil material and also by a large extent of undisturbed or weakly disturbed Luvisols at the study plot. These results can be attributed to the specific profile of Luvisols with the well-structured argic horizon representing a stable and hardly erodible layer.

The study showed that the colluvial soils developing in Luvisol areas can be delineated using topographic derivatives as the relationship between colluvial soil and topography is significant. The delineation model proposed in the Chernozem region will be applied in the next step of the research.

**Acknowledgements.** The study was supported by Grant No. 13-07516P of the Czech Science Foundation and by Project No. QJ1230319 of the Ministry of Agriculture of the Czech Republic. Authors thank to O. JAKŠÍK, M. FÉR, and A. KLEMENT for their help with fieldwork. Authors thank to C. ASH for language revision.

## References

- BRONICK C.J., LAL R. (2005): Soil structure and management: a review. *Geoderma*, **124**: 3–22.
- CANTÓN Y., SOLÉ-BENET A., ASENSIO C., CHAMIZO S., PUIGDEFÁBREGAS J. (2009): Aggregate stability in range sandy loam soils relationships with runoff and erosion. *Catena*, **77**: 192–199.
- CHLUPÁČ I., BRZOBHATÝ R., KOVANDA J., STRANÍK Z. (2002): Geological History of the Czech Republic. Academia, Praha. (in Czech)
- FLORINSKY I.V., EILERS R.G., MANNING G.R., FULLER L.G. (2002): Prediction of soil properties by digital terrain modelling. *Environmental Modelling & Software*, **17**: 295–311.
- KADEREIT A., KÜHN P., WAGNER G.A. (2010): Holocene relief and soil changes in loess-covered areas of southwestern Germany: The pedosedimentary archives of Bretten-Bauerbach (Kraichgau). *Quaternary International*, **222**: 96–119.
- KLIMEK K. (2010): Past and present interaction between the catchment and the valley floor: Upper Osoblaha basin,

- NE Sudetes slope and foreland. *Quaternary International*, **220**: 112–121.
- KLIMOWICZ Z., UZIAK S. (2001): The influence of long-term cultivation on soil properties and patterns in an undulating terrain in Poland. *Catena*, **43**: 177–189.
- LAL R. (2001): Soil degradation by erosion. *Land Degradation and Development*, **12**: 519–539.
- LANG A., HÖNSCHEIDT S. (1999): Age and source of colluvial sediments at Vaihingen–Enz, Germany. *Catena*, **38**: 89–107.
- LE BISSONNAIS Y. (1996): Aggregate stability and assessment of soil crustability and erodibility: I. Theory and methodology. *European Journal of Soil Science*, **47**: 425–437.
- LEOPOLD M., VÖLKELE J. (2007): Colluvium: Definition, differentiation, and possible suitability for reconstructing Holocene climate data. *Quaternary International*, **162–163**: 133–140.
- MARTIN W.K.E., TIMMER V.R. (2006): Capturing spatial variability of soil and litter properties in a forest stand by landform segmentation procedures. *Geoderma*, **132**: 169–181.
- MCKENZIE N.J., RYAN P.J. (1999): Spatial prediction of soil properties using environmental correlation. *Geoderma*, **89**: 67–94.
- MOORE I.D., GESSLER P.E., NIELSEN G.A., PETERSON G.A. (1993): Soil attribute prediction using terrain analysis. *Soil Science Society of America Journal*, **57**: 443–452.
- NĚMEČEK J., MÜHLHANSELOVÁ M., MACKŮ J., VOKOUN J., VAVŘÍČEK D., NOVÁK P. (2011): Czech Taxonomic Classification System of Soils. ČZU, Praha. (in Czech)
- ODEH I.O.A., McBRATNEY A.B., CHITTLEBOROUGH D.J. (1995): Further results on prediction of soil properties from terrain attributes: heterotopic cokriging and regressionkriging. *Geoderma*, **67**: 215–226.
- PENÍŽEK V., BORŮVKA L. (2004): Processing of conventional soil survey data using geostatistical methods. *Plant, Soil and Environment*, **50**: 352–357.
- PENÍŽEK V., BORŮVKA L. (2006): Soil depth prediction supported by primary terrain attributes: a comparison of methods. *Plant, Soil and Environment*, **52**: 424–430.
- POREBA G., SNIESZKO Z., MOSKA P. (2011): Some aspects of age assessment of Holocene loess colluvium: OSL and <sup>137</sup>Cs dating of sediment from Biała agricultural area, South Poland. *Quaternary International*, **240**: 44–51.
- RITCHIE J.C., MCCARTY G.W., VENTERIS E.R., KASPAR T.C. (2007): Soil and soil organic carbon redistribution on the landscape. *Geomorphology*, **89**: 1–2.
- SCHWANGHART W., JARMER T. (2011): Linking spatial patterns of soil organic carbon to topography – A case study from south-eastern Spain. *Geomorphology*, **126**: 252–263.
- SKJEMSTAD J.O., BALDOCK J.A. (2008): Total and organic carbon. In: CARTER M.R., GREGORICH E.G. (eds): *Soil Sampling and Method of Analysis*. Canadian Society of Soil Science, Taylor and Francis Group, Boca Raton, 225–237.
- TERHORST B. (2000): The influence of Pleistocene landforms on soil-forming processes and soil distribution in a loess landscape of Baden-Württemberg. *Catena*, **41**: 165–179.
- VANWALLEGHEM T., POESSEN J., McBRATNEY A., DECKERS J. (2010): Spatial variability of soil horizon depth in natural loess-derived soils. *Geoderma*, **157**: 37–45.
- WIESMEIER M., HÜBNER R., BARTHOLD F., SPÖRLEIN P., GEUSS U., HANGEN E., REISCHL A., SCHILLING B., VON LÜTZOW M., KÖGEL-KNABNER I. (2013): Amount, distribution and driving factors of soil organic carbon and nitrogen in cropland and grassland soils of southeast Germany (Bavaria). *Agriculture, Ecosystems & Environment*, **176**: 39–52.
- WOLF D., FAUST D. (2013): Holocene sediment fluxes in a fragile loess landscape (Saxony, Germany). *Catena*, **103**: 87–102.
- YOUNG F.J., HAMMER R.D. (2000): Soil–landform relationships on a loess-mantled upland landscape in Missouri. *Soil Science Society of America Journal*, **64**: 1443–1454.
- ZÁDOROVÁ T., PENÍŽEK V. (2011): Problems in correlation of Czech national soil classification and World Reference Base 2006. *Geoderma*, **168**: 54–60.
- ZÁDOROVÁ T., CHUMAN T., ŠEFRNA L. (2008): A method proposal for colluvisol delineation in Chernozem's region. *Soil and Water Research*, **3**: 215–222.
- ZÁDOROVÁ T., PENÍŽEK V., ŠEFRNA L., ROHOŠKOVÁ M., BORŮVKA L. (2011): Spatial delineation of organic carbon-rich Colluvial soils in Chernozem regions by Terrain analysis and fuzzy classification. *Catena*, **85**: 22–33.
- ZÁDOROVÁ, T., PENÍŽEK, V., ŠEFRNA, L., DRÁBEK, O., MIHALJEVIČ, M., VOLF, Š., CHUMAN, T. (2013): Identification of Neolithic to Modern erosion-sedimentation phases using geochemical approach in a loess covered sub-catchment of South Moravia, Czech Republic. *Geoderma*, **195–196**: 56–69.

Received for publication August 15, 2012

Accepted after corrections December 17, 2013

---

*Corresponding author:*

Mgr. TEREZA ZÁDOROVÁ, Česká zemědělská univerzita, Fakulta agrobiologie, potravinových a přírodních zdrojů, katedra pedologie a ochrany půd, Kamýcká 129, 165 21 Praha 6, Česká republika; e-mail: zadorova@af.czu.cz

---


## 5.6 Influence of former lynchets on soil cover structure and soil organic carbon storage in agricultural land, Central Czechia

---

- Zádorová, T., Penížek, V., **Žížala, D.**, Matějovský, J., Vaněk, A., 2018. Influence of former lynchets on soil cover structure and soil organic carbon storage in agricultural land, Central Czechia. *Soil Use and Management*. 34 (1). p. 60-71 [doi: 10.1111/sum.12406]



# Influence of former lynchets on soil cover structure and soil organic carbon storage in agricultural land, Central Czechia

T. ZÁDOROVÁ , V. PENÍZEK, D. ŽÍŽALA, J. MATĚJOVSKÝ & A. VANĚK

Department of Soil Science and Soil Protection, Czech University of Life Sciences, Kamýcká 129, 160 00 Praha 6-Suchbát, Prague, Czech Republic

## Abstract

Lynchets represent a traditional landscape element in agricultural landscapes having multiple functions in soil material redistribution, water retention, biodiversity and landscape character. They act as a barrier to translocated soil matter, and they can store a significant amount of soil material and soil organic carbon. Lynchets developed in many regions during formation of agriculture landscape as field boundaries or path networks. Further management led to unleveling of the fields and development of lynchets. During the 20th century, a large number of lynchets disappeared in Central and Western Europe due to land consolidation, intensification and industrialization of agriculture. This study was performed at a large agricultural study plot with dissected relief (Central Czechia) with the aim of assessing the influence of former but now completely levelled lynchets on actual soil stratigraphy, depth, soil organic carbon stocks and structure of soil units. The soil profiles in 20-m-long transects perpendicular to former lynchets were analysed, and statistical relationships between the positions above, in and below the former lynchets were assessed. The results showed high variability of studied soil characteristics in the areas of former lynchets. Statistically significant greater A horizon thickness (50–100 cm) and SOC stock (12.7 kg/m<sup>2</sup>) were observed in the location of a former lynchet, where colluvial soils were identified. Other areas of accumulation were identified below a lynchet, at the former break-in-slope. The strip above a lynchet was identified as a sediment delivery area, having a partly truncated soil profile. SOC concentration and SOC stock in A horizon did not differ significantly in the positions in, above or below a lynchet.

**Keywords:** Land use, land consolidation, soil redistribution, soil erosion, soil thickness

## Introduction

Structure of the soil cover, spatial arrangement of soil units and characteristics of a soil profile result from a long-term pedogenetic process mirroring a specific set of soil-forming factors and conditions (McBratney *et al.*, 2003). In an undulating relief, terrain morphology plays an important role in soil formation, mainly due to controlling the redistribution of water and soil matter (Wang *et al.*, 2010). Tillage and other agricultural practices historically changed the landscape morphology and soil cover due to enhanced soil erosion, landscape fragmentation and soil translocation by tillage. The soil redistribution within field limits led to the formation of anthropogenic landforms that relate to local

soil erosion and accumulation processes such as ridges and furrows, headlands and lynchets (Chartin *et al.*, 2011; Nyssen *et al.*, 2014). In this process, field borders act as barriers to tillage- and water erosion-induced soil matter fluxes, especially when they are covered in vegetation (Govers *et al.*, 1994; De Alba, 2003).

In Europe (most commonly in Central Europe and Western Europe), a mosaic of fields of a few hectares lined by a diverse mosaic of landscape elements was formed over centuries, due to fragmented ownership and diversity in crop cultivation. Lynchets (in some studies referred to as to cultivation or ploughed-on terraces) represent the most common landscape element, providing an example of an anthropogenic landform resulting from agricultural practices. An example of such a landscape with preserved agricultural landforms (SW Romania) is provided in Figure 1. A lynchet is a linear landform shaped by the progressive accumulation

Correspondence: T. Zádorová. E-mail: zadorova@af.czu.cz  
Received November 2016; accepted after revision January 2018



**Figure 1** Agricultural landscape with preserved landscape elements (lynchets, groves and solitaire trees) in SW Romania.

of soil material by water or tillage translocation upslope of a field border (Follain *et al.*, 2007; Chartin *et al.*, 2011). Bell (1992) refers to the term lynchets as the morphological response on a hillslope to the presence of field boundaries in cultivated landscapes. The prehistoric and historical lynchets have resulted from the soil redistribution due to repeated tillage, even with simple implements, and water erosion (Stolz, 2011; Nyssen *et al.*, 2014).

The lynchets are formed of two major parts: a gentle slope in the accumulation part of the lynchets, where a colluvium develops, and an associated break-in-slope of different height below the field border (Salvador-Blanes *et al.*, 2006; Chartin *et al.*, 2013). Nyssen *et al.* (2014) depict the development of a lynchets by a process where the topsoil is removed from the upper part of the interlynchets area, sometimes down to the parent material and then redeposited in the lynchets, where it forms a triangular wedge with the thickest deposit of colluvium at the position of the lynchets's shoulder. The lynchets increase gradually in depth and width. It develops from a few centimetres high terrain undulation to a distinct landform of height of tens of centimetres up to 1–2 m. Examples of initial and mature stages of a lynchets development are shown in Figure 2. Often, it is vegetated. The young lynchets are mostly grassed over; mature massive lynchets are covered with trees and shrubs.

Lynchets have multiple functions in the agricultural landscape. Primarily, they act as a barrier to translocated soil material and as such represent an effective anti-erosion element. They divide the slope and slow down the surface run-off (Vieira & Dabney, 2011). Each lynchets usually acts as a line of zero flux (Van Oost *et al.*, 2000). Despite their limited width, they can store a significant amount of material and soil organic carbon (Walter *et al.*, 2003; Follain *et al.*, 2007), depending on the thickness of the colluvium formed in the

accumulation part of the lynchets, and thus represent an important pool of sequestered SOC in the landscape. Apart from their functions in material redistribution, they provide important biological corridors and places of increased biodiversity in tilled land, and they retain the surplus run-off increasing the amount of water retained in the watershed and, last but not least, represent a key landscape component resulting from long-term agricultural management. A common occurrence of lynchets in the agricultural landscape, both historical and present, has been described worldwide: in France (Chartin *et al.*, 2011; Froehlicher *et al.*, 2016), Belgium (Nyssen *et al.*, 2014), Poland (Patro *et al.*, 2008), Germany (Moldenhauer *et al.*, 2010; Stolz, 2011; Larsen *et al.*, 2016), Spain (Poesen *et al.*, 1997), North America (Vieira & Dabney, 2011), South America (Dercon *et al.*, 2007) and Africa (Lewis, 1992; Nyssen *et al.*, 2000), most often in undulating dynamic landscapes with a prevalence of small farms. In Great Britain (Favis-Mortlock *et al.*, 1997) and Denmark (Nielsen & Dalsgaard, 2017), prehistoric lynchets have been studied related to Celtic settlements. In some studies, lynchets are referred to as field balks (Tesař *et al.*, 2008; Stolz, 2011) or ploughed-on terraces (Patro *et al.*, 2008).

During the 20th century, a large part of the area of lynchets disappeared from Europe. This was due to intensification and industrialization of agriculture, logically demanding larger agricultural fields. The land consolidation was initialized in the first decades of the 20th century (Dotterweich, 2013) and was intensified during its second half (Foucher *et al.*, 2014). The process was evident over the whole of Europe. Since the early 1950s, agriculture collectivization and land consolidation became a political instrument of newly established communist regimes in countries of Central and Eastern Europe (Jepsen *et al.*, 2015).

In Czechia, the forced collectivization of agricultural land resulted in spatial enlargement of fields to the extent of several hundreds of hectares and the destruction of thousands of hectares of vegetation in lynchets, groves and alleys (Beranová & Kubačák, 2010). The ploughing up of lynchets, which until then had been the most frequent anthropogenic landform feature in the agricultural landscape, was the most visible representative of the idea of a collective ownership. It was a practical, political and psychological action. Technically, the destruction of lynchets differed according to the technological equipment of each farming cooperative. Tractors with heavy ploughs and bulldozers were usually used. The ploughing up, as it was depicted in a number of photographs and political agitation movies and periodicals (Figure 3), was performed along the lynchets, starting at the upper part of the lynchets. The material was redistributed mostly downwards with the aim of levelling the terrain and filling up the area under the break-in-slope. During the following years, mostly all the terrain undulations – remnants of the former lynchets – were levelled by intensive tillage and cannot be recognized even



**Figure 2** Lynchets in initial (left) and mature (right) stage of development. Black lines represent cross sections of depicted lynchets.

from high-resolution DEMs (Zádorová *et al.*, 2015). The process of land consolidation and destruction of linear landscape elements with antierosional functions had, in the regions with dissected relief and vulnerable soil cover, a massive impact on the erosional stability of the landscape and led to severe erosion (Van Rompaey *et al.*, 2003). A parallel even from other Central European countries is difficult to find (Zádorová *et al.*, 2013).

Nowadays, we can see a slow and mainly local reformation of the lynchet system in Czechia, mainly owing to the return of nationalized land into private ownership or the division of large fields belonging to the modern agriculture cooperatives. Simultaneously, intentionally built lynchets are being reintroduced into the erosion-affected areas as an effective tool within the erosion control measures of a complex land consolidation programme (Figure 4). They are formed mainly on large, sloping agricultural blocks to slow down the surface run-off water and retain surplus water and material on the field. The antierosion lynchets are



**Figure 3** The destruction of lynchets as an act of a political propaganda in the 1950s (Šperk, 2013).

designed as contour-oriented landforms combining a low vegetated terrace and an adjacent shallow ditch (State Land Office, 2014).

The aim of this study was to identify the remnants of the former lynchets in this soil and assess their influence on the soil stratigraphy, depth, soil organic carbon stocks and structure of soil units.

#### Regional setting

The study plot is situated in Central Bohemia, in the vicinity of the town of Sedlčany (Vysoký Chlumeč municipality) in

the geomorphological region of Central Bohemian uplands (Figure 5). The area of the plot is 33 ha (49.616°N, 14.367°E), and altitude varies from 459 to 542 masl. The parent material is formed from Palaeozoic contact metamorphic greywacke and siltstone (Chlupáč *et al.*, 2002). The climate is cool (mean annual temperature of 7.1 °C), with mean annual precipitation of 660 mm. The study plot is represented by a slope system with two side valleys divided by an elevation (Figure 6). The plot has a marked



Figure 4 Newly built lynchets constructed within antierosion arrangements.

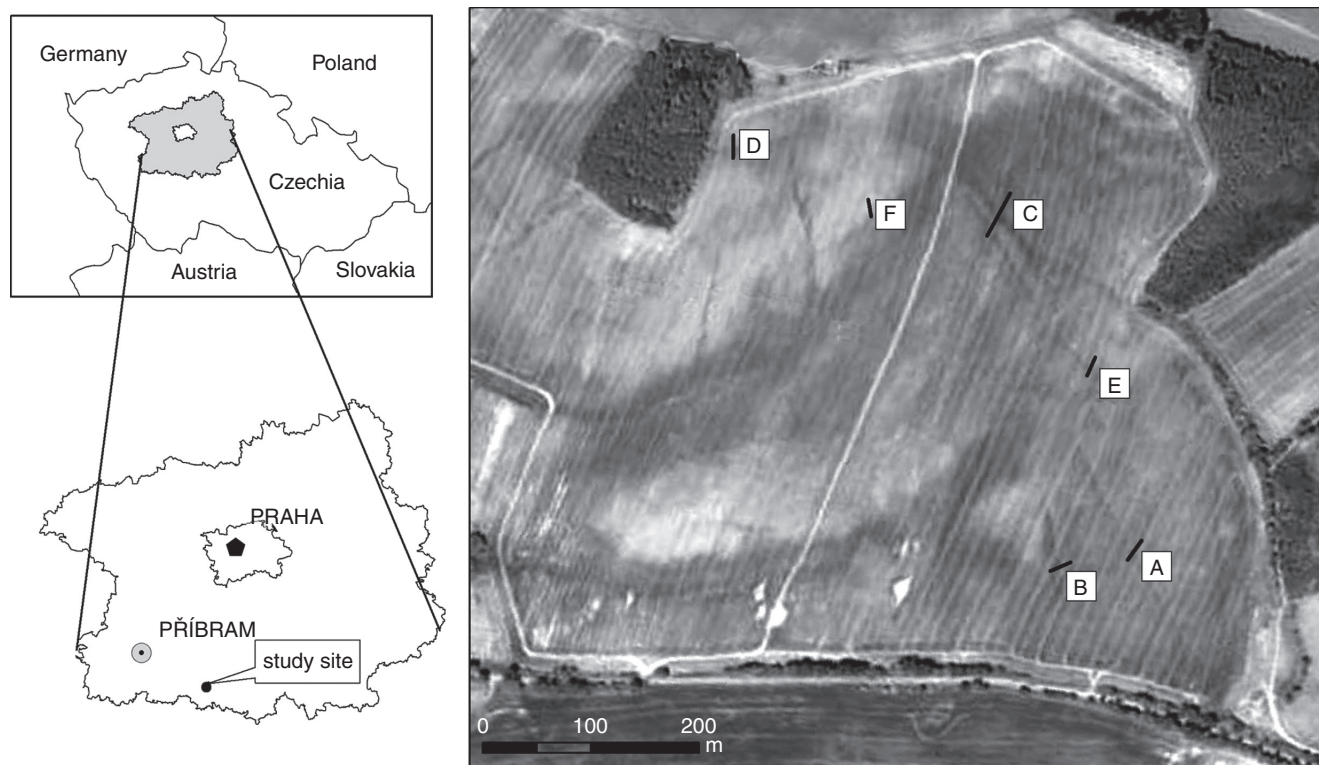


Figure 5 Location of the study plot with the study transects marked out.

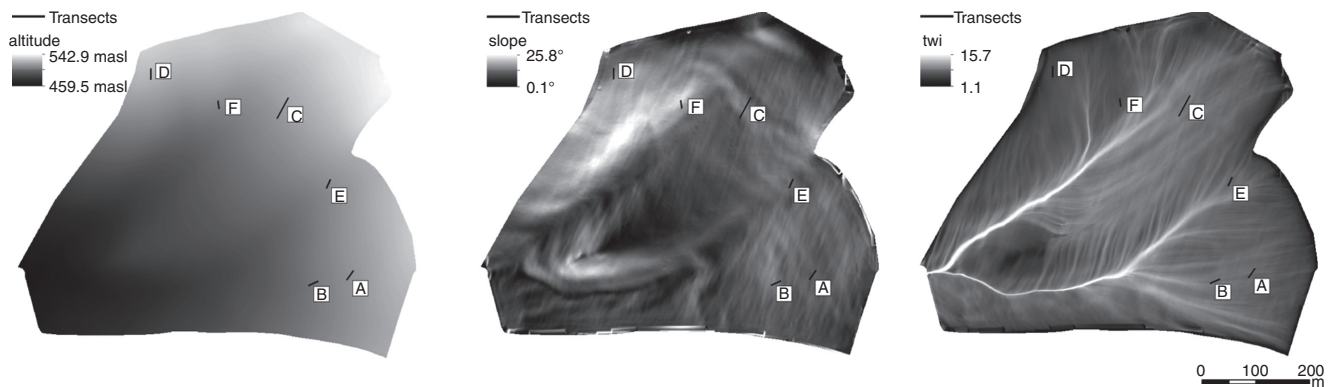


Figure 6 Selected terrain attributes at the study site (according to Zádorová *et al.*, 2015).

north–south slope, with a maximal gradient of 25°. The flat parts (0–2°) are situated in the south part of the plot adjacent to a road. The mean slope of the plot is 7°. Cambisols cover both the flat parts and the lower and middle slopes. Leptic Cambisols and Leptosols are found on the steepest slopes. Colluvial soils with maximum depths of 100 cm form at the base of the accumulation positions. Stagnic properties developed in the soils occurring at the confluence of the two side valleys (Zádorová *et al.*, 2015).

## Methods

### Identification of former lynchets

The localization of former lynchets was based on visual analysis of historical field boundary maps (stable municipality from 1842) and orthorectified aerial pictures. Figure 7 shows the field mosaic and the process of advancing elimination of lynchets in different years. The character of the ‘baroque’ landscape with a mosaic of small fields and numerous landscape elements is shown in the first map from 1842. The situation in 1949 depicts the land use before the collectivization and establishing of the Agricultural Cooperative. Slow enlargement of single fields and disappearance of lynchets is evident during the 1950s. Nevertheless, the landscape character was maintained including the presence of the main lynchets. The most intensive land consolidation took place in the late 1960s and 1970s. In 1976, the study locality was merged into one block and all the lynchets were eliminated. The last landscape element, a vegetated part of the side valley, disappeared in 1980s. The last aerial photograph shows the present situation; the former lynchets, though not detectable in the field, are still visible due to the identification of patterns from the air.

Six main lynchets selected for the study are shown in Figure 5. In field, the former lynchets were localized using a differential GPS device. The auger observations (soil profile stratigraphy, A horizon thickness) were realized every 2 m in

transects A–F perpendicular to the selected lynchets (Figure 5). Soil thickness, soil stratigraphy and soil type were recorded. Mixed samples for analysis of soil organic carbon were taken every 20 cm from the auger drillings to the depth of 1 m.

Soil organic carbon content was measured using the wet oxidation method (ISO, 14235:1998). Wet oxidation ( $K_2Cr_2O_7$ ) was followed by potentiometric titration with ferrous ammonium sulphate.

SOC stock was assessed using the widely applied equation (e.g. Wang *et al.*, 2010; Zádorová *et al.*, 2015):

$$SOC_{stock} = \sum(SOC \times \rho \times H/10) \quad 1$$

where  $SOC_{stock}$  is the SOC stock at the sampling point ( $kg/m^2$ ), SOC is the SOC concentration (%) in different soil layers,  $\rho$  is the bulk density in different soil layers ( $g/cm^3$ ), and  $H$  is the soil layer thickness (cm). SOC content was measured for each 20-cm-thick layer. Bulk density was assigned to each 20-cm-thick layer according to previous measurements already utilized in Zádorová *et al.* (2015).

For the statistical analysis, the set of points was divided into three parts: subset of points located in the area of the former lynchets (LYN), subset of points located above the lynchets (UP\_LYN) and subset of points located below the lynchets (DOWN\_LYN) (Figure 8).

Statistical analysis was used to find out whether the observed soil characteristics differed significantly in each of the subsets. Firstly, the Shapiro–Wilk test of normality and Levene’s test of equality of variances have been applied to select the appropriate analysis of variance. In the case of normal data distribution and equal variances, the parametrical one-way ANOVA was applied to assess the significance of differences among the subsets. In case of a significant difference, the post hoc Tukey’s test was applied to find out which of the subsets differed significantly. Analogically, nonparametrical ANOVA (Kruskal–Wallis analysis of variance) and post hoc Dunn’s test were used in case of non-normal data set distribution or nonequal variances.

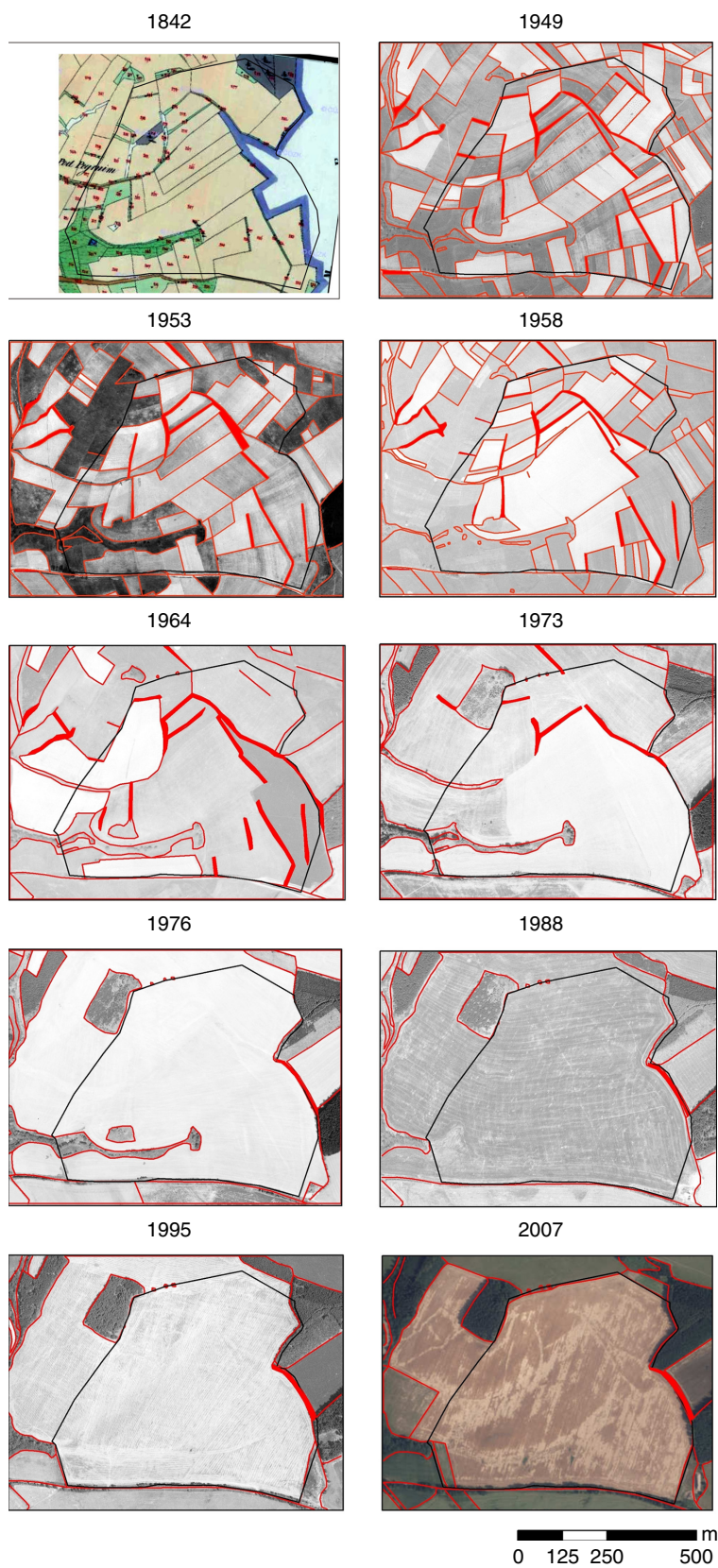


**Figure 7** Character of land use and localization of lynchets and field borders in different years according to aerial photographs and old maps.

Principal component analysis (PCA) was applied to display the structure of the data set. All statistical calculations were performed using the software R (R Core team, 2014).

**Results**

The soil profile stratigraphy in the studied transects is shown in Figure 9. The plots show the line of terrain, sequence of

soil horizons in each auger boring and the distribution of A horizon thickness. Localization of former lynchets is marked with arrows. Figure 10 shows summary statistics for the observed characteristics in the three positions.

The profile stratigraphy shows marked differences according to the position of profile within a transect. The majority of profiles have A-Bw-(B/C)-C stratigraphy with different thickness of each horizon and are classified as Cambisols. Some of the profiles, classified as Leptosols, are truncated with A-C stratigraphy. Some profiles are formed by a thick humus horizon with the thickness exceeding 50 cm and can be classified as colluvial soils. The thickness of the A horizon fluctuates between 25 cm (plough layer) and 100 cm. Table 1 gives the differences in A horizon thickness between three positions according to former lynchet. According to analysis of variance, the differences in the three positions are significant. Significantly greater values of A horizon thickness (range 40–100 cm, mean 71 cm) were observed in the area of the former lynchets, ranking the majority of observed profiles into colluvial soils. The values decrease in both directions away from the lynchets. The shallowest A horizons were observed in the upper parts of the transects, in the potential accumulation area of former

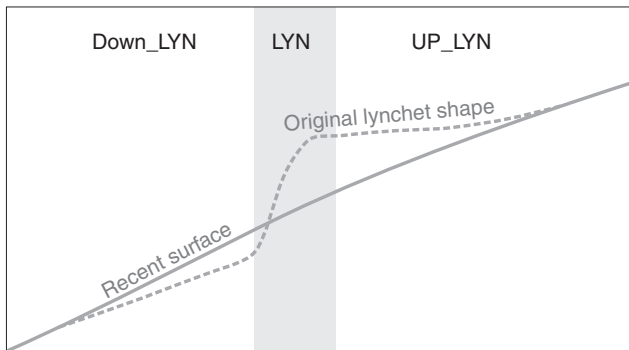


**Figure 8** Cross section of a lynchet with location of the three studied positions.

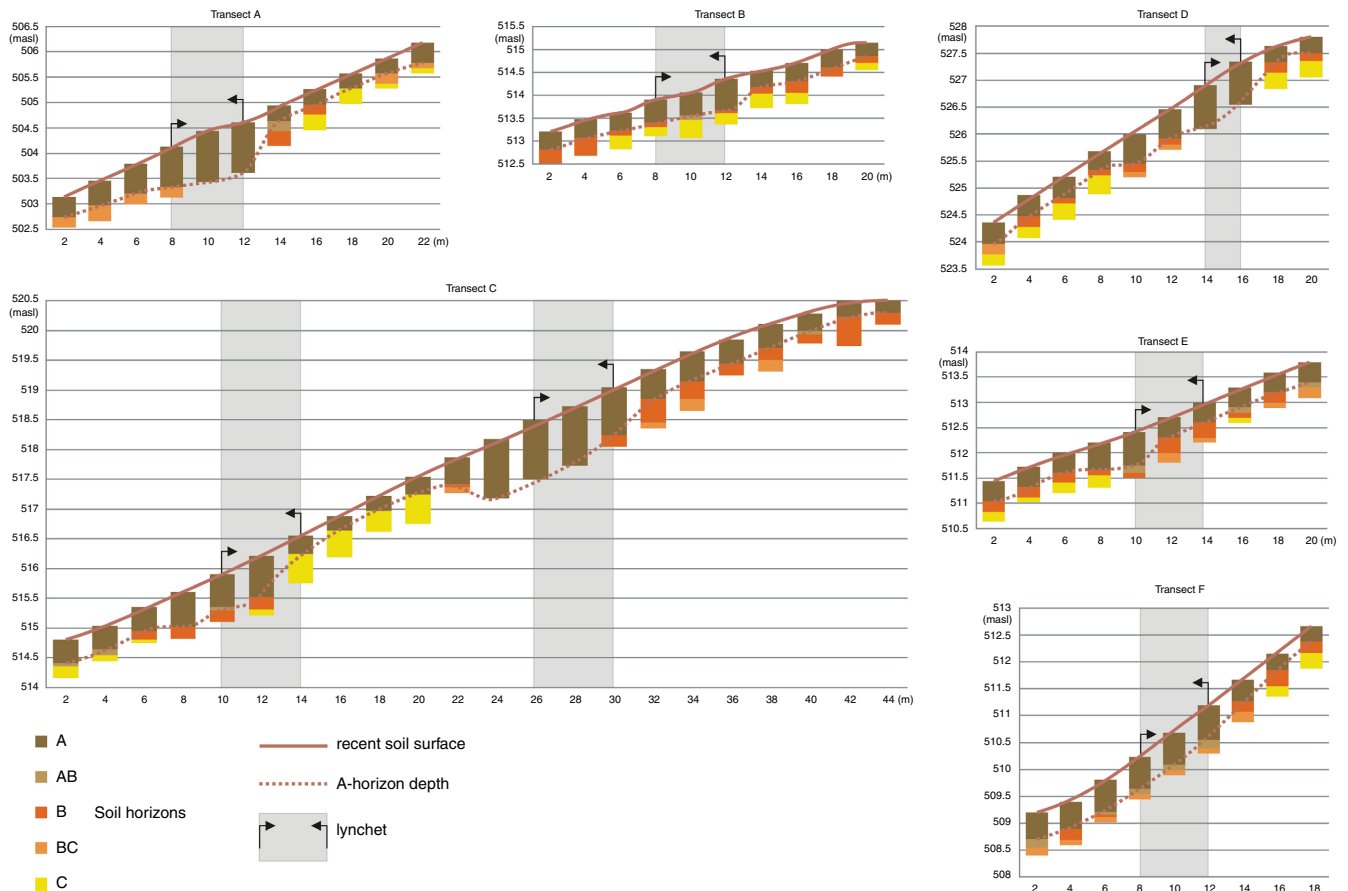


**Figure 9** Soil profile stratigraphy in the studied transects.

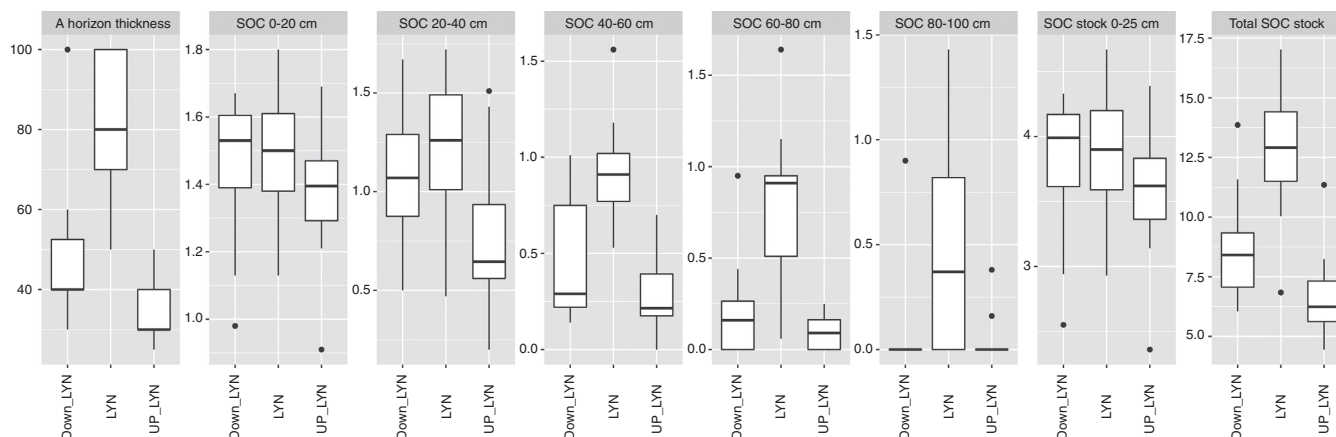


**Figure 10** Summary statistical indicators in the three studied positions (median, upper quartile, lower quartile, upper Whisker, lower Whisker and outliers).

lynchets. The values range from 25 to 50 cm (mean 35 cm), and some of the profiles are truncated with A-(B/C)-C stratigraphy. In contrast, the position below the former lynchets shows larger amounts of humus material with A horizons thickness from 30 to 100 cm (mean 47 cm). In transect E, we observed thicker A horizons below the former lynchets than in the lynchets itself.

Soil organic carbon concentration in the plough layer in the three positions shows similar trends as in the case of A horizon thickness, but the differences are not significant for any of the positions (Table 1). The values in LYN and DOWN\_LYN positions are very similar, and the UP\_LYN position shows smaller SOC concentrations. The situation is different in subsoil, where the difference between each position increases. The profiles situated in the lynchets area have significantly greater SOC concentration in the analysed depths between 40 and 100 cm. At 20–40 cm depth, a significantly smaller concentration was observed at the UP\_LYN position.

SOC stock was assessed for the topsoil and entire soil profile. In the topsoil, the SOC amount deposited in each position did not differ significantly; the largest mean stocks were observed in the lynchets ( $3.89 \text{ kg/m}^2$ ), whereas the smallest values were observed in the UP\_LYN position ( $3.60 \text{ kg/m}^2$ ). The SOC stock in the entire profile (0–100 cm) showed significantly greater values in LYN position (mean  $12.74 \text{ kg/m}^2$ ) and significantly smaller values in the UP\_LYN position ( $6.53 \text{ kg/m}^2$ ).

Results of PCA analysis are depicted in Figure 11. Component 1 and component 2 explain 80.1% of the data variability. The plot shows a significant influence of A horizon thickness, total SOC stock and SOC concentrations in deeper parts of the profile on the variability in the data set. In contrast, SOC concentration and stock in the topsoil had less significance in the data set distribution. The lynchets position is clearly distinguishable in the plot forming an

isolated cluster, while the positions out of the lynchets are partially overlapping.

## Discussion

The results showed high variability of studied soil characteristics in the areas of former lynchets. The deep humus horizons (50–100 cm) and occurrence of colluvial soils in the lynchets positions depict the amount of organic matter that has been accumulated behind and in the lynchets since the period of their formation. This is consistent with studies assessing the A horizon thickness distribution according to lynchets position. Chartin *et al.* (2011) described mean soil thickness 1.08 m in the lynchets areas with greater variability in soil thickness perpendicularly to lynchets than along their axes. These results indicate increases in soil thickness from the upslope to the downslope of a lynchets. Vieira & Dabney (2011) and Ghazavi *et al.* (2008) show similar soil accumulation in positions above and in the lynchets, but a significant decrease below the lynchets, where the soil removal processes prevail. This is in contradiction to our results, as we observed deeper soils with larger SOC concentrations in positions in and below the lynchets. The shift of the material from the area above to the area below the lynchets can be explained by two different events: the primary abrupt and short-term impulse and secondary long-term processes. The first distinct intervention in the material distribution was the destruction of the lynchets itself. One of the aims of ploughing up the lynchets was, apart from the primary consolidation of smaller fields into bigger plots, the decrease in relief roughness to be easily accessed by heavy machinery. This was only possible by the collapsing of the lynchets edge and movement of material downslope, into the former erosion position below the lynchets. Once the lynchets were destroyed and the slope was smoothed and elongated,



**Table 1** Position-specific differences in mean values of studied soil characteristics (A horizon thickness, SOC concentrations and SOC stock in different depths) in the three landscape positions. (a) Statistical analysis of variance. (b) Mean, standard deviation and position-specific differences in mean values of studied soil characteristics

Position	Analysis of variance			Post hoc test
(a)				
A horizon thickness (cm)	Kruskal–Wallis test chi-squared = 40.095, df = 2, P = 0.000			DOWN_LYN-LYN P = 0.001 DOWN_LYN – UP_LYN P = 0.001 LYN – UP_LYN P = 0.000
SOC (%) 0–20 cm	Kruskal–Wallis test chi-squared = 4.770, df = 2, P = 0.092			–
SOC (%) 20–40 cm	One-way ANOVA df = 2, F = 10.06 P = 0.000			DOWN_LYN-LYN P = 0.550 DOWN_LYN – UP_LYN P = 0.004 LYN – UP_LYN P = 0.000
SOC (%) 40–60 cm	Kruskal–Wallis test Chi-squared = 23.957, df = 2, P = 0.000			DOWN_LYN-LYN P = 0.002 DOWN_LYN – UP_LYN P = 0.070 LYN – UP_LYN P = 0.000
SOC (%) 60–80 cm	Kruskal–Wallis test chi-squared = 23.167, df = 2, P = 0.000			DOWN_LYN-LYN P = 0.001 DOWN_LYN – UP_LYN P = 0.168 LYN – UP_LYN P = 0.000
SOC (%) 80–100 cm	Kruskal–Wallis test chi-squared = 20.645, df = 2, P = 0.000			DOWN_LYN-LYN = 0.000 DOWN_LYN – UP_LYN = 0.813 LYN – UP_LYN = 0.000
SOC stock 0–25 cm (kg/m <sup>2</sup> )	Kruskal–Wallis test chi-squared = 4.7697 df = 2, P = 0.092			–
Total SOC stock (kg/m <sup>2</sup> )	Kruskal–Wallis test chi-squared = 28.138, df = 2, P = 0.000			DOWN_LYN-LYN = 0.007 DOWN_LYN – UP_LYN = 0.007 LYN – UP_LYN = 0.000
(b)				
Position	LYN Mean (SD)	DOWN_LYN Mean (SD)	UP_LYN Mean (SD)	Position-specific differences in mean values
A horizon thickness (cm)*	70.79 (19.28)	47.12 (13.31)	35.19 (6.72)	LYN>DOWN_LYN>UP_LYN
SOC (%) 0–20 cm	1.50 (0.16)	1.48 (0.18)	1.38 (0.17)	LYN=DOWN_LYN=UP_LYN
SOC (%) 20–40 cm*	1.22 (0.34)	1.09 (0.29)	0.74 (0.33)	LYN=DOWN_LYN>UP_LYN
SOC (%) 40–60 cm*	0.93 (0.25)	0.46 (0.30)	0.28 (0.17)	LYN>DOWN_LYN=UP_LYN
SOC (%) 60–80 cm*	0.78 (0.40)	0.20 (0.23)	0.09 (0.09)	LYN>DOWN_LYN=UP_LYN
SOC (%) 80–100 cm*	0.47 (0.51)	0.05 (0.20)	0.03 (0.09)	LYN>DOWN_LYN=UP_LYN
SOC stock 0–25 cm (kg/m <sup>2</sup> )	3.89 (0.42)	3.83 (0.46)	3.60 (0.45)	LYN=DOWN_LYN=UP_LYN
Total SOC stock (kg/m <sup>2</sup> )*	12.74 (2.55)	8.53 (8.53)	6.53 (1.51)	LYN>DOWN_LYN>UP_LYN

\*Significantly different mean values according to analysis of variance at  $P < 0.01$ . Position-specific differences in mean values according to post hoc tests, positions with symbols < and > are significantly different at  $P < 0.01$ .

the soil material redistribution significantly increased; partly due to enhanced run-off, partly due to intensive tillage. Chartin *et al.* (2013) simulated the erosion processes after land consolidation and lynchets destruction and indicated that the tillage erosion generated 95% of soil redistribution movements at the plot. They noted that land consolidation contributed to the acceleration of soil redistribution within the field through the conversion of depositional areas into sediment delivering areas. Similarly, Follain *et al.* (2006)

assessed the movement of soil particles over a long-term horizon (100–1200 yrs) with or without the presence of lynchets at the studied site. The results showed that the absence of former lynchets led to the removal of soil material from the formerly accumulation areas above the lynchet to the formerly eroded areas below the lynchet.

In contrast to soil and A horizon thickness, the concentration of SOC in the first 40 cm does not show significant differences in relation to the profile position,

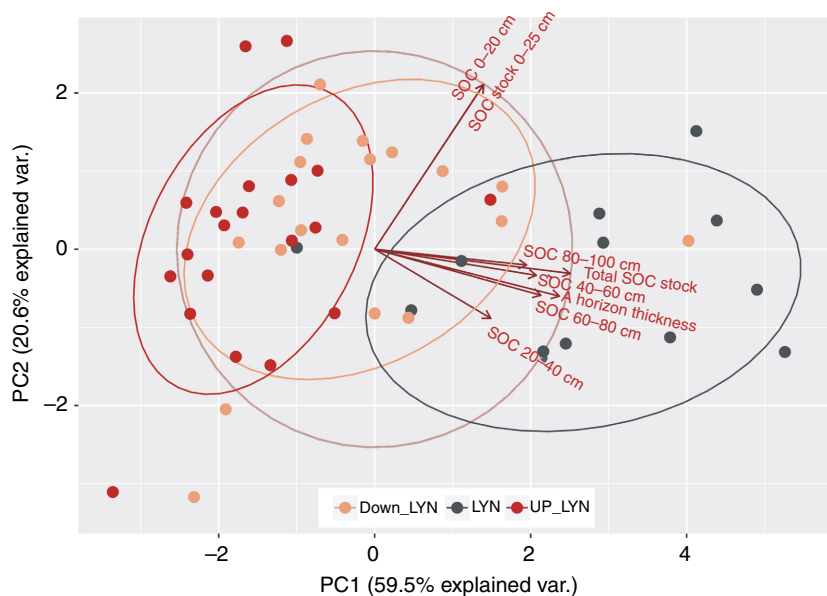


**Figure 11** Principal component analysis biplot.

although we observed larger values in and below the lynchet. The differences between LYN and both UP\_LYN and DOWN\_LYN positions become significant in the deeper part of the profiles, reflecting the different amount of accumulated material and correlating with A horizon thickness. In the 40–100 cm depth, the difference between the positions out of the lynchets (UP\_LYN and DOWN\_LYN) gradually decreases. Follain *et al.* (2007) correlated the SOC content at various depths with primary terrain parameters and geographical distance from the hedges (both present and past). The majority of the higher values were concentrated in the areas of present hedges and in a strip of 20 m along the hedges; the values decreased with increasing geographical distance to the hedge. The previous hedges did not have any significant influence on SOC concentration variability. The insignificant increase in SOC topsoil concentration in the lynchet areas can be attributed to long-term agricultural usage at the plot and rapid mineralization and homogenization in the topsoil due to tillage.

The study confirmed the large potential of lynchets in carbon sequestration as observed by Follain *et al.* (2006, 2007), Walter *et al.* (2003) and Chartin *et al.* (2013): the large SOC stocks in the areas in and below the lynchet significantly exceeded the adjacent values and demonstrate considerable SOC storage in these positions, even several decades after their destruction. The SOC stocks in the lynchets and along the lynchets are comparable with the SOC stocks in the two side valleys, forming the main accumulation area at the study plot, where the 80–100 cm deep colluvial soils prevail (Zádorová *et al.*, 2015).

Another issue connected with the redistribution of soil characteristics due to former anthropogenic structures (particularly lynchets and field borders) is that it can vastly influence the effectiveness of mathematical models simulating

the spatial variability of soil cover and properties (Follain *et al.*, 2007). In particular, it is the case of models that use terrain properties as explanatory variables in their predictions. Zádorová *et al.* (2015) simulated the distribution of SOC stock at the presented study plot, using DEM-based prediction methods (support vector machine). Based on the result of this study, in the areas of former lynchets, the SOC stock was significantly underestimated. The reason was a zero effect of former lynchets on recent relief resulting in omitting these areas from the model. The root mean square error (RSME) for the between predicted and recently observed SOC stocks was  $3.71 \text{ kg/m}^2$ , exceeding the RSME of the model itself ( $2.38 \text{ kg/m}^2$ ) given in Zádorová *et al.* (2015). Moreover, the RSME varied significantly according to the position: it was small in the UP\_LYN positions ( $1.83 \text{ kg/m}^2$ ), similar to model error in the DOWN\_LYN positions ( $2.80 \text{ kg/m}^2$ ), but very large in the LYN positions ( $6.17 \text{ kg/m}^2$ ). The DEM-based model performed well in the positions out of the lynchets, but was not satisfactory in the lynchet positions. The presented study proves that, in the areas where lynchets previously existed, the models predicting soil cover variability should assess the zones of former lynchets and field borders as areas of abrupt local change in soil properties.

## Conclusions

The results of the study showed that, tens of years after their destruction, the former lynchets still influence the spatial distribution of the depth of soil A horizon, stratigraphy and carbon storage in agricultural land.

The areas of former lynchets and strips along them represent localities with increased soil depth and A horizon thickness and spots of significant carbon storage. Compared

to the localities with existing lynchets or other linear landscape elements, the main storage of SOC is related to the positions in place of the former lynchets and below it, where the break-in-slope was filled during the destruction of the lynchets. The following period of intensive tillage leads to other redistribution of soil material, namely the removal of soil from the past accumulation positions above the lynchets, where we have not observed any significant increase in soil depth or SOC stock. The three positions (in, above and below the lynchets) showed significant differences in A horizon thickness, total SOC stock and SOC concentration in deeper parts of the soil profile. In contrast, SOC concentration and SOC stock in topsoil did not differ significantly. In each of the positions, specific soil units were classified, according to the soil profile stratigraphy.

The study demonstrated that the colluvia developed within the lynchets represent an important pool of organic carbon in an agricultural landscape with SOC stocks comparable to the natural accumulation areas (toe slopes, side valleys). We presume that their reformation, whether deliberate due to retransformation of agricultural blocks or purposeful within an antierosion arrangement, can prevent an enhanced loss of organic matter from the agricultural fields and establish a new important pool of organic carbon in the farmland.

The comparison with the previous research predicting the SOC stock at the study plot found that the models predicting soil cover variability should assess the zones of former lynchets and field borders as areas of abrupt local change in soil properties.

### Acknowledgements

The study was supported by grants nr. 13-07516P and nr. 17-27726S of the Czech Science Foundation.

### References

- Bell, M. & Boardman, J. 1992. *Past and present soil erosion: Archaeological and Geographical Perspectives*. Oxbow Books, Oxford.
- Beranová, M. & Kubačák, A. 2010. *Dějiny zemědělství v Čechách a na Moravě*. Libri, Praha (in Czech).
- Chartin, C., Bourennane, H., Salvador-Blanes, S., Hirschberger, F. & Macaire, J.-J. 2011. Classification and mapping of anthropogenic landforms on cultivated hillslopes using DEMs and soil thickness data – Example from the SW Parisian Basin, France. *Geomorphology*, **135**, 8–20.
- Chartin, C., Evrard, O., Salvador-Blanes, S., Hirschberger, F., Van Oost, K., Lefèvre, I., Daroussin, J. & Macaire, J. 2013. Quantifying and modelling the impact of land consolidation and field borders on soil redistribution in agricultural landscapes (1954–2009). *Catena*, **110**, 184–195.
- Chlupáč, I., Brzobohatý, R., Kovanda, J. & Straník, Z. 2002. *Geologická minulost České republiky*. Academia, Praha (in Czech).
- De Alba, S. 2003. Simulating long-term soil redistribution generated by different patterns of mouldboard ploughing in landscapes of complex topography. *Soil and Tillage Research*, **71**, 71–86.
- Dercon, G., Govers, G., Poesen, J., Sanchez, H., Rombaut, K., Vandenbroeck, E., Loaiza, G. & Deckers, J. 2007. Animal-powered tillage erosion assessment in the southern Andes region of Ecuador. *Geomorphology*, **87**, 4–15.
- Dotterweich, M. 2013. The history of human-induced soil erosion: geomorphic legacies, early descriptions and research, and the development of soil conservation—A global synopsis. *Geomorphology*, **201**, 1–34.
- Favis-Mortlock, D., Boardman, J. & Bell, M. 1997. Modelling long-term anthropogenic erosion of a loess cover: South Downs, UK. *Holocene*, **7**, 79–89.
- Follain, S., Minasny, B., McBratney, A.B. & Walter, C. 2006. Simulation of soil thickness evolution in complex agricultural landscape at fine spatial and temporal scales. *Geoderma*, **133**, 71–86.
- Follain, S., Walter, C., Legout, A., Lemerrier, B. & Dutin, G. 2007. Induced effect of hedgerow networks on soil organic carbon storage within an agricultural landscape. *Geoderma*, **142**, 80–95.
- Foucher, A., Salvador-Blanes, S., Evrard, O., Simonneau, A., Chapron, E., Courp, T., Cerdan, I., Adriaensens, H., Lecompte, F. & Desmet, M. 2014. Increase in soil erosion after agricultural intensification: evidence from a lowland basin in France. *Anthropocene*, **7**, 30–41.
- Froehlicher, L., Schwartz, D., Ertlen, D. & Trautmann, M. 2016. Hedges, colluvium and Lynchets along a reference toposequence (Habsheim, Alsace, France): history of erosion in a loess area. *Quaternaire*, **27**, 173–185.
- Ghazavi, G., Thomas, Z., Hamon, Y., Marie, J.C., Corson, M. & Merot, P. 2008. Hedgerow impacts on soil-water transfer due to rainfall interception and root-water uptake. *Hydrological Processes*, **22**, 4723–4735.
- Govers, G., Vandaele, K., Desmet, P., Poesen, J. & Bunte, K. 1994. The role of tillage in soil redistribution on hillslopes. *European Journal of Soil Science*, **45**, 469–478.
- ISO 14235. 1998. Soil quality – determination of organic carbon by sulfochromic oxidation. Technical Committee ISO/TC 190.
- Jepsen, M.R., Kuemmerle, T., Muller, D., Erb, K., Verburg, P.H., Haberl, H., Vesterager, J.P., Andrić, M., Antrop, M., Austrheim, G. & Björn, I. 2015. Transition in European land-management regimes between 1800 and 2010. *Land Use Policy*, **49**, 53–64.
- Larsen, A., Robin, V., Heckmann, T., Fülling, A., Larsen, J.R. & Bork, H.-R. 2016. The influence of historic land-use changes on hillslope erosion and sediment redistribution. *Holocene*, **26**, 1248–1261.
- Lewis, L.A. 1992. Terracing and accelerated soil loss on Rwandan steepplands: a preliminary investigation of the implications of human activities affecting soil movement. *Land Degradation and Rehabilitation*, **3**, 241–246.
- McBratney, A.B., Santos, M.L.M. & Minasny, B. 2003. On digital soil mapping. *Geoderma*, **117**, 3–52.
- Moldenhauer, K.-M., Heinrich, J. & Vater, A. 2010. Causes and history of multiple soil erosion processes in the northern Odenwald uplands. *Erde*, **14**, 171–186.
- Nielsen, N.H. & Dalsgaard, K. 2017. Dynamics of Celtic fields—A geoarchaeological investigation of Øster Lem Hede, Western Jutland, Denmark. *Geoarchaeology*, **32**, 414–434.

- Nyssen, J., Poesen, J., Haile, M., Moeyersons, J. & Deckers, J. 2000. Tillage erosion on slopes with soil conservation structures in the Ethiopian highlands. *Soil and Tillage Research*, **57**, 115–127.
- Nyssen, J., Debever, M., Poesen, J. & Deckers, J. 2014. Lynchets in eastern Belgium – a geomorphic feature resulting from non-mechanised crop farming. *Catena*, **121**, 164–175.
- Patro, M., Węgorzek, T. & Zubala, T. 2008. Ploughed-on terraces in loess landscape of strongly developed high plains. *Annals of Warsaw University of Life Sciences – SGGW. Land Reclamation*, **39**, 95–101.
- Poesen, J., Van Wesemael, B., Govers, G., Martinez-Fernandez, J., Desmet, P., Vandaele, K., Quine, T. & Degraer, G. 1997. Patterns of rock fragment cover generated by tillage erosion. *Geomorphology*, **18**, 183–197.
- R Core Team 2014. *R: A language and environment for statistical computing*. R Foundation for Statistical Computing, Vienna, Austria.
- Salvador-Blanes, S., Cornu, S., Couturier, A., King, D. & Macaire, J.-J. 2006. Morphological and geochemical properties of soil accumulated in hedge-induced terraces in the Massif Central, France. *Soil and Tillage Research*, **85**, 62–77.
- Šperk, J. (2013). *Kolektivizace v ČSR*. <http://www.moderni-dejiny.cz/clanek/kolektivizace-v-csr/>; accessed 1/11/2016.
- State Land Office 2014. *Land Consolidation*. [http://www.spucr.cz/frontend/webroot/uploads/files/2015/06/pozemkove\\_upravy\\_2014782.pdf](http://www.spucr.cz/frontend/webroot/uploads/files/2015/06/pozemkove_upravy_2014782.pdf); accessed 11/6/2017.
- Stolz, C. 2011. Spatiotemporal budgeting of soil erosion in the abandoned fields area of the “Rahnstätter Hof” near Michelbach (Taunus Mts., Western Germany). *Erdkunde*, **65**, 355–370.
- Tesař, M., Syrovátka, O., Šír, M., Lichner, L., Váchal, J. & Krejča, M. 2008. Storm runoff in the foothill headwater area Senotín. *Soil and Water Research*, **3**, 168–174.
- Van Oost, K., Govers, G. & Desmet, P. 2000. Evaluating the effects of changes in landscape structure on soil erosion by water and tillage. *Landscape Ecology*, **15**, 577–589.
- Van Rompaey, A., Krasa, J., Dostal, T. & Govers, G. 2003. Modelling sediment supply to rivers and reservoirs in Eastern Europe during and after the collectivisation period. *Hydrobiologia*, **494**, 169–176.
- Vieira, D.A.N. & Dabney, S.M. 2011. Modeling edge effect of tillage erosion. *Soil and Tillage Research*, **111**, 197–207.
- Walter, C., Mérot, P., Layer, B. & Dutin, G. 2003. The effect of hedgerows on soil organic carbon storage in hillslopes. *Soil Use and Management*, **19**, 201–207.
- Wang, Z., Govers, G., Steegen, A., Clymans, W., Van den Putte, A., Langhans, C., Merckx, R. & Van Oost, K. 2010. Catchment-scale carbon redistribution and delivery by water erosion in an intensively cultivated area. *Geomorphology*, **124**, 65–74.
- Zádorová, T., Penížek, V., Vašát, R., Žížala, D., Chuman, T. & Vaněk, A. 2015. Colluvial soils as a soil organic carbon pool in different soil regions. *Geoderma*, **253**, 122–134.
- Zádorová, T., Penížek, V., Šefrna, L., Drábek, O., Mihaljevič, M. & Volf, Š., & Chuman, T. 2013. Identification of Neolithic to Modern erosion-sedimentation phases using geochemical approach in a loess covered sub-catchment of South Moravia, Czech Republic. *Geoderma*, **195–196**, 56–69.

## 6 Sumární diskuze

---

Ve výzkumu ovlivnění dynamiky SOC erozními procesy je stále řada nedostatečně dořešených vědeckých otázek. Nejistoty panují zejména v ovlivnění SOC v různých fázích erozního procesu a sedimentace a nedostatečném poznání některých biochemických procesů v rámci rozkladu, stabilizace a nahrazování organické hmoty v erozně-akumulačních podmínkách (Kuhn et al., 2012; Kirkels et al., 2014; Doetterl et al., 2015a). Pro celkové porozumění v této oblasti a odstranění nejistot ve vědeckých závěrech mohou přispět nejen výzkumy popisu procesů tvorby a mineralizace SOC, či popisu osudu erozí transportované případně akumulované organické hmoty na bázi biochemického výzkumu, ale také vhodné způsoby podrobného plošného mapování redistribuce SOC. K tomuto účelu mohou sloužit metody digitálního mapování půd s využitím dat dálkového průzkumu Země. Mapování SOC pomocí progresivních pedometrických a spektroskopických metod je však obecně problematické v oblastech s vysokou variabilitou půdních vlastností, která se často vyskytuje právě v erozně ovlivněných oblastech. Předmětem této práce bylo tedy nalézt způsoby podrobného mapování redistribuce SOC, koncentrace a zásob SOC jak v erodovaných, tak v akumulačních částech terénu v podmínkách České republiky a popsat a zhodnotit možnosti a přesnosti jejich využití. Předložené výsledky prezentované souborem publikovaných recenzovaných článků ukazují, že zmíněné metody pro mapování variability a redistribuce SOC lze v podmínkách zemědělských půd ČR vhodně uplatnit. Využití a nasazení těchto metod však obecně není triviální, vyžaduje široké znalosti řešené problematiky, nejen v oblasti věd o půdě, ale i technické dovednosti pro zpracování dat (GIS, statistika, programování v R) a znalosti o možnostech, výhodách a nedostacích použití metod pro konkrétní účely (Minasny, 2018; Minasny a Ma, 2018). Poznatky plynoucí z představených výsledků v tomto ohledu přispívají k rozšíření vědomostí potřebných k jejich uplatnění a jako takové budou v následující pasáži diskutovány s cílem kriticky zhodnotit a posoudit jejich relevanci pro budoucí nasazení na různých úrovních mapování SOC.

Úroveň variability SOC na lokální úrovni může dosahovat v závislosti na příčinných faktorech značných hodnot odpovídajících míře variability na regionální úrovni (Goidts

et al., 2009; Stevens et al., 2015). Ve všech zájmových lokalitách vybraných na základě potenciální erozní ohroženosti byla v rámci detailního terénního průzkumu sledána rozmanitá mozaika půdních jednotek a velká vnitropolní heterogenita jako pravděpodobný důsledek intenzivního působení redistribuce materiálu erozně-akumulačními pochody. Výsledná erozní katéna zahrnovala relativně neovlivněné autochtonní půdy (černozemě, hnědozemě, kambizemě), erodované půdy na sklonitých částech (regozemě, rankery) a koluviální půdy v nižších a plochých částech svahů charakteristické akumulovaným erozním materiálem a všechny přechodné typy. Současně koncentrace SOC v orničním horizontu dosahovala značné variability, variační rozpětí dosahovalo na jednotlivých lokalitách velkých hodnot od 0,71 do 1,78 % SOC (černozem - 0,50-1,75 - Brumovice; 0,84-2,62 - Šardice, hnědozem - 0,7-1,41 - Jičín, luvizemě - 0,70-1,40 - Vidim, kambizem - 0,44-2,22 - Chlumec; 0,61-1,88 - Přestavlký; 0,56-1,44 - Nová Ves). Vertikální rozložení uhlíku v profilu se ale může velice dynamicky měnit i v závislosti na změně stratigrafie profilu, přičemž v akumulovaných půdách je profil zásob uhlíku značně heterogenní, závislý na místních podmínkách (Zádorová et al., 2013). Přesné prostorové a 3D mapování je tedy zapotřebí s ohledem na určení přesných zásob uhlíku v půdách. Jak ukázaly předkládané výsledky, prostorová či hloubková generalizace může vést k značným chybám v odhadech celkového množství zásob uhlíku. Většina studií zásob uhlíku byla nicméně směřována pouze na orniční horizont, případně svrchních 50 cm (López-Fando a Pardo, 2011; Schwanghart a Jarmer, 2011; Cambule et al., 2014) až 100 cm (Don et al., 2007; De Gryze et al., 2008; Fang et al., 2012; Khalil et al., 2013). I v hlubších koluviálních půdách může být koncentrována značná zásoba uhlíku (Zádorová a Penížek, 2018), čemuž věnovala pozornost dosud jen omezená část studií (Tang et al., 2010; Meersmans a Quine, 2013; Chaopricha a Marín-Spiotta, 2014; Wang et al., 2014b).

Vzhledem k velké heterogenitě jednotlivých zmapovaných ploch byly v rámci studia možností mapování obsahu SOC v půdách České republiky testovány pedometrické přístupy s využitím různých druhů podpůrných dat v závislosti na zdrojích variability SOC v půdách. Nicméně i při využití stejných vstupních dat (vysvětlujících proměnných) je v rámci různých půdních podmínek efektivita a přesnost metod digitálního mapování půd různá právě v závislosti na zdroji variability SOC v půdách. Pokud jejím zdrojem jsou hlavně vlastnosti, které lze dobře a přesně popsat vstupními daty (deterministická proměnlivost), např. terénními vlastnostmi, tak lze redistribuci organického uhlíku

predikovat poměrně přesně. Jestliže je variabilita ovlivněna zvýšenou heterogenitou špatně prostorově mapovaných faktorů, např. půdních substrátů, je predikce zatížena větší chybovostí. Zdrojem variability mohou být také jiné příčiny, které je nemožné podrobně mapovat (např. vlivy větrné eroze – Šardice, eroze orbou – různé směry pojezdů, či ostatní vlivy činnosti člověka – různé způsoby obhospodařování pozemků, vliv historického využití území apod.). S větším vlivem této, z pohledu modelu stochastické proměnlivosti, je predikce dále obtížnější a méně přesná a zvyšuje se podíl modelem nepopsané variability. Jak např. ukázaly výsledky předkládané studie Zádorová et al. (2018) - článek 5.6, staré krajinné prvky, které již desítky let nejsou součástí krajiny, stále ovlivňují distribuci zásob uhlíku v zemědělských půdách. Studie ukázala, že v rámci modelování je nutno tyto struktury zahrnout do návrhu modelu a vzorkovací sítě, jinak mohou modely značně reálně podhodnotit zásoby uhlíku a to i bez toho, aby se to projevilo ve statistikách prokazující efektivitu predikčního modelu. Obdobné závěry předkládají i Follain et al., (2007). V případě, že vzorkovací síť tyto struktury náhodně postihne a nejsou zohledněny v modelu, může naopak dojít k nadhodnocení zásob a nižší predikční schopnosti modelu. Proto je zapotřebí zohlednit případné vlivy již v rámci návrhu vzorkovací sítě a přípravy podpůrných dat. Při větším plošném záběru mapování na regionální úrovni je již nutné brát v úvahu i variabilitu způsobenou různou historií hospodaření na pozemcích, která se projevuje ve zvýšené variabilitě SOC na úrovni krajiny (Stevens et al., 2015).

Specifikem erozně ovlivněných oblastí je zvýšená variabilita koncentrace a zásob SOC způsobená různorodým působením erozně-akumulačních procesů a vlivem různých lokálních podmínek pro transport, sedimentaci a mineralizaci SOC. Různá kombinace preferenčního (plošná a mezirýhová eroze) a nepreferenčního (rýhová eroze, eroze zpracováním půdy) odnosu organické hmoty v závislosti na podmínkách stanoviště ovlivňuje různé obohacení sedimentu o SOC (Hu et al., 2013; Chaplot et al., 2015; Müller-Nedebock a Chaplot, 2015). Výsledkem jsou značné rozdíly v redistribuci SOC ve svrchní vrstvě půdy. V oblastech s intenzivním erozním poškozením může navíc docházet k odnosu již podorničních horizontů s menším obsahem organické hmoty a při akumulaci tohoto materiálu k retrográdnímu vývoji koluviálních půd. Tento efekt byl popsán na úrovni terénního průzkumu zejména ve studovaných černozemních oblastech, ale taktéž v kambizemních. Na rozdíl od zjištění Schmid et al. (2016) a Hill a Schütt (2000) tak akumulované půdy mohou mít následně snížený obsah organického uhlíku v povrchové vrstvě oproti původním autochtonním půdám. V rámci prezentované studie

(Žižala et al., 2018 - článek 5.3) se tento popsany efekt projevil při využití dat DPZ ve velmi slabé spektrální separabilitě erozních a akumulacních forem půd identifikovaných při terénním průzkumu. Při predikčním mapování se zmíněné efekty projeví ve vyšším podílu nevysvětlené variability popsané modely a tedy sníženou predikční schopností modelů v závislosti na vertikálním rozlišení mapování (Zádorová et al., 2015 - článek 5.4). Zatímco vliv terénních vlastností na redistribuci lze modely popsat, stochastická proměnlivost spojená zejména se způsobem hospodaření a charakterem srážkových událostí, ovlivňujících intenzitu a opakovanost erozně-akumulacních událostí, může způsobovat sníženou efektivitu modelů, obzvláště v predikcích zásob a koncentrací ve svrchní vrstvě půdy. V rámci intenzivního působení procesů větrné eroze může docházet k další výrazné redistribuci půdního materiálu a organického uhlíku, která vede k dalšímu zvýšení komplexity výsledné redistribuce znesnadňující prostorové predikce.

Z výsledků prezentovaných studií vyplývá, že obecně největší zásoby SOC se koncentrují v pozicích neovlivněných erozními pochody, tedy na plošinách s neerodovanými organominerálními horizonty a nevýrazným pohybem materiálu a zejména v akumulacních polohách na patách svahů a dnech úpadů a bočních údolí. Z hlediska terénních parametrů jsou tyto polohy definované nízkým sklonem, konkávním zakřivením, vysokými hodnotami hydrologických indexů indikujícími vyšší půdní vlhkost, a nízkými hodnotami topografických indexů indikujícími silnou geomorfologickou závislost zásob SOC. Tyto výsledky korespondují s výsledky dalších výzkumů (Ritchie et al., 2007; Schwanghart a Jarmer, 2011; Doetterl et al., 2013; Wiesmeier et al., 2014), kdy autoři uvádějí závislost zásob SOC na pozici v reliéfu, zakřivení a vlhkostním indexu. Na základě výsledků bylo nicméně zjištěno, že hodnocení zásob a koncentrace SOC v erozně ovlivněných půdách v různých půdních regionech nelze provádět na základě modelů využívající konkrétní terénní vlastnosti, kterými by bylo primárně možno popsat redistribuci SOC v ploše, respektive výsledné rozložení zásob SOC. Redistribuce, jak vyplývá z výše uvedeného, je velice místně specifická (*site-specific*). Použití obecných modelů je tak nesnadné a pro přesnou prostorovou predikci je potřeba velké množství vstupních vzorků. Predikční schopnost modelů založených pouze na terénních vlastnostech se významně liší v závislosti na lokalitě a hloubkovém intervalu řešené zásoby SOC. V černozemních a luvizemních lokalitách modely popisují variabilitu z více jak 80 % (kdy nejlépe popisujícími proměnnými je příspěvková plocha



a topografický vlhkostní index), zatímco u kambizemních oblastí jen 63 % u celkové zásoby a pouhých 23 % u zásoby ve svrchní 25cm vrstvě.

Faktor reliéfu je společně s dalšími funkčními faktory z koncepčního hlediska chápán jako jeden z půdotvorných faktorů, který má značný vliv na redistribuci SOC v krajině. Jak již bylo dříve uvedeno, redistribuci SOC však nelze plně mapovat pouze pomocí těchto faktorů vzhledem k problematice jejich přesného prostorového zmapování a dostupnosti těchto dat. Výsledky (Žížala et al., 2017 - článek 5.1; Gholizadeh et al., 2018 - článek 5.2) stejně tak jako řada recentních studií (Franceschini et al., 2015; Stevens et al., 2015; Steinberg et al., 2016; Castaldi et al., 2018) prokázaly, že vhodnými podpůrnými daty pro predikční modelování tak mohou být spektrální data, nejlépe obrazová spektrální data, tedy materiály dálkového průzkumu Země. Tato data nepopisují faktory ovlivňující redistribuci, ale zprostředkovávají informaci, která je již důsledkem redistribuce, tzn. změněnou spektrální informaci. Data DPZ tak popisují současný stav půdního pokryvu a mohou popsat složku variability, kterou není možné popsat jiným dostupným způsobem. Využívaná optická data DPZ ze své podstaty řeší pouze svrchní část půdního pokryvu, a je tedy možné je využít jen pro mapování obsahu SOC ve svrchní vrstvě půdy, případně v orničním horizontu, pokud uvažujeme homogenizaci vrstvy vlivem orby, či jako podpůrnou informaci při mapování zásob SOC.

Pro účely ověření možností mapování redistribuce organického uhlíku byla využita zejména letecká hyperspektrální data, která splňují požadavky na vysoké prostorové i spektrální rozlišení. Výsledky (Žížala et al., 2017 - článek 5.1; Gholizadeh et al., 2018 - článek 5.2) ukázaly, že využití těchto spektrálních dat pro mapování koncentrací SOC ve svrchní vrstvě může být velice vhodné. Modely koncentrace SOC popisovaly 80 – 91 % ( $R^2 = 0,80 - 0,91$ ) variability v závislosti na půdních podmínkách, přičemž střední chyba predikce se pohybovala mezi 0,07 a 0,12 % SOC. Tyto výsledky jsou srovnatelné s výsledky dosaženými v obdobných studiích (Uno et al., 2005; Selige et al., 2006; Hively et al., 2011; Hbirkou et al., 2012; Stevens et al., 2012; Denis et al., 2014). SOC je obecně nejčastěji a nejúspěšněji predikovaná půdní komponenta ( $R^2$  mezi 0,65 a 0,96) s využitím hyperspektrálních dat (viz Tabulka 3 v příloze). Uváděné hodnoty přesnosti predikce SOC ( $R^2$  a RMSE) z předchozích studií jsou nicméně velice variabilní a nelze je plně srovnat s výsledky ze studií v ČR s ohledem na velkou heterogenitu lokálních podmínek (charakteristiky povrchu půdy – vlhkost, drsnost povrchu, vegetační zbytky), počtu

využitých vzorků pro kalibraci, velikosti sledované plochy, charakteristik použitých senzorů a geometrie snímání či použitých technik predikce. Zatím malý počet studií v této problematice tak neumožňuje provádět zobecňující závěry o příčinách kolísání přesnosti predikce. Doporučení tak mohou být stanovena pouze na bázi expertních odhadů a hypotéz a nikoli z výsledků statisticky ověřených porovnání. Z předkládaných výsledků nicméně vyplývá, že predikční schopnost modelů koncentrace SOC je ovlivněna nejen vnějšími parametry spojenými s pořízením dat, ale i lokálními podmínkami. Provedené experimenty ukázaly, že v substrátově homogenních oblastech, kterými je např. sprašová oblast jižní Moravy, se využití dat DPZ v digitálním mapování půd ukázalo jako velice přesné. Nicméně i při nízkých obsazích a v substrátově heterogennějších oblastech je stále predikční schopnost modelů vysoká, vyšší než u jiných půdních komponent a s menší variabilitou. Obecně lze tedy určit hypotézu, že lepší predikční schopnosti je dosahováno tam, kde je obsah SOC vysoký a má ve spektru značný vliv a půdní vlastnosti (např. v závislosti na substrátu) jsou více homogenní. Obdobné závěry jsou prezentovány i v dalších studiích (Gomez et al., 2012; Vaudour et al., 2016a; Castaldi et al., 2018).

Byť hyperspektrální data prokázala své výhody při mapování SOC, je jejich pořízení pro praktické využití poměrně finančně náročné a vyžaduje náročné zpracování. Jak však ukázala analýza využití volně dostupných dat z družic Sentinel 2 (Gholizadeh et al., 2018 - článek 5.2), tak i tato data jsou vhodná pro mapování SOC. Predikce pomocí těchto dat dosahovala obecně nižší přesnosti (RMSE 0,08 – 0,24 % SOC a  $R^2 = 0,57 - 0,89$ ), nicméně výsledky jsou stále vyhovující, obzvláště v kontextu analýzy prostorové distribuce, kdy se prokázalo, že lze mapovat stejné prostorové trendy jako s výrazně přesnějšími hyperspektrálními leteckými daty. Výsledky jsou opět srovnatelné s výzkumy v jiných částech světa využívajícími satelitní data (Ray et al., 2004; Ballabio et al., 2014; Castaldi et al., 2016).

Využití spektrálních obrazových dat na různé úrovni má ale řadu omezení. Pro mapování půdních vlastností je lze využít pouze na holé půdě. Přímé pozorování půdy je tak v podmínkách mírného klimatu omezeno na období s minimem vegetace (jaro, podzim). V souvislosti s mozaikou pěstovaných plodin a střídání ozimých a jarních plodin v osevních postupech a honech a s výskytem oblačnosti je možné na jednom snímku zachytit holé půdy jen na několika půdních blocích. Pro hodnocení ve větším plošném rozsahu je tak zapotřebí využít širší časové řady snímků, jak bylo představeno ve studii

(Žížala et al., 2018 - článek 5.3). Multitemporální analýza pro regionální predikci půdních vlastností vyžaduje tedy buď vytvoření kompozitu (mozaiky) holých půd dle např. konceptu Dieka et al. (2017) či Rogge et al. (2018), nebo zpracování každého obrazu odděleně kvůli minimalizaci vlivu geometrických podmínek (využito ve studii Žížala et al., 2018 - článek 5.3). Satelitní a letecká data jsou totiž ovlivněna různou geometrií snímání v závislosti na době akvizice (výška a azimut Slunce, směr letu). Odstranění, respektive minimalizace tohoto efektu vyžaduje provedení precizních korekcí obrazu. Spektrální informace získaná ze satelitních či leteckých snímků je rovněž ovlivňována půdní vlhkostí, geometrickými parametry povrchu půdy (drsnost povrchu) a variabilitou dalších půdních vlastností, jako jsou textura, velikost půdních agregátů či přítomnost půdního škraloupu (Goldshleger et al., 2010; Ben-Dor a Demattê, 2015; Demattê et al., 2015; Schmid et al., 2016). Obzvláště při použití v regionálním mapování je potřebné najít postupy, které umožní minimalizaci těchto vlivů, jakožto i vlivů nefotosyntetizující vegetace na povrchu půdy (rostlinné zbytky), obzvláště v kontextu zvýšeného používání metod bezorebných technologií. V předkládaných studiích (Žížala et al., 2017 - článek 5.1 a Gholizadeh et al., 2018 - článek 5.2) vyhodnocení probíhalo na lokální úrovni, na blocích s provedenou předset'ovou přípravou (holá půda s minimalizací drsnosti povrchu) a suchým povrchem (minimálně 5 dní po posledním dešti) a vyhodnocení vlivu zmíněných parametrů tak nebylo možné.

Metody digitálního mapování půd, které byly pro mapování a predikci redistribuce SOC použity, jsou obecně závislé na kvalitě vstupních dat a použitých statistických metod. Vstupními daty v případě předkládaných studií byly na jedné straně (vysvětlující proměnné) hlavně data DPZ a terénní vlastnosti. Obě datové sady lze výhodně využít pro predikci koncentrace či zásob SOC nebo klasifikaci různě saturovaných půd. Pro dosažení nejlepších výsledků mapování a predikce je však vhodné využít kombinace všech relevantních dat. Další doplnění mohou představovat např. výsledky erozních či jiných environmetálních modelů či kombinace regresních metod s geostatistickými metodami v podobě regrese krigingu, kdy je při zachování podmínek (normální rozdělení reziduí) možné geostatisticky modelovat prostorovou korelaci reziduí modelu. Tyto možnosti jsou však předmětem dalšího plánovaného testování.

Důležitým aspektem mapování je cílové rozlišení jak v horizontálním měřítku, tak i ve vertikálním (mapování orniční vrstvy, celého profilu, jednotlivých horizontů). Obecnou

snahou při mapování půdních vlastností je dosáhnout co největší prostorové přesnosti. S rozvojem metod sběru digitálních dat přichází i vývoj v prostorové přesnosti dat, která jsou následně použita jako doplňková data v predikčních modelech. V současnosti je tak možno použít velice přesná data. Jak nicméně ukazují diskuze mezi odborníky a výsledky současných studií, lepší přesnosti často bývá dosaženo při využití dat s menším prostorovým rozlišením (Hannam, 2017; Malone, 2017; Samuel-Rosa, 2017). Při predikci půdních vlastností prezentované v předkládané studii (Žížala et al., 2017 - článek 5.1) se ukázalo, že je výhodnější použít směsné vzorky z plochy odpovídající rozlišení cílového mapování než využít bodových odběrů. Tomuto faktu je zapotřebí přizpůsobit i metodu terénního vzorkování. Kvalitu výsledných modelů zásadně ovlivňuje i počet a rozmístění vzorků (vysvětlovaná proměnná) (Brus et al., 2011; ten Caten et al., 2013; Biswas a Zhang, 2018). Optimální počet vzorků je nicméně velice obtížné předem stanovit. Obecně se dá doporučit pro větší území s větší heterogenitou půdních podmínek volit větší počet vstupních vzorků. S počtem vzorků obecně vzrůstá efektivita modelů a přesnost finálních map (Brodský et al., 2013), nicméně finální počet je vždy kompromisem mezi náklady na vzorkování a dostatečnou cílovou přesností. Rozmístění vzorků je předmětem řady metod založených na statistických či modelových analýz. Cílem by vždy však mělo být optimální pokrytí geografického prostoru a zároveň pokrytí kovariačního prostoru. Pro digitální mapování půd je nejčastěji doporučována metoda vzorkování pomocí redukční pravděpodobnostní metody podmíněných Latinských hyperkrychlí (cLHS) (Minasny a McBratney, 2006; Penížek et al., 2014). Tato metoda je přesto i kritizována (Ließ, 2017a, 2017b), že její schopnost zachytit heterogenitu a tedy pedodiverzitu krajiny je velice limitována a její použití při vzorkování může v důsledku vést k vychýleným (*biased*) predikčním modelům.

Na počtu vstupních dat a charakteristice studovaných závislostí závisí i vhodný způsob výběru použité statistické regresní metody. Častým způsobem je výběr optimálního modelu na základě zkušeností či expertního odhadu. Jak ukázaly prezentované studie, pro danou úlohu a prostor nemusí existovat jediné optimální řešení. Výsledky testování různých vícerozměrných metod ukázaly různou míru predikční schopnosti v závislosti na půdních podmínkách, počtu vzorků použitých pro kalibraci či použité metodě přípravy dat. Vhodným přístupem je tak otestovat více modelů, z nich vybrat ten s nejlepší predikční schopností nebo modely kombinovat s využitím nějaké *ensemble* metody. Výsledky testování v rámci předkládaných studií ukázaly, že pro sady s malým počtem

vzorků (30 - 50) lépe vyhovují metody SVM či neuronové sítě, u metody náhodných lesů (*random forest*) dochází k přeučení a není tedy vhodná pro malou sadu dat. Nicméně se stoupajícím počtem vzorků je tato metoda velice vhodná a často v současných studiích využívána (Viscarra Rossel a Behrens, 2010; Stevens et al., 2013; Veronesi et al., 2014; Were et al., 2015). Lineární metody jako testovaná metoda PLSR nedosáhly při mapování SOC s pomocí menšího počtu vzorků, kdy se vyskytují často nelineární vztahy ve vícerozměrném prostoru proměnných, takové přesnosti jako nelineární metody. Přesto je tato metoda v predikčním mapování a obecně při využití spektrálních dat stále často používána (Hbirkou et al., 2012; Siegmann et al., 2012; Denis et al., 2014; Pascucci et al., 2014; Franceschini et al., 2015; Vaudour et al., 2016a; Castaldi et al., 2018). Její výhodou je snazší interpretabilita oproti snížené až nemožné u nelineárních metod strojového učení. Výsledky navíc prokázaly, že pokles v predikční schopnosti oproti nelineárním metodám nemusí být zásadní. Presentované studie se nicméně zaobíraly převážně lokálně trénovanými modely (pro jeden až několik půdních bloků), čímž jsou výsledky zkresleny a predikční schopnost těchto modelů je tak pravděpodobně vyšší, než by tomu bylo u regionálních modelů (Stevens et al., 2012; Vaudour et al., 2016a). Současné studie často pracují právě na bázi jednotlivých půdních bloků a studie v regionálním měřítku jsou zatím sporadické a zatíženy vysokou chybovostí (Goidts et al., 2009; Stevens et al., 2015). Kalibrace empirických modelů je totiž účinná především lokálně a jejich aplikace na jiné podmínky či oblasti je často obtížná či nemožná (Casa et al., 2013a; Castaldi et al., 2018) a vyžaduje velký počet vstupních vzorků. Stevens et al. (2012) pro trénování regionálních modelů navrhuje inovativní metody křížové validace, které mohou optimalizovat kalibraci těchto modelů, jakožto jedno z možných řešení.

Jak ukázaly dřívější studie (Gholizadeh et al., 2013; Minu et al., 2016), ale rovněž i prezentované výsledky, důležitým aspektem v kvalitě modelů využívajících hyperspektrální data může být i způsob předzpracování dat. Jeho význam na jedné straně stoupá s vyšším spektrálním rozlišením dat, respektive s vyšší mírou šumu v datech (nižší poměr *signal to noise*), tam kde je zapotřebí míru šumu omezit a tedy data zhladit. Metody předzpracování spekter rovněž mohou sloužit k maskování vlivu environmentálních faktorů na spektrální absorpční pásy a zlepšit tak výsledky predikčních modelů. Tento efekt lze vhodně využít při laboratorním zpracování, kde je již efekt environmentálních faktorů vlivem standardizace vzorků (vysušení, analytická jemnost) částečně odstraněn. Nicméně v rámci sledování *in-situ* (což se děje v případě metod DPZ) mohou fyzikální

charakteristiky, které mají vliv na celkový posun albeda, přinášet další důležitou informaci (např. vlivem korelace mezi obsahem SOC a tvorbou agregátů, vlhkostí apod.). Z výsledků předkládaných studií vyplývá, že metody předzpracování spekter (hlavně metoda Savitzky-Golay) dokáží redukovat vliv nevhodných podmínek při pořízení leteckých hyperspektrálních dat.

Jak je z předešlé diskuze zřejmé, testované metody mapování redistribuce SOC mohou dosáhnout velice přesných výsledků, nicméně jejich uchopení a aplikace není triviální, je náročná zejména z hlediska potřebné kvalifikace, datového a softwarového vybavení a velice časově náročná zejména ve fázi přípravy dat. Přínosy těchto metod jsou však zřejmé a v porovnání s tradičními metodami mohou přinést přesnější, prostorově distribuované výsledky s menšími náklady. I přestože se metody digitálního mapování půd etabloují již od 90. let 20. století, stále existuje řada plně nedorozřešených otázek (Zhang et al., 2017) vyvolávající diskuze nad korektním výkladem nejen výsledků, ale i jednotlivých přístupů (Heuvelink, 2017; Rossiter, 2017). Při analýze přesnosti metod je tak třeba dbát zvýšené pozornosti na správnou interpretaci výsledků a statistických ukazatelů přesnosti predikce a hledat způsoby jak optimálně validovat, respektive ohodnotit modely, stanovit nepřesnosti a nejistoty v nevizorkovaných prostorech a analyzovat šíření chyb v modelech. Jak totiž ukazuje srovnání současných vědeckých studií, řada prací neudává adekvátní míry přesnosti (např. *bias*) a nezaobírá se externí validací (Selige et al., 2006; Stevens et al., 2008; Gomez et al., 2012; Kanning et al., 2016 oproti Hbirkou et al., 2012; Stevens et al., 2013) či jiným způsobem kvantifikace chyby v nevizorkovaných místech a srovnání a vyvozování adekvátních podložených závěrů je tak velice obtížné.

## 7 Závěr

---

Tato disertační práce předložená formou souboru publikovaných článků svými výsledky ukázala, že metody digitálního mapování půd s využitím dostupných spektrálních obrazových dat a modelu terénu lze uplatnit pro mapování redistribuce organického uhlíku i v erozně ovlivněných půdách v různých půdních podmínkách České republiky. Na základě podrobného terénního průzkumu byla popsána vysoká lokální variabilita koncentrací a zásob uhlíku ovlivněných erozně-akumulačními pochody dosahující míry variability na úrovni krajiny a lokální specifičnost redistribuce v různých podmínkách.

S pomocí leteckých hyperspektrálních dat se podařilo sestavit predikční modely pro mapování distribuce obsahu organického uhlíku ve svrchní vrstvě půdy s úrovní přesnosti na základě validace  $R^2 = 0,80 - 0,91$  a  $RMSE = 0,07 - 0,12$  % SOC. Při testování satelitních multispektrálních dat pro stejné účely bylo dosaženo menší přesnosti ( $R^2 = 0,57 - 0,89$  a  $RMSE 0,08 - 0,24$ ). Bylo však prokázáno, že s jejich využitím lze mapovat stejné prostorové trendy jako s využitím prostorově i spektrálně přesnějších dat. Vzhledem k nákladům a technickým požadavkům na zpracování hyperspektrálních dat se volně dostupná satelitní data jeví jako vhodná alternativa pro mapování SOC. Z hlediska půdních podmínek bylo obecně dosaženo lepších výsledků v oblastech s většími koncentracemi uhlíku a s menší variabilitou půdních vlastností, např. v oblastech s homogenním půdním substrátem (sprašové oblasti).

S využitím morfometrických dat odvozených z digitálního modelu terénu je možno vytvořit predikční modely nejen koncentrace organického uhlíku ve svrchní vrstvě půdy, ale i zásob uhlíku v celém půdním profilu. Prostorové modely zásoby SOC v celém profilu dosahovaly přesnosti  $R^2 = 0,62 - 0,99$  a  $RMSE = 0,28 - 2,38$   $\text{kg}\cdot\text{m}^{-2}$ . Modely zásob SOC pouze v orničním horizontu dosahovaly méně přesných a více rozkolísaných výsledků ( $R^2 = 0,23 - 0,91$  a  $RMSE = 0,17 - 0,89$   $\text{kg}\cdot\text{m}^{-2}$ ). Výsledná přesnost je značně místně specifická v závislosti na míře působení dalších faktorů ovlivňující redistribuci a dynamiku SOC nespjatých přímo s pozicí v terénu (srážky, způsob hospodaření apod.).

Předložené výsledky tak potvrdily iniciální hypotézu a využití metody predikčního modelování ukázaly, že jak s využitím pouze terénních dat, tak pouze s využitím spektrálních obrazových dat lze mapování SOC provést s vysokou mírou přesnosti. Současné využití obou typů dat v jednom predikčním modelu slibuje další zvýšení predikční schopnosti. Popsané metody se tak mohou stát vhodným nástrojem pro analýzu

redistribuce půdního uhlíku a studie ovlivnění koloběhu uhlíku v půdě, možnosti sekvestrace či studie ovlivnění uhlíku během erozně akumulčních procesů na lokální úrovni. Uplatnění ovšem mohou nalézt i v širším kontextu regionálního a celostátního mapování. Potřebná data pro mapování na této úrovni jsou již dnes dostupná a v blízké budoucnosti lze očekávat další vývoj např. v souvislosti s vypuštěním nových satelitních hyperspektrálních senzorů (EnMAP, PRISMA, SHALOM). Další možnosti jsou spojeny s využitím starších půdních dat, tzv. „*legacy dat*“. V rámci České republiky se jedná zejména o data Komplexního průzkumu zemědělských půd, která budou brzy k dispozici v digitální podobě. Jejich využití paralelně s poznatky z předkládané práce je plánováno v běžícím výzkumném projektu „Vytvoření podrobných aktuálních map půdních vlastností ČR na základě využití dat Komplexního průzkumu půd a metod digitálního mapování půd“.

V rámci práce byla nicméně popsána řada omezení, kritických předpokladů a nejistot spojených s aplikací použitých postupů. Metody nejsou stále dostatečně etablovány a je tedy zapotřebí se adekvátně věnovat minimalizaci všech rizik spojených s využitím dat, důsledné kvantifikaci chyb, nejistot a přesnosti predikčních modelů. Budoucí výzkum by měl být zároveň zaměřen na rozvoj metod sloužících k minimalizaci faktorů negativně ovlivňujících výslednou přesnost mapování a k rozvoji metod souvisejících s uplatněním popsaných principů při mapování v regionálním měřítku. U spektrálních obrazových dat se jedná zejména o metody redukcující vliv maskujících faktorů (vegetace, vlhkost, drsnost povrchu, zrnitost) a metody multispektrální analýzy. U nástrojů digitálního mapování se pak jedná o vývoj v metodách kalibrace modelů, optimalizaci jednotlivých vícerozměrných metod, případně metod určování vlivu vstupních proměnných na popis výsledné variability.

S vývojem digitálních metod je rovněž spojena tendence k zanedbávání klasického pedologického terénního průzkumu, který je ovšem nezbytný. Je nutné získávat aktuální analytické informace o půdním prostředí a to v dostatečné kvalitě i kvantitě, protože ty, jak bylo ukázáno, značně ovlivňují kvalitu výsledků, a nespolehat se jen na dostupná starší půdní data. Prezentované metody je tak nutné chápat jako podpůrné nástroje, které ovšem mohou přinést jinak těžko získatelné a nákladné informace, které jsou velice potřebné v kontextu ochrany půdy před degradačními vlivy, udržitelnosti hospodaření na půdě a adaptace na očekávané klimatické změny. Použití těchto metod není triviální,



vyžaduje široké znalosti a schopnosti v oborech jako statistika, geoinformatika, pedologie a je tedy velice vhodné je studovat a využívat v rámci širší týmové spolupráce.

## 8 Seznam použité literatury

---

- Adhikari, K., Hartemink, A.E., Minasny, B., Bou Kheir, R., Greve, M.B., Greve, M.H., 2014. Digital mapping of soil organic carbon contents and stocks in Denmark. *PLoS One*. 9 (8). 1–13. doi: 10.1371/journal.pone.0105519
- Afshar, F.A., Ayoubi, S., Jalalian, A., 2010. Soil redistribution rate and its relationship with soil organic carbon and total nitrogen using <sup>137</sup>Cs technique in a cultivated complex hillslope in western Iran. *Journal of Environmental Radioactivity*. 101 (8). 606–614. doi: 10.1016/j.jenvrad.2010.03.008
- Aïchi, H., Fouad, Y., Walter, C., Viscarra Rossel, R.A., Chabaane, Z.L., Sanaa, M., 2009. Regional predictions of soil organic carbon content from spectral reflectance measurements. *Biosystems Engineering*. 104 (3). 442–446. doi: 10.1016/j.biosystemseng.2009.08.002
- Aldana-Jague, E., Sommer, M., Saby, N.P.A., Cornelis, J.-T., Van Wesemael, B., Van Oost, K., 2016. High resolution characterization of the soil organic carbon depth profile in a soil landscape affected by erosion. *Soil and Tillage Research*. 3., 156. 185–193. doi: 10.1016/j.still.2015.05.014
- Alvarez, R., 2005. A review of nitrogen fertilizer and conservation tillage effects on soil organic carbon storage. *Soil Use and Management*. 21 (1). 38–52. doi: 10.1079/SUM2005291
- Anne, N.J.P., Abd-Elrahman, A.H., Lewis, D.B., Hewitt, N.A., 2014. Modeling soil parameters using hyperspectral image reflectance in subtropical coastal wetlands. *International Journal of Applied Earth Observation and Geoinformation*. 33. 47–56. doi: 10.1016/j.jag.2014.04.007
- Awale, R., Chatterjee, A., Franzen, D., 2013. Tillage and N-fertilizer influences on selected organic carbon fractions in a North Dakota silty clay soil. *Soil and Tillage Research*. 134. 213–222. doi: 10.1016/j.still.2013.08.006
- Ayoubi, S., Mokhtari Karchegani, P., Mosaddeghi, M.R., Honarjoo, N., 2012. Soil aggregation and organic carbon as affected by topography and land use change in western Iran. *Soil and Tillage Research*. 121. 18–26. doi: 10.1016/j.still.2012.01.011

- Bajracharya, R.M., Lal, R., Kimble, J.M., 2000. Erosion Effects on Carbon Dioxide Concentration and Carbon Flux from an Ohio Alfisol. *Soil Science Society of America Journal*. 64 (2). 694. doi: 10.2136/sssaj2000.642694x
- Bajwa, S.G., Tian, L.F., 2005. Soil fertility characterization in agricultural fields using hyperspectral remote sensing. *Transactions of the ASAE*. 48 (6). 2399–2406.
- Ballabio, C., Panagos, P., Montanarella, L., 2014. Predicting soil organic carbon content in Cyprus using remote sensing and Earth observation data. In: Hadjimitsis, D.G., Themistocleous, K., Michaelides, S., Papadavid, G., (ed.). *Proceedings of SPIE - the International Society for Optical Engineering*. s. 92290F. doi: 10.1117/12.2066406
- Banwart, S.A., Black, H., Cai, Z., Gicheru, P.T., Joosten, H., Victoria, R.L., Milne, E., Noellemeyer, E., Pascual, U., 2015. The Global Challenge for Soil Carbon. In: Banwart, S.A., Noellemeyer, E., Milne, E., (ed.). *Soil Carbon: Science, Management and Policy for Multiple Benefits*. CAB International, s. 1–9. ISBN: 978 1 78064 532 2.
- Barančíková, G., Halás, J., Gutteková, M., Makovníková, J., Nováková, M., Skalský, R., Tarasovičová, Z., 2010. Application of RothC model to predict soil organic carbon stock on agricultural soils of Slovakia. *Soil and Water Research*. 5 (1). 1–9.
- Bartholomeus, H.M., Kooistra, L., Stevens, A., Van Leeuwen, M., Van Wesemael, B., Ben-Dor, E., Tychon, B., 2011. Soil Organic Carbon mapping of partially vegetated agricultural fields with imaging spectroscopy. *International Journal of Applied Earth Observation and Geoinformation*. 13 (1). 81–88. doi: 10.1016/j.jag.2010.06.009
- Bartholomeus, H.M., Schaepman, M.E., Kooistra, L., Stevens, A., Hoogmoed, W.B., Spaargaren, O.S.P., 2008. Spectral reflectance based indices for soil organic carbon quantification. *Geoderma*. 145 (1–2). 28–36. doi: 10.1016/j.geoderma.2008.01.010
- Batjes, N.H., 1995. *World Soil Carbon Stocks and Global Change*. Wageningen: ISRIC.
- Batjes, N.H., 1996. Total carbon and nitrogen in the soils of the world. *European Journal of Soil Science*. 47 (6). 151–163.
- Batjes, N.H., Wesemael, B. Van, 2015. Measuring and Monitoring Soil Carbon. In: Banwart, S.A., Noellemeyer, E., Milne, E., (ed.). *Soil Carbon: Science, Management and Policy for Multiple Benefits*. CAB International, s. 459–492.
- Battle-Aguilar, J., Brovelli, A., Porporato, A., Barry, D.A., 2011. Modelling Soil Carbon

- and Nitrogen Cycles During Land Use Change. In: Lichtfouse, E., Hamelin, M., Navarrete, M., Debaeke, P., (ed.). *Sustainable Agriculture Volume 2*. Dordrecht: Springer Netherlands, s. 499–527. ISBN: 978-94-007-0393-3. doi: 10.1007/978-94-007-0394-0\_23
- Baumgardner, M.F., Kristof, S.J., Johannsen, C.J., Zachary, A.L., 1970. Effects of Organic Matter on the Multispectral Properties of Soils. In: *Proceeding of the Indian Academy of Science. Journal Paper n°3939*. Purdue University Agricultural Experiment Station, s. 413–422.
- Bayer, A.D., Pugh, T.A.M., Krause, A., Arneith, A., 2015. Historical and future quantification of terrestrial carbon sequestration from a Greenhouse-Gas-Value perspective. *Global Environmental Change*. 32. 153–164. doi: 10.1016/j.gloenvcha.2015.03.004
- Bellinaso, H., Demattê, J.A.M., Romeiro, S.A., 2010. Soil Spectral Library and Its Use in Soil Classification. *Revista Brasileira de Ciência do Solo*. 34 (1). 861–870.
- Bellon-Maurel, V., McBratney, A., 2011. Near-infrared (NIR) and mid-infrared (MIR) spectroscopic techniques for assessing the amount of carbon stock in soils - Critical review and research perspectives. *Soil Biology and Biochemistry*. 43 (7). 1398–1410. doi: 10.1016/j.soilbio.2011.02.019
- Ben-Dor, E., Chabrillat, S., Demattê, J.A.M., Taylor, G.R., Hill, J., Whiting, M.L., Sommer, S., 2009. Using Imaging Spectroscopy to study soil properties. *Remote Sensing of Environment*. 113 (SUPPL. 1). S38–S55. doi: 10.1016/j.rse.2008.09.019
- Ben-Dor, E., Demattê, J.A.M., 2015. Remote Sensing of Soil in the Optical Domains. In: Thenkabail, P.S., (ed.). *Land Resources Monitoring, Modeling, and Mapping with Remote Sensing*. Remote Sen. Boca Raton: CRC Press, s. 733–787.
- Ben-Dor, E., Heller, D., Chudnovsky, A., 2008a. A Novel Method of Classifying Soil Profiles in the Field using Optical Means. *Soil Science Society of America Journal*. 72 (4). 1113. doi: 10.2136/sssaj2006.0059
- Ben-Dor, E., Inbar, Y., Chen, Y., 1997. The reflectance spectra of organic matter in the visible near-infrared and short wave infrared region (400-2500 nm) during a controlled decomposition process. *Remote Sensing of Environment*. 61 (1). 1–15. doi: 10.1016/S0034-4257(96)00120-4

- Ben-Dor, E., Irons, J.R., Epema, G.F., 1999. Soil Reflectance. In: Rencz, A.N., Ryerson, R.A., (ed.). *Manual of Remote Sensing: Remote Sensing for Earth Science*. 3. vyd. s. 111–187. ISBN: ISBN: 978-0-471-29405-4.
- Ben-Dor, E., Ong, C., Lau, I.C., 2015. Reflectance measurements of soils in the laboratory: Standards and protocols. *Geoderma*. 5., 245–246. 112–124. doi: 10.1016/j.geoderma.2015.01.002
- Ben-Dor, E., Patkin, K., Banin, A., Karnieli, A., 2002. Mapping of several soil properties using DAIS-7915 hyperspectral scanner data - a case study over clayey soils in Israel. *International Journal of Remote Sensing*. 23 (6). 1043–1062. doi: 10.1080/01431160010006962
- Ben-Dor, E., Taylor, G.R., Hill, J., Demattê, J.A.M., Whiting, M.L., Chabrillat, S., Sommer, S., 2008b. Imaging spectrometry for soil applications. *Advances in Agronomy*. 97. 321–392.
- Berhe, A.A., Harden, J.W., Torn, M.S., Harte, J., 2008. Linking soil organic matter dynamics and erosion-induced terrestrial carbon sequestration at different landform positions. *Journal of Geophysical Research: Biogeosciences*. 113 (4). 1–12. doi: 10.1029/2008JG000751
- Berhe, A.A., Harte, J., Harden, J.W., Torn, M.S., 2007. The Significance of the Erosion-induced Terrestrial Carbon Sink. *BioScience*. 57 (4). 337–346. doi: 10.1641/B570408
- Bhunia, G.S., Kumar Shit, P., Pourghasemi, H.R., 2017. Soil organic carbon mapping using remote sensing techniques and multivariate regression model. *Geocarto International*. 6049 (September). 1–12. doi: 10.1080/10106049.2017.1381179
- Bielek, P., Jurčová, O., 2010. *Metodika bilancie pôdnej organickej hmoty a stanovenia potreby organického hnojenia poľnohospodárskych pôd*. Bratislava: Výzkumný ústav pôdozvedectva a ochrany pôdy. ISBN: 978-80-89128-80-8.
- Biswas, A., Zhang, Y., 2018. Sampling Designs for Validating Digital Soil Maps: A Review. *Pedosphere*. 28 (1). 1–15. doi: 10.1016/S1002-0160(18)60001-3
- Bou Kheir, R., Greve, M.H., Bøcher, P.K., Greve, M.B., Larsen, R., McCloy, K., 2010. Predictive mapping of soil organic carbon in wet cultivated lands using classification-tree based models: The case study of Denmark. *Journal of Environmental Management*. 91 (5). 1150–1160. doi:

10.1016/j.jenvman.2010.01.001

- Bouwman, A.F., 1989. Modelling soil organic matter decomposition and rainfall erosion in two tropical soils after forest clearing for permanent agriculture. *Land Degradation and Development*. 1 (2). 125–140. doi: 10.1002/ldr.3400010205
- Brodský, L., Vašát, R., Klement, A., Zádorová, T., Jakšík, O., 2013. Uncertainty propagation in VNIR reflectance spectroscopy soil organic carbon mapping. *Geoderma*. 199. 54–63. doi: 10.1016/j.geoderma.2012.11.006
- Brodský, L., Klement, A., Penížek, V., Kodešová, R., Borůvka, L., 2011a. Building soil spectral library of the czech soils for quantitative digital soil mapping. *Soil and Water Research*. 6 (4). 165–172.
- Brodský, L., Zádorová, T., Klement, A., Jakšík, O., Borůvka, L., 2011b. Utilization of VNIR diffuse reflectance spectroscopy to map soil erosion Study on two arable fields. In: Adamchuk, V.I., Viscarra Rossel, R. A., (ed.). *The Second Global Workshop on Proximal Soil Sensing*. s. 84–87.
- Brown, D.J., Shepherd, K.D., Walsh, M.G., Dewayne Mays, M., Reinsch, T.G., 2006. Global soil characterization with VNIR diffuse reflectance spectroscopy. *Geoderma*. 132 (3–4). 273–290. doi: 10.1016/j.geoderma.2005.04.025
- Brus, D.J., Kempen, B., Heuvelink, G.B.M., 2011. Sampling for validation of digital soil maps. *European Journal of Soil Science*. 62 (3). 394–407. doi: 10.1111/j.1365-2389.2011.01364.x
- Buschiazzo, D.E., Zobeck, T.M., Abascal, S.A., 2007. Wind erosion quantity and quality of an Entic Haplustoll of the semi-arid pampas of Argentina. *Journal of Arid Environments*. 4., 69 (1). 29–39. doi: 10.1016/j.jaridenv.2006.08.013
- Buschiazzo, D.E., Funk, R., 2015. Wind Erosion of Agricultural Soils and the Carbon Cycle. In: Banwart, S.A., Noellemeyer, E., Milne, E., (ed.). *Soil Carbon: Science, Management and Policy for Multiple Benefits*. CAB International, s. 161–168.
- Cambule, A.H., Rossiter, D.G., Stoorvogel, J.J., Smaling, E.M.A., 2014. Soil organic carbon stocks in the Limpopo National Park, Mozambique: Amount, spatial distribution and uncertainty. *Geoderma*. 213. 46–56. doi: 10.1016/j.geoderma.2013.07.015
- Campbell, C. A, Mcconkey, B.G., Zentner, R.P., Selles, F., Curtin, D., 1996. Long-term

- Effects of Tillage and Crop Rotations on Soil Organic C and Total N in a Clay Soil in Southwestern Saskatchewan. *Agriculture*. 76. 395–401.
- Casa, R., Castaldi, F., Pascucci, S., Palombo, A., Pignatti, S., 2013a. A comparison of sensor resolution and calibration strategies for soil texture estimation from hyperspectral remote sensing. *Geoderma*. 197–198. 17–26. doi: 10.1016/j.geoderma.2012.12.016
- Casa, R., Castaldi, F., Pascucci, S., Basso, B., Pignatti, S., 2013b. Geophysical and Hyperspectral Data Fusion Techniques for In-Field Estimation of Soil Properties. *Vadose Zone Journal*. 12 (4). 0. doi: 10.2136/vzj2012.0201
- Castaldi, F., Casa, R., Castrignanò, A., Pascucci, S., Palombo, A., Pignatti, S., 2014. Estimation of soil properties at the field scale from satellite data: a comparison between spatial and non-spatial techniques. *European Journal of Soil Science*. 65 (6). 842–851. doi: 10.1111/ejss.12202
- Castaldi, F., Chabrillat, S., Jones, A., Vreys, K., Bomans, B., Van Wesemael, B., 2018. Soil Organic Carbon Estimation in Croplands by Hyperspectral Remote APEX Data Using the LUCAS Topsoil Database. *Remote Sensing*. 10 (2). 153–172. doi: 10.3390/rs10020153
- Castaldi, F., Palombo, A., Santini, F., Pascucci, S., Pignatti, S., Casa, R., 2016. Evaluation of the potential of the current and forthcoming multispectral and hyperspectral imagers to estimate soil texture and organic carbon. *Remote Sensing of Environment*. 179. 54–65. doi: 10.1016/j.rse.2016.03.025
- Cécillon, L., Barthès, B.G., Gomez, C., Ertlen, D., Genot, V., Hedde, M., Stevens, A., Brun, J.J., 2009. Assessment and monitoring of soil quality using near-infrared reflectance spectroscopy (NIRS). *European Journal of Soil Science*. 60 (5). 770–784. doi: 10.1111/j.1365-2389.2009.01178.x
- Ceddia, M.B., Villela, A.L.O., Pinheiro, É.F.M., Wendroth, O., 2015. Spatial variability of soil carbon stock in the Urucu river basin, Central Amazon-Brazil. *Science of the Total Environment*. 526. 58–69. doi: 10.1016/j.scitotenv.2015.03.121
- Chabrillat, S., Kaufmann, H., Merz, B., Mueller, A., Bens, O., Lemmnitz, C., 2003. Development of relationships between reflectance and erosion modelling : Test site preliminary field spectral analysis. In: *3rd EARSeL Workshop on Imaging*

*Spectroscopy, 13-16 May 2003*. Herrsching: EARSeL, s. 13–16.

- Chaopricha, N.T., Marín-Spiotta, E., 2014. Soil burial contributes to deep soil organic carbon storage. *Soil Biology and Biochemistry*. 69. 251–264. doi: 10.1016/j.soilbio.2013.11.011
- Chaplot, V., Abdalla, K., Alexis, M., Bourennane, H., Darboux, F., Dlamini, P., Everson, C., Mchunu, C., Muller-Nedebeck, D., Mutema, M., Quenea, K., Thenga, H., Chivenge, P., 2015. Surface organic carbon enrichment to explain greater CO<sub>2</sub> emissions from short-term no-tilled soils. *Agriculture, Ecosystems & Environment*. 203. 110–118. doi: 10.1016/j.agee.2015.02.001
- Chaplot, V., McHunu, C.N., Manson, A., Lorentz, S., Jewitt, G., 2012. Water erosion-induced CO<sub>2</sub> emissions from tilled and no-tilled soils and sediments. *Agriculture, Ecosystems and Environment*. 159. 62–69. doi: 10.1016/j.agee.2012.06.008
- Chaplot, V., Cooper, M., 2015. Soil aggregate stability to predict organic carbon outputs from soils. *Geoderma*. 243–244. 205–213. doi: 10.1016/j.geoderma.2014.12.013
- Chen, F., Kissel, D.E., West, L.T., Adkins, W., Rickman, D., Luvall, J.C., 2006. Feature selection and similarity analysis of crop fields for mapping organic carbon concentration in soil. *Computers and Electronics in Agriculture*. 54 (1). 8–21. doi: 10.1016/j.compag.2006.06.003
- Chen, F., Kissel, D.E., West, L.T., Adkins, W., Rickman, D., Luvall, J.C., 2008. Mapping Soil Organic Carbon Concentration for Multiple Fields with Image Similarity Analysis. *Soil Science Society of America Journal*. 72 (1). 186. doi: 10.2136/sssaj2007.0028
- Chen, F., Kissel, D.E., West, L.T., Adkins, W., 2000. Field-Scale Mapping of Surface Soil Organic Carbon Using Remotely Sensed Imagery. *Soil Science Society of America Journal*. 64 (2). 746. doi: 10.2136/sssaj2000.642746x
- Chenu, C., Rumpel, C., Lehmann, J., 2015. Methods for Studying Soil Organic Matter: Nature, Dynamics, Spatial Accessibility, and Interactions with Minerals. In: Paul, E.A., (ed.). *Soil Microbiology, Ecology, and Biochemistry*. fourth. Elsevier Inc., s. 343–412. ISBN: 978-0-12-415955-6.
- Chepil, W.S., 1960. Conversion of Relative Field Erodibility to Annual Soil Loss by Wind. *Soil Science Society of America Proceedings*. 24 (2). 143–145.



- Conant, R.T., Ryan, M.G., Ågren, G.I., Birge, H.E., Davidson, E. A., Eliasson, P.E., Evans, S.E., Frey, S.D., Giardina, C.P., Hopkins, F.M., Hyvönen, R., Kirschbaum, M.U.F., Lavallee, J.M., Leifeld, J., Parton, W.J., Steinweg, J.M., Wallenstein, M.D., Wetterstedt, J.Å.M., Bradford, M.A., 2011. Temperature and soil organic matter decomposition rates - synthesis of current knowledge and a way forward. *Global Change Biology*. 17 (11). 3392–3404. doi: 10.1111/j.1365-2486.2011.02496.x
- Conant, R.T., Ogle, S.M., Paul, E.A., Paustian, K., 2010. Measuring and monitoring soil organic carbon stocks in agricultural lands for climate mitigation. *Frontiers in Ecology and the Environment*. 9 (3). 169–173. doi: 10.1890/090153
- Croft, H., Kuhn, N.J., Anderson, K., 2012. On the use of remote sensing techniques for monitoring spatio-temporal soil organic carbon dynamics in agricultural systems. *Catena*. 94. 64–74. doi: 10.1016/j.catena.2012.01.001
- Das, B.S., Sarathjith, M.C., Santra, P., Sahoo, R.N., Srivastava, R., Routray, A., Ray, S.S., 2015. Hyperspectral remote sensing : opportunities , status and challenges for rapid soil assessment in India. *Current Science*. 108 (5). 860–868.
- De Gruijter, J.J., McBratney, A.B., Taylor, J., 2010. Sampling for High-Resolution Soil Mapping. In: Viscarra Rossel, R.A., McBratney, A.B., Minasny, B., (ed.). *Proximal Soil Sensing SE - 1*. Springer Netherlands, Progress in Soil Science, s. 3–14. ISBN: 978-90-481-8858-1. doi: 10.1007/978-90-481-8859-8\_1
- De Gryze, S., Six, J., Bossuyt, H., Van Oost, K., Merckx, R., 2008. The relationship between landform and the distribution of soil C, N and P under conventional and minimum tillage. *Geoderma*. 144 (1–2). 180–188. doi: 10.1016/j.geoderma.2007.11.013
- Demattê, J.A.M., Morgan, C.L.S., Chabrillat, S., Rizzo, R., Franceschini, M.H.D., Terra, F. D., Vasques, G.M., Wetterlind, J., 2015. Spectral Sensing From Ground to Space in Soil Science: State of the Art, Applications, Potential and Perspectives. In: Thenkabail, P.S., (ed.). *Land Resources Monitoring, Modeling, and Mapping with Remote Sensing*. Remote Sen. Boca Raton: CRC Press, s. 661–732.
- Denis, A., Stevens, A., Van Wesemael, B., Udelhoven, T., Tychon, B., 2014. Soil organic carbon assessment by field and airborne spectrometry in bare croplands: Accounting for soil surface roughness. *Geoderma*. 226–227 (1). 94–102. doi:

10.1016/j.geoderma.2014.02.015

- DeTar, W.R., Chesson, J.H., Penner, J. V., Ojala, J.C., 2008. Detection of Soil Properties with Airborne Hyperspectral Measurements of Bare Fields. *Transactions of the ASABE*. 51 (2). 463–470. doi: 10.13031/2013.24388
- Diek, S., Fornallaz, F., Schaepman, M.E., De Jong, R., 2017. Barest Pixel Composite for agricultural areas using landsat time series. *Remote Sensing*. 9 (12). doi: 10.3390/rs9121245
- Dlugoß, V., 2011. *Impacts of Soil Redistribution Processes on Soil Organic Carbon Stocks and Fluxes in a Small Agricultural Catchment*. Universität zu Köln.
- Dlugoß, V., Fiener, P., Schneider, K., 2010. Layer-Specific Analysis and Spatial Prediction of Soil Organic Carbon Using Terrain Attributes and Erosion Modeling. *Soil Science Society of America Journal*. 74 (3). 922. doi: 10.2136/sssaj2009.0325
- Dlugoß, V., Fiener, P., Van Oost, K., Schneider, K., 2012. Model based analysis of lateral and vertical soil carbon fluxes induced by soil redistribution processes in a small agricultural catchment. *Earth Surface Processes and Landforms*. 37 (2). 193–208. doi: 10.1002/esp.2246
- Doetterl, S., Berhe, A.A., Nadeu, E., Wang, Z., Sommer, M., Fiener, P., 2015a. Erosion, deposition and soil carbon: A review of process-level controls, experimental tools and models to address C cycling in dynamic landscapes. *Earth-Science Reviews*. doi: 10.1016/j.earscirev.2015.12.005
- Doetterl, S., Six, J., Van Wesemael, B., Van Oost, K., 2012. Carbon cycling in eroding landscapes: Geomorphic controls on soil organic C pool composition and C stabilization. *Global Change Biology*. 18 (7). 2218–2232. doi: 10.1111/j.1365-2486.2012.02680.x
- Doetterl, S., Stevens, A., Six, J., Merckx, R., Van Oost, K., Casanova Pinto, M., Casanova-Katny, A., Muñoz, C., Boudin, M., Zagal Venegas, E., Boeckx, P., 2015b. Soil carbon storage controlled by interactions between geochemistry and climate. *Nature Geoscience*. 8 (10). 780–783. doi: 10.1038/ngeo2516
- Doetterl, S., Stevens, A., Van Oost, K., Quine, T. A., Van Wesemael, B., 2013. Spatially-explicit regional-scale prediction of soil organic carbon stocks in cropland using environmental variables and mixed model approaches. *Geoderma*. 204–205 (7). 31–

42. doi: 10.1016/j.geoderma.2013.04.007

- Don, A., Schumacher, J., Scherer-Lorenzen, M., Scholten, T., Schulze, E.-D., 2007. Spatial and vertical variation of soil carbon at two grassland sites — Implications for measuring soil carbon stocks. *Geoderma*. 141 (3–4). 272–282. doi: 10.1016/j.geoderma.2007.06.003
- Du, C., Zhou, J., 2009. Evaluation of Soil Fertility Using Infrared Spectroscopy – A Review. In: *Climate Change, Intercropping, Pest Control and Beneficial Microorganisms*. Dordrecht: Springer Netherlands, s. 453–483. ISBN: 978-90-481-2715-3. doi: 10.1007/978-90-481-2716-0\_16
- Ebengo, D.M., Vaudour, E., Gilliot, J., Hadjar, D., Baghdadi, N., 2018. Potential of combined Sentinel 1 / Sentinel 2 images for mapping topsoil organic carbon content over cropland taking into account soil roughness. In: *Geophysical Research Abstracts, vol. 20, EGU General Assembly 2018*. Wien: EGU, s. 14368.
- Eglin, T., Ciais, P., Piao, S.L., Barre, P., Bellassen, V., Cadule, P., Chenu, C., Gasser, T., Koven, C., Reichstein, M., Smith, P., 2010. Historical and future perspectives of global soil carbon response to climate and land-use changes. *Tellus*. 62B (5). 700–718. doi: 10.1111/j.1600-0889.2010.00499.x
- Falloon, P., Jones, C.D., Ades, M., Paul, K., 2011. Direct soil moisture controls of future global soil carbon changes: An important source of uncertainty. *Global Biogeochemical Cycles*. 25 (3). doi: 10.1029/2010GB003938
- Fang, X., Xue, Z., Li, B., An, S., 2012. Soil organic carbon distribution in relation to land use and its storage in a small watershed of the Loess Plateau, China. *Catena*. 88 (1). 6–13. doi: 10.1016/j.catena.2011.07.012
- Feller, C., Bernoux, M., 2008. Historical advances in the study of global terrestrial soil organic carbon sequestration. *Waste Management*. 28 (4). 734–740. doi: 10.1016/j.wasman.2007.09.022
- Fiener, P., Dlugob, V., Korres, W., Schneider, K., 2012. Spatial variability of soil respiration in a small agricultural watershed - Are patterns of soil redistribution important? *Catena*. 94. 3–16. doi: 10.1016/j.catena.2011.05.014
- Fiener, P., Dlugob, V., Van Oost, K., 2015. Erosion-induced carbon redistribution, burial and mineralisation — Is the episodic nature of erosion processes important? *Catena*.

133. 282–292. doi: 10.1016/j.catena.2015.05.027

- Florinsky, I. V, Eilers, R.G., Manning, G.R., Fuller, L.G., 2002. Prediction of soil properties by digital terrain modelling. *Environmental Modelling & Software*. 17 (3). 295–311. doi: 10.1016/S1364-8152(01)00067-6
- Follain, S., Walter, C., Legout, A., Lemercier, B., Dutin, G., 2007. Induced effects of hedgerow networks on soil organic carbon storage within an agricultural landscape. *Geoderma*. 142 (1–2). 80–95. doi: 10.1016/j.geoderma.2007.08.002
- Franceschini, M.H.D., Demattê, J.A.M., Da Silva Terra, F., Vicente, L.E., Bartholomeus, H.M., De Souza Filho, C.R., 2015. Prediction of soil properties using imaging spectroscopy: Considering fractional vegetation cover to improve accuracy. *International Journal of Applied Earth Observation and Geoinformation*. 38. 358–370. doi: 10.1016/j.jag.2015.01.019
- Frank, D., Reichstein, M., Bahn, M., Thonicke, K., Frank, D., Mahecha, M.D., Smith, P., Van der Velde, M., Vicca, S., Babst, F., Beer, C., Buchmann, N., Canadell, J.G., Ciais, P., Cramer, W., Ibrom, A., Miglietta, F., Poulter, B., Rammig, A., Seneviratne, S.I., Walz, A., Wattenbach, M., Zavala, M. A, Zscheischler, J., 2015. Effects of climate extremes on the terrestrial carbon cycle: concepts, processes and potential future impacts. *Global Change Biology*. 21 (8). 2861–2880. doi: 10.1111/gcb.12916
- Gao, Y., Cui, L., Lei, B., Zhai, Y., Shi, T., Wang, J., Chen, Y., He, H., Wu, G., 2014. Estimating Soil Organic Carbon Content with Visible-Near-Infrared (Vis-NIR) Spectroscopy. *Applied Spectroscopy*. 68 (7). 712–722. doi: 10.1366/13-07031
- Ge, Y., Morgan, C.L.S., Grunwald, S., Brown, D.J., Sarkhot, D. V., 2011. Comparison of soil reflectance spectra and calibration models obtained using multiple spectrometers. *Geoderma*. 161 (3–4). 202–211. doi: 10.1016/j.geoderma.2010.12.020
- Gerighausen, H., Menz, G., Kaufmann, H., 2012. Spatially Explicit Estimation of Clay and Organic Carbon Content in Agricultural Soils Using Multi-Annual Imaging Spectroscopy Data. *Applied and Environmental Soil Science*. 2012. 1–23. doi: 10.1155/2012/868090
- Gholizadeh, A., Borůvka, L., Saberioon, M., Vašát, R., 2013. Visible, near-infrared, and mid-infrared spectroscopy applications for soil assessment with emphasis on soil

- organic matter content and quality: State-of-the-art and key issues. *Applied Spectroscopy*. 67 (12). 1349–1362. doi: 10.1366/13-07288
- Gholizadeh, A., Žižala, D., Saberioon, M., Borůvka, L., 2018. Soil Organic Carbon and Clay Monitoring and Mapping using Airborne and Sentinel-2 Spectral Imaging. In: *Sixth International Conference on Remote Sensing and Geoinformation of Environment*. Aliathon: Cyprus Remote Sensing Society.
- Gmur, S., Vogt, D., Zabowski, D., Moskal, L.M., 2012. Hyperspectral Analysis of Soil Nitrogen, Carbon, Carbonate, and Organic Matter Using Regression Trees. *Sensors*. 12 (8). 10639–58. doi: 10.3390/s120810639
- Goidts, E., Van Wesemael, B., Crucifix, M., 2009. Magnitude and sources of uncertainties in soil organic carbon (SOC) stock assessments at various scales. *European Journal of Soil Science*. 60 (5). 723–739. doi: 10.1111/j.1365-2389.2009.01157.x
- Goldshleger, N., Ben-Dor, E., Lugassi, R., Eshel, G., 2010. Soil Degradation Monitoring by Remote Sensing: Examples with Three Degradation Processes. *Soil Science Society of America Journal*. 74 (5). 1433–1445. doi: 10.2136/sssaj2009.0351
- Gomez, C., Lagacherie, P., Coulouma, G., 2012. Regional predictions of eight common soil properties and their spatial structures from hyperspectral Vis-NIR data. *Geoderma*. 189–190. 176–185. doi: 10.1016/j.geoderma.2012.05.023
- Gomez, C., Viscarra Rossel, R. A., McBratney, A.B., 2008. Soil organic carbon prediction by hyperspectral remote sensing and field vis-NIR spectroscopy: An Australian case study. *Geoderma*. 146 (3–4). 403–411. doi: 10.1016/j.geoderma.2008.06.011
- Grunwald, S., 2009. Multi-criteria characterization of recent digital soil mapping and modeling approaches. *Geoderma*. 152 (3–4). 195–207. doi: 10.1016/j.geoderma.2009.06.003
- Grunwald, S., Vasques, G.M., Rivero, R.G., 2015. Fusion of Soil and Remote Sensing Data to Model Soil Properties. In: Sparks, D.L., (ed.). *Advances in Agronomy*. Elsevier, s. 1–109. ISBN: 978-0-12-802136-1. doi: 10.1016/bs.agron.2014.12.004
- Hancock, G.R., Murphy, D., Evans, K.G., 2010. Hillslope and catchment scale soil organic carbon concentration: An assessment of the role of geomorphology and soil

- erosion in an undisturbed environment. *Geoderma*. 155 (1–2). 36–45. doi: 10.1016/j.geoderma.2009.11.021
- Hannam, J., 2017. Why use a fine paintbrush when a broad brush will do? *Pedometron*. (41). 32–33.
- Hbirkou, C., Pätzold, S., Mahlein, A.K., Welp, G., 2012. Airborne hyperspectral imaging of spatial soil organic carbon heterogeneity at the field-scale. *Geoderma*. 175–176. 21–28. doi: 10.1016/j.geoderma.2012.01.017
- Hengl, T., Gruber, S., Shrestha, D.P., 2004. Reduction of errors in digital terrain parameters used in soil-landscape modelling. *International Journal of Applied Earth Observation and Geoinformation*. 5. 97–112. doi: 10.1016/j.jag.2004.01.006
- Heuvelink, G., 2017. We can avoid confusion and misunderstanding if we make the change. *Pedometron*. (41). 24.
- Hiederer, R., Köchy, M., 2011. *Global Soil Organic Carbon Estimates and the Harmonized World Soil Database*. EUR 25225. Luxembourg: Publications Office of the European Union. ISBN: 978-92-79-23108-7. doi: 10.2788/13267
- Hill, J., Schütt, B., 2000. Mapping complex patterns of erosion and stability in dry mediterranean ecosystems. *Remote Sensing of Environment*. 74 (3). 557–569. doi: 10.1016/S0034-4257(00)00146-2
- Hively, W.D., McCarty, G.W., Reeves, J.B., Lang, M.W., Oesterling, R. A., Delwiche, S.R., 2011. Use of Airborne Hyperspectral Imagery to Map Soil Properties in Tilled Agricultural Fields. *Applied and Environmental Soil Science*. 2011. 1–13. doi: 10.1155/2011/358193
- Hoffmann, C., Funk, R., Li, Y., Sommer, M., 2008. Effect of grazing on wind driven carbon and nitrogen ratios in the grasslands of Inner Mongolia. *Catena*. 75 (2). 182–190. doi: 10.1016/j.catena.2008.06.003
- Houghton, R.A., 1995. Changes in the Storage of Terrestrial Carbon Since 1850. In: Lal, R., Kimble, J.M., Levine, E.R., Stewart, B.A., (ed.). *Soils and Global Change*. CRC Press, s. 45–65.
- Houghton, R.A., 2012. *Recarbonization of the Biosphere*. Dordrecht: Springer Netherlands. ISBN: 978-94-007-4158-4. doi: 10.1007/978-94-007-4159-1
- Hu, Y., Kuhn, N.J., 2014. Aggregates reduce transport distance of soil organic carbon:

- are our balances correct? *Biogeosciences Discussions*. 11 (6). 8829–8859. doi: 10.5194/bgd-11-8829-2014
- Hu, Y., Fister, W., Kuhn, N., 2013. Temporal Variation of SOC Enrichment from Interrill Erosion over Prolonged Rainfall Simulations. *Agriculture*. 3 (4). 726–740. doi: 10.3390/agriculture3040726
- Huang, J., Li, Z., Zeng, G., Zhang, J., Li, J., Nie, X., Ma, W., Zhang, X., 2013. Microbial responses to simulated water erosion in relation to organic carbon dynamics on a hilly cropland in subtropical China. *Ecological Engineering*. 60. 67–75. doi: 10.1016/j.ecoleng.2013.07.040
- Izaurrealde, R.C., Williams, J.R., McGill, W.B., Rosenberg, N.J., 2001. Simulating Soil Carbon Dynamics, Erosion and Tillage with EPIC. In: *First National Conference on Carbon Sequestration, May 14-17, 2001*. Washington: Department of Energy—National Energy Technology Laboratory, s. 1–12. ISBN: 2026465029.
- Izaurrealde, R.C., Rice, C.W., Wielopolski, L., Ebinger, M.H., Reeves, J.B., Thomson, A.M., Harris, R., Francis, B., Mitra, S., Rappaport, A.G., Etchevers, J.D., Sayre, K.D., Govaerts, B., McCarty, G.W., 2013. Evaluation of Three Field-Based Methods for Quantifying Soil Carbon. *PLoS One*. 8 (1). doi: 10.1371/journal.pone.0055560
- Jaber, S.M., Lant, C.L., Al-Qinna, M.I., 2011. Estimating spatial variations in soil organic carbon using satellite hyperspectral data and map algebra. *International Journal of Remote Sensing*. 32 (18). 5077–5103. doi: 10.1080/01431161.2010.494637
- Jacinthe, P. A., Lal, R., Owens, L.B., Hothem, D.L., 2004. Transport of labile carbon in runoff as affected by land use and rainfall characteristics. *Soil and Tillage Research*. 77 (2). 111–123. doi: 10.1016/j.still.2003.11.004
- Jacinthe, P.A., Lal, R., Kimble, J.M., 2001. Assessing Water Erosion Impacts on Soil Carbon Pools and Fluxes. In: Lal, R., Kimble, J.M., Follet, R.F., Steward, B.A., (ed.). *Assessment Methods for Soil Carbon*. Boca Raton, Florida, Florida: Lewis Publishers, s. 427–450.
- Jandl, R., Rodeghiero, M., Martinez, C., Cotrufo, M.F., Bampa, F., Van Wesemael, B., Harrison, R.B., Guerrini, I.A., Richter, D. DeB, Rustad, L., Lorenz, K., Chabbi, A., Miglietta, F., 2014. Current status, uncertainty and future needs in soil organic carbon monitoring. *Science of the Total Environment*. 468–469. 376–383. doi:

10.1016/j.scitotenv.2013.08.026

- Jarmer, T., Hill, J., Mader, S., 2007. The use of hyperspectral remote sensing data for the assessment of chemical properties of dryland soils in se-spain. In: *5th EARSeL Workshop on Imaging Spectroscopy*. s. 1–9.
- Jarmer, T., Hill, J., Lavée, H., Sarah, P., 2010. Mapping Topsoil Organic Carbon in Non-agricultural Semi-arid and Arid Ecosystems of Israel. *Photogrammetric Engineering & Remote Sensing*. 76 (1). 85–94. doi: 10.14358/PERS.76.1.85
- Jastrow, J.D., Amonette, J.E., Bailey, V.L., 2007. Mechanisms controlling soil carbon turnover and their potential application for enhancing carbon sequestration. *Climatic Change*. 80 (1–2). 5–23. doi: 10.1007/s10584-006-9178-3
- Jenny, H., 1941. *Factors of Soil Formation*. New York: McGraw.
- Ji, W., Viscarra Rossel, R. A., Shi, Z., 2015. Improved estimates of organic carbon using proximally sensed vis-NIR spectra corrected by piecewise direct standardization. *European Journal of Soil Science*. 66 (4). 670–678. doi: 10.1111/ejss.12271
- Joosten, H., 2015. Current soil carbon loss and land degradation globally – where are the hotspots and why there? In: Banwart, S.A., Noellemeyer, E., Milne, E., (ed.). *Soil Carbon: Science, Management and Policy for Multiple Benefits*. CAB International, s. 228–281.
- Kadlec, V., Holubík, O., Procházková, E., Urbanová, J., Tipl, M., 2012. Soil organic carbon dynamics and its influence on the soil erodibility factor. *Soil and Water Research*. 7 (3). 97–108.
- Kanning, M., Siegmann, B., Jarmer, T., 2016. Regionalization of uncovered agricultural soils based on organic carbon and soil texture estimations. *Remote Sensing*. 8 (927). 1–17. doi: 10.3390/rs8110927
- Khalil, M.I., Kiely, G., O'Brien, P., Müller, C., 2013. Organic carbon stocks in agricultural soils in Ireland using combined empirical and GIS approaches. *Geoderma*. 193–194. 222–235. doi: 10.1016/j.geoderma.2012.10.005
- Kirkels, F.M.S. A., Cammeraat, L.H., Kuhn, N.J., 2014. The fate of soil organic carbon upon erosion, transport and deposition in agricultural landscapes – A review of different concepts. *Geomorphology*. 226. 94–105. doi: 10.1016/j.geomorph.2014.07.023



- Klement, A., 2014. *Možnosti využití infračervené spektrometrie pro predikci půdních vlastností. Disertační práce.* Česká zemědělská univerzita v Praze.
- Kopačková, V., Ben-Dor, E., 2016. Normalizing reflectance from different spectrometers and protocols with an internal soil standard. *International Journal of Remote Sensing*. 37 (6). 1276–1290. doi: 10.1080/01431161.2016.1148291
- Kuhn, N.J., 2007. Erodibility of soil and organic matter: independence of organic matter resistance to interrill erosion. *Earth Surface Processes and Landforms*. 32 (5). 794–802. doi: 10.1002/esp.1486
- Kuhn, N.J., Armstrong, E.K., 2012. Erosion of organic matter from sandy soils: Solving the mass balance. *Catena*. 98. 87–95. doi: 10.1016/j.catena.2012.05.014
- Kuhn, N.J., Hoffmann, T., Schwanghart, W., Dotterweich, M., 2009. Agricultural soil erosion and global carbon cycle: controversy over? *Earth Surface Processes and Landforms*. 6. doi: 10.1002/esp.1796
- Kuhn, N.J., Van Oost, K., Cammeraat, E., 2012. Soil erosion, sedimentation and the carbon cycle. *Catena*. 94. 1–2. doi: 10.1016/j.catena.2011.11.007
- Kuhn, N.J., 2013. Assessing lateral organic Carbon movement in small agricultural catchments. *Jahrestagung der Schweizerischen Geomorphologischen Gesellschaft*. 9. 151–164.
- Kusumo, B.H., Hedley, C.B., Hedley, M.J., Hueni, A., Tuohy, M.P., Arnold, G.C., 2008. The use of diffuse reflectance spectroscopy for in situ carbon and nitrogen analysis of pastoral soils. *Australian Journal of Soil Research*. 46 (6–7). 623–635. doi: 10.1071/SR08118
- Ladoni, M., Bahrami, H.A., Alavipanah, S.K., Norouzi, A.A., 2010. Estimating soil organic carbon from soil reflectance: A review. *Precision Agriculture*. 11 (1). 82–99. doi: 10.1007/s11119-009-9123-3
- Lal, R., 2004. Soil Carbon Sequestration Impacts on Global Climate Change and Food Security. *Science*. 304 (5677). 1623–1627. doi: 10.1126/science.1097396
- Lal, R., 1995. Global Soil Erosion by Water and Carbon Dynamics. In: Lal, R., Kimble, J.M., Levine, E., Steward, B.A., (ed.). *Soils and Global Change*. Boca Raton, Florida, Florida: CRC Press, s. 131–142.
- Lal, R., 2003. Soil erosion and the global carbon budget. *Environment International*. 29

- (4). 437–450. doi: 10.1016/S0160-4120(02)00192-7
- Lal, R., 2005. Soil erosion and carbon dynamics. *Soil and Tillage Research*. 81 (2). 137–142. doi: 10.1016/j.still.2004.09.002
- Lal, R., 2010. Depletion and Restoration of Carbon in the Pedosphere. *Japanese Society of Pedology*. 53 (3). 19–32.
- Lal, R., Griffin, M., Apt, J., Lave, L., Morgan, M. G., 2004a. Managing Soil Carbon. *Science*. 304 (5669). 393–393. doi: 10.1126/science.1093079
- Lal, R., Griffin, M., Apt, J., Lave, L., Morgan, M. G., 2004b. Response to Comments on „Managing Soil Carbon". *Science*. 305 (5690). 1567d–1567d. doi: 10.1126/science.1101271
- Lee, J., Laca, E. A., Van Kessel, C., Rolston, D.E., Hopmans, J.W., Six, J., 2009. Tillage Effects on Spatiotemporal Variability of Particulate Organic Matter. *Applied and Environmental Soil Science*. 2009. 1–14. doi: 10.1155/2009/219379
- Li, Q., Yue, T., Wang, C., Zhang, W., Yu, Y., Li, B., Yang, J., Bai, G., 2013. Spatially distributed modeling of soil organic matter across China: An application of artificial neural network approach. *Catena*. 104. 210–218. doi: 10.1016/j.catena.2012.11.012
- Ließ, M., 2017a. Can conditioned Latin hypercube sampling capture pedodiversity? In: *Abstract Book Pedometrics 2017*. s. 138.
- Ließ, M., 2017b. Subsampling for dataset optimisation. In: *EGU General Assembly 2017*. Vienna, Austria: EGU, s. 2175. Dostupné z: <http://meetingorganizer.copernicus.org/EGU2017/EGU2017-2175.pdf>
- Lindstrom, M.J., Schumacher, J.A., Schumacher, T.E., 2000. TEP: A Tillage Erosion Prediction model to calculate soil translocation rates from tillage. *Journal of Soil and Water Conservation*. 55 (1). 105–108.
- Liu, H., Shi, T., Chen, Y., Wang, J., Fei, T., Wu, G., 2017. Improving Spectral Estimation of Soil Organic Carbon Content through Semi-Supervised Regression. *Remote Sensing*. 9 (1). 29. doi: 10.3390/rs9010029
- Liu, S., Bliss, N., Sundquist, E., Huntington, T.G., 2003. Modeling carbon dynamics in vegetation and soil under the impact of soil erosion and deposition. *Global Biogeochemical Cycles*. 17 (2). 43/1-43/24. doi: <http://dx.doi.org/10.1029/2002GB002010>.

- López-Fando, C., Pardo, M.T., 2011. Soil carbon storage and stratification under different tillage systems in a semi-arid region. *Soil and Tillage Research*. 111 (2). 224–230. doi: 10.1016/j.still.2010.10.011
- Lu, P., Wang, L., Niu, Z., Li, L., Zhang, W., 2013. Prediction of soil properties using laboratory VIS-NIR spectroscopy and Hyperion imagery. *Journal of Geochemical Exploration*. 132. 26–33. doi: 10.1016/j.gexplo.2013.04.003
- Luo, Z., Yaolin, L., Jian, W., Jing, W., 2008. Quantitative Mapping of Soil Organic Material Using Field Spectrometer and Hyperspectral Remote Sensing. In: *The International Archives of the Photogrammetry, Remote Sensing and Spatial Information Sciences. Vol. XXXVII. Part B8. Beijing 2008*. s. 901–906. ISBN: 978-0-7695-3682-8.
- Madari, B.E., Reeves, J.B., Machado, P.L.O. A, Guimarães, C.M., Torres, E., McCarty, G.W., 2006. Mid- and near-infrared spectroscopic assessment of soil compositional parameters and structural indices in two Ferralsols. *Geoderma*. 136 (1–2). 245–259. doi: 10.1016/j.geoderma.2006.03.026
- Malone, B., 2017. Connected multi-scale digital soil mapping, rather than producing finest grain soil map. *Pedometron*. (41). 31–32.
- Manzoni, S., Porporato, A., 2009. Soil carbon and nitrogen mineralization: Theory and models across scales. *Soil Biology and Biochemistry*. 41 (7). 1355–1379. doi: 10.1016/j.soilbio.2009.02.031
- Marchetti, A., Piccini, C., Francaviglia, R., Mabit, L., 2012. Spatial Distribution of Soil Organic Matter Using Geostatistics: A Key Indicator to Assess Soil Degradation Status in Central Italy. *Pedosphere*. 22 (2). 230–242. doi: 10.1016/S1002-0160(12)60010-1
- Martin, M.P., Wattenbach, M., Smith, P., Meersmans, J., Jolivet, C., Boulonne, L., Arrouays, D., 2011. Spatial distribution of soil organic carbon stocks in France. *Biogeosciences*. 8 (5). 1053–1065. doi: 10.5194/bg-8-1053-2011
- Martínez-Mena, M., López, J., Almagro, M., Albaladejo, J., Castillo, V., Ortiz, R., Boix-Fayos, C., 2012. Organic carbon enrichment in sediments: Effects of rainfall characteristics under different land uses in a Mediterranean area. *Catena*. 94. 36–42. doi: 10.1016/j.catena.2011.02.005

- Matarrese, R., Ancona, V., Salvatori, R., Muolo, M.R., Uricchio, V.F., Vurro, M., 2014. Detecting soil organic carbon by CASI hyperspectral images. In: *2014 IEEE Geoscience and Remote Sensing Symposium*. IEEE, s. 3284–3287. ISBN: 978-1-4799-5775-0. doi: 10.1109/IGARSS.2014.6947181
- McBratney, A.B., Mendonça Santos, M.L., Minasny, B., 2003. On digital soil mapping. *Geoderma*. 117 (1–2). 3–52. doi: 10.1016/S0016-7061(03)00223-4
- McBratney, A.B., Pringle, M.J., 1999. Estimating Average and Proportional Variograms of Soil Properties and Their Potential Use in Precision Agriculture. *Precision Agriculture*. 1 (2). 125–152. doi: 10.1023/A:1009995404447
- McBratney, A.B., Odeh, I.O. A, Bishop, T.F. A, Dunbar, M.S., Shatar, T.M., 2000. *An overview of pedometric techniques for use in soil survey*. ISBN: 6129351321. doi: 10.1016/S0016-7061(00)00043-4
- McCarty, G.W., Ritchie, J.C., 2002. Impact of soil movement on carbon sequestration in agricultural ecosystems. *Environmental Pollution*. 116 (3). 423–430. doi: 10.1016/S0269-7491(01)00219-6
- Meersmans, J., Van Wesemael, B., Van Molle, M., 2009. Determining soil organic carbon for agricultural soils: a comparison between the Walkley & Black and the dry combustion methods (north Belgium). *Soil Use and Management*. 25 (4). 346–353. doi: 10.1111/j.1475-2743.2009.00242.x
- Meersmans, J., Martin, M.P., De Ridder, F., Laccarce, E., Wetterlind, J., De Baets, S., Le Bas, C., Louis, B.P., Orton, T.G., Bispo, A., Arrouays, D., 2012. A novel soil organic C model using climate, soil type and management data at the national scale in France. *Agronomy for Sustainable Development*. 32 (4). 873–888. doi: 10.1007/s13593-012-0085-x
- Meersmans, J., Quine, T., 2013. Refining regional SOC estimates: Accounting for erosion induced within field variability of the vertical distribution of SOC. In: *Geophysical Research Abstracts*. EGU General Assembly. EGU, s. 12846. Dostupné z: <http://adsabs.harvard.edu/abs/2013EGUGA..1512846M>
- Milne, E., Banwart, S. A., Noellemeyer, E., Abson, D.J., Ballabio, C., Bampa, F., Bationo, A., Batjes, N.H., Bernoux, M., Bhattacharyya, T., Black, H., Buschiazzo, D.E., Cai, Z., Cerri, C.E., Cheng, K., Compagnone, C., Conant, R., Coutinho, H.L.C.,

- De Brogniez, D., Balieiro, F.D.C., Duffy, C., Feller, C., Fidalgo, E.C.C., Da Silva, C.F., Funk, R., Gaudig, G., Gicheru, P.T., Goldhaber, M., Gottschalk, P., Goulet, F., Goverse, T., Grathwohl, P., Joosten, H., Kamoni, P.T., Kihara, J., Krawczynski, R., La Scala, N., Lemanceau, P., Li, L., Li, Z., Lugato, E., Maron, P.-A., Martius, C., Melillo, J., Montanarella, L., Nikolaidis, N., Nziguheba, G., Pan, G., Pascual, U., Paustian, K., Piñeiro, G., Powelson, D., Quiroga, A., Richter, D., Sigwalt, A., Six, J., Smith, J., Smith, P., Stocking, M., Tanneberger, F., Termansen, M., Van Noordwijk, M., Van Wesemael, B., Vargas, R., Victoria, R.L., Waswa, B., Werner, D., Wichmann, S., Wichtmann, W., Zhang, X., Zhao, Y., Zheng, J., Zheng, J., 2015. Soil carbon, multiple benefits. *Environmental Development*. 13 (14). 33–38. doi: 10.1016/j.envdev.2014.11.005
- Minasny, B., 2018. Classic Art as Covariates in Digital mapping. *Pedometron*. (42). 16.
- Minasny, B., Ma, Y., 2018. Highway to the Danger Zones. *Pedometron*. (42). 26–27.
- Minasny, B., McBratney, A.B., 2015. Digital soil mapping: A brief history and some lessons. *Geoderma*. 16. 2022. doi: 10.1016/j.geoderma.2015.07.017
- Minasny, B., McBratney, A.B., 2006. A conditioned Latin hypercube method for sampling in the presence of ancillary information. *Computers & Geosciences*. 32 (9). 1378–1388. doi: 10.1016/j.cageo.2005.12.009
- Minasny, B., McBratney, A.B., Malone, B.P., Wheeler, I., 2013. *Digital Mapping of Soil Carbon*. ISBN: 978-0-12-4059429. doi: 10.1016/B978-0-12-405942-9.00001-3
- Minu, S., Shetty, A., Gopal, B., Filchev, L.H., 2016. Review of preprocessing techniques used in soil property prediction from hyperspectral data. *Cogent Geoscience*. 1–16. doi: 10.1080/23312041.2016.1145878
- Mondal, A., Khare, D., Kundu, S., Mondal, S., Mukherjee, S., Mukhopadhyay, A., 2017. Spatial soil organic carbon (SOC) prediction by regression kriging using remote sensing data. *The Egyptian Journal of Remote Sensing and Space Science*. National Authority for Remote Sensing and Space Sciences, 20 (1). 61–70. doi: 10.1016/j.ejrs.2016.06.004
- Morgan, R.P.C., 2005. *Soil Erosion and Conservation*. 3. vyd. Oxford: Blackwell Publishing. ISBN: 1-4051-1781-8.
- Mulder, V.L., De Bruin, S., Schaepman, M.E., Mayr, T.R., 2011. The use of remote

- sensing in soil and terrain mapping - A review. *Geoderma*. 162 (1–2). 1–19. doi: 10.1016/j.geoderma.2010.12.018
- Müller-Nedebock, D., Chaplot, V., 2015. Soil carbon losses by sheet erosion: a potentially critical contribution to the global carbon cycle. *Earth Surface Processes and Landforms*. 3758. doi: 10.1002/esp.3758
- Nadeu, E., Berhe, A. A., De Vente, J., Boix-Fayos, C., 2012. Erosion, deposition and replacement of soil organic carbon in Mediterranean catchments: A geomorphological, isotopic and land use change approach. *Biogeosciences*. 9 (3). 1099–1111. doi: 10.5194/bg-9-1099-2012
- Nocita, M., Kooistra, L., Bachmann, M., Müller, A., Powell, M., Weel, S., 2011. Predictions of soil surface and topsoil organic carbon content through the use of laboratory and field spectroscopy in the Albany Thicket Biome of Eastern Cape Province of South Africa. *Geoderma*. 167–168. 295–302. doi: 10.1016/j.geoderma.2011.09.018
- Nocita, M., Stevens, A., Noon, C., Van Wesemael, B., 2013. Prediction of soil organic carbon for different levels of soil moisture using Vis-NIR spectroscopy. *Geoderma*. 199. 37–42. doi: 10.1016/j.geoderma.2012.07.020
- Nocita, M., Stevens, A., Van Wesemael, B., Brown, D.J., Shepherd, K.D., Towett, E., Vargas, R., Montanarella, L., 2015. Soil spectroscopy: an opportunity to be seized. *Global Change Biology*. 21 (1). 10–11. doi: 10.1111/gcb.12632
- Noon, C., Stevens, A., Van Oost, K., Six, J., 2013. Mid-infrared spectroscopy as a tool to identify and quantify soil organic carbon size fractions. In: *Geophysical Research Abstracts, Vol. 15, EGU General Assembly 2013*. Wien: EGU, s. 3836.
- Nowkandeh, S.M., Homae, M., Noroozi, A A, 2013. Mapping Soil Organic Matter Using Hyperion Images. *International Journal of Agronomy and Plant Production*. 4 (8). 1753–1759.
- O'Rourke, S.M., Holden, N.M., 2011. Optical sensing and chemometric analysis of soil organic carbon - a cost effective alternative to conventional laboratory methods? *Soil Use and Management*. 27 (2). 143–155. doi: 10.1111/j.1475-2743.2011.00337.x
- Odeh, I.O.A., McBratney, A.B., Chittleborough, D.J., 1995. Further results on prediction of soil properties from terrain attributes: heterotopic cokriging and regression-

- kriging. *Geoderma*. 67 (3–4). 215–226. doi: 10.1016/0016-7061(95)00007-B
- Parton, W.J., Del Grosso, S.J., Plante, A.F., Adair, E.C., Lutz, S.M., 2015. Modeling the Dynamics of Soil Organic Matter and Nutrient Cycling. In: Paul, E.A., (ed.). *Soil Microbiology, Ecology and Biochemistry (Fourth Edition)*. 4. vyd. Natural Resource Ecology Laboratory and Department of Soil and Crop Sciences, Colorado State University Fort Collins: Elsevier, s. 505–537. doi: 10.1016/B978-0-12-415955-6.00017-7
- Pascucci, S., Casa, R., Belviso, C., Palombo, A., Pignatti, S., Castaldi, F., 2014. Estimation of soil organic carbon from airborne hyperspectral thermal infrared data: a case study. *European Journal of Soil Science*. 65 (6). 865–875. doi: 10.1111/ejss.12203
- Patzold, S., Mertens, F.M., Bornemann, L., Koleczek, B., Franke, J., Feilhauer, H., Welp, G., 2008. Soil heterogeneity at the field scale: A challenge for precision crop protection. *Precision Agriculture*. 9 (6). 367–390. doi: 10.1007/s11119-008-9077-x
- Peng, X., Shi, T., Song, A., Chen, Y., Gao, W., 2014. Estimating soil organic carbon using VIS/NIR spectroscopy with SVMR and SPA methods. *Remote Sensing*. 6 (4). 2699–2717. doi: 10.3390/rs6042699
- Penížek, V., 2005. *Testování různých pedometrických metod pro zpracování výsledků půdního průzkumu. Disertační práce*. Česká zemědělská univerzita v Praze.
- Penížek, V., Zádorová, T., Kodešová, R., Klement, A., 2014. *Optimalizace vzorkovací sítě pomocí využití analýzy reliéfu pro popis prostorové variability půdních vlastností v rámci půdních bloků : certifikovaná metodika*. Praha: Česká zemědělská univerzita v Praze. ISBN: 978-80-213-2533-3.
- Pennock, D.J., Frick, A. H., 2001. The role of field studies in landscape-scale applications of process models: An example of soil redistribution and soil organic carbon modeling using CENTURY. *Soil and Tillage Research*. 58 (3–4). 183–191. doi: 10.1016/S0167-1987(00)00167-7
- Pimstein, A., Notesco, G., Ben-Dor, E., 2011. Performance of Three Identical Spectrometers in Retrieving Soil Reflectance under Laboratory Conditions. *Soil Science Society of America Journal*. 75 (2). 746. doi: 10.2136/sssaj2010.0174
- Plante, A.F., Parton, W.J., 2007. The Dynamics of Soil Organic Matter and Nutrient

- Cycling. In: Paul, E.A., (ed.). *Soil Microbiology and Biochemistry*. third edit. Elsevier, s. 433–470. ISBN: 9780125468077.
- Polyakov, V., Lal, R., 2004. Modeling soil organic matter dynamics as affected by soil water erosion. *Environment International*. 30 (4). 547–556. doi: 10.1016/j.envint.2003.10.011
- Polyakov, V., Lal, R., 2008. Soil organic matter and CO<sub>2</sub> emission as affected by water erosion on field runoff plots. *Geoderma*. 143 (1–2). 216–222. doi: 10.1016/j.geoderma.2007.11.005
- Powelson, D.S., Whitmore, A. P., Goulding, K.W.T., 2011. Soil carbon sequestration to mitigate climate change: A critical re-examination to identify the true and the false. *European Journal of Soil Science*. 62 (1). 42–55. doi: 10.1111/j.1365-2389.2010.01342.x
- Quine, T.A., Van Oost, K., 2007. Quantifying carbon sequestration as a result of soil erosion and deposition: Retrospective assessment using caesium-137 and carbon inventories. *Global Change Biology*. 13 (12). 2610–2625. doi: 10.1111/j.1365-2486.2007.01457.x
- Quinton, J.N., Catt, J. A., Wood, G. A., Steer, J., 2006. Soil carbon losses by water erosion: Experimentation and modeling at field and national scales in the UK. *Agriculture, Ecosystems and Environment*. 112 (1). 87–102. doi: 10.1016/j.agee.2005.07.005
- Quinton, J.N., Govers, G., Van Oost, K., Bardgett, R.D., 2010. The impact of agricultural soil erosion on biogeochemical cycling. *Nature Geoscience*. 3 (5). 311–314. doi: 10.1038/ngeo838
- Ranatunga, K., Hill, M.J., Probert, M.E., Dalal, R.C., 2001. Comparative Application of APSIM, RothC and Century to Predict Soil Carbon Dynamics. In: Ghassemi, F., Whetton, P., Little, R., Littleboy, M., (ed.). *MODSIM2001, International Congress on Modelling and Simulation*. Canberra: ANU, s. 733–738.
- Ray, S.S., Singh, J.P., Das, G., Panigrahy, S., Group, A.R., Centre, S.A., Potato, C., 2004. Use of High Resolution Remote Sensing Data For Generatin Site-Specific Soil Mangement Plan. In: *XX ISPRS Congress, Commission VII, Working Group VII/2, The International Archives of the Photogrammetry, Remote Sensing and Spatial*



*Information Sciences*. s. 127–131.

- Reeves, J.B., 2010. Near- versus mid-infrared diffuse reflectance spectroscopy for soil analysis emphasizing carbon and laboratory versus on-site analysis: Where are we and what needs to be done? *Geoderma*. 158 (1–2). 3–14. doi: 10.1016/j.geoderma.2009.04.005
- Reicosky, D.C., Lindstrom, M.J., Schumacher, T.E., Lobb, D.E., Malo, D.D., 2005. Tillage-induced CO<sub>2</sub> loss across an eroded landscape. *Soil and Tillage Research*. 81 (2). 183–194. doi: 10.1016/j.still.2004.09.007
- Renwick, W.H., Smith, S. V, Slezzer, R.O., Buddemeier, R.W., 2004. Comment on „Managing Soil Carbon" (II). *Science*. 305 (5690). 1567c–1567c. doi: 10.1126/science.1100447
- Rienzi, E.A., Mijatovic, B., Mueller, T.G., Matocha, C.J., Sikora, F.J., Castrignanò, A., 2014. Prediction of Soil Organic Carbon under Varying Moisture Levels Using Reflectance Spectroscopy. *Soil Science Society of America Journal*. 78 (3). 958. doi: 10.2136/sssaj2013.09.0408
- Ritchie, J.C., McCarty, G.W., Venteris, E.R., Kaspar, T.C., 2007. Soil and soil organic carbon redistribution on the landscape. *Geomorphology*. 89 (1–2 SPEC. ISS.). 163–171. doi: 10.1016/j.geomorph.2006.07.021
- Roberts, D.F., Adamchuk, V.I., Shanahan, J.F., Ferguson, R.B., Schepers, J.S., 2011. Estimation of surface soil organic matter using a ground-based active sensor and aerial imagery. *Precision Agriculture*. 12 (1). 82–102. doi: 10.1007/s11119-010-9158-5
- Rodríguez-Lado, L., Martínez-Cortizas, A., 2015. Modelling and mapping organic carbon content of topsoils in an Atlantic area of southwestern Europe ( Galicia , NW-Spain ). *Geoderma*. 245–246. 65–73. doi: 10.1016/j.geoderma.2015.01.015
- Rogge, D., Bauer, A., Zeidler, J., Mueller, A., Esch, T., Heiden, U., 2018. Building an exposed soil composite processor (SCMaP) for mapping spatial and temporal characteristics of soils with Landsat imagery (1984–2014). *Remote Sensing of Environment*. 205. 1–17. doi: 10.1016/j.rse.2017.11.004
- Rosenbloom, N. A., Harden, J.W., Neff, J.C., Schimel, D.S., 2006. Geomorphic control of landscape carbon accumulation. *Journal of Geophysical Research*:

- Biogeosciences*. 111 (1). 1–10. doi: 10.1029/2005JG000077
- Rossiter, D.G., 2017. Maps and models are never valid, but they can be evaluated. *Pedometron*. (41). 19–21.
- Samuel-Rosa, A., 2017. Why do we always want higher resolution covariates? *Pedometron*. (41). 29–30.
- Sanderman, J., Chappell, A., 2013. Uncertainty in soil carbon accounting due to unrecognized soil erosion. *Global Change Biology*. 19 (1). 264–272. doi: 10.1111/gcb.12030
- Sato, J.H., Figueiredo, C.C. De, Marchão, R.L., Madari, B.E., Benedito, L.E.C., Busato, J.G., Souza, D.M. De, 2014. Methods of soil organic carbon determination in Brazilian savannah soils. *Scientia Agricola*. 71 (4). 302–308. doi: 10.1590/0103-9016-2013-0306
- Schils, R., Kuikman, P., Liski, J., Van Oijen, M., Smith, P., Webb, J., Alm, J., Somogyi, Z., Van den Akker, J., Billett, M., Emmett, B., Evans, C., Lindner, M., Palosuo, T., Bellamy, P., Jandl, R., Hiederer, R., 2008. *Review of existing information on the interrelations between soil and climate change. (ClimSoil). Final report*. doi: 10.2779/12723
- Schmid, T., Rodriguez-Rastrero, M., Escribano, P., Palacios-Orueta, A., Ben-Dor, E., Plaza, A., Milewski, R., Huesca, M., Bracken, A., Cicuendez, V., Pelayo, M., Chabrillat, S., 2016. Characterization of Soil Erosion Indicators Using Hyperspectral Data From a Mediterranean Rainfed Cultivated Region. *IEEE Journal of Selected Topics in Applied Earth Observations and Remote Sensing*. 9 (2). 845–860. doi: 10.1109/JSTARS.2015.2462125
- Schwanghart, W., Jarmer, T., 2011. Linking spatial patterns of soil organic carbon to topography - A case study from south-eastern Spain. *Geomorphology*. 126 (1–2). 252–263. doi: 10.1016/j.geomorph.2010.11.008
- Selige, T., Böhner, J., Schmidhalter, U., 2006. High resolution topsoil mapping using hyperspectral image and field data in multivariate regression modeling procedures. *Geoderma*. 136 (1–2). 235–244. doi: 10.1016/j.geoderma.2006.03.050
- Shi, Z., Ji, W., Viscarra Rossel, R. A., Chen, S., Zhou, Y., 2015. Prediction of soil organic matter using a spatially constrained local partial least squares regression and the

- Chinese vis-NIR spectral library. *European Journal of Soil Science*. 1–9. doi: 10.1111/ejss.12272
- Shibu, M.E., Leffelaar, P. A., Van Keulen, H., Aggarwal, P.K., 2006. Quantitative description of soil organic matter dynamics-A review of approaches with reference to rice-based cropping systems. *Geoderma*. 137 (1–2). 1–18. doi: 10.1016/j.geoderma.2006.08.008
- Siegmann, B., Jarmer, T., Selige, T., Lilienthal, H., Richter, N., Hofle, B., 2012. Using hyperspectral remote sensing data for the assessment of topsoil organic carbon from agricultural soils. In: Neale, C.M.U., Maltese, A., (ed.). *Remote Sensing for Agriculture, Ecosystems, and Hydrology XIV*. ISBN: 0277-786X. doi: Artn 85312c\rDoi 10.1117/12.974509
- Sleutel, S., De Neve, S., Singier, B., Hofman, G., 2007. Quantification of Organic Carbon in Soils: A Comparison of Methodologies and Assessment of the Carbon Content of Organic Matter. *Communications in Soil Science and Plant Analysis*. 38 (19–20). 2647–2657. doi: 10.1080/00103620701662877
- Smith, J., Smith, P., Wattenbach, M., Zaehle, S., Hiederer, R., Jones, R.J. A, Montanarella, L., Rounsevell, M.D. A, Reginster, I., Ewert, F., 2005a. Projected changes in mineral soil carbon of European croplands and grasslands, 1990–2080. *Global Change Biology*. 11. 2141–2152. doi: 10.1111/j.1365-2486.2005.01075.x
- Smith, P., 2006. Organic Matter Modeling. In: Lal, R., (ed.). *Encyclopedia of Soil Science*. second edi. Boca Raton, Florida: Taylor and Francis/CRC Press, s. 1196–1202. ISBN: 9780849338304.
- Smith, P., Andrén, O., Karlsson, T., Perälä, P., Regina, K., Rounsevell, M., Van Wesemael, B., 2005b. Carbon sequestration potential in European croplands has been overestimated. *Global Change Biology*. 11 (12). 2153–2163. doi: 10.1111/j.1365-2486.2005.01052.x
- Smith, P., Gottschalk, P., Smith, J., 2015. Climate Change and Soil Carbon Impacts. In: Banwart, S.A., Noellemeyer, E., Milne, E., (ed.). *Soil Carbon: Science, Management and Policy for Multiple Benefits*. CAB International, s. 235–242.
- Smith, S. V, Renwick, W.H., Buddemeier, R.W., Crossland, C.J., 2001. Budgets of soil erosion and deposition for sediments and sedimentary organic carbon across the

- conterminous United States. *Global Biogeochemical Cycles*. 15 (3). 697–707. doi: 10.1029/2000GB001341
- Song, X., Brus, D.J., Liu, F., Li, D., Zhao, Y., Yang, J., Zhang, G., 2016. Mapping soil organic carbon content by geographically weighted regression: A case study in the Heihe River Basin, China. *Geoderma*. Elsevier B.V., 261. 11–22. doi: 10.1016/j.geoderma.2015.06.024
- Starr, G.C., Lal, R., Malone, R., Hothem, D., Owens, L., Kimble, J., 2000. Modeling Soil Carbon Transported By Water Erosion Processes. *Land Degradation & Development*. 11. 83–91.
- Steinberg, A., Chabrillat, S., Stevens, A., Segl, K., Foerster, S., 2016. Prediction of Common Surface Soil Properties Based on Vis-NIR Airborne and Simulated EnMAP Imaging Spectroscopy Data: Prediction Accuracy and Influence of Spatial Resolution. *Remote Sensing*. 8 (7). 613–633. doi: 10.3390/rs8070613
- Stenberg, B., Viscarra Rossel, R.A., Mouazen, A.M., Wetterlind, J., 2010. Visible and Near Infrared Spectroscopy in Soil Science. In: *Advances in Agronomy*. s. 163–215. ISBN: 0065-2113 978-0-12-381033-5. doi: 10.1016/S0065-2113(10)07005-7
- Stevens, A., Wesemael, B. Van, Touré, S., Vandenschrack, G., Tychon, B., 2004. Can hyperspectral techniques improve estimates of carbon stocks in agricultural soils? In: *Proceedings of the Airborne Imaging Spectroscopy Workshop - Bruges, 8 October 2004*.
- Stevens, A., Miralles, I., Van Wesemael, B., 2012. Soil Organic Carbon Predictions by Airborne Imaging Spectroscopy: Comparing Cross-Validation and Validation. *Soil Science Society of America Journal*. 76 (6). 2174. doi: 10.2136/sssaj2012.0054
- Stevens, A., Nocita, M., Tóth, G., Montanarella, L., Van Wesemael, B., 2013. Prediction of Soil Organic Carbon at the European Scale by Visible and Near InfraRed Reflectance Spectroscopy. *PLoS One*. 19.6., 8 (6). e66409. doi: 10.1371/journal.pone.0066409
- Stevens, A., Udelhoven, T., Denis, A., Tychon, B., Liroy, R., Hoffmann, L., Van Wesemael, B., 2010. Measuring soil organic carbon in croplands at regional scale using airborne imaging spectroscopy. *Geoderma*. 158 (1–2). 32–45. doi: 10.1016/j.geoderma.2009.11.032

- Stevens, A., Van Wesemael, B., Bartholomeus, H.M., Rosillon, D., Tychon, B., Ben-Dor, E., 2008. Laboratory, field and airborne spectroscopy for monitoring organic carbon content in agricultural soils. *Geoderma*. 144 (1–2). 395–404. doi: 10.1016/j.geoderma.2007.12.009
- Stevens, A., Van Wesemael, B., Vandenschrick, G., Touré, S., Tychon, B., 2006. Detection of Carbon Stock Change in Agricultural Soils Using Spectroscopic Techniques. *Soil Science Society of America Journal*. 70 (3). 844–850. doi: 10.2136/sssaj2005.0025
- Stevens, F., Bogaert, P., Wesemael, B. Van, 2015. Detecting and quantifying field-related spatial variation of soil organic carbon using mixed-effect models and airborne imagery. *Geoderma*. 259–260. 93–103. doi: 10.1016/j.geoderma.2015.05.008
- Stockman, U., Adams, M., Crawford, J., Field, D., Henakaarchchi, N., Jenkins, M., McBratney, A., De Courcelles, V.D.R., Singh, K., Stockmann, U., Wheeler, I., 2011. *Managing the soil-plant system to mitigate atmospheric CO<sub>2</sub>*.
- Summers, D., Lewis, M., Ostendorf, B., Chittleborough, D., 2011. Visible near-infrared reflectance spectroscopy as a predictive indicator of soil properties. *Ecological Indicators*. 11 (1). 123–131. doi: 10.1016/j.ecolind.2009.05.001
- Tang, X., Liu, S., Liu, J., Zhou, G., 2010. Effects of vegetation restoration and slope positions on soil aggregation and soil carbon accumulation on heavily eroded tropical land of Southern China. *Journal of Soils and Sediments*. 10 (3). 505–513. doi: 10.1007/s11368-009-0122-9
- Ten Caten, A., Dalmolin, R.S.D., Pedron, F.A., Ruiz, L.F.C., Da Silva, C.A., 2013. An appropriate data set size for digital soil mapping in Erechim, Rio Grande do Sul, Brazil. *Revista Brasileira de Ciência do Solo*. 37 (2). 359–366. doi: 10.1590/S0100-06832013000200007
- Tiwari, S.K., Saha, S.K., Kumar, S., 2015. Prediction Modeling and Mapping of Soil Carbon Content Using Artificial Neural Network, Hyperspectral Satellite Data and Field Spectroscopy. *Advances in Remote Sensing*. 4 (1). 63–72. doi: 10.4236/ars.2015.41006
- Todd-Brown, K.E.O., Randerson, J.T., Post, W.M., Hoffman, F.M., Tarnocai, C., Schuur, E. a G., Allison, S.D., 2013. Causes of variation in soil carbon simulations from

- CMIP5 Earth system models and comparison with observations. *Biogeosciences*. 10 (3). 1717–1736. doi: 10.5194/bg-10-1717-2013
- Toure, S., Tychon, B., 2004. Airborne hyperspectral measurements and superficial soil organic matter. In: *Proceedings of the Airborne Imaging Spectroscopy Workshop-Bruges*. s. 1–6. Dostupné z: <http://eo.belspo.be/Docs/Resources/Publications/bruhyp2004/toure.pdf>
- Touré, S., Tychon, B., 2003. Estimation of Surface Soil Organic Matter by Means of Hyperspectral Data Analysis. In: *Thematic day of the Belgian Soil Science Society Carbon sequestration in terrestrial ecosystems*. Brussels: Ghent University, Université Catholique de Louvain, s. 27–32.
- Uno, Y., Prasher, S., Patel, R., Strachan, I., Pattey, E., Karimi, Y., 2005. Development of field-scale soil organic matter content estimation models in Eastern Canada using airborne hyperspectral imagery. *Canadian Biosystems Engineering/Le génie des biosystèmes au Canada*. 47. 1–9.
- Van Hemelryck, H., Fiener, P., Van Oost, K., Govers, G., Merckx, R., 2010. The effect of soil redistribution on soil organic carbon: An experimental study. *Biogeosciences*. 7 (12). 3971–3986. doi: 10.5194/bg-7-3971-2010
- Van Hemelryck, H., Govers, G., Van Oost, K., Merckx, R., 2011. Evaluating the impact of soil redistribution on the in situ mineralization of soil organic carbon. *Earth Surface Processes and Landforms*. 36 (4). 427–438. doi: 10.1002/esp.2055
- Van Oost, K., Cerdan, O., Quine, T. A., 2009. Accelerated sediment fluxes by water and tillage erosion on European agricultural land. *Earth Surface Processes and Landforms*. 34 (12). 1625–1634. doi: 10.1002/esp.1852
- Van Oost, K., Govers, G., Quine, T. A., Heckrath, G., 2004. Comment on „Managing Soil Carbon" (I). *Science*. 305 (5690). 1567b–1567b. doi: 10.1126/science.1100273
- Van Oost, K., Govers, G., Van Muysen, W., 2003. A process-based conversion model for caesium-137 derived erosion rates on agricultural land: an integrated spatial approach. *Earth Surface Processes and Landforms*. 28 (2). 187–207. doi: 10.1002/esp.446
- Van Oost, K., Govers, G., Quine, T. A., Heckrath, G., Olesen, J.E., De Gryze, S., Merckx, R., 2005. Landscape-scale modeling of carbon cycling under the impact of soil

- redistribution: The role of tillage erosion. *Global Biogeochemical Cycles*. 19 (4). 1–13. doi: 10.1029/2005GB002471
- Van Oost, K., Quine, T.A., Govers, G., De Gryze, S., Six, J., Harden, J.W., Ritchie, J.C., McCarty, G.W., Heckrath, G., Kosmas, C., Giraldez, J.V., Da Silva, J.R.M., Merckx, R., 2007. The impact of agricultural soil erosion on the global carbon cycle. *Science*. 318 (5850). 626–629. doi: 10.1126/science.1145724
- VandenBygaart, A. J., Gregorich, E.G., Angers, D. A., 2003. Influence of agricultural management on soil organic carbon: A compendium and assessment of Canadian studies. *Canadian Journal of Soil Science*. 83 (4). 363–380. doi: 10.4141/S03-009
- VandenBygaart, A.J., Gregorich, E.G., Helgason, B.L., 2015. Cropland C erosion and burial: Is buried soil organic matter biodegradable? *Geoderma*. 239–240. 240–249. doi: 10.1016/j.geoderma.2014.10.011
- Varvel, G.E., Schlemmer, M.R., Schepers, J.S., 1999. Relationship Between Spectral Data from an Aerial Image and Soil Organic Matter and Phosphorus Levels. *Precision Agriculture*. 1. 291–300.
- Vasques, G.M., Grunwald, S., Sickman, J.O., 2008. Comparison of multivariate methods for inferential modeling of soil carbon using visible/near-infrared spectra. *Geoderma*. 146 (1–2). 14–25. doi: 10.1016/j.geoderma.2008.04.007
- Vaudour, E., Gilliot, J.M., Bel, L., Lefevre, J., Chehdi, K., 2016a. Regional prediction of soil organic carbon content over temperate croplands using visible near-infrared airborne hyperspectral imagery and synchronous field spectra. *International Journal of Applied Earth Observation and Geoinformation*. 49. 24–38. doi: 10.1016/j.jag.2016.01.005
- Vaudour, E., Gilliot, J.M., Bel, L., Lefevre, J., Chehdi, K., 2016b. Regional prediction of soil organic carbon content over temperate croplands using visible near-infrared airborne hyperspectral imagery and synchronous field spectra. *International Journal of Applied Earth Observation and Geoinformation*. 49 (June). 24–38. doi: 10.1016/j.jag.2016.01.005
- Veronesi, F., Corstanje, R., Mayr, T., 2014. Landscape scale estimation of soil carbon stock using 3D modelling. *Science of the Total Environment*. 487. 578–586. doi: 10.1016/j.scitotenv.2014.02.061

- Victoria, R., Banwart, S., Black, H., Ingram, J., Joosten, H., Milne, E., Noellemeyer, E., Baskin, Y., 2012. The Benefits of Soil Carbon: Managing soils for multiple economic, societal and environmental benefits. In: UNEP, (ed.). *UNEP Year Book: Emerging Issues in our Global Environment 2012*. Nairobi: United Nations Environmental Programme, s. 19–33. ISBN: 978-92-807-3214-6. Dostupné z: [http://www.unep.org/yearbook/2012/pdfs/UYB\\_2012\\_CH\\_2.pdf](http://www.unep.org/yearbook/2012/pdfs/UYB_2012_CH_2.pdf)
- Vindušková, O., 2013. *Metody odlišení fosilní a recentní organické hmoty v půdách výsypek. Diplomová práce*. Univerzita Karlova v Praze.
- Viscarra Rossel, R. A., Minasny, B., Roudier, P., McBratney, A. B., 2006a. Colour space models for soil science. *Geoderma*. 133 (3–4). 320–337. doi: 10.1016/j.geoderma.2005.07.017
- Viscarra Rossel, R. A., Walvoort, D.J.J., McBratney, A. B., Janik, L.J., Skjemstad, J.O., 2006b. Visible, near infrared, mid infrared or combined diffuse reflectance spectroscopy for simultaneous assessment of various soil properties. *Geoderma*. 131 (1–2). 59–75. doi: 10.1016/j.geoderma.2005.03.007
- Viscarra Rossel, R.A., Behrens, T., 2010. Using data mining to model and interpret soil diffuse reflectance spectra. *Geoderma*. 158 (1–2). 46–54. doi: 10.1016/j.geoderma.2009.12.025
- Viscarra Rossel, R. A., 2009. The Soil Spectroscopy Group and the development of a global soil spectral library. In: *Geophysical Research Abstracts, EGU 2009*.
- Voroney, R.P., Van Veen, J.A., Paul, E.A., 1981. Organic C Dynamics in Grassland Soils. Model Validation and Simulation of the Long-term Effects of Cultivation and Rainfall Erosion. *Canadian Journal of Soil Science*. 61 (2). 211–224. doi: 10.4141/cjss81-026
- Výzkumný ústav meliorací a ochrany půdy, 2015. *Větrná eroze* [vid. 23. červenec 2015]. Dostupné z: <http://geoportal.vumop.cz/index.php?projekt=vetrna>
- Wang, J., He, T., Lv, C., Chen, Y., Jian, W., 2010a. Mapping soil organic matter based on land degradation spectral response units using Hyperion images. *International Journal of Applied Earth Observation and Geoinformation*. 12 (SUPPL. 2). S171–S180. doi: 10.1016/j.jag.2010.01.002
- Wang, X., Cammeraat, E.L.H., Romeijn, P., Kalbitz, K., 2014a. Soil Organic Carbon



- Redistribution by Water Erosion – The Role of CO<sub>2</sub> Emissions for the Carbon Budget. *PLoS ONE*. 6.5., 9 (5). e96299. doi: 10.1371/journal.pone.0096299
- Wang, Z., Van Oost, K., Lang, A., Quine, T., Clymans, W., Merckx, R., Notebaert, B., Govers, G., 2014b. The fate of buried organic carbon in colluvial soils: a long-term perspective. *Biogeosciences*. 11 (3). 873–883. doi: 10.5194/bg-11-873-2014
- Wang, Z., Govers, G., Steegen, A., Clymans, W., Van den Putte, A., Langhans, C., Merckx, R., Van Oost, K., 2010b. Catchment-scale carbon redistribution and delivery by water erosion in an intensively cultivated area. *Geomorphology*. 124 (1–2). 65–74. doi: 10.1016/j.geomorph.2010.08.010
- Watson, R.T., Noble, I.R., Bolin, B., Ravindranath, N.H., Verardo, D.J., Dokken, D.J., 2000. *Models*.
- Webb, N.P., Chappell, A., Strong, C.L., Marx, S.K., McTainsh, G.H., 2012. The significance of carbon-enriched dust for global carbon accounting. *Global Change Biology*. 18 (11). 3275–3278. doi: 10.1111/j.1365-2486.2012.02780.x
- Were, K., Bui, D.T., Dick, Ø.B., Singh, B.R., 2015. A comparative assessment of support vector regression, artificial neural networks, and random forests for predicting and mapping soil organic carbon stocks across an Afromontane landscape. *Ecological Indicators*. 52. 394–403. doi: 10.1016/j.ecolind.2014.12.028
- West, T.O., Wali, M.K., 2002. Modeling Regional Carbon Dynamics and Soil Erosion in Disturbed and Rehabilitated Ecosystems as Affected by Land Use and Climate. *Water, Air, and Soil Pollution*. 138 (1/4). 141–164. doi: 10.1023/A:1015552330945
- Wiesmeier, M., Barthold, F., Spörlein, P., Geuß, U., Hangen, E., Reischl, A., Schilling, B., Angst, G., Von Lützwow, M., Kögel-Knabner, I., 2014. Estimation of total organic carbon storage and its driving factors in soils of Bavaria (southeast Germany). *Geoderma Regional*. 1. 67–78. doi: 10.1016/j.geodrs.2014.09.001
- Wu, C., Wu, J., Luo, Y., Zhang, L., DeGloria, S.D., 2009. Spatial Prediction of Soil Organic Matter Content Using Cokriging with Remotely Sensed Data. *Soil Science Society of America Journal*. 73 (4). 1202–1208. doi: 10.2136/sssaj2008.0045
- Xiaojun, N., Jianhui, Z., Zhengan, S., 2013. Dynamics of Soil Organic Carbon and Microbial Biomass Carbon in Relation to Water Erosion and Tillage Erosion. *PLoS ONE*. 8 (5). 1–7. doi: 10.1371/journal.pone.0064059

- Xin, Z., Qin, Y., Yu, X., 2016. Spatial variability in soil organic carbon and its influencing factors in a hilly watershed of the Loess Plateau, China. *Catena*. 137. 660–669. doi: 10.1016/j.catena.2015.01.028
- Xu, D., Ma, W., Chen, S., Jiang, Q., He, K., Shi, Z., 2018. Assessment of Important Soil Properties Related to Chinese Soil Taxonomy Based on vis – NIR Reflectance Spectroscopy Assessment of important soil properties related to Chinese Soil Taxonomy based on vis – NIR reflectance spectroscopy. *Computers and Electronics in Agriculture*. 144 (41461063). 1–8. doi: 10.1016/j.compag.2017.11.029
- Yadav, V., Malanson, G.P., 2009. Modeling impacts of erosion and deposition on soil organic carbon in the Big Creek Basin of southern Illinois. *Geomorphology*. 106 (3–4). 304–314. doi: 10.1016/j.geomorph.2008.11.011
- Young, C.J., Liu, S., Schumacher, J. A., Schumacher, T.E., Kaspar, T.C., McCarty, G.W., Napton, D., Jaynes, D.B., 2014. Evaluation of a model framework to estimate soil and soil organic carbon redistribution by water and tillage using <sup>137</sup>Cs in two U.S. Midwest agricultural fields. *Geoderma*. 232–234. 437–448. doi: 10.1016/j.geoderma.2014.05.019
- Zádorová, T., Penížek, V., 2018. Formation, morphology and classification of colluvial soils: a review. *European Journal of Soil Science*. 69 (4). 577–591. doi: 10.1111/ejss.12673
- Zádorová, T., 2009. *Koluvizemě - jejich charakteristika a problematika plošného vymezení ve vybraných oblastech České republiky. Disertační práce*. Praha. Univerzita Karlova v Praze.
- Zádorová, T., Penížek, V., Žížala, D., Matějovský, J., Vaněk, A., 2018. Influence of former lynchets on soil cover structure and soil organic carbon storage in agricultural land, Central Czechia. *Soil Use and Management*. 34 (1). 60–71. doi: 10.1111/sum.12406
- Zádorová, T., Penížek, V., Šefrna, L., Drábek, O., Mihaljevič, M., Volf, Š., Chuman, T., 2013. Identification of Neolithic to Modern erosion-sedimentation phases using geochemical approach in a loess covered sub-catchment of South Moravia, Czech Republic. *Geoderma*. 195–196. 56–69. doi: 10.1016/j.geoderma.2012.11.012
- Zádorová, T., Penížek, V., Šefrna, L., Rohošková, M., Borůvka, L., 2011. Spatial

- delineation of organic carbon-rich Colluvial soils in Chernozem regions by Terrain analysis and fuzzy classification. *Catena*. 85 (1). 22–33. doi: 10.1016/j.catena.2010.11.006
- Zádorová, T., Penížek, V., Vašát, R., Žížala, D., Chuman, T., Vaněk, A., 2015. Colluvial soils as a soil organic carbon pool in different soil regions. *Geoderma*. 253–254. 122–134. doi: 10.1016/j.geoderma.2015.04.012
- Zhang, G. Lin, Liu, F., Song, X. Dong, 2017. Recent progress and future prospect of digital soil mapping: A review. *Journal of Integrative Agriculture*. 16 (12). 2871–2885. doi: 10.1016/S2095-3119(17)61762-3
- Zhang, S.-R., Sun, B., Zhao, Q.-G., XIAO, P.-F., Shu, J.-Y., 2013a. Temporal-spatial variability of soil organic carbon stocks in a rehabilitating ecosystem. *Pedosphere*. 14 (4). 501–508.
- Zhang, S., Huang, Y., Shen, C., Ye, H., Du, Y., 2012. Spatial prediction of soil organic matter using terrain indices and categorical variables as auxiliary information. *Geoderma*. 171–172. 35–43. doi: 10.1016/j.geoderma.2011.07.012
- Zhang, T., Li, L., Zheng, B., 2013b. Estimation of agricultural soil properties with imaging and laboratory spectroscopy. *Journal of Applied Remote Sensing*. 7 (1). 073587-1-073587-24. doi: 10.1117/1.JRS.7.073587
- Zhang, T., Li, L., Zheng, B., 2009. Partial least squares modeling of Hyperion image spectra for mapping agricultural soil properties. In: Gao, W., Jackson, T.J., (ed.). *Remote Sensing and Modeling of Ecosystems for Sustainability VI*. s. 74540P–74540P–12. doi: 10.1117/12.824635
- Zheng, B., 2008. *Using Satellite Hyperspectral Imagery to Map Soil Organic Matter , Total Nitrogen And Total Phosphorus*. Indiana University.
- Žížala, D., Juřicová, A., Zádorová, T., Zelenková, K., Minařík, R., 2018. Mapping soil degradation using remote sensing data and ancillary data: South-East Moravia, Czech Republic. *European Journal of Remote Sensing*. 1–15. doi: 10.1080/22797254.2018.1482524
- Žížala, D., Zádorová, T., Kapička, J., 2017. Assessment of Soil Degradation by Erosion Based on Analysis of Soil Properties Using Aerial Hyperspectral Images and Ancillary Data, Czech Republic. *Remote Sensing*. 9 (1). 28. doi: 10.3390/rs9010028

## Příloha

---

Tabulka 1: Přehled vybraných výzkumů využívajících terénní vlastnosti pro predikci SOC

Autor	Predikovaná veličina	Počet vzorků	Terénní vlastnosti	Další charakteristiky	Rozlišení DMT (m)	Plocha studovaného území	Použité metody	R <sup>2</sup> predikce [* křížová validace]	RMSEP [* RMSEcv]
Song et al. (2016)	Obsah SOC Do 20 cm	548	Sklon, expozice, zakřivení, TWI	Půdní typ, land use, prům. roční srážky, prům. roční teplota, sluneční radiace, NDVI	30	50 810 km <sup>2</sup> Čína	MLR, GWR, GWRR, KED, GWRSK	0,8*; 0,84*; 0,84*; 0,87*; 0,85*	1,85*; 1,76*; 1,76*; 1,67*; 1,73* g·kg <sup>-1</sup>
Xin et al. (2016)	Obsah SOC Do 20 cm	180	Nadmoř. výška, sklon, CA, TWI	Land use, prům. roční srážky, NDVI	-	72 km <sup>2</sup> Čína	MLR, OK, IDW	0,31*; 0,2*; 0,19*	3,47*; 4,14*; 4,48* g·kg <sup>-1</sup>
Rodríguez-Lado a Martínez-Cortizas (2015)	Obsah SOC Do 30 cm	463	Nadmoř. výška	Mat. substrát, land use, prům. roční srážky, prům. roční a měsíční teplota, potenciální evapotranspirace, vodní bilance, index kontinentality	25	29 574 km <sup>2</sup> Galicie	PLSR, MLR, PCR	0,78; 0,75; 0,66	3,48; 3,73; 4,36 %
Were et al. (2015)	Zásoby SOC do 30 cm	320	Sklon, zakřivení, expozice, TWI	Land use, prům. roční srážky, prům. roční teplota, NDVI	30	650 km <sup>2</sup> Keňa	SVM, ANN, RF	0,64; 0,61; 0,53	1,45; 1,54; 1,83 kg·m <sup>-2</sup>
Ceddia et al. (2015)	Zásoby SOC do 1 m	96	Sklon, zakřivení, expozice, CTI	Půdní textura	5	80 km <sup>2</sup> Amazonie	OK, ICOK, HCOK	-	1,99; 2,00; 1,91 kg·m <sup>-2</sup>
Veronesi et al. (2014)	Zásoby SOC Celkové	435	Sklon, zakřivení, expozice	Půdní typ, land cover, geologie	50	13 948 km <sup>2</sup> Anglie	UCK	0,36*	-
Wiesmeier et al. (2014)	Zásoby SOC do 1 m	1460	Nadmoř. výška, expozice, sklon, zakřivení, CA, TWI	Půdní substrát, půdní typ, land use, prům. roční srážky, prům. roční teplota	25	70 549 km <sup>2</sup> Bavorsko	RF	0,39	9 kg·m <sup>-2</sup>
Adhikari et al. (2014)	Obsah SOC (0-5,5-15,15-30,30-60,60-100 cm)	40250	Nadmoř. výška, sklon, expozice, FA, TWI, AAC, délka svahu, hloubka údolí	Půdní typ, land use, geograf. regiony, typ krajiny, prům. roční srážky, sluneční radiace,	30	43 000 km <sup>2</sup> Dánsko	RK	0,61; 0,63; 0,51; 0,50; 0,28	1,73; 1,73; 4,57; 3,63; 3,02 g·kg <sup>-2</sup>

Autor	Predikovaná veličina	Počet vzorků	Terénní vlastnosti	Další charakteristiky	Rozlišení DMT (m)	Plocha studovaného území	Použité metody	R <sup>2</sup> predikce [* křížová validace]	RMSEP [* RMSEcv]
Li et al. (2013)	Obsah SOM Do 30 cm	5620	Sklon, CA, TWI	Půdní typ, land use, prům. roč. srážky, prům. roč. teplota, akumul. teplota nad 10 °C, rel. vlhkost, sluneční radiace, NDVI	1000	9,6 mil. km <sup>2</sup> Čína	ANN, MLR, RK	0,019 - 0,597	21,8; 28,4; 28,05 g·kg <sup>-2</sup>
Doetterl et al. (2013)	Zásoby SOC Do 1 m (do 20 cm)	100	Sklon, zakřivení, TPI, FA, FL, TCI	Pūd. textura, koncentrace C ve svrch. vrstvě půdy, prům. roční srážky a teplota, sezonalita teploty a srážek	5	500 km <sup>2</sup> Lucembursko	LMM	0,53-0,88 (0,36-0,66)	1,52-2,02 (0,43-0,78) kg·m <sup>-2</sup>
Zhang et al. (2012)	Obsah SOM Do 25 cm	469	Nadmoř. výška, sklon, expozice, LS, TWI, SPI	Půdní typ, textura, land use	25	2 230 km <sup>2</sup> Čína	OK, RK, SMLR	-	1,33; 1,26; 0,83
Dlugoš et al. (2010)	Obsah SOC (0-25,55-50,50-90 cm)	92	Nadmoř. výška, sklon, zakřivení, expozice, CA, TWI, SPI	Dlouhodobá eroze půdy – vodní a orbou z modelu WaTEM/SEDEM	6,25	4.2 ha Německo	RK, OK	-	0,12*; 0,19*; 0,13* % 0,12*; 0,20*; 0,15* %
Afshar et al. (2010)	Obsah SOC Do 30 cm	91	Nadmoř. výška, sklon, expozice, zakřivení, CA, TWI, STI	-	3	9 ha Írán	OK	0,96*	1,74* g·kg <sup>-2</sup>
Florinsky et al. (2002)	Obsah SOC Do 30 cm	210	Nadmoř. výška, sklon, expozice, zakřivení, CA, TWI, SPI	-	15	6,75 ha USA	MLR	0,37*	0,47* %

Poznámky: CA - přispívající plocha (catchment area), TWI – topografický vlhkostní index, TPI – topografický poziční index, LS – LS faktor z USLE, TCI – topografický konvergenční index, FA – akumulace odtoku, FL – délka odtoku, STI – transportní index sedimentů, SPI – index energie vodních toků, AAC – výška nad tokem, CTI – složený topografický index, NDVI – normalizovaný diferenční vegetační index

SVM – support vector machine, RF – random forest, ANN – artificial neural networks, LMM – linear mixed effect model, MLR – multiple linear regression, SMLR – stepwise multiple linear regression, GWR – geographically weighted regression, GWRR – geographically weighted ridge regression, KED – kriging with external drift, GWRSK – simple kriging with GWR, PLSR – partial least squares regression, PCR – principal component regression, OK – ordinary kriging, ICOK – isotopic co-kriging, HCOK – partially heterotopic cokriging, IDW – inverse distance weighting, LMM – linear mixed effect model, RK – regression kriging, UCK – universal co-kriging

Tabulka 2: Přehled vybraných současných studií využívajících bodovou spektroskopii při hodnocení SOC

Autor	Predikovaná veličina	Počet vzorků	Spektrometr	Spektrální rozlišení (nm)	Radiometrické rozlišení (nm)	Plocha území studovaného	Použité metody	R <sup>2</sup> predikce [* křížová validace]	RMSEP [* RMSEcv]
Liu et al. (2017)	SOC	252	ASD FieldSpec 3	350–2500	3-10	Čína	Co-LSSVMR	0,81	2,95 g·kg <sup>-1</sup>
Shi et al. (2015)	SOM	2732	ASD Fieldspec ProFR	350–2500	3-10	Čína	PLSR, local-PLSR, scL-PLSR	0,50; 0,69; 0,74	0,84; 0,66; 0,6 %
Ji et al. (2015)*	SOC	124	Fieldspec Pro FR	350 – 2500	3-10	11 polí (0,25 – 1 ha) Čína	PLSR	0,71	1,32 g·kg <sup>-1</sup>
Gao et al. (2014)	SOC	100	ASD FieldSpec Pro FR	350 – 2500	1	10 lokalit (0,02 – 200 ha) Čína	PLSR, SVMR	0,79; 0,86	2,33; 1,84 g·kg <sup>-1</sup>
Peng et al. (2014)	SOC	298	ASD FieldSpec 3	350–2500	1	3 lokality (každá cca 100 km <sup>2</sup> ) Čína	SVMR, PLSR	0,73; 0,62	2,78; 2,83 g·kg <sup>-1</sup>
Stevens et al. (2013)	SOC	Cca 20 000 LUCAS	XDS Rapid Content Analyzer	400-2500	0.5	23 států EU	PLSR, BRT, RF, SVMR, MARS, CR	0,86	7,3 g·kg <sup>-1</sup>
Gmur et al. (2012)	SOM	39	ASD FieldSpec 3	325 – 1075	3	Washington, Oregon USA	RT	0,98*	0,02* %
Brodský et al. (2011b)	SOC	181	ASD FieldSpec 3	350 – 2500	-	2 pole ČR	PLSR	0,72; 0,89	0,22; 0,14 %
Nocita et al. (2011)	SOC	113	ASD Fieldspec-Pro	350-2500	1	130 km transekt Jižní Afrika	PLSR	0,93	2,87 g·kg <sup>-1</sup>

Poznámky: \* měření In-situ (jinak laboratorně),

RT – regression trees, PLSR – partial least square regression, BRT – boosted regression trees, RT – regression trees, RF – random forest, SVMR – support vector machine regression, MARS – multivariate adaptive regression splines, CR – cubist regression

Tabulka 3: Přehled studií využívajících obrazovou spektroskopii při predikci obsahu SOC

Autoři	Predikovaná veličina	Počet vzorků	Nosič	Typ senzoru	Senzor	Spektrální a radiometrické rozlišení	Prostorové rozlišení (m)	Plocha studovaného území	Použité statistické metody	R <sup>2</sup> predikce [* křížová validace]	RMSEP [* RMSEcv]
Castaldi et al. (2018)	SOC	84 a 54	Letadlo	Hyperspektrální	APEX	313 pásem 400–2500 nm	2,5	462 a 145 km <sup>2</sup> Belgie a Lucembursko	PLSR	-	1,5 a 4,9 g·kg <sup>-1</sup>
Bhunia et al. (2017)	SOC	50	Satelit Landsat 4-5	Multispektrální	TM	7 pásem VNIR-SWIR	30	323 km <sup>2</sup> Indie	MLR	0,71*	1,11 %
Mondal et al. (2017)	SOC	210	Družice IRS-P6	Multispektrální	LISS-III	4 pásma VNIR-SWIR	23,5	20 km <sup>2</sup>	RK	-	0,28 %
Steinberg et al. (2016)	SOC	81	Letadlo	Hyperspektrální	AHS-160	Využito 20 pásem v VNIR	2,6	7 km <sup>2</sup> Lucembursko	PLSR	0,74	2,2 g·kg <sup>-1</sup>
"	"	"	Satelit	Hyperspektrální	EnMAP - simulovaný	242 pásem 420-2450 nm	30	"	"	0,67	2,8 g·kg <sup>-1</sup>
Kanning et al. (2016)	SOC	40	Letadlo	Hyperspektrální	AISA-DUAL	367 pásem 400-2500 nm	3	80 a 120 ha Německo	PLSR	0,89*	0,27 %*
Vaudour et al. (2016)	SOC	267	Letadlo	Hyperspektrální	AISA-Eagle	126 pásem 400–1000 nm	1	221 km <sup>2</sup> Francie	Bootstrap PLSR	0,25	3,73 a 4,49 g·kg <sup>-1</sup>
Franceschini et al., (2015)	SOM	89	Letadlo	Hyperspektrální	ProSpecTIR V-S sensor	357 pásem 400-2500 nm	1	100 ha Brazílie	PLSR	0,33	3,82 g·kg <sup>-1</sup>
Stevens et al. (2015)	Použito výsledků (Stevens et al., 2012)										
Tiwari et al. (2015)	SOC	65	Satelit EO-1	Hyperspektrální	Hyperion	220 pásem VNIR-SWIR	30	189 km <sup>2</sup> Indie	ANN	0,93	0,04 %



Autoři	Predikovaná veličina	Počet vzorků	Nosič	Typ senzoru	Senzor	Spektrální a radiometrické rozlišení	Prostorové rozlišení (m)	Plocha studovaného území	Použité statistické metody	R <sup>2</sup> predikce [* křížová validace]	RMSEP [* RMSEcv]
Matarrese et al. (2014)	SOC		Letadlo	Hyperspektrální	CASI 1500	288 pásem 380-1050 nm	0,2	Itálie	Korelace druhé derivace a SOC	0,85	-
Pascucci et al. (2014)	SOC	65	Letadlo	Hyperspektrální	TASI 600	32 pásem 8000 – 11500 nm	1	3 pole (2–3,5 ha) Itálie	PLSR, CR	0,24*; 0,53*	0,31*; 0,26* %
Denis et al. (2014)	SOC	165	Letadlo	Hyperspektrální	AHS-160	63 pásem 430-2540 nm	2,6	42 km <sup>2</sup> Lucembursko	PLSR	0,96*	3,68* g·kg <sup>-1</sup>
Castaldi et al. (2014)	SOM	72	Satelit EO-1	Hyperspektrální	Hyperion ALI	220 pásem VNIR-SWIR	30	29 ha Itálie	PLSR, OLS	-	0,41*; 0,27* %
Ballabio et al. (2014)	SOC	90	Satelit Landsat	Multispektrální	ETM+	8 pásem VNIR-SWIR	30	9 251 km <sup>2</sup> Kypr	SVMR	0,81*	-
Anne et al. (2014)	Lehké frakce SOM, Labilní SOC		Satelit EO-1 Landsat	Hyperspektrální Multispektrální	Hyperion TM	220 pásem VNIR-SWIR	30	Florida	PLSR	0,67*; 0,93*	4,67* %; 6,72* g·kg <sup>-1</sup>
Lu et al. (2013)	SOC	49	Satelit EO-1	Hyperspektrální	Hyperion	220 pásem VNIR-SWIR	30	~300 km <sup>2</sup> Čína	PLSR, SMLR	0,63*; 0,5	1,6* g·kg <sup>-1</sup>
Zhang et al. (2013b)	SOM	28	Satelit EO-1	Hyperspektrální	Hyperion	220 pásem VNIR-SWIR	30	~300 km <sup>2</sup> Indiana USA	PLSR	0,74	0,66 %
Casa et al. (2013)	SOC	72	Satelit PROBA	Hyperspektrální	CHRIS	37 pásem 442–1019 nm	17	29 ha Itálie	RK PLSR	-	1,06 a 1,16 g·kg <sup>-1</sup>
Nowkandeh et al. (2013)	SOM	40	Satelit EO-1	Hyperspektrální	Hyperion	220 pásem	30	100 km <sup>2</sup>	SMLR, ANN	0,47; 0,53	0,78; 0,33 %

Autoři	Predikovaná veličina	Počet vzorků	Nosič	Typ senzoru	Senzor	Spektrální a radiometrické rozlišení	Prostorové rozlišení (m)	Plocha studovaného území	Použité statistické metody	R <sup>2</sup> predikce [* křížová validace]	RMSEP [* RMSEcv]
						VNIR-SWIR		Írán			
Stevens et al. (2012)	SOC	456	Letadlo	Hyperspektrální	AHS-160	63 pásem 430 – 2540 nm	2,6	420 km <sup>2</sup> Lucembursko	PLSR, PSR, SVMR	0,79*; 0,78*; 0,81*	3,9*; 4,0*; 3,8* g·kg <sup>-1</sup>
Siegmann et al. (2012)	SOC	32	Letadlo	Hyperspektrální	AISA-DUAL	367 pásem 400-2500 nm	3	2 pole (100 a 21 ha) Německo	PLSR	0,93*	2,48* g·kg <sup>-1</sup>
Hbirkou et al. (2012)	SOC	204	Letadlo	Hyperspektrální	HyMap	126 pásem 450-2500 nm	4	4 pole 2,5-9 ha Německo	PLSR	0,83	1,1 g·kg <sup>-1</sup>
Gomez et al. (2012)	SOC	95	Letadlo	Hyperspektrální	HyMap	126 pásem 400-2500 nm	5	24,6 km <sup>2</sup> Francie	PLSR	0,02*	2,6* g·kg <sup>-1</sup>
Gerighausen et al. (2012)	SOC	20,38,11	Letadlo	Hyperspektrální	HyMap	128 pásem 450-2480 nm	4	~200 km <sup>2</sup> Německo	PLSR	0,62; 0,71; 0,45	2,13; 1,64; 1,61 g·kg <sup>-1</sup>
Schwanghart a Jarmer (2011)	SOC	61	Letadlo	Hyperspektrální	HyMap	126 pásem 420-2480 nm	6	23 km <sup>2</sup> Španělsko	PLSR <sup>#</sup>	0,77*	0,13* %
Hively et al. (2011)	SOM	315	Letadlo	Hyperspektrální	HyperSpecTIR	178 pásem 400 – 2450 nm	2,5	6 polí (7,1 – 14,6 ha) USA	PLSR	0,75*	0,5 %
Bartholomeus et al. (2011)	SOC	68	Letadlo	Hyperspektrální	AHS-160	63 pásem 430 – 2540 nm	2,6	12 ha Belgie	PLSR	0,43 – 0,53	2,42 – 3,05 g·kg <sup>-1</sup>
Roberts et al. (2011)	SOM	217	Letadlo	Multispektrální	digital sensor system	3 pásma Green, red, NIR	0,3	6 polí (13 – 25 ha) USA	MLR	0,8	4,3 g·kg <sup>-1</sup>

Autoři	Predikovaná veličina	Počet vzorků	Nosič	Typ senzoru	Senzor	Spektrální a radiometrické rozlišení	Prostorové rozlišení (m)	Plocha studovaného území	Použité statistické metody	R <sup>2</sup> predikce [* křížová validace]	RMSEP [* RMSEcv]
Jarmer et al. (2010)	SOC	53 a 80	Satelit Landsat 5	Multispektrální	TM	7 pásem VNIR-SWIR	30	1 800 km <sup>2</sup> Izrael	MLR	0,91* a 0,79*	2,83* a 2,11* g·kg <sup>-1</sup>
Jaber et al. (2011)	SOC	303	Satelit EO-1	Hyperspektrální	Hyperion	220 pásem VNIR-SWIR	30	134 km <sup>2</sup> Illinois, USA	ANN	0,79*	11,3 t·ha <sup>-1</sup>
Stevens et al. (2010)	SOC	325	Letadlo	Hyperspektrální	AHS-160	63 pásem 430 – 2540 nm	2,6	420 km <sup>2</sup> Lucembursko	PLSR, PSR, SVMR	0,88; 0,89; 0,84	3,22; 3,13; 4,20 g·kg <sup>-1</sup>
Wang et al. (2010a)	SOM	-	Satelit EO-1	Hyperspektrální	Hyperion	220 pásem VNIR-SWIR	30	96 km <sup>2</sup> Čína	MLR	0,56 – 0,98	0,28 – 0,43 %
Zhang et al. (2009)	SOM	-	Satelit EO-1	Hyperspektrální	Hyperion	220 pásem VNIR-SWIR	30	Indiana, USA	PLSR	0,89	-
Chen et al. (2008)	SOC	-	Letadlo	Multispektrální	NASA ATLAS	15 pásem VNIR-SWIR	2	7 polí	SMLR	0,63	0,22 %
Stevens et al. (2008)	SOC	110	Letadlo	Hyperspektrální	AHS-160	63 pásem 430 – 2540 nm	2,6	10 polí Belgie	PLSR	-	6,96 g·kg <sup>-1</sup>
Patzold et al. (2008)	SOC	9	Letadlo	Hyperspektrální	HyMap	128 pásem 450-2500 nm	4	9 polí Německo	PLSR	0,74*	1,6* g·kg <sup>-1</sup>
DeTar et al. (2008)	SOM	173+14 8	Letadlo	Hyperspektrální	AVNIR	60 pásem 429–1010 nm	1,2	72 + 63 ha Kalifornie	MLR	0,49	0,08 %
Zheng (2008)	SOM	70	Satelit EO-1	Hyperspektrální	Hyperion	220 pásem VNIR-SWIR	30	3 lokality (420 – 824 km <sup>2</sup> ) USA	PLSR	0,74	1,42 %
Luo et al. (2008)	SOM	60	Satelit EO-1	Hyperspektrální	Hyperion	220 pásem	30	42.8 km <sup>2</sup>	MLR	0,78	0,45 %

Autoři	Predikovaná veličina	Počet vzorků	Nosič	Typ senzoru	Senzor	Spektrální a radiometrické rozlišení	Prostorové rozlišení (m)	Plocha studovaného území	Použité statistické metody	R <sup>2</sup> predikce [* křížová validace]	RMSEP [* RMSEcv]
Gomez et al. (2008)	SOC		Satelit EO-1	Hyperspektrální	Hyperion	VNIR-SWIR 220 pásem VNIR-SWIR	30	Čína cca 17 km <sup>2</sup> Austrálie	PLSR	0,49*	0,8* %
Jarmer et al. (2007)	SOC	77	Letadlo	Hyperspektrální	HyMap	126 pásem 450-2500 nm	6	Španělsko	MLR <sup>#</sup>	0,79*	0,11* %
Selige et al. (2006)	SOC, textura	72	Letadlo	Hyperspektrální	HyMap	128 pásem VNIR-SWIR	6	700 ha Německo	MLR, PLSR	0,89	0,22*; 0,29*
Stevens et al. (2006)	SOC	138+100	Letadlo	Hyperspektrální	CASI-2	96 pásem 405-950 nm	6; 2,5	2 lokality Belgie	PLSR	0,85	5,1 g·kg <sup>-1</sup>
Chen et al. (2006)	SOC	45	Letadlo	Multispektrální	NASA ATLAS	15 pásem VNIR-SWIR	2	2 pole USA	MLR	0,81	-
Uno et al. (2005)	SOM	50	Letadlo	Hyperspektrální	CASI	72 pásem VNIR 408 – 947 nm	14	30 ha Kanada	ANN, MLR	0,74*; 0,59*	0,49*; 0,59* %
Bajwa a Tian (2005)	SOM	-	Letadlo	Hyperspektrální	RDACS/H-3	120 pásem 471–828 nm	-	4 pole USA	PLSR	0,66	-
Toure a Tychon (2004)	SOM	100	Letadlo	Hyperspektrální	CASI-2	96 pásem 405-950 nm	2,5	50 km <sup>2</sup> Belgie	MLR	0,85-0,88	0,27-0,37 %
Stevens et al. (2004)	SOC	138	Letadlo	Hyperspektrální	CASI-2	96 pásem 405-950 nm	6	13 polí 35 km <sup>2</sup> Belgie	PLSR	0,87	0,34 %
Ray et al. (2004)	SOM	35	Satelit IKONOS	Multispektrální	IKONOS	4 pásma VIS-VNIR	4	4.43 ha Indie	SMLR	0,73	-

Autoři	Predikovaná veličina	Počet vzorků	Nosič	Typ senzoru	Senzor	Spektrální a radiometrické rozlišení	Prostorové rozlišení (m)	Plocha studovaného území	Použité statistické metody	R <sup>2</sup> predikce [* křížová validace]	RMSEP [* RMSEcv]
Touré a Tychon (2003)	SOM	135	Letadlo	Hyperspektrální	CASI-2 + SASI		2,5	14 polí (50 km <sup>2</sup> ) Belgie	SMLR	0,83	0,33* %
Ben-Dor et al. (2002)	SOM	62	Letadlo	Hyperspektrální	DAIS-7915	72 pásem 400 – 2500 nm	8	20 km <sup>2</sup> Izrael	MLR	0,83	0,02 %
Chen et al. (2000)	SOC	28+32	Letadlo	Barevný	Skenovaný barevný snímek	RGB	2	115 ha Georgie (USA)	MLR	0,98	-
Hill a Schütt (2000)	SOC	92	Satelit Landsat	Multispektrální	TM	7 pásem VNIR-SWIR	30	Cca 20 km <sup>2</sup> Španělsko	MLR	0,89*	-
(Varvel et al., 1999)	SOM	2200	letadlo	Barevný	Barevný snímek	RGB + NIR	~1	Nebraska USA	korelace	R~0,5	

Poznámky: šedě podbarvené pole ukazují studie využívající satelitní data, # - Model vytvořený nad laboratorně změřenými daty a přenesený na obrazová data,

MLR – multiple linear regression, SMLR – stepwise multiple linear regression, PLSR – partial least square regression, ANN – artificial neural network, PSR – penalized-spline signal regression, SVMR – support vector machine regression, OLS – ordinary least squares regression, LMEM – linear mixed effect model, CR – cubist regression, RK – regresní kriging